Dissertation zur Erlangung des Doktorgrades
der Fakultät für Chemie und Pharmazie
der Ludwig-Maximilians-Universität München

Efficient distance-including integral screening for Møller-Plesset perturbation theory of second order and symmetry-adapted perturbation theory

Simon Andreas Maurer

aus

Waiblingen

2014

Erklärung

Diese Dissertation wurde im Sinne von §7 der Promotionsordnung vom 28. November 2011 von Herrn Prof. Dr. C. Ochsenfeld betreut.

Eidesstattliche Versicherung

Diese Dissertation wurde eigenständig und ohne unerlaubte Hilfe erarbeitet.

München, 23. Januar 2014

(Simon Maurer)

Dissertation eingereicht am:	23.01.2014
1. Gutachter:	Prof. Dr. Christian Ochsenfeld
2. Gutachter:	Prof. Dr. Hubert Ebert
Mündliche Prüfung am:	07.03.2014

Danksagung

Bei Prof. Dr. Christian Ochsenfeld bedanke ich mich für die spannende Aufgabenstellung, die gute Betreuung dieser Arbeit und die äußerst angenehme Zusammenarbeit. Prof. Dr. Hubert Ebert danke ich für die Zeit und Mühe der Erstellung des Zweitgutachtens.

Meinem Kollegen Matthias Beer danke ich herzlich für die umfassende Unterstützung sowie für viele lehrreiche und anregende Gespräche. Ebenso gilt mein Dank allen Mitgliedern des Arbeitskreises, die mich die letzten Jahre begleitet haben, für viele kleine und große Hilfestellungen und die ausgesprochen nette Atmosphäre.

Meine Eltern danke ich dafür, dass sie den Grundstein für diese Arbeit gelegt haben, indem sie mein Interesse für naturwissenschaftliche Fragen weckten.

Mein besonderer Dank gilt meiner Frau Tara für all das, was mir neben jeder Arbeit im Leben wichtig ist.

Zusammenfassung

Die vorliegende Arbeit beschreibt Beiträge zur Entwicklung effizienter quantenchemischer Methoden für Berechnungen an großen molekularen Systemen. Zentraler Bestandteil dieser Entwicklungen sind effiziente Abschätzungen für Elektronen-Repulsions-Integrale, welche die Coulomb-Wechselwirkung zwischen zwei Ladungsverteilungen beschreiben. Solche Integralabschätzungen können in verschiedenen quantenchemischen Methoden zur Anwendung kommen, um eine Vorauswahl derjenigen Energiebeiträge zu treffen, die wesentlich für das Gesamtergebnis sind, und damit die unnötige Berechnung sehr kleiner Beiträge zu vermeiden. Die im Rahmen dieser Arbeit entwickelten QQR-Integralabschätzungen haben gegenüber bestehenden Ansätzen den Vorteil, dass der Abstand zwischen den beteiligten Ladungsverteilungen passend berücksichtigt wird, wodurch die Abschätzungen für größere Abstände massiv verbessert werden. Insbesondere bei der Vorauswahl signifikanter Beiträge in der Berechnung kurzreichweitiger Effekte, wie der Elektronenkorrelation in einem System oder der Dispersionwechselwirkung zwischen zwei Molekülen, ist eine solche Abstandsabhängigkeit der Integralabschätzungen unerlässlich für eine effiziente Selektion.

Neben der Entwicklung der QQR-Abschätzungen steht in dieser Arbeit deshalb die Berechnung der Korrelationsenergie mittels Møller-Plesset Störungstheorie in zweiter Ordnung (MP2) und die Berechnung der Dispersionsenergie im Rahmen der Symmetrie-adaptierten Störungstheorie (SAPT) im Mittelpunkt. In beiden Fällen ist eine geeignete lokale Formulierung der Theorien erforderlich, die es ermöglicht, die Berechnung auf signifikante kurzreichweitige Beiträge zu beschränken. Grundlage der vorgestellten Entwicklungen ist die Atomorbital-basierte (AO-)MP2-Theorie. Es wurde im Rahmen der Arbeit gezeigt, dass die Verwendung der QQR-Abschätzungen in AO-MP2 mit skaliertem Beitrag der Elektronen gegensätzlichen Spins (*scaled opposite-spin* AO-MP2, SOS-AO-MP2) die Berechnungen für große Moleküle gegenüber konventionellen Ansätzen massiv beschleunigt und der Anstieg der Rechenzeit mit der Molekülgröße auf das optimale, aymptotisch lineare Skalenverhalten reduziert werden kann. Durch die effiziente Selektion signifikanter Beiträge werden mit der QQR-basierten SOS-AO-MP2-Methode Berechnungen der Korrelationsenergie von sehr großen biochemischen Molekülen mit mehr als 2000 Atomen ermöglicht.

Berechnungen an derart großen Molekülen verwenden notwendigerweise eher kleine Basissätze. Um auch Berechnungen mit größeren Basissätzen für Systeme mit mehreren hundert Atomen effizient durchführen zu können, wurden die QQR-Abschätzungen auch im Rahmen unserer MP2-Methode mit Cholesky-zerlegten Pseudodichten (*Cholesky-decomposed pseudo-densities MP2*, CDD-MP2) angewendet, die auf der AO-MP2-Methode aufbaut. Durch die Zerlegung werden zwei der auftretenden Summen im MP2-Ausdruck auf einen redundanzfreien Satz von besetzten Orbitalen beschränkt, deren Anzahl nur an die Zahl der Elektronen im System gekoppelt ist, was die Verwendung größerer Basissätze begünstigt. Es wurde zudem der Ansatz einer Zerlegung der Identität (*resolution-of-the-identity*, RI) verwendet, um bereits für Systemgrößen ab 100 Atomen eine effiziente Berechnung zu ermöglichen. Mit Hilfe der QQR-Abschätzungen und unter Verwendung spezieller Algorithmen für den Umgang mit den auftretenden dünn besetzten Matrizen wurde eine sehr effiziente RI-basierte CDD-MP2-Methode entwickelt, bei der der Rechenaufwand asymptotisch kubisch mit der Molekülgröße ansteigt und die Berechnungen an Systemen mit bis zu 500 Atomen in der größeren cc-pVTZ-Basis ermöglicht.

Die effiziente Berechnung von SAPT-Dispersionsenergien wurde auf Grundlage einer Atomorbital-basierten Formulierung analog zum AO-MP2-Ansatz realisiert. Hier ermöglicht der Einsatz der QQR-Abschätzungen, die Berechnung der Dispersionswechselwirkung zwischen zwei Molekülen auf die tatsächlich beitragenden Bereiche in der Nähe der Kontaktfläche zu beschränken. Diese effiziente Methode zur Berechnung des Dispersionsbeitrags wurde mit bestehenden linear-skalierenden Beschreibungen der übrigen klassischen Wechselwirkungsbeiträge und der zugehörigen nicht-klassischen Austauschterme kombiniert, die ebenfalls in unserem Arbeitskreis entwickelt wurden. Der Austauschterm des Dispersionsbeitrags wurde in einem neuen Verfahren vernachlässigt und durch eine Skalierung der Dispersionswechselwirkung effizient ersetzt, wobei die Skalierung gleichzeitig den Gesamtfehler insbesondere mit kleinen Basissätzen massiv reduziert. Eine effiziente Berechnung von Wechselwirkungsenergien ist so auch für große Moleküle möglich, was unter anderem für die Berechnung der Wechselwirkung eines Enzymausschnitts von mehr als 1000 Atomen mit einem Molekül in seiner aktiven Tasche demonstriert wird.

Abstract

In this thesis, contributions to the development of efficient quantum-chemical methods for calculations on large molecular system are presented. A key feature of these developments are efficient estimates for electron repulsion integrals which describe the Coulomb interaction between two charge distributions. Such integral estimates can be applied in different quantum-chemical methods to preselect energy contributions that are significant for the final result and to avoid the unnecessary computation of very small contributions. In contrast to conventional approaches, the QQR integral estimates developed in this work have the advantage that they take the distance between the charge distributions into account which leads to greatly improved estimates in the case of larger distances. This distance dependence of the integral estimates is especially crucial for an efficient preselection of significant contributions in the calculation of short-ranged effects like the electron correlation in a system or the dispersion interactions between two molecules.

In addtion to the development of the QQR estimates, this work therefore focuses on the calculation of the correlation energy using Møller-Plesset perturbation theory of second order (MP2) and the calculation of the dispersion energy in the context of symmetry-adapted perturbation theory (SAPT). In both cases, a local formulation of the theory is required that allows to restrict the calculation on significant short-ranged contributions. The basis of the current developments is atomic orbital-based (AO-)MP2 theory. It has been shown in this work, that the application of QQR estimates in AO-MP2 with a scaled contribution of electrons with opposite-spin (SOS-AO-MP2) leads to massive speedups for large systems compared to conventional methods and the increase of the computational cost with molecular size is reduced to the optimal, asymptocally linear scaling. Due to the efficient selection of significant contributions, the QQR-based SOS-AO-MP2 method enables calculations of the correlation energy of very large biochemical systems with more than 2000 atoms.

Calculations on molecules of this size necessarily employ rather small basis sets. For an efficient calculations using larger basis sets on systems with several hundred atoms, we also applied our QQR estimates in our MP2 method with Cholesky-decomposed pseudo-densities (CDD-MP2) which is based on our AO-MP2 method.

By the use of the decomposition, two summations in the MP2 expression become restricted to a non-redundant set of occupied orbitals whose number is coupled to the number of electrons in the systems which is favorable for larger basis sets. Furthermore, the resolution-of-the-identity (RI) approach has been applied to allow for efficient calculations already at system sizes around 100 atoms. Owing to the QQR estimates and with the use of special algorithms for the treatment of the sparse matrices involved in the calculations, a very efficient RI-based CDD-MP2 method was developed which shows an asymptotically cubic increase of the computational cost with system size and allows to perform calculations on systems with up to 500 atoms in the larger cc-pVTZ basis.

The efficient calculation of SAPT dispersion energies was realized using an atomic orbital-based formulation analogous to the AO-MP2 approach. In this formulation, using the QQR estimates allows to restrict the calculation of the dispersion interaction between two molecules to those parts of the systems close to the contact surface that actually contribute to the interaction. This efficient method for the evaluation of the dispersion contribution was combined with existing linear-scaling formulations of the remaining classical interaction contributions and their corresponding non-classical exchange terms that also have been developed in our group. The exchange term of the dispersion contribution was neglected and efficiently substituted by a scaling of the dispersion interaction in a novel approach where the scaling at the same time greatly reduces the total error with small basis sets. An efficient calculation of interaction energies of large molecules is therefore possible as demonstrated for the calculation of the interaction of an enzyme cutout with more than 1000 atoms with a molecule in its active pocket.

Contents

List of publications **1**

1 Introduction **3**

2 Theory **7**

2.1 Hartree-Fock 7

2.1.1 Basic theory 7

2.1.2 Linear-scaling formulation 9

2.1.3 Improvements in the screening procedure 10

2.2 Møller-Plesset perturbation theory 12

2.2.1 Basic theory and conventional implementation 12

2.2.2 Low-order scaling MP2 methods 13

2.2.3 Atomic orbital-based MP2 theory 14

2.2.4 Cholesky-decomposed pseudo-density MP2 17

2.2.5 Cubic-scaling scaled opposite-spin MP2 20

2.3 Symmetry-adapted perturbation theory 22

2.3.1 Basic theory 22

2.3.2 Recent developments 23

2.3.3 Linear- and sublinear-scaling SAPT 24

3 Conclusion and outlook **25**

4 Bibliography **26**

5 Publications **31**

5.1 Paper I: "Distance-dependent Schwarz-based integral estimates for two-electron integrals: Reliable tightness vs. rigorous upper bounds", S. A. Maurer, D. S. Lambrecht, D. Flaig, C. Ochsenfeld, *J. Chem. Phys.*, **136**, 144107 (2012) 31

5.2 Paper II: "Efficient distance-including integral screening in linear-scaling Møller-Plesset perturbation theory",
S. A. Maurer, D. S. Lambrecht, J. Kussmann, C. Ochsenfeld,
J. Chem. Phys., **138**, 014101 (2013) 73
5.3 Paper III: "Cholesky-decomposed density MP2 with density fitting: accurate MP2 and double-hybrid DFT energies for large systems",
S. A. Maurer, L. Clin, C. Ochsenfeld, (submitted) 93
5.4 Paper IV: "Linear-scaling symmetry-adapted perturbation theory with scaled dispersion",
S. A. Maurer, M. Beer, D. S. Lambrecht, C. Ochsenfeld,
J. Chem. Phys., **139**, 184104 (2013) 121

Curriculum vitae **135**

List of publications

This work is a cumulative dissertation. The results of this thesis were so far published in four peer-reviewed journal papers which are considered the main part of this work. The following list specifies the contributions of the author in each of the publications in italics. All four publications and their corresponding supplementary material are collected at the second part of this work and are referred to in the text as paper **I** - **IV**:

(**I**): Simon A. Maurer, Daniel S. Lambrecht, Denis Flaig, and Christian Ochsenfeld, "Distance-dependent Schwarz-based integral estimates for two-electron integrals: Reliable tightness vs. rigorous upper bounds", *J. Chem. Phys.*, **136**, 144107 (2012).

Contribution by S. A. Maurer: *All derivations, the implementation of the revised MBIE and the new QQR estimates, all calculations, and most of the writing.*

(**II**): Simon A. Maurer, Daniel S. Lambrecht, Jörg Kussmann, and Christian Ochsenfeld, "Efficient distance-including integral screening in linear-scaling Møller-Plesset perturbation theory", *J. Chem. Phys.*, **138**, 014101 (2013).

Contribution by S. A. Maurer: *Implementation of the QQR-based screening procedure, all calculations, and most of the writing.*

(**III**): Simon A. Maurer, Lucien Clin, and Christian Ochsenfeld, "Cholesky-decomposed density MP2 with density fitting: accurate MP2 and double-hybrid DFT energies for large systems", (submitted).

Contribution by S. A. Maurer: *Complete reimplementation of the RI-CDD-MP2 method based on QQR-type screening and sparse matrix algebra, proofs of properties of the Cholesky decomposition, development and implementation of an RI-CDD-MP2 variant with local RI fitting, all calculations, and most of the writing.*

(**IV**): Simon A. Maurer, Matthias Beer, Daniel S. Lambrecht, and Christian Ochsenfeld, "Linear-scaling symmetry-adapted perturbation theory with scaled dispersion", *J. Chem. Phys.*, **139**, 184104 (2013).

Contribution by S. A. Maurer: *Development of the scaled-dispersion SAPT method, reimplementation of the complete dispersion term based on QQR-type screening, all calculations, and most of the writing.*

Chapter 1

Introduction

Theoretical studies of large molecular systems are often limited by the computational cost of the calculations. The treatment of systems with several thousand atoms, like whole proteins or large DNA segments, is conventionally only possible using rather simple models based on a mechanical description of bonds and interactions as spring models and classical potentials. While this molecular mechanics (MM) approach is very fast, most MM models are unable to describe chemical reactions and calculations of molecular properties like spectroscopic data are not possible. Furthermore, the parameters in the MM models are empirically fitted for a particular class of systems and the transferability of a particular method might be limited.

Reliable studies therefore often require more advanced models which are based on a quantum-mechanical (QM) description of the electronic structure in the system. These methods are either directly based on the electron distribution, as in density-functional theory (DFT) [1], or use the concept of an electronic wave function as (approximate) solution to the fundamental Schrödinger equation. In studies of biochemical systems, the quantum-chemical methods are often applied within a combined quantum-mechanics/molecular-mechanics (QM/MM) approach where only the region which is in the focus of the study, e.g., the active pocket of an enzyme, is treated with a quantum-chemical method (QM region) and the remaining outer part of the system is described with simpler MM models. The QM/MM approach significantly reduces the system sizes that have to be treated with the more expensive quantum-chemical methods and convergence with system size has been found to require QM regions of a few hundred up to 1000 atoms depending on the molecular system [2].

The DFT approach to quantum-chemical calculations, usually based on the Kohn-Sham formulation of DFT, is widely-used in theoretical studies as it provides reasonable results in many situations and is cheap compared to most of the wave function-based methods. Despite its efficiency, DFT theory in the present formulations has some less appealing features which are connected to the fact that the exact energy functional is unknown. While physically well-founded DFT functionals have been proposed, succesful application to molecular systems usually requires to include undesired empirical fitting parameters in the functionals. The description of London dispersion effects is a particularly challenging problem for DFT and conventional functionals do not provide a reasonable dispersion description. To take dispersion into account, special functionals with a very large number of fitting parameters have to be used or empirical dispersion corrections similar to an MM description have to be added to the conventional results [3].

Among the wave function-based quantum-chemical methods, Hartree-Fock theory [4, 5] is the most fundamental one and serves as a basis for many, more advanced, models. In the Hartree-Fock method, the electron-electron interaction is described in an averaged way as each electron interacts with the mean-field of the remaining electrons. The uncorrelated Hartree-Fock model has some shortcomings and, like conventional DFT, does not account for dispersion effects, but there are several methods that start from the Hartree-Fock wave function and improve the model by including the correlation between electrons. Rigorous post-Hartree-Fock theories that provide a hierarchy up to the exact solution for the wave function (within the chosen basis) are provided by configuration interaction and coupled-cluster theory [5]. Nowadays, coupled-cluster theory is usually the preferred approach for high accuracy calculations as it provides a size-extensive solution. The coupled-cluster model including single and double excitations and a perturbative triples correction (CCSD(T)) provides an accuracy which is more than sufficient for most of the applications in quantum chemistry and is therefore sometimes referred to as the "gold standard" of quantum-chemical methods. Unfortunately, the computational cost for conventional CCSD(T) calculations increases as N^7 with the molecular size N and the application of CCSD(T) is therefore limited to very small molecules.

Another pathway to correlated methods is provided by perturbation theory. The Møller-Plesset perturbation theory [4] is based on the Hartree-Fock solution and uses the difference between the Hartree-Fock model hamiltonian and the exact hamiltonian as perturbation, which gives a series of perturbative corrections to the Hartree-Fock energy. The convergence behavior of this series is not satisfactory, nevertheless the lowest-order terms have been found to provide good results at comparably low computational cost. Nowadays, most of the development is concentrated on the first energy correction to the Hartree-Fock model which is obtained at second order in the Møller-Plesset perturbation expansion (MP2). The MP2 method is the cheapest wave function-based correlation method that is able to provide a reasonable description of dispersion effects. However, the cost of conventional MP2 calculations still scales as the fifth-power with system size which limits the applicability. In the last decades, much work has been dedicated to the development of efficient MP2 methods with reduced scaling [6]. In this thesis, contributions to the development of low-scaling MP2 methods are presented with a special focus on the preselection of significant contributions in these theories using estimates for the electron-repulsion integrals which are the central quantity in MP2 calculations.

The novel integral estimates introduced in this work are denoted as QQR and cover all the essential spatial couplings between the four functions involved in an electron repulsion integral. The important improvement over the conventional Schwarz estimates [7] is the appropriate description of the decay with increasing separation between the charge distributions of bra and ket which is based on an analysis of the multipole expansion of the integral. The QQR estimates were first introduced and extensively studied in the context of Hartree-Fock theory as discussed in section 2.1.3 and paper **I**. A comparison to the previous attempt of multipole-based integral estimates (MBIE) [8, 9] is given in this work and the advantages of the QQR approach are discussed. While Hartree-Fock calculations can be realized with linear-scaling cost also with the conventional Schwarz estimate, the use of our QQR-based integral screening in the evaluation of the exchange matrix is shown to reduce the number of selected integrals significantly, up to a factor of 2 when calculations with the same accuracy are compared.

In MP2 theory, the use of distance-dependent integral estimates is mandatory to efficiently preselect significant contributions and to restrict the calculation to a linear-scaling number of integrals. We introduced our QQR estimates into our atomic orbital-based (AO-)MP2 method [10] where an asymptotic linear-scaling behavior of the computational cost with system size can be achieved. The theory and results are summarized in section 2.2.3 and presented in detail in paper **II**. The implementation is focused on the opposite-spin term within the scaled opposite-spin (SOS-)AO-MP2 method where our efficient QQR-type screening enables calculations on very large biochemical systems with more than 2000 atoms.

Further developments focusing on MP2 calculations with larger basis sets are based on the Cholesky decomposition of the pseudo-densities (CDD-)MP2 approach [11] and are described in section 2.2.4 and paper **III**. In the CDD-MP2 method a non-redundant basis of local functions is obtained by the decomposition which leads to equally favourable performance in both small and large basis sets. Using the resolution-of-the-identity (RI) approximation and sparse matrix algebra, a very efficient, asymptotically cubic scaling MP2 method is obtained which is shown to provide significant speedups compared to conventional RI-MP2 already for system sizes of around 150 atoms. Due to the low scaling of the computational cost, the range of systems that can be treated with an RI-CDD-MP2 calculation in a triple-zeta basis on a single computing node is extended to more than 500 atoms as demonstrated in calculations on DNA systems.

While regular quantum-chemical calculations evaluate the total energy of a molecular system and interaction energies are obtained as the energy difference between the interacting complex and the individual monomer calculations, a direct evaluation of interaction energies is also possible using symmetry-adapted perturbation theory (SAPT). In the SAPT method, the total interaction energy is calculated as a sum of individual terms that can be identified with the classical interactions – electrostatic, induction and dispersion interaction – and additional non-classical exchange terms. A linear-scaling atomic orbital-based implementation of the electrostatic and induction terms including their exchange counterparts was developed by Beer [12] in our group. A linear-scaling evaluation of the SAPT dispersion term, which is similar to the opposite-spin term of AO-MP2, was realized in the present work using QQR-based screening. The work of Beer and the QQR-based dispersion term were combined into an novel SAPT method based on zeroth-order SAPT (SAPT0) where the dispersion term is scaled to account for the neglect of the dispersion-exchange term and to partially correct the basis set incompleteness error. This scaled dispersion (sd-)SAPT0 method is described in section 2.3 and paper **IV**. Efficient screening procedures are used in all time-determining steps which allow to greatly reduce the number of evaluated contributions due to the limited range of the interaction forces. This makes our sd-SAPT0 method an efficient tool for studies of interactions in large systems as demonstrated for the case of an enzyme cutout with more than 1000 atoms interacting with a molecule in its active pocket.

In the following sections, brief discussions of the methods and the contributions of this thesis are given. While concise discussions of the conventional theories can be found in textbooks and reviews, the aim of the following presentation is to introduce the notations and conventions used in the publications and review some basic aspects of the theories which are presumed in the discussions in the papers. Furthermore, an overview of the existing work in the field is provided to put the contributions of this thesis into perspective. Details are presented in the papers in the second part of this work. Furthermore, section 2.2.5 describes a novel, yet unpublished MP2 method which was derived as part of this work and for which an efficient implementation is currently under development in our group.

Chapter 2

Theory

2.1 Hartree-Fock

2.1.1 Basic theory

The basic Hartree-Fock (HF) theory as given in this section is textbook knowledge. A comprehensive discussion of the Hartree-Fock approach and the derivation of the working formulas can be found in Ref. [4].

In the Hartree-Fock method, the wave-function of a system is approximated as a Slater determinant over single-electron functions, the molecular orbitals (MOs). This ansatz ultimately leads to a model, where interactions between electrons are no longer described individually but each electron only interacts with the mean field of all the other electrons.

In practical calculations, a molecular orbital $\varphi_i(\mathbf{r})$ is expressed as a linear combination of basis functions

$$\varphi_i(\mathbf{r}) = \sum_\mu c_{\mu i} \chi_\mu(\mathbf{r}) \tag{2.1}$$

which is usually referred to as the *linear combination of atomic orbitals* (LCAO) ansatz. The basis functions $\chi_\mu(\mathbf{r})$ are typically constructed from Gaussian-type primitive functions in such a way that a few of them combined model the regular atomic orbitals, i.e, the orbitals of independent atoms. While there is no one-to-one correspondence between atomic orbitals and basis functions in all but minimal basis sets, both sets are atom-centered and share the same symmetry properties and it is therefore common practice to refer to the functions $\chi_\mu(\mathbf{r})$ as atomic orbitals (AOs). The MO coeffcients $c_{\mu i}$ are determined by minimizing the energy expectation value of the Slater determinant as it is known from the variation principle that the exact wave-function corresponds to the lowest energy. The lowest energy solution is therefore the best approximation with respect to the energy criterion.

The energy minimization is an iterative procedure where the essential steps in each iteration are the formation of the Fock matrix and the subsequent solution of the Roothaan-Hall equation. The expression for the Fock matrix in the AO basis reads

$$F_{\mu\nu} = h_{\mu\nu} + 2\sum_{\lambda\sigma} P_{\lambda\sigma}(\mu\nu|\lambda\sigma) - \sum_{\lambda\sigma} P_{\lambda\sigma}(\mu\lambda|\nu\sigma) \tag{2.2}$$

where

$$(\mu\nu|\lambda\sigma) = \int \chi_\mu(\boldsymbol{r}_1)\chi_\nu(\boldsymbol{r}_1)\frac{1}{r_{12}}\chi_\lambda(\boldsymbol{r}_2)\chi_\sigma(\boldsymbol{r}_2)\mathrm{d}\boldsymbol{r}_1\mathrm{d}\boldsymbol{r}_2 \tag{2.3}$$

are two-electron integrals which are also known as *electron repulsion integrals* (ERIs). Throughout this work, real-valued basis functions are employed. The density matrix $\mathbf{P}$ is constructed from the coefficients of the occupied MOs

$$P_{\mu\nu} = \sum_i c_{\mu i}c_{\nu i} \tag{2.4}$$

and $h_{\mu\nu}$ are AO contributions to the one-electron energies, i.e., the kinetic energy as well as the potential energy in the field of the nuclei.

The Roothaan-Hall equation

$$\mathbf{FC} = \mathbf{SC}\boldsymbol{\varepsilon} \tag{2.5}$$

is a generalized eigenvalue problem where $\mathbf{S}$ is the overlap matrix in the AO basis. The matrix of MO coefficients $\mathbf{C}$ and the diagonal matrix $\boldsymbol{\varepsilon}$ including the orbital energies are obtained as solutions. The Hartree-Fock solution only depends on the occupied MOs which are those orbitals with the lowest orbital energies with their number equal to the number of electrons in the system. The solution of the Roothaan-Hall equation provides a much larger number of MOs equal to the number of atomic orbitals. The unoccupied orbitals are important in methods that include electron correlation (see sections 2.2 and 2.3). The unoccupied MOs are called virtual orbitals and will be subscripted with $a, b, \ldots$ while we continue to use indices $i, j, \ldots$ for occupied orbitals. Summations are implicitly meant to be restricted to the corresponding set of occupied and virtual functions.

The iterative process of building the Fock matrix and solving the Roothaan-Hall equation is continued to convergence. The Hartree-Fock energy is finally obtained as

$$E_{HF} = \sum_{\mu\nu} h_{\mu\nu}P_{\mu\nu} + \sum_{\mu\nu} F_{\mu\nu}P_{\mu\nu}. \tag{2.6}$$

It should be noted, that the commonly applied Kohn-Sham formulation of density-functional theory (DFT) is closely connected to the solution of the Hartree-Fock problem described above. While the Fock matrix is expanded by an additional exchange-correlation term, the general iterative procedure is essentially unchanged and the developments described below can be readily applied to DFT calculations with hybrid functionals like the famous B3LYP functional [13, 14].

2.1.2 Linear-scaling formulation

The time determining step in a Hartree-Fock calculation is usually the formation of the Fock matrix Eq. 2.2 where the expensive part are the contractions of the density-matrix with the two-electron integrals in the last two terms. The computational cost for these steps would scale as the fourth power of the molecular size in a trivial implementation. Using more advanced techniques, it is possible to achieve linear-scaling with the molecular size as described below.

A first step to improve the scaling behavior is the preselection of significant contributions using integral estimates. The most famous estimate is based on the Cauchy-Schwarz inequality which was first applied to two-electron integrals in quantum chemistry by Whitten in 1973 [7]. This estimate, known as the *Schwarz estimate*,

$$|(\mu\nu|\lambda\sigma)| \leq (\mu\nu|\mu\nu)^{\frac{1}{2}}(\lambda\sigma|\lambda\sigma)^{\frac{1}{2}} = Q_{\mu\nu}Q_{\lambda\sigma} \tag{2.7}$$

provides an upper bound to the integral. The product on the right hand side is very cheap to evaluate and can be used to sort out very small integrals which can be neglected without introducing significant errors. As the two-electron integrals depend on products of basis functions and since function values of these products are negligible if the two functions are far apart and localized in space like the atomic orbitals, for each value of one index only an asymptotically constant number of the second index gives significant integrals. In the following, we refer to such index pairs as 'coupled indices'. Due to the coupling of both μ and ν as well as λ and σ the total number of significant AO integrals in large systems scales quadratically with system size.

In the evaluation of the exchange term $\sum_{\lambda\sigma} P_{\lambda\sigma}(\mu\lambda|\nu\sigma)$, estimates for each AO contribution

$$|P_{\lambda\sigma}(\mu\lambda|\nu\sigma)| \leq |P_{\lambda\sigma}|Q_{\mu\lambda}Q_{\nu\sigma} \tag{2.8}$$

are used and only contributions for which the right hand side of the inequality is larger than a chosen threshold are taken into account. For systems with significant HOMO-LUMO gap, which includes most of the common chemical systems but excludes conductive materials and systems with strong delocalization, the number of significant elements of the density matrix scales linearly with system size [15,16]. More specifically, the index pairs are limited to functions in close vicinity (the decay is exponential [16]) so that the indices of the density matrix are stronlgy coupled. In combination with the coupling of indices in a function product, all indices in Eq. 2.8 are coupled with each other and only a linear-scaling number of significant contributions exists which can be preselected using the Schwarz estimate.

While the calculation of estimates is rather cheap, for very large systems this step might become a bottleneck. A linear-scaling formulation of the screening step can be achieved using the ONX [17] or the more efficient LinK [18, 19] screening schemes which allows for a fully linear-scaling evaluation of the exchange contribution.

The Coulomb term $2\sum_{\lambda\sigma} P_{\lambda\sigma}(\mu\nu|\lambda\sigma)$ can be calculated with linear-scaling cost using the multipole expansion in combination with a tree structure of boxes as, e.g., used in the continous fast multipole method (CFMM) [20, 21]. In this approach, the Coulomb interaction between well-separated parts of the molecule is not calculated as a large sum of individual AO contributions but rather expressed as the interaction of two large charge distributions. The interaction energy for these collections of AO distributions can be efficiently calculated using the multipole expansion. Both the multipole-based evaluation of the long-range interaction as well as the cost for the remaining short-range terms which require explicit integral evaluations scale linearly with system size.

The computational cost for the diagonalization step in the solution of the Roothaan-Hall equation increases cubically with system size but has a very small prefactor when highly optimized library routines are applied. Usually, the time required for this step is negligible compared to the formation of the Fock matrix but for very large systems it might become significant or even dominating so that linear-scaling alternatives have been developed. These methods directly determine an improved density matrix from the Fock matrix without calculation of the intermediate (delocalized) MOs. A comparison of different diagonalization alternatives can be found in Ref. [22].

2.1.3 Improvements in the screening procedure

A two-electron integral $(\mu\nu|\lambda\sigma)$ can be understood as the Coulomb interaction of two charge distributions where each distribution (in bra and ket) is described by a product of two basis functions. Besides the coupling of the two functions of such a product as described in the previous section, the integral also exhibits a decay with increasing separation of the bra and ket charge distribution (see Fig. I in paper **II**). This decay can be analyzed using the multipole expansion of the two-electron integrals [5] which is valid if the charge distribution of bra and ket do not overlap. The slowest decaying term in the expansion is the monopole-monopole interaction which corresponds to the classical Coulomb interaction of two point charges and decays as $1/R$ with the bra-ket separation which is therefore identical to the asymptotic decay behavior of the integral value.

Based on the multipole expansion, improved integral estimates can be derived that take the decay with the bra-ket separation into account. The first such attempt were the multipole based integral estimates (MBIE) introduced by Lambrecht and Ochsenfeld in 2005 [8, 9]. A revised derivation of these estimates was developed as part of this thesis and can be found in appendix A of paper **I**. The MBIE estimates are upper bounds to the integral value

$$|(\mu\nu|\lambda\sigma)| \leq \frac{\mathcal{M}'^{(0)}_{\mu\nu}\mathcal{M}'^{(0)}_{\lambda\sigma}}{R - \mathrm{ext}_{\mu\nu} - \mathrm{ext}_{\lambda\sigma}} \tag{2.9}$$

and reflect the correct asymptotic $1/R$ decay of the integral value. The quantities $\mathcal{M}'^{(0)}_{\mu\nu}$ are calculated such that they are upper bound on the corresponding absolute multipole integrals

$$\mathcal{M}'^{(0)}_{\mu\nu} \geq \int |\chi_\mu(\boldsymbol{r})\chi_\nu(\boldsymbol{r})|\,\mathrm{d}\boldsymbol{r} \tag{2.10}$$

In principle, an exact evaluation of these quantities is possible but requires expensive numerical integration. An efficient approach uses exact solutions for primitive Gaussian distributions and a transformation to contracted function pairs using absolute values of the contraction coefficients. Detailed formulas for both $\mathcal{M}'^{(0)}_{\mu\nu}$ and the corresponding extents $\mathrm{ext}_{\mu\nu}$, are given in appendix A of paper **I**.

The MBIE approach provides more accurate estimates for integrals with large bra-ket separation than the Schwarz estimate while the latter is always employed for near-field integrals where the bra and ket charge distribution overlap and the multipole expansion is not valid.

MBIE theory provides a rigorous way to derive distance-dependent upper bounds to ERIs. Nevertheless the absolute value involved in the definition of the absolute multipole integrals Eq. 2.10 leads to significant overestimation of the integral value despite the correct decay behavior. We therefore explored a different approach in this work which formally replaces the absolute multipole integrals by the Schwarz integrals. A detailed discussion is given in paper **I**. We denote these new integral estimates as QQR according to the quantities involved in the calculation

$$|(\mu\nu|\lambda\sigma)| \approx \frac{Q_{\mu\nu}Q_{\lambda\sigma}}{R - \mathrm{ext}_{\mu\nu} - \mathrm{ext}_{\lambda\sigma}}. \tag{2.11}$$

As the extents $\mathrm{ext}_{\mu\nu}$ in MBIE theory depend on the values of the absolute multipole integrals, a different definition has to be used in the QQR approach. We found that the well-separatedness extents known from CFMM theory are a suitable choice (detailed definitions are provided in appendix B of paper **I**).

In paper **I**, both MBIE and QQR estimates were extensively studied and applied in the calculation of the exchange term in Hartree-Fock theory. In contrast to MBIE theory, the QQR estimates are no longer upper bounds but they provide estimates much closer to the exact value than previous methods. The superior performance of QQR was confirmed in extensive benchmarks including calculations on a large benchmark set which was developed as part of this work. The results show that QQR screening allows to reduce the number of exchange integrals that have to be calculated for a given accuracy by a factor of up to 2 and consistently shows an improved error-to-number-of-integrals ratio. While the scaling behavior of the calculation remains unchanged (linear-scaling is already achieved with pure Schwarz screening) significant savings can be achieved with the distance-including QQR screening. As the QQR estimates show better performance than MBIE and the difference is even more significant for electron correlation methods, where transformed functions occur (see next chapter) and the absolute value in the MBIE integrals has an even more detrimental effect, in the following we focus exclusively on the use of the efficient QQR-type estimates.

2.2 Møller-Plesset perturbation theory

2.2.1 Basic theory and conventional implementation

A concise discussion of Møller-Plesset perturbation theory and a derivation of the working equations can be found in Ref. [4]. In the following, we will focus on the implications of the theory and on computational aspects of the conventional implementation.

Møller-Plesset perturbation theory allows to improve upon the independent-particle model of Hartree-Fock theory by expanding both the energy and the wave-function in a pertubation series where the perturbation is the correction of the Hartree-Fock model Hamiltonian to the exact (non-relativistic) Hamiltonian in the Born-Oppenheimer approximation. The sum of zeroth and first order energy is identical to the Hartree-Fock energy so that the first improvement is obtained with the second-order energy correction (MP2). The MP2 expression in canonical space orbitals reads

$$E_{MP2} = -\sum_{ijab} \frac{2(ia|jb)(ia|jb) - (ia|jb)(ib|ja)}{\epsilon_a + \epsilon_b - \epsilon_i - \epsilon_j} \tag{2.12}$$

The MP2 energy is the cheapest method which provides a wave-function based description of dispersive interactions and is therefore an important quantum-chemical tool for studying large systems. Furthermore, similar methods based on DFT calculations have also been developed and are considered to be very accurate approximations [23]: The recently introduced class of *double-hybrid* density functionals [23] evaluates Eq. 2.12 with the orbitals from a DFT rather than a Hartree-Fock calculation. Therefore these modern DFT functionals also depend on an efficient evaluation of the MP2 expression.

The time determining step in a conventional MP2 calculation is the transformation of the two-electron integrals from the AO basis to the basis of the canonical MOs

$$(ia|jb) = \sum_{\mu\nu\lambda\sigma} c_{\mu i} c_{\nu a} c_{\lambda j} c_{\sigma b} (\mu\nu|\lambda\sigma) \tag{2.13}$$

This transformation can be implemented in four consecutive steps where each step has a fifth-order scaling with system size.

An important improvement in reducing prefactors was the introduction of the resolution-of-the-identity (RI) approximation in MP2 theory by Feyereisen in 1993 [24], where the regular four-center two-electron integrals are build from two- and three-center intermediates

$$(ia|jb) = \sum_{PQ} (ia|P) \left[\mathbf{J}^{-1}\right]_{PQ} (Q|jb) \tag{2.14}$$

where the matrix $\mathbf{J}$ is the matrix of two-center two-electron integrals $(P|Q)$ in the basis of auxiliary functions.

The RI approach (also known as density fitting) does largely reduce the prefactor of the calculations as only two-fold transformations are necessary to build the $(ia|P)$ intermediates and each transformation step scales only as the fourth power of the system size. On the other hand, the total scaling behavior remains unchanged as the final step in the contraction to the MO integrals in Eq. 2.14 exhibits a fifth-order scaling and is usually dominant. Nevertheless, the RI approach allows to extend the applicability of MP2 theory not only because of the reduced prefactor but also because of the largely reduced hard disk requirements. Instead of the huge number of regular four-center integrals only the reduced amount of three-center integrals has to be stored on disk for efficient evaluation.

Besides the RI approach a closely connected method is based on the Cholesky decomposition of the matrix of two-electron integrals in the AO basis, which can be considered as an on-the-fly creation of a density fitting auxiliary basis [25] and was applied to MP2 theory and other correlation methods [26, 27]. As in the standard RI approach, the scaling behavior remains unchanged.

2.2.2 Low-order scaling MP2 methods

There has been significant work on reducing the scaling behavior of MP2 calculations. One of the early attempts has been the *local* approach pioneered by Pulay and Saebø [28, 29]. To obtain a reduced scaling, local methods abandon the closed formula Eq. 2.12 which is based on canonical (delocalized) orbitals and their corresponding orbital energies and instead use an iterative procedure based on the minimization of the Hylleraas functional [29]. This approach allows to use localized orbitals which are usually obtained by unitary transformation among the occupied orbitals using an appropriate locality measure, e.g., the sum of orbital variances, as objective function. For the virtual orbitals, the convergence of regular localization procedures is slow and an alternative projection of the AO functions on the virtual space is usually applied which yields a redundant set of projected atomic orbitals. Only recently, viable alternatives have been developed [30–32] that allow for a full optimization of a non-redundant set of virtual orbitals.

A lot of work has been done on the local MP2 method [33–35] and linear-scaling cost with molecular size is possible [35]. Nevertheless, efficient use of the local approximation leads to significant truncation errors. These errors can be largely reduced using explicitly correlated wave-functions [36] where the linear scaling behavior can be retained but the prefactor is significantly increased as additional expensive terms arise from the explicitly correlated treatment.

Another approach to linear-scaling MP2 is based on the Laplace transform of the denominator which allows to express the MP2 energy purely in the AO basis. The AO-MP2 method was introduced by Almlöf and Häser in 1991-1993 [37–39] and linear-scaling formulations have been developed by Ayala and Scuseria [40] and our group (see Ref. [10] and paper **II**). Details of the AO-MP2 method as well as the improvements developed within this work are discussed in the next section.

Other linear-scaling methods are based on a fragmentation of the molecular system like the divide-and-conquer [41] approach or the fragment molecular orbital (FMO-)MP2 theory [42]. Very large FMO-MP2 calculations on massively parallel computers have been reported [43] but the accuracy of these large scale calculations could not yet be determined due to the lack of comparative calculations [6]. An alternative to the common a-priori restrictions in local MP2 methods based on the Pulay/Saebø approach has been recently introduced with the divide-expand-consolidate MP2 method [44] where the local correlation space is dynamically expanded.

2.2.3 Atomic orbital-based MP2 theory

In the regular MP2 expression Eq. 2.12 the four sums over MO indices are coupled via the energy denominator which hinders a straightforward change of basis. The solution of Almlöf and Häser [37–39] is a Laplace transform of the denominator which is evaluated as a finite quadrature sum

$$\frac{1}{\epsilon_a + \epsilon_b - \epsilon_i - \epsilon_j} = \int_0^\infty e^{-(\epsilon_a + \epsilon_b - \epsilon_i - \epsilon_j)t} \mathrm{d}t \approx \sum_\alpha \omega^{(\alpha)} e^{-\epsilon_a t^{(\alpha)}} e^{-\epsilon_b t^{(\alpha)}} e^{\epsilon_i t^{(\alpha)}} e^{\epsilon_j t^{(\alpha)}} \tag{2.15}$$

where typically 5-6 points are sufficient for errors well below 350 μHartree or 1 kJ/mol for systems with significant HOMO-LUMO gap as shown in extensive benchmark calculations in the papers **II** and **III**. The multiplicative expression on the right hand side of Eq. 2.15 decouples the MO indices. In combination with the LCAO expansion 2.1 applied to the MO functions of the two-electron integrals this approach finally allows to evaluate the MO sums of the MP2 expression and contract the MO coefficients and the exponential terms of the Laplace expansion into occupied and virtual *pseudo-densities*

$$\begin{aligned}\underline{P}_{\mu\nu} &= (\omega_\alpha)^{\frac{1}{4}} \sum_i c_{\mu i} e^{\epsilon_i t_\alpha} c_{\nu i} \\ \overline{P}_{\mu\nu} &= (\omega_\alpha)^{\frac{1}{4}} \sum_a c_{\mu a} e^{-\epsilon_a t_\alpha} c_{\nu a}.\end{aligned} \tag{2.16}$$

The resulting expression for the AO-MP2 energy reads

$$E_{AO-MP2} = -\sum_\alpha \sum_{\substack{\mu\nu\lambda\sigma \\ \mu'\nu'\lambda'\sigma'}} \underline{P}_{\mu\mu'} \overline{P}_{\nu\nu'} \underline{P}_{\lambda\lambda'} \overline{P}_{\sigma\sigma'} (\mu\nu|\lambda\sigma) \left[2(\mu'\nu'|\lambda'\sigma') - (\mu'\sigma'|\lambda'\nu') \right]. \tag{2.17}$$

The pseudo-densities are sparse for large systems and only have significant entries for index pairs of AOs that are in close vicinity. As the AO functions are localized on single atoms, the AO-MP2 expression provides a local description of correlation.

The MP2 energy is often formally split into Coulomb-type contributions

$$e_J^{(\alpha)} = \sum_{\substack{\mu\nu\lambda\sigma \\ \mu'\nu'\lambda'\sigma'}} \underline{P}_{\mu\mu'} \overline{P}_{\nu\nu'} \underline{P}_{\lambda\lambda'} \overline{P}_{\sigma\sigma'} (\mu\nu|\lambda\sigma)(\mu'\nu'|\lambda'\sigma') \tag{2.18}$$

and exchange-type contributions

$$e_K^{(\alpha)} = \sum_{\substack{\mu\nu\lambda\sigma \\ \mu'\nu'\lambda'\sigma'}} \underline{P}_{\mu\mu'} \overline{P}_{\nu\nu'} \underline{P}_{\lambda\lambda'} \overline{P}_{\sigma\sigma'} (\mu\nu|\lambda\sigma)(\mu'\sigma'|\lambda'\nu') \tag{2.19}$$

where the sum yields the total AO-MP2 energy

$$E_{AO-MP2} = -\sum_\alpha (2e_J^{(\alpha)} - e_K^{(\alpha)}). \tag{2.20}$$

There is only an asymptotically linear scaling number of Coulomb and exchange-type contributions to the AO-MP2 energy as discussed in Ref. [10] and paper **II**. In the exchange-type term Eq. 2.19, the indices are coupled via the basis function products of bra and ket and via the sparsity of the pseudo-densities similar to the Hartree-Fock exchange term described in section 2.1.2 and the significant products can be preselected using the Schwarz estimate [10, 39].

The Coulomb-type term can be rewritten with half-transformed integrals

$$(\underline{\mu}\overline{\nu}|\lambda\sigma) = \sum_{\mu'\nu'} \underline{P}_{\mu\mu'}\overline{P}_{\nu\nu'}(\mu'\nu'|\lambda\sigma). \tag{2.21}$$

as

$$e_J^{(\alpha)} = \sum_{\mu\nu\lambda\sigma} (\underline{\mu}\overline{\nu}|\lambda\sigma)(\mu\nu|\underline{\lambda}\overline{\sigma}) \tag{2.22}$$

which is the most convenient form for both estimation of significant contributions and efficient evaluation of the contributions. As discussed in paper **II**, the multipole expansion can be used to explain the linear-scaling number of contributions: Both of the two half-transformed integrals show an asymptotic $1/R^2$ decay with increasing separation of the bra and ket charge distributions. This decay is stronger than for the case of regular AO integrals since the products of transformed functions, e.g., $\underline{\mu}$ and $\overline{\nu}$, do not have a net charge and the first term in the multipole expansion, the slowly decaying monopole-monopole term, vanishes. As each half-transformed integral decays as $1/R^2$, the product of two such integrals shows a strong $1/R^4$ decay with the bra-ket separation which couples all the four indices and leads to a linear-scaling number of significant contributions.

Based on the success of our QQR estimates in Hartree-Fock theory, we developed Schwarz-based distance-including QQR-type screening for AO-MP2 as part of this work (paper **II**) which allows to efficiently preselect significant contributions in AO-MP2 theory. For a half-transformed integral the estimate reads

$$(\underline{\mu}\overline{\nu}|\lambda\sigma) \approx \frac{Z_{\underline{\mu}\overline{\nu}} Q_{\lambda\sigma}}{(R - \mathrm{ext}_{\underline{\mu}\overline{\nu}} - \mathrm{ext}_{\lambda\sigma})^2} \tag{2.23}$$

where $Q_{\lambda\sigma}$ is the regular Schwarz integral (see Eq. 2.7) and $Z_{\underline{\mu}\overline{\nu}}$ is an approximation to the corresponding transformed integral $(\underline{\mu}\overline{\nu}|\underline{\mu}\overline{\nu})^{\frac{1}{2}}$ (cf. Ref. [39]). The definition for the extents $\mathrm{ext}_{\underline{\mu}\overline{\nu}}$ of the transformed function products is given in section II B of paper **II** while the untransformed extents $\mathrm{ext}_{\lambda\sigma}$ are defined in appendix B of paper **I**.

We applied our new QQR-type estimates within the scaled-opposite spin (SOS) AO-MP2 method, where only the Coulomb term is calculated for which the use of our distance-including screening is essential to achieve linear-scaling. In the SOS-MP2 method the neglect of the exchange-term is approximately compensated by a scaling factor for the Coulomb term

$$E_{SOS-AO-MP2} = -c_{OS} \sum_{\alpha} e_J^{(\alpha)} \tag{2.24}$$

where the factor c_{OS} was determined as 1.3 [45].

We performed extensive benchmark studies on our linear-scaling SOS-AO-MP2 method in paper **II** which showed a consistently good performance of our QQR-type screening procedure. While the errors are comparable to the rigorous Schwarz screening the distance-including QQR-type screening achieves huge speedups for larger systems due to the reduced scaling behavior. Linear-scaling could be demonstrated on timings on DNA systems where the calculation on a very large system with 16 base pairs and more than 1000 atoms / 10000 basis functions could be performed on a single CPU core. Calculations on even larger systems are possible using efficient parallelization techniques. We performed an SOS-AO-MP2 calculation on cutouts of the MutM repair enzyme in complex with DNA where the calculated system comprised 2025 atoms and 20371 basis functions in a 6-31G** basis. Using 20 computing nodes and 160 CPU cores the MP2 contribution for this huge system could be calculated in 8.5 days. All details and benchmark results of our QQR-based SOS-AO-MP2 method are given in paper **II**.

2.2.4 Cholesky-decomposed pseudo-density MP2

The products of atomic orbitals in AO-MP2 are very compact and provide a local description of correlation. But in contrast to the canonical MO formulation Eq. 2.12 where the occupied indices are restricted to the number of electrons in the system and the virtual index corresponds to the unoccupied MOs, in AO-MP2 theory every atomic orbital index runs over all basis functions. This leads to high computational cost when large basis sets are used, i.e., while the cost of the method still scales linearly with system size, the prefactor might be large in these cases.

To combine the advantage of a local non-iterative formulation with a restriction to occupied and virtual indices and therefore good performance for large basis sets, our group developed the Cholesky-decomposed pseudo-densities (CDD-)MP2 method [11]. This approach is similar to the decomposition of the regular density matrix which was studied by Aquilante [46] as an alternative route to localized Hartree-Fock orbitals. Based on the AO-MP2 expression, the Cholesky decomposition of the pseudo-densities Eq. 2.16 provides local functions.

$$\underline{\mathbf{P}} = \underline{\mathbf{L}\mathbf{L}}^T \qquad \overline{\mathbf{P}} = \overline{\mathbf{L}\mathbf{L}}^T \tag{2.25}$$

The columns of the matrices $\underline{\mathbf{L}}$ and $\overline{\mathbf{L}}$ are the coefficients of local pseudo-MOs (LPMOs). Using a Cholesky decomposition algorithm with complete pivoting, the number of LPMOs is exactly equal to the rank of the decomposed pseudo-density (a proof is given in appendix A of paper **III**). The number of occupied/virtual LPMOs is therefore equal to the number of occupied/virtual canonical MOs or in some situations slightly smaller as discussed in appendix A of paper **III**. A visual comparison of the occupied coefficient matrices in MO-MP2, AO-MP2 and CDD-MP2 is given in figure 2.1 for a linear alkane. The occupied canonical MOs

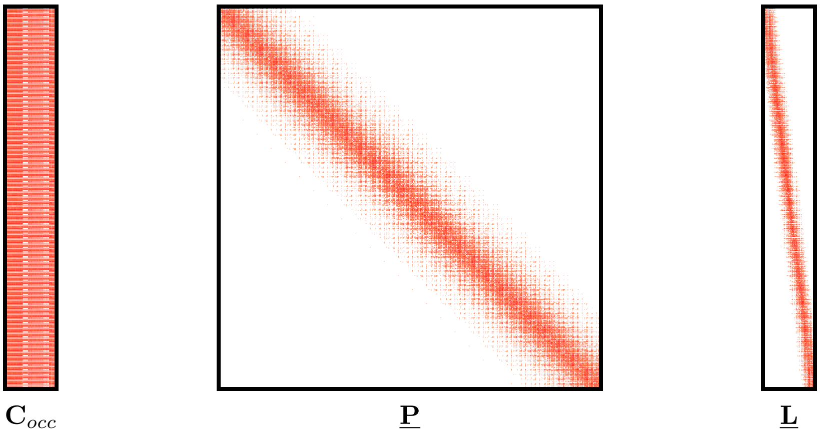

Figure 2.1: Sparsity pattern of the coefficient matrix of occupied canonical MOs $\mathbf{C}_{occ}$, the occupied pseudo-density $\underline{\mathbf{P}}$ and the coefficient matrix of the occupied Cholesky pseudo-MOs $\underline{\mathbf{L}}$ for a linear alkane with 80 carbon atoms. Matrix elements larger than 10^{-6} a.u. are marked as red dots.

are delocalized but their number is restricted to the number of electrons and the pseudo-density in AO-MP2 defines local but redundant functions and their number is equal to the total number of atomic orbitals. The Cholesky pseudo-MOs show good locality and are at the same time restricted to the number of occupied MOs. The same behavior is observed for the virtual functions but the number of virtual orbitals and atomic orbitals is rather similar especially for large basis sets so that the small number of occupied functions is the crucial advantage of the CDD-MP2 method.

The energy expression in CDD-MP2 reads

$$E_{CDD-MP2} = -\sum_{\alpha}\sum_{ij}^{\text{occ}}\sum_{ab}^{\text{virt}}\left[2(\underline{i}\bar{a}|\underline{j}\bar{b}) - (\underline{i}\bar{b}|\underline{j}\bar{a})\right](\underline{i}\bar{a}|\underline{j}\bar{b}). \tag{2.26}$$

Similar to the AO-MP2 case, the transformed charge distributions described by the products of an occupied and a virtual LPMO do not have a net charge as proven in appendix B of paper **III**. In the multipole expansion of the integrals $(\underline{i}\bar{a}|\underline{j}\bar{b})$, both the monopole-monopole and the two monopole-dipole terms vanish and the asymptotic decay of the integral value with increasing bra-ket separation is $1/R^3$ (see the discussion in paper **II**). The integral products of the Coulomb-type term therefore decay as $1/R^6$ which gives a strong coupling between the functions of bra and ket. To fully exploit the coupling, QQR-type estimates of the form

$$(\underline{i}\bar{a}|\underline{j}\bar{b}) \approx \frac{Z_{\underline{i}\bar{a}}Z_{\underline{j}\bar{b}}}{(R_{\underline{i}\bar{a},\underline{j}\bar{b}} - \text{ext}_{\underline{i}\bar{a}} - \text{ext}_{\underline{j}\bar{b}})^3} \tag{2.27}$$

are used where the definitions of centers and extents are found in appendix C of paper **III**. An efficient calculation of the of the four-fold transformed integrals $(\underline{i}\overline{a}|\underline{j}\overline{b})$ is possible using the RI approximation Eq. 2.14 which leads to an asymptotic cubic-scaling cost with system size.

In paper **III**, we present for the first time results of a full RI-CDD-MP2 implementation. Key features of the new implementation, that was developed in this work, are the use of efficient sparse matrix multiplications in the transformation steps of the RI integrals and the application of our new and tight QQR-type estimates in the screening procedure. Our method shows small and well-controlled errors, has a very small prefactor and an early crossover with the conventional RI-MP2 method. For DNA systems, RI-CDD-MP2 is faster than RI-MP2 for systems with two or more DNA base pairs and significant speedups are observed for systems larger than 200 atoms. For a fixed molecular size, the increase in calculation time when going from a smaller to a larger basis set is the same in RI-CDD-MP2 and conventional RI-MP2 so that similar speedups are observed for small and large basis sets. Using our RI-CDD-MP2 method, calculations on systems with more than 5000 basis functions can be performed on a single CPU core and parallelization extends the accessible system size to more than 1000 atoms / 16 DNA base pairs in a double-zeta basis or more than 500 atoms / 8 DNA base pairs in a triple-zeta basis on one computing node with multiple cores.

We also explored the use of local restrictions on the auxiliary RI basis along the lines of Werner et al. [35]. In principle, this approach allows to reduce the total scaling behavior of our method to linear but the benchmark calculations on linear alkanes presented in paper **III** show that the crossover to the method with full auxiliary basis is rather late for systems with roughly 80 carbon atoms. Therefore, the regular cubic scaling RI-CDD-MP2 method with full auxiliary basis is preferable for any realistic calculation at this stage of development.

The success of the cubic-scaling RI-CDD-MP2 approach is encouraging. Based on the present work two possible further improvements are currently under investigation in our group: Instead of discarding small integrals with large bra-ket separation, cheap dipole approximations might be used instead, similar to the approach of Riplinger et al. [47]. With this approach it might be possible to achieve the same accuracy with less tight screening thresholds and therefore at smaller costs. Furthermore, when less integrals with large separation are treated explicitly, this reduces the auxiliary space in the local fitting approach significantly so that it might allow calculations with reduced scaling on realistic systems. The second project, which was started as part of this thesis, attempts further localization of the LPMOs using a trust region minimization algorithm [31, 32] that is able to provide both local occupied and virtual functions. Based on the results of Aquilante et al. [46] in the context of Hartree-Fock orbitals, it can be assumed that the localization of Cholesky LPMOs is still suboptimal. The localization procedure for LPMOs is more difficult than for the regular MOs as the LPMOs are non-orthogonal. Using a generalization of the existing theory, more local LPMOs might be obtained which would reduce the number of significant energy contributions and further speed up RI-CDD-MP2 calculations.

2.2.5 Cubic-scaling scaled opposite-spin MP2

While AO-MP2 and RI-CDD-MP2 provide very efficient ways to calculate the MP2 energy for large systems, their efficient implementation requires rather complicated code for the screening procedure and bookkeeping. Furthermore, the most economical implementations of these methods usually requires to store transformed integrals on disk so that costly integral evaluations do not have to be repeated. In the following, we will present a novel method which allows to calculate the scaled opposite-spin MP2 energy with asymptotically cubic scaling cost that does not require complicated screening procedures and can be implemented in a way that all transformation steps are performed only once while all data can be kept in main memory and no I/O is necessary.

The new method is based on the efficient SOS-RI-MP2 implementation of Jung et al. [48] which has a fourth-order scaling. Our method uses an atomic orbital-based formulation in combination with efficient transformations using sparse-matrix multiplications (as in RI-CDD-MP2) and allows to reduce the scaling behavior of the computational cost to a cubic increase with system size. It should be noted, that there exists another cubic scaling variant of SOS-RI-MP2 developed by Jung et al. [49,50] but it is based on a local fitting metric in the RI approximation to restrict the number of significant three-center integrals. No such restriction is necessary in our approach. Furthermore, in contrast to the existing approach, our method does not require I/O operations, essentially no bookkeeping, and is particularly suited for calculations using graphics processing units (GPUs) as discussed below.

We start from the RI-AO-MP2 expression for the Coulomb term

$$E^{OS}_{RI-AO-MP2} = -\sum_{\alpha} \sum_{\substack{\mu\nu\lambda\sigma \\ \mu'\nu'\lambda'\sigma'}} \sum_{PQRS} \underline{P}_{\mu\mu'} \overline{P}_{\nu\nu'} \underline{P}_{\sigma\sigma'} \overline{P}_{\lambda\lambda'} \\ (\mu\nu|P) \left[\mathbf{J}^{-1}\right]_{PQ} (Q|\lambda\sigma)(\mu'\nu'|R) \left[\mathbf{J}^{-1}\right]_{RS} (S|\lambda'\sigma') \tag{2.28}$$

which can be compactly expressed as

$$E^{OS}_{RI-AO-MP2} = -\sum_{\alpha} \sum_{PQ} \tilde{Y}_{PQ} \tilde{Y}_{QP} \tag{2.29}$$

with

$$\tilde{\mathbf{Y}} = \mathbf{Y}\mathbf{J}^{-1} \tag{2.30}$$

and

$$\begin{aligned} Y_{PQ} &= \sum_{\mu\nu\mu'\nu'} (P|\mu'\nu')\underline{P}_{\mu\mu'}\overline{P}_{\nu\nu'}(\mu\nu|Q) \\ &= \sum_{\mu\nu}(P|\underline{\mu}\overline{\nu})(\mu\nu|Q) \end{aligned} \tag{2.31}$$

An efficient algorithm might therefore include the following steps:

(1)	Calculation of $\mathbf{J}^{-1}$	$\mathcal{O}(\mathrm{N}^3)$
(2)	Calculation of pseudo-densities	$\mathcal{O}(\mathrm{N}^3)$
(3)	Calculation of $(P|\mu\nu)$	$\mathcal{O}(\mathrm{N}^2)$
(4)	Transformation to $(P|\underline{\mu}\overline{\nu})$	$\mathcal{O}(\mathrm{N}^2)$
(5)	Contraction $\sum_{\mu\nu}(P|\underline{\mu}\overline{\nu})(\mu\nu|Q)$	$\mathcal{O}(\mathrm{N}^3)$
(6)	Multiplication $\mathbf{Y}\mathbf{J}^{-1}$	$\mathcal{O}(\mathrm{N}^3)$
(7)	Contraction $\sum_{PQ}\tilde{Y}_{PQ}\tilde{Y}_{QP}$	$\mathcal{O}(\mathrm{N}^2)$

The final quadratic step has negligible cost. Steps (1), (2), and (6) can be performed using very efficient and well-parallelized BLAS routines which make these steps extremely efficient even for very large systems. In principle, step (3) has to be performed only once as the integrals might be reused for every Laplace point. To completely eliminate I/O operations, this quadratic step can be repeated for every Laplace point as the prefactor is rather small. The time determining steps are the transformation of the three-center integrals (4) and the contraction step (5). Step (4) can be performed using efficient BCSR sparse matrix multiplications as in the RI-CDD-MP2 method which leads to an asymptotically quadratic scaling. Step (5) has an asymptotic cubic scaling, but efficient BLAS routines for the calculation of the dot product are available. In our CPU based pilot implementation, step (4) and (5) show roughly the same cost for a linear alkane model system with 40 carbon atoms.

An I/O free implementation can be realized by performing steps (3), (4), and (5) in batches of P. For each batch of this auxiliary index, all three-center integrals can be kept in memory. The transformation is performed in memory and in step (5) the untransformed integrals are calculated on-the-fly and directly contracted so that all operations can be performed without any hard disk access.

The expensive contraction step (5) is also particularly suited for calculations on GPUs. For a fixed index P, the contraction with the three-center integrals $(\mu\nu|Q)$ is similar to the formation of the Coulomb matrix in Hartree-Fock theory for which extremely efficient code has been developed in our group [51]. A very efficient implementation of our SOS-RI-MP2 method might therefore be realized using GPUs for step (5). In this case, only quadratic steps or cubic steps with very small prefactor have to be evaluated on CPU and no I/O operations limit the efficiency of parallelization. A GPU-based implementation is under development in our group.

2.3 Symmetry-adapted perturbation theory

2.3.1 Basic theory

In this section, the basic concept of symmetry-adapted perturbation theory is reviewed along the lines of Ref. [52]. A more detailed discussion can be found in recent reviews [52, 53].

Symmetry-adapted perturbation theory (SAPT) is the name of a class of methods which try to describe the interaction energy between two monomers using a perturbative expansion while enforcing a solution with the correct antisymmetry (consistent with the Pauli exclusion principle). The SAPT method is a very elegant way to obtain interaction energies because the SAPT energy contributions can be interpreted as the classical interaction contributions, i.e., the electrostatic interaction, induction and dispersion as well as additional exchange effects. The direct calculation of the interaction energy in SAPT is conceptually very different from the conventional supermolecular approach where the interaction energy is calculated as the difference of the total energy of the interacting complex and the two independent calculations of the monomers. As the interaction energy is several orders of magnitude smaller than the total energy of the system, the calculation as a difference of total energies is a disadvantage both in terms of accuracy and also computational efficiency as much of the work is spent on terms that ultimately cancel. The direct calculation in SAPT therefore offers an efficient and chemically interpretable way to study interacting sytems.

While there are in principle several ways to derive a symmetry-adapted pertubation theory (see Ref. [53] for an overview) the results at the lowest orders are very similar for the different methods [52]. Therefore, SAPT nowadays usually refers to the simplest approach, the symmetrized Rayleigh-Schrödinger (SRS) method. The SRS theory is based on a separation of the Hamiltonian of the interacting system

$$\hat{H} = \hat{H}^A + \hat{H}^B + \hat{H}^{AB} \tag{2.32}$$

into operators that act solely on particles of monomer A ($\hat{H}^A$) or B ($\hat{H}^B$) and the remaining terms that are interaction operators ($\hat{H}^{AB}$). Provided that independent solutions for the monomers A and B are known, the interacting system can be described with a perturbation expansion using the interaction operators as perturbation. To account for the Pauli exclusion principle, the solutions are then antisymmetrized by constructing all possible intermonomer permutations and adding them up with appropriate sign. The interaction energies are then calculated based on the antisymmetrized perturbed wave-function.

As the exact solutions for the monomers are in general unknown, a double perturbation expansion based on the Hartree-Fock solutions can be used. The intramonomer correlation is described in analogy to the Møller-Plesset theory (cf. section 2.2.1) with a pertubative correction on the Hartree-Fock hamiltonian, e.g., $\hat{H}^A = \hat{H}_0^A + \hat{W}^A$ while the second perturbation is the intermolecular interaction operator $\hat{H}^{AB}$. The exact hamiltonian of the interacting system is therefore expanded as

$$\hat{H} = (\hat{H}_0^A + \hat{H}_0^B) + \lambda_1(\hat{W}^A + \hat{W}^B) + \lambda_2\hat{H}^{AB} \tag{2.33}$$

and a hierarchy of SAPT methods is available based on the expansion order in the intramonomer and intermonomer perturbations. Szalewicz [52] discusses high accuracy of SAPT comparable to the very accurate coupled-cluster singles and double with perturbative triples (CCSD(T)) method when SAPT terms up to second-order in the intermonomer potential are included and some terms in the intramonomer perturbation are summed to infinite order. The resulting SAPT method shows the same $\mathcal{O}(\mathrm{N}^7)$ scaling with system size as CCSD(T). If the intramonomer perturbation is neglected (zeroth-order SAPT, SAPT0), the accuracy is roughly comparable to MP2 and both methods share a $\mathcal{O}(\mathrm{N}^5)$ scaling in the conventional formulation.

Besides the Møller-Plesset-type treatment of intramonomer correlation, SAPT methods based on a DFT description of the monomers were also developed. The two available methods SAPT(DFT) [54] and DFT-SAPT [55, 56] are slightly different but provide very similar results [52].

2.3.2 Recent developments

In the last decade, efficient RI-based implementations of SAPT contributions have been developed [57–59] where most of the development focuses on DFT-based SAPT. An atomic-orbital based formulation of the electrostatic and induction energies together with the corresponding exchange-terms has been derived by Hesselmann et al. [57].

The most accurate SAPT calculations are possible using a coupled-cluster description of the monomers as derived by Korona and Jeziorski [60–62]. To reduce the basis set requirements, Řezáč and Hobza [63] proposed a scaling of the dispersion term and its exchange counterpart in DFT-SAPT which allows to obtain good results already with an augmented double-zeta basis.

2.3.3 Linear- and sublinear-scaling SAPT

The first linear-scaling implementation of the non-dispersive terms was developed by Beer [12] using methods from linear-scaling Hartree-Fock and coupled-perturbed self-consistent-field theory (CPSCF) based on the AO formulation of Hesselmann [57]. An AO-based approach for the dispersion term was developed by Lambrecht [64] based on the closely connected AO-MP2 expression.

In this work, the AO expression of the dispersion term was reimplemented using our efficient QQR-type screening. It is combined with the most recent developments of the non-dispersive terms of Beer that use our efficient density matrix-based Laplace-transformed (DL-)CPSCF method [65]. A novel SAPT0 method is proposed in paper **IV** that combines these linear-scaling formulations in an approach similar to scaled opposite-spin MP2 [48] where the exchange-dispersion SAPT term is neglected and the dispersion term is scaled appropriately. The scaling parameter was optimized for the S22 set [66]. It was found that the best fit can be obtained using a modest 6-31G** basis where the neglect of the exchange-dispersion term and the basis set incompleteness error lead to rather balanced total errors for hydrogen-bonded and dispersion bound systems which can be efficiently cured using a single scaling parameter. The good performance of our new scaled dispersion (sd-)SAPT0 method in combination with the 6-31G** basis was confirmed in extensive benchmark calculations where the accuracy was roughly comparable to supermolecular RI-MP2 calculations in the much larger cc-pVTZ basis.

Due to the limited range of the interaction forces, significant contributions are mainly associated with those parts of one monomer which are close to the second molecule. Our AO-SAPT approach provides a local description of the interaction components and allows to exploit this local effect of interaction forces. When one of the interacting monomers is extended in a region far away from the second monomer, the calculation time for the SAPT terms increases sublinearly with the size of the monomer. This feature is demonstrated in timings on cellulose fragments in paper **IV**. It should be noted that the underlying Hartree-Fock calculations of the monomers still scale linearly with system size but the expensive SAPT calculation shows a sublinear scaling. For systems where the contact surface increases with system size, like DNA double strands, linear-scaling is observed. One particularly suited example of the application of our new sd-SAPT0 method is the interaction of an enzyme with a molecule in its active pocket. With our new method, a calculation of a 12 $\AA$ cutout of the MutM repair enzyme with 1100 atoms interacting with a DNA lesion was performed on a single CPU core.

Chapter 3

Conclusion and outlook

In this work, we introduced the distance-dependent QQR estimates for electron repulsion integrals. These estimates allow for an efficient preselection of significant integrals in quantum-chemical methods and successful applications in Hartree-Fock, MP2, and SAPT theory have been demonstrated in this work.

In Hartree-Fock theory, the number of exchange integrals that have to be evaluated in the calculation of the Fock matrix can be reduced by a factor of up to 2 using QQR-based screening compared to calculations with the conventional Schwarz screening at the same accuracy. While the predecessor of the QQR approach, the MBIE estimates, were also studied in the Hartree-Fock context, it was shown that the QQR estimates are preferable in terms of performance and better suited for adaptation to correlation methods.

The use of QQR-based screening in our SOS-AO-MP2 method yields an efficient linear-scaling method for the calculation of correlation energies of very large systems. Extensive benchmark calculations were performed that demonstrate the reliable accuracy of our approach and timings for systems with up to 1000 atoms calculated on a single CPU core have been presented. Using parallelization, the range of applicability of our SOS-AO-MP2 method is further extended. Calculations on systems with more than 2000 atoms and 20000 basis functions are feasible as demonstrated on a large cutout of an enzyme-DNA complex which makes our SOS-AO-MP2 method a useful tool for studying large biochemical systems. Our method is furthermore particularly suited to study the convergence of the correlation contribution with increasing size of the cutout in layered models like the combined quantum-mechanics/molecular-mechanics (QM/MM) approach as it reaches far beyond the system sizes commonly selected for the quantum-chemical treatment in these models.

An efficient MP2 method for larger basis sets was developed based on our RI-CDD-MP2 approach which provides an expression of the MP2 energy in the basis of local pseudo-MOs obtained from a Cholesky decomposition. The introduction of QQR-type screening into the RI-CDD-MP2 method in combination with efficient sparse matrix algebra for the integral transformations lead to a small prefactor and an early crossover with conventional RI-MP2. Despite an asymptotic cubic scaling, the range of accesible system sizes is significantly increased and systems with more than 500 atoms in a triple-zeta basis can be calculated using parallelization on one computing node with multiple cores. Further improvements of the RI-CDD-MP2 method using dipole approximations for integrals with large separation and novel localization techniques for the local pseudo-MOs are currently explored in our group. Besides the RI-CDD-MP2 method, another efficient cubic scaling MP2 approach restricted to scaled opposite-spin MP2 has been presented in section 2.2.5. It is designed for evaluation on GPUs and can be implemented without any I/O operation. An efficient implementation is currently developed in our group.

For the direct calculation of interaction energies in large molecular systems, the sd-SAPT0 method was developed which uses an efficient scaling of the dispersion term that compensates the neglect of the exchange-dispersion contribution and at the same time cures the basis set incompleteness error to a large extent. The sd-SAPT0 energies in a modest 6-31G** basis set are found to provide results roughly comparable to much more expensive MP2 calculations in a triple-zeta basis. In our sd-SAPT0 method, the expensive dispersion term is efficiently evaluated using an atomic orbital-based formulation with a QQR-based screening procedure while the remaining non-dispersive terms are calculated using the efficient AO-based implementation developed previously in our group which employs linear-scaling techniques from Hartree-Fock and coupled-perturbed self-consistent field theory. Due to the efficient screening procedures in our method, the computational cost of our sd-SAPT0 implementation is hardly affected by molecular parts which are too far away from the contact surface to contribute to the interaction energy. Our method is therefore particularly suited for systems like the important case of an enzyme interacting with a molecule in its active pocket. The efficiency of our method was demonstrated for an enzyme cutout with more than 1000 atoms where the interaction with a DNA lesion in the active site was calculated in the 6-31G** basis on a single CPU core. While our sd-SAPT0 method is already a powerful tool for studies of large systems, future developments might include the implementation of sd-SAPT0 into a QM/MM scheme that would further reduce the computational cost and might enable to routinely perform calculations of molecules interacting with enzymes that are converged with the size of the QM region.

Bibliography

[1] R. G. Parr and W. Yang, *Density-Functional Theory of Atoms and Molecules*, Oxford University Press, New York, 1994.

[2] D. Flaig, M. Beer, and C. Ochsenfeld, *J. Chem. Theory Comput.* **8**, 2260 (2012).

[3] S. Grimme, *WIREs Comput. Mol. Sci.* **1**, 211 (2011).

[4] A. Szabo and N. Ostlund, *Modern Quantum Chemistry: Introduction to Advanced Electronic Structure Theory*, Dover Books on Chemistry Series, Dover Publications, 1996.

[5] T. Helgaker, P. Jørgensen, and J. Olsen, *Molecular electronic-structure theory*, Wiley-VCH, Weinheim, 2000.

[6] D. Cremer, *WIREs Comput. Mol. Sci.* **1**, 509 (2011).

[7] J. L. Whitten, *J. Chem. Phys.* **58**, 4496 (1973).

[8] D. S. Lambrecht and C. Ochsenfeld, *J. Chem. Phys.* **123**, 184101 (2005).

[9] D. S. Lambrecht and C. Ochsenfeld, *J. Chem. Phys.* **136**, 149901 (2012).

[10] B. Doser, D. S. Lambrecht, J. Kussmann, and C. Ochsenfeld, *J. Chem. Phys.* **130**, 064107 (2009).

[11] J. Zienau, L. Clin, B. Doser, and C. Ochsenfeld, *J. Chem. Phys.* **130**, 204112 (2009).

[12] M. Beer, *Effiziente 'ab-initio' Berechnung molekularer Eigenschaften großer Systeme*, PhD thesis, Ochsenfeld group, University of Munich (LMU), 2011.

[13] A. D. Becke, *J. Chem. Phys.* **98**, 5648 (1993).

[14] P. J. Stephens, F. J. Devlin, C. F. Chabalowski, and M. J. Frisch, *J. Phys. Chem.* **98**, 11623 (1994).

[15] C. Ochsenfeld and M. Head-Gordon, *Chem. Phys. Lett.* **270**, 399 (1997).

[16] P. E. Maslen, C. Ochsenfeld, C. A. White, M. S. Lee, and M. Head-Gordon, *J. Phys. Chem. A* **102**, 2215 (1998).

[17] E. Schwegler, M. Challacombe, and M. Head-Gordon, *J. Chem. Phys.* **106**, 9708 (1997).

[18] C. Ochsenfeld, C. A. White, and M. Head-Gordon, *J. Chem. Phys.* **109**, 1663 (1998).

[19] C. Ochsenfeld, *Chem. Phys. Lett.* **327**, 216 (2000).

[20] C. A. White, B. G. Johnson, P. M. W. Gill, and M. Head-Gordon, *Chem. Phys. Lett.* **230**, 8 (1994).

[21] C. A. White, B. G. Johnson, P. M. W. Gill, and M. Head-Gordon, *Chem. Phys. Lett.* **253**, 268 (1996).

[22] E. Rudberg and E. H. Rubensson, *J. Phys.: Condens. Matter* **23**, 075502 (2011).

[23] S. Grimme, *J. Chem. Phys.* **124**, 034108 (2006).

[24] M. Feyereisen, G. Fitzgerald, and A. Komornicki, *Chem. Phys. Lett.* **208**, 359 (1993).

[25] T. B. Pedersen, F. Aquilante, and R. Lindh, *Theoretical Chemistry Accounts* **124**, 1 (2009).

[26] H. Koch, A. Sánchez de Merás, and T. B. Pedersen, *J. Chem. Phys.* **118**, 9481 (2003).

[27] J. Boström, M. Pitoňák, F. Aquilante, P. Neogrády, T. B. Pedersen, and R. Lindh, *J. Chem. Theory Comput.* , 120501091244000 (2012).

[28] P. Pulay, *Chem. Phys. Lett.* **100**, 151 (1983).

[29] P. Pulay and S. Saebø, *Theor. Chim. Acta* **69**, 357 (1986).

[30] J. E. Subotnik, A. D. Dutoi, and M. Head-Gordon, *J. Chem. Phys.* **123**, 114108 (2005).

[31] B. Jansík, S. Høst, K. Kristensen, and P. Jørgensen, *J. Chem. Phys.* **134**, 194104 (2011).

[32] I.-M. Høyvik, B. Jansik, and P. Jørgensen, *J. Chem. Theory Comput.* **8**, 3137 (2012).

[33] G. Hetzer, M. Schütz, H. Stoll, and H.-J. Werner, *J. Chem. Phys.* **113**, 9443 (2000).

[34] S. Saebø and P. Pulay, *J. Chem. Phys.* **115**, 3975 (2001).

[35] H.-J. Werner, F. R. Manby, and P. J. Knowles, *J. Chem. Phys.* **118**, 8149 (2003).

[36] T. B. Adler, H.-J. Werner, and F. R. Manby, *J. Chem. Phys.* **130**, 054106 (2009).

[37] J. Almlöf, *Chem. Phys. Lett.* **181**, 319 (1991).

[38] M. Häser and J. Almlöf, *J. Chem. Phys.* **96**, 489 (1992).

[39] M. Häser, *Theoret. Chim. Acta* **87**, 147 (1993).

[40] P. Y. Ayala and G. E. Scuseria, *J. Chem. Phys.* **110**, 3660 (1999).

[41] M. Kobayashi, T. Akama, and H. Nakai, *J. Chem. Phys.* **125**, 204106 (2006).

[42] D. G. Fedorov and K. Kitaura, *J. Chem. Phys.* **121**, 2483 (2004).

[43] Y. Mochizuki, K. Yamashita, T. Murase, T. Nakano, K. Fukuzawa, K. Takematsu, H. Watanabe, and S. Tanaka, *Chem. Phys. Lett.* **457**, 396 (2008).

[44] K. Kristensen, I.-M. Høyvik, B. Jansík, P. Jørgensen, T. Kjærgaard, S. Reine, and J. Jakowski, *Phys. Chem. Chem. Phys.* **14**, 15706 (2012).

[45] Y. Jung, R. C. Lochan, A. D. Dutoi, and M. Head-Gordon, *J. Chem. Phys.* **121**, 9793 (2004).

[46] F. Aquilante, T. B. Pedersen, A. Sánchez de Merás, and H. Koch, *J. Chem. Phys.* **125**, 174101 (2006).

[47] C. Riplinger and F. Neese, *J. Chem. Phys.* **138**, 034106 (2013).

[48] Y. Jung, R. C. Lochan, A. D. Dutoi, and M. Head-Gordon, *J. Chem. Phys.* **121**, 9793 (2004).

[49] Y. Jung and M. Head-Gordon, *Phys. Chem. Chem. Phys.* **8**, 2831 (2006).

[50] Y. Jung, Y. Shao, and M. Head-Gordon, *J. Comput. Chem.* **28**, 1953 (2007).

[51] J. Kussmann and C. Ochsenfeld, *J. Chem. Phys.* **138**, 134114 (2013).

[52] K. Szalewicz, *WIREs Comput. Mol. Sci.* **2**, 254 (2012).

[53] K. Szalewicz, K. Patkowski, and B. Jeziorski, *Struct. Bond.* **116**, 43 (2005).

[54] H. L. Williams and C. F. Chabalowski, *J. Phys. Chem. A* **105**, 646 (2001).

[55] G. Jansen and A. Hesselmann, *J. Phys. Chem. A* **105**, 11156 (2001).

[56] A. Hesselmann and G. Jansen, *Chem. Phys. Lett.* **357**, 464 (2002).

[57] A. Hesselmann, G. Jansen, and M. Schütz, *J. Chem. Phys.* **122**, 014103 (2005).

[58] R. Podeszwa, R. Bukowski, and K. Szalewicz, *J. Chem. Theory Comput.* **2**, 400 (2006).

[59] E. G. Hohenstein, R. M. Parrish, C. D. Sherrill, J. M. Turney, and H. F. Schaefer, *J. Chem. Phys.* **135**, 174107 (2011).

[60] T. Korona and B. Jeziorski, *J. Chem. Phys.* **128**, 144107 (2008).

[61] T. Korona, *J. Chem. Phys.* **128**, 224104 (2008).

[62] T. Korona, *J. Chem. Theory Comput.* **5**, 2663 (2009).

[63] J. Řezáč and P. Hobza, *J. Chem. Theory Comput.* **7**, 685 (2011).

[64] D. Lambrecht, *Development of rigorous and efficient integral bounds and strategies for the linear-scaling quantum chemical calculation of large molecules*, PhD thesis, Ochsenfeld group, University of Tübingen, 2011.

[65] M. Beer and C. Ochsenfeld, *J. Chem. Phys.* **128**, 221102 (2008).

[66] P. Jurecka, J. Sponer, J. Cerný, and P. Hobza, *Phys. Chem. Chem. Phys.* **8**, 1985 (2006).

Chapter 5

Publications

5.1 Paper I: ”Distance-dependent Schwarz-based integral estimates for two-electron integrals: Reliable tightness vs. rigorous upper bounds”, S. A. Maurer, D. S. Lambrecht, D. Flaig, C. Ochsenfeld, *J. Chem. Phys.*, 136, 144107 (2012)

THE JOURNAL OF CHEMICAL PHYSICS **136**, 144107 (2012)

Distance-dependent Schwarz-based integral estimates for two-electron integrals: Reliable tightness vs. rigorous upper bounds

Simon A. Maurer, Daniel S. Lambrecht,[a] Denis Flaig, and Christian Ochsenfeld[b]
Chair of Theoretical Chemistry, Department of Chemistry, University of Munich (LMU), Butenandtstr. 7, D-81377 München, Germany

(Received 19 September 2011; accepted 20 February 2012; published online 11 April 2012)

A new integral estimate for four-center two-electron integrals is introduced that accounts for distance information between the bra- and ket-charge distributions describing the two electrons. The screening is denoted as QQR and combines the most important features of the conventional Schwarz screening by Häser and Ahlrichs published in 1989 [J. Comput. Chem. **10**, 104 (1989)] and our multipole-based integral estimates (MBIE) introduced in 2005 [D. S. Lambrecht and C. Ochsenfeld, J. Chem. Phys. **123**, 184101 (2005)]. At the same time the estimates are not only tighter but also much easier to implement, so that we recommend them instead of our MBIE bounds introduced first for accounting for charge-distance information. The inclusion of distance dependence between charge distributions is not only useful at the SCF level but is particularly important for describing electron-correlation effects, e.g., within AO-MP2 theory, where the decay behavior is at least $1/R^4$ or even $1/R^6$. In our present work, we focus on studying the efficiency of our QQR estimates within SCF theory and demonstrate the performance for a benchmark set of 44 medium to large molecules, where savings of up to a factor of 2 for exchange integrals are observed for larger systems. Based on the results of the benchmark set we show that reliable tightness of integral estimates is more important for the screening performance than rigorous upper bound properties. © *2012 American Institute of Physics*. [http://dx.doi.org/10.1063/1.3693908]

I. INTRODUCTION

Discarding negligible contributions in quantum-chemical calculations that are zero or very close to zero is of central importance for efficient calculations. In this respect, one of the key quantities in many quantum-chemical methods are the four-center two-electron integrals either in their untransformed form such as in Hartree-Fock (HF) (Ref. 1) or density-functional theory (DFT) (Ref. 2) methods or in their transformed form in wavefunction-based electron-correlation methods.[3]

For several decades it has been known that many of the formally M^4 scaling number of four-center two-electron integrals arising in self-consistent field (SCF) calculations are negligibly small, so that the number of numerically significant integrals reduces asymptotically to $\mathcal{O}(M^2)$. Therefore, there have been several attempts to estimate the integral values with the aim of discarding small contributions: In the early stages, employed integral estimates were either upper bounds restricted to a specific class of integrals[4] or approximations without bound properties.[5,6] Already in 1973, Whitten[7] applied the Schwarz inequality in formulating a rigorous upper bound to two-electron integrals. A breakthrough was the introduction of Schwarz estimates into direct SCF algorithms by Häser and Ahlrichs in 1989.[8] The Schwarz estimates account for the exponential coupling of the commonly used Gaussian-type basis functions and they are, at the same time, upper bounds applicable to all angular momenta with estimates that are closer to the true integral value than previous attempts.[8] While some extensions have been proposed,[9] the original Schwarz bound is still the standard scheme for estimating integrals in quantum chemistry allowing to reduce the asymptotic scaling of the two-electron integrals to $\mathcal{O}(M^2)$.

The computational effort can be further reduced by so-called linear-scaling methods where a multitude of approaches has been developed over the last decades (see, e.g., Refs. 10–16). In our present work, we will not focus on linear-scaling methods themselves, but instead on screening integrals as necessary in most quantum-chemical approaches. Nevertheless, we perform also in our present work the screening tests within the most efficient methods available to us: We employ the continuous fast multipole method (CFMM) approach[10,17] for the Coulomb part and the LinK method[14,18] for the HF exchange. They allow to achieve linear scaling in evaluating the Fock matrix for systems with a nonvanishing HOMO-LUMO gap. In combination with linear-scaling numerical integration for the exchange-correlation part in DFT or hybrid DFT approaches,[19,20] SCF calculations for molecules with more than 1000 atoms are nowadays accessible on simple workstation computers (see, e.g., Refs. 16 and 21) and even molecular property calculations are possible for such large molecular systems (e.g., Refs. 22 and 23) by employing related techniques in density-matrix-based reformulations of response theory.[24–26]

While Schwarz estimates successfully exploit the locality of the atomic orbitals in forming the charge distributions, they do not account for the distance dependence between the

---

[a] Present address: Department of Chemistry, University of California, Berkeley, California 94720, USA.
[b] Electronic mail: christian.ochsenfeld@uni-muenchen.de.

This article is copyrighted as indicated in the article. Reuse of AIP content is subject to the terms at: http://scitation.aip.org/termsconditions. Downloaded to IP: 92.230.182.222 On: Sat, 14 Dec 2013 21:59:43

"bra" and "ket" part of the two-electron integral, which arises due to the $1/r_{12}$ operator. A first remedy to this issue was introduced by means of multipole-based integral estimates (MBIE) by Lambrecht and Ochsenfeld in 2005.[27] Distance-dependent integral estimates do not only lead to speedups for SCF theories but are particularly important for electron-correlation theories such as, e.g., Laplace-based AO-MP2 theory[28–33] where the $1/R$ coupling of charge distributions turns into a $1/R^4$ or even $1/R^6$ decay, so that the conventional $\mathcal{O}(\mathrm{M}^5)$ scaling of the computational effort for MO-MP2 theory can be reduced for AO-MP2 to linear.[33] In this way, AO-MP2 calculations for DNA and RNA systems with more than 1000 atoms and more than 10 000 basis functions became possible.[34,35]

While MBIE[27] focuses on a correct description of the bra-ket separation, it tends to overestimate the magnitude of the bra and ket charge distributions, due to the use of absolute multipoles. In our present work, we introduce a new integral estimate that combines the favorable features of (1) a decent estimate of the magnitude of the charge distributions, (2) the $1/R$ distance coupling of charge distributions, and (3) technical simplicity of the estimate (which is much simpler to implement than our previously advocated MBIE theory).

The only seeming drawback of our new estimates denoted as QQR screening is at first sight their empiricism by the loss of being a rigorous upper bound to the four-center two-electron integrals. However, we will show that (reliable) tightness of an integral estimate is more important than a true upper bound. We will demonstrate that our new QQR screening significantly reduces the number of estimated exchange integrals, while the tightness of the error distribution as compared to both the original Schwarz estimates and MBIE is significantly improved. The performance of our new QQR screening is compared to the one of Schwarz and MBIE screening: Beside tests for the well-known S22 set[36] consisting of small interacting molecules, we present benchmark calculations on a set of 44 medium to large systems with up to 1707 atoms that cover covalent, ionic, radical, and delocalized systems as an extensive test for the screening performance. Based on our new benchmark set,[37] a general procedure to assess integral screening methods is described and we advocate the use of this test set for performance assessment of reduced-scaling approaches.

II. THEORY

The screening we propose here is inspired by the multipole-based integral estimates that were first published by Lambrecht and Ochsenfeld in 2005.[27] A revised version of these estimates is derived in Appendix A as they are connected to our new empirical estimates introduced in the present work. According to the new MBIE derivation (we focus on MBIE-0, where just absolute multipole integrals up to zeroth order are included and which is always denoted as MBIE in the following), the two-electron integrals are rigorously bound by

$$|(\mu\nu \mid \lambda\sigma)| \leq \frac{\mathcal{M}'^{(0)}_{\mu\nu}\mathcal{M}'^{(0)}_{\lambda\sigma}}{R - \mathrm{ext}_{\mu\nu} - \mathrm{ext}_{\lambda\sigma}}, \qquad (1)$$

if the absolute multipole integrals $\mathcal{M}'^{(0)}_{\mu\nu}$ and $\mathcal{M}'^{(0)}_{\lambda\sigma}$ are calculated according to Eq. (A16) and the extents $\mathrm{ext}_{\mu\nu}$ and $\mathrm{ext}_{\lambda\sigma}$ satisfy inequality (A17). The bra-ket distance R needs to be larger than the sum of $\mathrm{ext}_{\mu\nu}$ and $\mathrm{ext}_{\lambda\sigma}$ and the bra and ket charge distributions are required to be well separated in order to justify the validity of the multipole expansion. As well-separatedness criterion we require the distance R to be larger than the sum of the well-separatedness extents known from CFMM theory[10] in order to allow for the applicability of Eq. (1). Integrals with bra and ket charge distributions that are well separated in this sense will be referred to as far-field integrals in the following, while the remaining ones are subsumed as near-field integrals. Explicit definitions of the centers and well-separatedness extents for contracted basis functions are given in Appendix B.

In MBIE theory, the absolute multipole integrals characterize the dependence of the integral value on the properties of the bra and ket charge distribution, respectively, similar to what the Schwarz two-center integrals describe within the Schwarz bounds. Here, the two-center integrals $(\mu\nu|\mu\nu)^{1/2}$ are an excellent measure for the dependence of the two-electron integrals on the bra (or ket) charge distribution, while, in contrast, the need to use absolute multipole integrals within MBIE automatically leads to an overestimation of all integrals.

In our present work, we combine the positive features of Schwarz and MBIE estimates leading to estimates that we denote as QQR, where we use Schwarz integrals to describe the exponential coupling between function pairs within bra and ket in combination with the $1/R$ dependence on the bra-ket separation derived from MBIE theory. There are two similar viewpoints that both lead to the QQR working equation: One could either start with the MBIE equation (1) and formally substitute the absolute multipole integrals by the Schwarz integrals or alternatively start with the common Schwarz bound and introduce the $1/R$ factor from MBIE theory. Following the first viewpoint, the question arises whether there is a direct relation between the values of the absolute multipole integral and the Schwarz integrals that are used as replacement. Simple relations can only be derived for a few special cases, while in the general case of contracted basis functions and arbitrary angular momenta this is obstructed by the absolute value in the integrand of the MBIE integrals (see Appendix C for a discussion of this point). Therefore, this viewpoint is considered as a formal way to draw a comparison between QQR and MBIE.

Following the second viewpoint, the $1/R$ factor derived in MBIE theory is applied as a distance-dependent scaling factor to the Schwarz estimate which thereby reintroduces the correct asymptotic dependence on the bra-ket separation. A further discussion about the dimension of the $1/R$ factor can be found in Appendix D. Since the definition of the extents in inequality (A17) is meaningless when abandoning absolute multipoles, they are substituted by the (usually much larger) well-separatedness extents (that were also used as conservative estimate for defining the far-field in our original MBIE method). This is necessary, since the $1/R$ decay behavior can only be described in a regime where the multipole expansion

This article is copyrighted as indicated in the article. Reuse of AIP content is subject to the terms at: http://scitation.aip.org/termsconditions. Downloaded to IP: 92.230.182.222 On: Sat, 14 Dec 2013 21:59:43

is also valid. Therefore, the working equation for the far-field QQR estimates reads (in atomic units):

$$|(\mu\nu \mid \lambda\sigma)| \approx \frac{Q_{\mu\nu} Q_{\lambda\sigma}}{R - \mathrm{ext}'_{\mu\nu} - \mathrm{ext}'_{\lambda\sigma}}, \tag{2}$$

where we again use the definitions given in Appendix B. It should be noted that, in principle, a dimensional factor of 1 a.u. of length appears on the right hand side to make the $1/R$ factor dimensionless, but that factor can be skipped assuming all quantities in atomic units (cf. Appendix D for a discussion). Since Eq. (2) is only applicable for well-separated charge-distributions, near-field integrals are estimated by the conventional Schwarz bound just as in MBIE theory.

The QQR estimates Eq. (2) exhibit several features that make them the preferred screening method: (1) The error-to-number-of-integrals-ratio of the screening was the best in all our tests; (2) the estimates show the correct functional behavior with the $\mu\nu$ and $\lambda\sigma$ distances within the basis function pairs forming the charge distributions; (3) the dependence on the bra-ket separation is derived from the multipole expansion and the estimates therefore show the appropriate $1/R$ asymptotic distance dependence; (4) the estimates exhibit a tight error distribution, as will be discussed in detail in Sec. III A; (5) they are simple and easy to implement; (6) in contrast to MBIE theory, where the absolute value in the integrand of the multipole integrals forces the use of absolute contraction coefficients, there is no such problem when using Schwarz estimates in the numerator of our QQR screening. This point is of special importance once the screening is extended to correlation methods, an issue we will address in detail in an upcoming paper.[38]

While already the MBIE bounds allow for significant savings in SCF calculations (or more specifically for an improved error vs. number of integrals ratio), the performance of the QQR screening has been found to be clearly superior. This is remarkable at first sight since the QQR estimate is no longer a rigorous upper bound to the two-electron integral. As this observation stands in contrast to our previous argumentation[27] and also to the one of earlier work in the literature,[39] we will explain in the following why we have become convinced that it is advantageous in the present context to drop the rigorous bound property for (reliable) tightness:

First, an upper bound for (neglecting) individual integrals or single energy contributions does not necessarily lead to a useful upper bound for the error in the total energy. An integral estimate like, e.g., the common Schwarz bound is always combined with a (empirical) threshold that balances cost and accuracy—clearly, loose integral bounds lead to meaningless bounds in the total energy. As an illustrative and conservative example consider one SCF iteration with a converged density for a DNA system with two base pairs (DNA$_2$) where the HF/6-31G* exchange energy is about −530 hartree. In the following, the error in the exchange energy in a single iteration is considered:

- Common Schwarz screening in the exchange part with a threshold of 10^{-8} leads to a small error of 2 μhartree.
- In a hypothetical exact screening (simulated based on the true integral values) neglecting, e.g., shells with maxima between 10^{-8} and 10^{-9} would correspond to 2×10^{9} neglected integrals. If these contributions would all by chance be close to the shell maximum the error would be in the order of several hartrees!
- Using a hypothetical exact screening and neglecting all shells with maxima below 10^{-8} (based on a Schwarz prescreening with $\vartheta_{\mathrm{K}} = 10^{-13}$), the unsigned sum of all neglected contributions (simulating missing error compensation) would still add up to an error of 975 μhartree, nearly three orders of magnitude larger than the Schwarz error with the same threshold.

We thus conclude that even screening based on rigorous upper bounds heavily relies on significant error cancellation. With rigorous but non-tight estimates reasonable thresholds (concerning the cost) do not offer a meaningful bound on the total error. The example demonstrates that applying rigorous upper bounds is not the most important property of a screening procedure in the present context. In contrast, tightness of the screening is much more important.

Second, as will be discussed in detail in Sec. III C, it can be observed that screening performance of a rigorous screening might be improved by scaling down the values of the estimates for improving tightness (while the rigorous bound property is lost). The reason for introducing such a scaling can be understood by recalling that the screening thresholds are purely empirical parameters which may have different optimal values for different screening methods in near- and far-field screening. Scaling the estimates, which is identical to choosing a less tight threshold for the distance-dependent far-field estimates, can improve tightness considerably. In the same way, a non-rigorous screening, such as the one proposed in our present work, can be understood as a rigorous one with an empirical scaling factor, as long as the underestimation behaves systematically and is limited in practice.

In the following, we study the usefulness of the QQR estimates in comparison to Schwarz or MBIE estimates for the formation of the Fock matrix in the SCF procedure. Since the widely used CFMM method covers most of the far-field interactions in evaluating the Coulomb part of the Fock matrix, we focus on the selection of exchange integrals where significant savings can be achieved as will be shown in detail in Sec. III C.

III. COMPUTATIONAL DETAILS

All calculations were performed with a development version of Q-CHEM.[40] The density convergence criterion was fixed to a DIIS error of 10^{-5} in all calculations. To assess the performance in real applications we performed full SCF calculations with the specified screening parameters and report errors in the final energies. The Coulomb and exchange parts of the Fock matrix were evaluated separately and CFMM in the Coulomb part was automatically used when beneficial as decided by the autograin code in Q-CHEM. The exchange part was evaluated using the LinK[14] screening scheme in all but the statistics calculations which has of course no influence on the results. If not denoted otherwise the threshold for determination of significant shell pairs[41] as well as the screening threshold for Coulomb integrals was fixed to 10^{-10}, while the

This article is copyrighted as indicated in the article. Reuse of AIP content is subject to the terms at: http://scitation.aip.org/termsconditions. Downloaded to IP: 92.230.182.222 On: Sat, 14 Dec 2013 21:59:43

screening threshold for exchange integrals—denoted as ϑ_K, in the following—was varied. The threshold for determination of the well-separatedness extent was chosen such that the error of the multipole expansion is confined to less than 10% of the integral value for the case of spherical Gaussian functions which corresponds to a threshold value of 10^{-1}.[3] For the MBIE bounds the parameter n_{max} was chosen to be 5 (cf. Appendix A). As initial guess we used the superposition of atomic densities.[40] Difference densities for updating the Fock matrix were used throughout. The DIIS method[42] was applied to extrapolate Fock matrices for all molecules except for the radicaloid systems, where the geometric direct minimization method[43] was used. The basis sets 6-31G*,[44,45] SV(P),[46] cc-pVTZ,[47] and aug-cc-pVTZ[48] were used as noted.

A. Error statistics

For a successful screening it is of course important that the estimates be as close as possible to the true value of the integral. We therefore used the ratio between the estimate and the exact integral value $F = I_{estimate}/I_{exact}$ to assess the quality of Schwarz (QQ), MBIE, and QQR estimates. For both $I_{estimate}$ and I_{exact} we used the maximum value per shell quartet. It should be noted that near-field integrals are always estimated according to the Schwarz bounds.

Our screening procedure works as follows: First, we preselect potentially significant integrals based on Schwarz screening. In the case of MBIE or QQR screening this integral list is skimmed further by employing the chosen far-field screening. This procedure avoids unnecessary calculation of the $1/R$ factors. For all screenings a threshold $\vartheta_K = 10^{-8}$ was applied that usually leads to an accuracy in the final energy of 1 kJ/mol or 400 μhartree or better for molecular systems on the order of 100–1500 atoms. For very large systems it is well known that the error increases roughly linearly with system size, while the error per atom is roughly constant. All calculations were performed in standard nuclear orientation.[49] Since the statistics routines are quite expensive for large molecules, we restricted the calculations to smaller systems of our new benchmark set described in Sec. III C (amylose$_8$, angiotensin, angiotensin deprotonated, angiotensin zwitterion, beta-carotene, carbon nanotubes CNT$_{20}$ and CNT$_{40}$, DNA$_2$, diamond$_{102}$, graphite$_{54}$, $(H_2O)_{68}$, polyethyne$_{64}$, polyyne$_{64}$, and $(S_8)_5$) using 6-31G*, SV(P), and cc-pVTZ basis sets.

A typical example of the collected statistical information is shown in Figure 1. The datapoints correspond to the accumulated number of estimated integrals with ratio F smaller than the given abscissa. In Figure 1(a) the performance of combining Schwarz near-field estimates and MBIE or QQR, respectively, for estimating the exchange contributions (near- and far-field) are shown, whereas in Figure 1(b) only far-field integrals are counted, for which the MBIE or QQR far-field estimate, respectively, is smaller than the Schwarz estimate. The latter leads to different total integral counts for MBIE and QQR but allows to obtain the statistically relevant information for the far-field screenings.

Both figures demonstrate the rigorous bound property of MBIE estimates, while QQR sometimes underestimates the true integral value. At the same time, the QQR estimates accumulate closer to the exact values compared to the MBIE results. In Figure 1(a) the QQR distribution is broadened due to the superposition with the QQ distribution for near-field integrals that are significantly overestimated. This effect is not observed for MBIE since the overestimation in near- and far-field are of similar size in this case. For far-field integrals the MBIE and QQR curves in Figure 1(b) are similar which is the reason why a screening performance comparable to QQR can be obtained if the MBIE estimates are scaled down by a constant factor as discussed below.

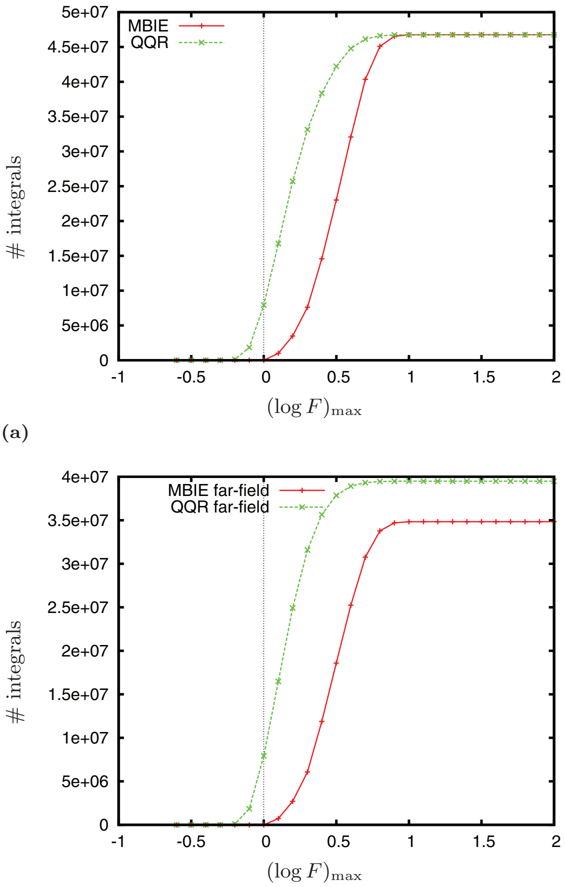

(a)

(b)

FIG. 1. Error distribution of (a) combined and (b) pure far-field estimates for the DNA$_2$ test system in the 6-31G* basis. The plot shows the number of integrals with $\log(F)$ smaller than $(\log F)_{\max}$, where F is defined as $F = I_{estimate}/I_{exact}$. In (b) only integrals were evaluated for which the MBIE/QQR estimate is lower than the Schwarz estimate, which causes different total integral counts for the two methods.

The statistical results over all test calculations using the 6-31G* basis are summarized in Figure 2 based on the ratio F of estimate to integral value. Pure Schwarz screening shows the broadest distribution of the three methods. Both the average and the maximum ratio F as well as the standard deviation decrease from Schwarz to MBIE and are even smaller for the QQR screening, while for the latter small underestimations with up to 0.45 times the integral value occur. The results for other basis sets are given in Table I. For the SV(P) and

This article is copyrighted as indicated in the article. Reuse of AIP content is subject to the terms at: http://scitation.aip.org/termsconditions. Downloaded to IP: 92.230.182.222 On: Sat, 14 Dec 2013 21:59:43

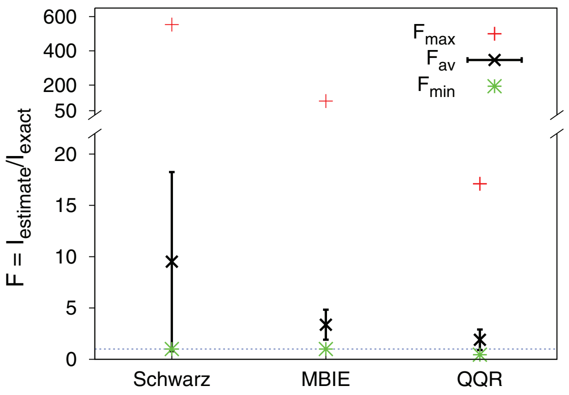

FIG. 2. Results of the error statistics in the 6-31G* basis corresponding to the values given in Table I.

cc-pVTZ basis, huge overestimations occur due to the poor Schwarz estimates for integrals involving p-functions. This deficiency is not observed for the 6-31G* basis since shared-*sp* shells are employed and the comparably accurate estimates for *s*-functions determine the shell maxima and therefore the ratio *F*. The statistical trends for SV(P) and cc-pVTZ are the same as for the 6-31G* basis with the QQR screening providing the smallest standard deviation and the average ratio *F* closest to 1, while underestimations are 0.33 times the integral value at most.

The same trends are observed for the statistics restricted to far-field integrals, where the corresponding data tables can be found in the supplementary information.[50] For these far-field statistics we also analyzed the standard deviation of log(*F*) which describes the broadness of the error distribution on the logarithmic scale as depicted in Figure 1(b). This value is unmodified when the far-field estimate is scaled by a constant factor. The logarithmic standard deviations listed in Table II are of similar magnitude for MBIE and QQR, so that it should be possible to reach similar performance as in the QQR screening once the MBIE estimates are scaled down. As discussed in Sec. II this is equivalent to choosing an independent threshold for the far-field screening. In fact, a screening based on MBIE estimates scaled by a factor of 0.3 performed almost as good as QQR in our benchmark calculations as discussed in detail in Sec. III C, although such a scaling destroys the rigorous upper-bound property of MBIE. Nevertheless, the main drawback of MBIE that remains is that it is technically much more complicated than our new QQR screening.

TABLE II. Comparison of the logarithmic standard deviation $\sigma(\log(F))$ of the ratio $F = I_{estimate}/I_{exact}$ for MBIE and QQR far-field integral estimates. The standard deviation was determined in each iteration and averaged over all calculations.

	$\sigma(\log(F))_{avg}$	
Basis	MBIE	QQR
6-31G*	0.18	0.17
SV(P)	0.38	0.34
cc-pVTZ	0.39	0.34

An interesting point which is hardly discussed in the literature is the dependence of screenings on the molecular orientation. The traditional Schwarz bounds as well as the QQR estimates are not rotationally invariant, since the Schwarz integrals depend on the overlap distribution of atomic orbitals and therefore depend on the orientation for all but s-type basis functions. Furthermore, since the electronic density is, in principle, rotationally invariant, the density-matrix elements have to change with the orientation of the atomic orbitals and hence also depend on the molecular orientation. We observed a noteworthy example of this dependence during our studies of the error statistics on preconverged densities of DNA systems. By extending the system from DNA_8 to DNA_{16}, the maximum ratio of estimate to exact integral value (maximum overestimation) in QQR calculations decreased from 18.8 to 16.7, which did not seem plausible at first sight. The higher value is due to a shell quadruple located near the third base pair, where the density is not expected to change much between the two systems. But the orientation of the two molecules is quite different and the key values of the screening change significantly: The maximum density element for the shell block decreases by nearly 38% and the shell block maximum of the Schwarz integrals is 27% smaller in the case of the DNA_{16} system. Due to these changes the estimate for the Fock matrix contribution decreases below the chosen screening threshold and the integral disappeared from the statistics. It should also be noted that this effect is not the result of distance-dependent estimates; the integral in question is a near-field integral estimated according to the conventional Schwarz bound.

While care has to be taken in special cases as the one described above, the orientation dependence is usually not a major issue in SCF calculations. The largest energy difference we observed in test calculations is on the order of a few μhartree (depending on the convergence threshold, while the integral threshold has been chosen tight enough) for a linear polyyne_{64} system. Nevertheless, the effect can be more pronounced in correlation methods which is the subject of ongoing studies.

TABLE I. Comparison of error statistics for MBIE and QQR integral estimates. Shown are the statistics of the ratio $F = I_{estimate}/I_{exact}$ as the average $\overline{F}$, its smallest and largest values (F_{min}, F_{max}), and the standard deviations of F averaged over all iterations.

	Schwarz				MBIE				QQR			
Basis	$\overline{F}$	F_{min}	F_{max}	$\sigma(F)_{avg}$	$\overline{F}$	F_{min}	F_{max}	$\sigma(F)_{avg}$	$\overline{F}$	F_{min}	F_{max}	$\sigma(F)_{avg}$
6-31G*	9.52	1.00	553.5	8.73	3.37	1.00	106.5	1.46	1.90	0.45	17.1	1.00
SV(P)	40.32	1.00	1×10^7	2527.36	6.54	1.00	2×10^6	167.54	3.31	0.37	2×10^6	134.21
cc-pVTZ	45.51	1.00	1×10^7	2122.28	8.31	1.00	2×10^6	156.20	3.23	0.33	2×10^6	81.14

This article is copyrighted as indicated in the article. Reuse of AIP content is subject to the terms at: http://scitation.aip.org/termsconditions. Downloaded to IP: 92.230.182.222 On: Sat, 14 Dec 2013 21:59:43

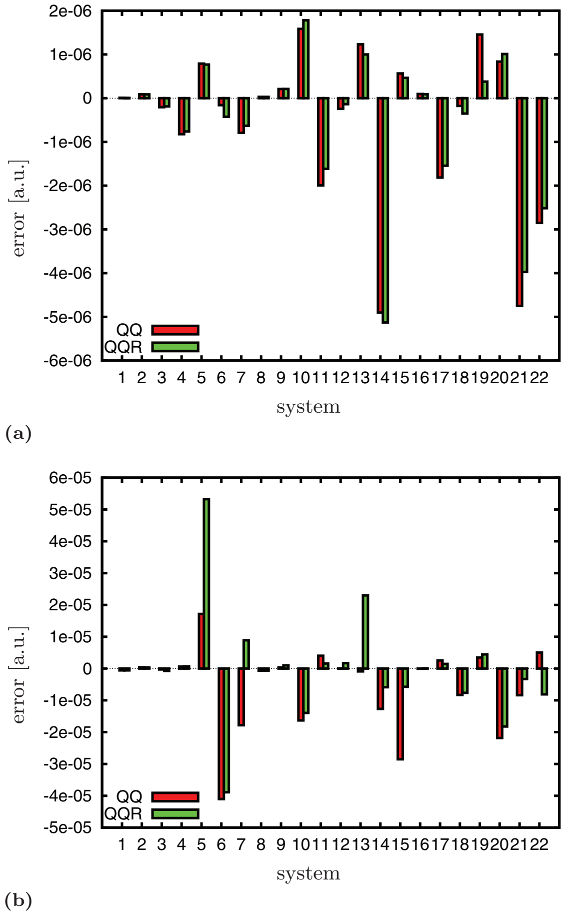

FIG. 3. Errors in S22 test set calculations with Schwarz and QQR screening with (a) SV(P) and (b) aug-cc-pVTZ basis sets ($\vartheta_K = 10^{-8}$). Reference for the errors are QQ ($\vartheta_K = 10^{-10}$) calculations.

B. Assessment of QQR on S22 test set

As a first test of the QQR screening we chose the well-known S22 test set of Hobza and co-workers.[36] While it mainly consists of small molecules (compared to the large systems discussed in Sec. III C) and therefore shows moderate influence of far-field screening, it is nevertheless a good starting point for studying new screening methods since the short calculation times allow for extensive testing. Besides the influence of the screening on the total energy error, we also investigated the dependence of the error on the interaction distance, the convergence behavior, and the error to integral ratio for different thresholds.

We performed QQR and Schwarz calculations on the S22 test set with $\vartheta_K = 10^{-8}$ and studied the error in total energies compared to Schwarz calculations with $\vartheta_K = 10^{-10}$. For the SV(P) basis set the errors are plotted in Figure 3(a). The errors of Schwarz and QQR using the same threshold criteria are typically of similar size, with the largest absolute deviation of 1.1 μhartree between the two screening methods.

Deviations for the S22 set using other basis sets such as 6-31G* and cc-pVTZ are very similar to the ones in the SV(P) basis with the largest deviation between QQ and QQR being 0.2 μhartree and 2.2 μhartree, respectively. The corresponding figures can be found in the supplementary information.[50] The aug-cc-pVTZ basis results are plotted in Figure 3(b). Employing a threshold ϑ_K of 10^{-8}, the errors of Schwarz screening and the QQR method reach up to 41 μhartree and 53 μhartree, respectively, which is about one order of magnitude larger than for the non-augmented basis sets. The maximum deviation of QQ and QQR is 36 μhartree in this case. For accuracies comparable to the other basis sets a tighter threshold of 10^{-9} needs to be chosen which reduces the maximum errors of both screenings to less than 2 μhartree and the deviation of QQ and QQR below 1 μhartree (see supplementary information[50] for the corresponding figure).

It is clear that the use of an additional far-field screening (rigorous or not) on top of the underlying Schwarz estimates (always the minimum of the different screening estimates is employed) will discard additional integrals. While this might provide a more balanced description of near- and far-field interactions, it may become necessary to choose tighter screening thresholds for obtaining similar accuracies, but these can be reached with a reduced number of integrals and lower costs. Therefore, it is important to carefully assess the balance between accuracy and performance of a screening procedure, which will be discussed in more detail at the end of this section.

To evaluate the observed deviations within the S22 test set in more detail, we further investigated the dependence of the error on the interaction distance for selected systems: For the non-augmented basis sets (6-31G*, SV(P), cc-pVTZ) we chose 2-pyridoxine · 2-aminopyridine (#6), benzene · HCN (#19), and the benzene dimer (#20), since they show comparatively large relative or absolute errors in their non-elongated forms. The more central processing unit (CPU) time intensive studies for the aug-cc-pVTZ basis were restricted to the uracil dimer (#5) where larger deviations with $\vartheta_K = 10^{-8}$ have been observed. Studying the distance-dependent error fluctuations allows to determine whether an observed deviation indicates a fundamental problem or lies within the range of arbitrary errors. Moreover, we wanted to make sure that the potential curve remains smooth with the distance-dependent QQR screening. As Figure 4(a) shows the error with QQR basically follows the Schwarz error and does not introduce any significant further discontinuities. Fluctuations in the error itself are much larger than deviations between QQR and Schwarz results, which shows the reliability of the new QQR screening. The behavior for systems #6, #19, and #20 using the non-augmented basis sets is very similar and the corresponding results can be found in the supplementary material.[50]

The results for system #5 using the aug-cc-pVTZ basis and $\vartheta_K = 10^{-8}$ are shown in Fig. 4(b): for distances below 1.8 Å relatively strong error fluctuations occur with up to almost 0.1 μhartree for both Schwarz and QQR screening. This indicates that for diffuse basis sets a (slightly) tighter threshold is necessary, which is also obvious from the increased number of iterations necessary for converging the SCF procedure as compared to the reference calculation with a threshold of $\vartheta_K = 10^{-10}$ for some of the chosen distances: at 1.3 Å for Schwarz, at 1.5 Å for QQR, and at 1.2 Å for both methods; for

This article is copyrighted as indicated in the article. Reuse of AIP content is subject to the terms at: http://scitation.aip.org/termsconditions. Downloaded to IP: 92.230.182.222 On: Sat, 14 Dec 2013 21:59:43

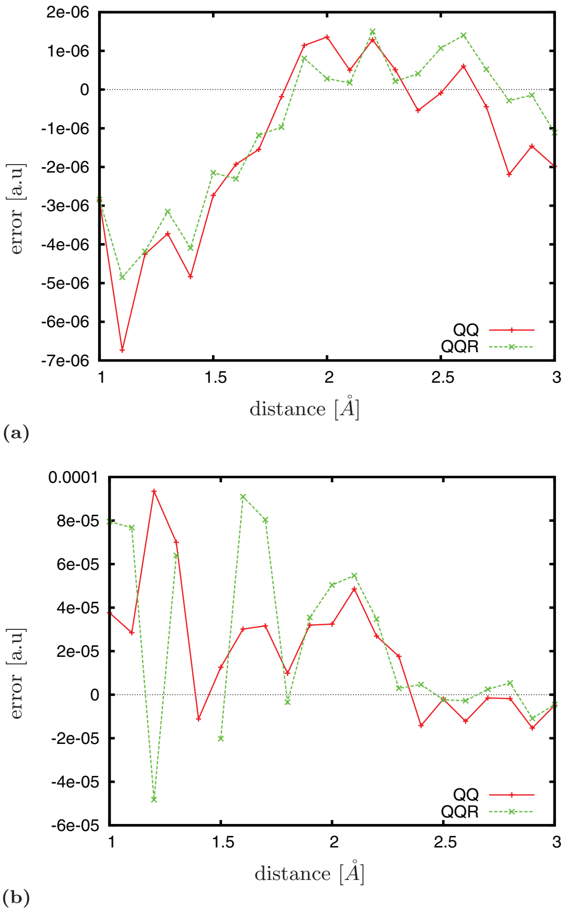

(a)

(b)

FIG. 4. Errors of Schwarz and QQR screening with respect to (a) the distance of hydrogen to the benzene plane in the benzene · HCN complex (#19) of the S22 test set with SV(P) basis and (b) the distance along the h-bonds in the h-bonded uracil dimer (#5) of the S22 test set with aug-cc-pVTZ basis ($\vartheta_K = 10^{-8}$). Note the big errors in (b) of up to 93 μhartree for both methods that indicate an insufficiently tight threshold for the augmented basis. At a distance of 1.4 Å the threshold is not tight enough to converge the SCF procedure with QQR screening.

a distance of 1.4 Å the threshold is not even tight enough to converge the QQR calculation. Such a behavior is sometimes observed also in the test set presented in Sec. III C when a large error of the Schwarz results indicates that the threshold is hardly tight enough to converge the SCF procedure. In such borderline cases the QQR method might fail to converge since it needs in general a slightly tighter threshold than Schwarz to reach the same accuracy level (and likewise convergence) as discussed above. With a tighter threshold ($\vartheta_K = 10^{-9}$) the distance dependence of the error reverts to fluctuations similar to the results for the other basis sets (see the supplementary information[50]).

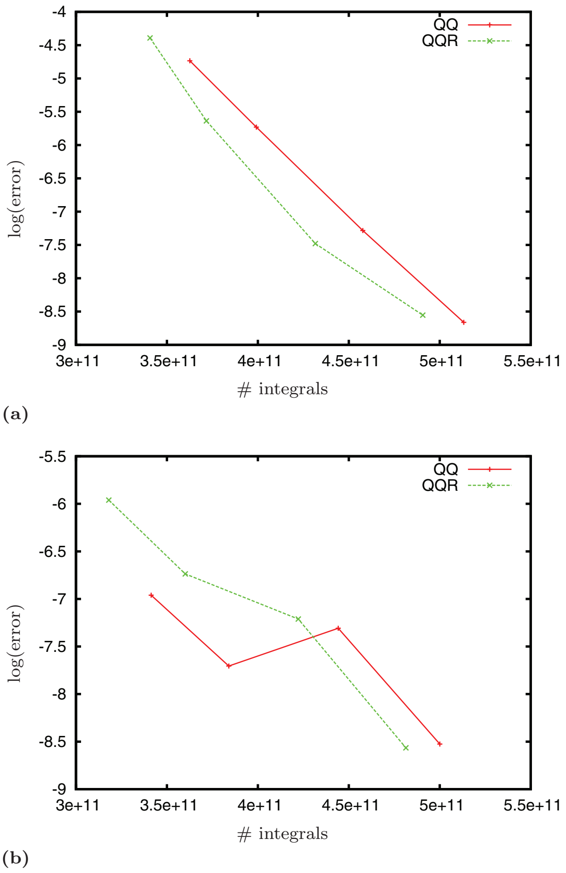

(a)

(b)

FIG. 5. Error vs. number of integrals for Schwarz and QQR screening with different thresholds ϑ_K in (a) the h-bonded uracil dimer (#5) and (b) the phenol dimer (#22) of the S22 test set with aug-cc-pVTZ basis set. The points correspond to calculations with ϑ_K values of 10^{-8}, 10^{-9}, 10^{-10}, and 10^{-11}. Note the anomalous behavior of the QQ curve in (b) due to fortuitous small errors for the less tight thresholds

While the errors for the same threshold may slightly differ between QQR and pure Schwarz, the error-to-integral ratio is consistently better with our new screening even in the more difficult aug-cc-pVTZ basis as exemplified for the hydrogen-bonded uracil dimer (#5) in Figure 5(a). The reference calculation for this plot was performed with integral thresholds for Coulomb and exchange part set to 10^{-13}. The data points were obtained for thresholds ϑ_K of 10^{-8}–10^{-11}, while the resulting error vs. the reference value and the number of resulting exchange integrals is shown. Figure 5(a) shows the typical behavior in which the logarithmic error reduces roughly linearly with the number of integrals. Therefore, the connecting lines between data points can be understood as rough interpolations for intermediate thresholds. Since the data points (and the line) for QQR are always located to the left of the corresponding Schwarz results, it shows that the QQR screening offers better accuracy for the same cost or requires less integrals for the same accuracy. A special case is depicted in Figure 5(b) where the errors of the Schwarz calculations for ϑ_K values of 10^{-8} and 10^{-9} are very good by pure chance, which is obvious since they are similar or even better than the error with $\vartheta_K = 10^{-10}$.

The latter case shows that it is not sufficient to study isolated diagrams of this kind, but instead such studies are necessary for a statistically relevant test set in order to judge the

This article is copyrighted as indicated in the article. Reuse of AIP content is subject to the terms at: http://scitation.aip.org/termsconditions. Downloaded to IP: 92.230.182.222 On: Sat, 14 Dec 2013 21:59:43

performance of a screening method. The remaining plots for the other systems of the S22 test set are provided in the supplementary information[50] and show consistently good performance of the QQR screening with only a few cases where the error fluctuation masks the improved screening performance for less tight thresholds as in the second example described above.

In this context we would like to note that the error in the total energy is not the only possible criterion to assess the accuracy of a calculation. An interesting alternative is the use of a unitary norm of an error matrix as described in Ref. 21. For the case depicted in Figure 5(b) we tested the Euclidean norm of the error in the converged density matrix. This error criterion shows much smaller fluctuations with the screening threshold leading to a monotonic decrease, but yet significant deviations from the expected linear correlation are observed. In the present work we focus on the total energy as error criterion since it offers good comparability with former results and can furthermore be used to study screening in correlation methods in the same way (which we are planning to report on soon).

C. Benchmark calculations for recommended testsuite

In order to reliably assess the performance of our new QQR screening method, we study in the following a large test set that we designed to be representative for various molecular systems. All coordinate files can be downloaded from our website.[37] The test set needs to be large enough in order to distinguish between random cases and systematic failures in certain situations. The chosen systems are listed in Table III and cover systems from insulators to molecules with small band gaps such as carbon nanotubes (CNTs). Furthermore, the dimensionality of the systems ranges from one-dimensional (e.g., polyenes) to three-dimensional (e.g., diamond), while the set contains neutral, ionic, and radicaloid systems, as well as a few third row elements and one copper complex. While some of the systems are biologically relevant (e.g., angiotensin) we also included some very artificial systems as the linear polyyne $C_{1024}H_2$ as tough tests.

The systems were reoriented using the Q-CHEM code according to the standard orientation introduced by Gill *et al.*[49] and are given in the final orientation. This point is significant since none of the screening methods (neither the original Schwarz screening, nor QQR) are rotationally invariant as discussed in Sec. III A.

Table III summarizes the results for the QQR method in the 6-31G* basis. Results in the SV(P) basis and for the smaller systems in the cc-pVTZ basis are reported in the supplementary information.[50] All errors and integral ratios (speedups) refer to calculations that require the same number of iterations for convergence as the reference calculations with a threshold of $\vartheta_K = 10^{-10}$. This is usually achieved with a ϑ_K value of 10^{-8}, but in some cases tighter thresholds are required as noted in the table.

For nearly all systems the new QQR screening leads to significant savings with speedups of up to 2.3 compared to the Schwarz calculation. The maximum speedup was observed for the largest water cluster using the SV(P) basis, while the error is of the same size as for the Schwarz method. The speedups increase with system size up to the point where the locality of the density matrix is dominant and effectively reduces the count of exchange integrals to a strictly linear-scaling number. For these cases the savings with QQR become independent of the system size as it is observed for the longest amylose chains. In a few cases (polyynes, triphenylmethyl, phthalocyanine complex, the larger LiF systems using SV(P) and cc-pVTZ as well as CNT(6,3)$_8$, and diamond$_{470}$ with SV(P)) the threshold for QQR needs to be tighter than in the Schwarz calculation. Even when the threshold ϑ_K is one order of magnitude tighter than in the Schwarz calculations about one third of these cases still show increased speed with QQR. Although the remaining cases show a slightly increased number of integrals compared to the Schwarz result with less tight threshold, much higher accuracies are achieved in return.

Since it is difficult to assess the performance of a screening method if there is a tradeoff of accuracy vs. number of integrals, the error-to-integral diagrams introduced in Sec. III B are helpful for this purpose. Figure 6 shows the QQR results with $\vartheta_K = 10^{-8}$ and $\vartheta_K = 10^{-9}$ for all systems calculated in the corresponding basis set. To include all data in a single plot and obtain a statistical tool for assessment of the screening, all results are plotted relative to the Schwarz errors and integral counts with $\vartheta_K = 10^{-8}$ for the corresponding system. The calculated data define the end-points of the plotted lines. For cases where only one calculation converged with the same number of iterations as the QQ ($\vartheta_K = 10^{-10}$) reference (see discussion above), the results are shown as single data points.

In these figures the intersections with the horizontal reference line allow to estimate the ratio of exchange-integral numbers selected by QQ vs. QQR—which corresponds to the estimated speedups—for reaching the same accuracy in both screening schemes. The speedups are typically of the order of 1.3–2.1 and about 1.1 for the less favorable systems. Alternatively, intersections with the vertical reference line show that QQR reduces the errors for the same number of integrals by about 0.2–1 order of magnitude or 30%–90%. Overall, the QQR screening provides results that are consistently (1) faster than Schwarz calculations with the same error and (2) more accurate than Schwarz results with the same number of integrals.

If one considers the results in Figures 6 in more detail, then those results outperforming the Schwarz calculations in both error and number of integrals are located in the bottom right box within the diagram. The QQR results for $\vartheta_K = 10^{-8}$ are mainly located near the right part of the horizontal reference line, while the calculations for $\vartheta_K = 10^{-9}$ often lie to the left of the vertical reference line. However, the latter provide higher accuracies for QQR than for pure Schwarz. All but one line pass below the reference point and therefore confirm the better performance of QQR compared to the old Schwarz estimates. The only exception in Figure 6(b) (green line) is the DNA system with 16 base pairs. However, this is solely due to a coincidentally small error of the Schwarz reference ($\vartheta_K = 10^{-8}$) of only 13.3 μhartree that is actually smaller than the error of the Schwarz ($\vartheta_K = 10^{-9}$) calculation of 17.1 μhartree. Here, the latter is again of the same size as

This article is copyrighted as indicated in the article. Reuse of AIP content is subject to the terms at: http://scitation.aip.org/termsconditions. Downloaded to IP: 92.230.182.222 On: Sat, 14 Dec 2013 21:59:43

TABLE III. QQR benchmark calculations in a 6-31G* basis. Errors are given with respect to the QQ ($\vartheta_K = 10^{-10}$) reference calculations. Speedups are given as the ratio of the number of integrals.

	QQ ($\vartheta_K = 10^{-8}$)		QQR ($\vartheta_K = 10^{-8}$)		
System	err [μhartree]	#int [10^6]	err [μhartree]	#int [10^6]	speedup
Amylose$_2$	−7.18	2574	−6.94	2229	1.15
Amylose$_4$	−11.85	7808	−11.86	5967	1.30
Amylose$_8$	−26.54	19482	−25.99	13950	1.39
Amylose$_{16}$	−51.17	42899	−50.11	29968	1.43
Amylose$_{32}$	−64.08	83312	−62.68	57623	1.44
Amylose$_{48}$	−96.49	126797	−94.44	87372	1.45
Amylose$_{64}$	−128.44	170311	−125.18	117159	1.45
Angiotensin	−12.62	20779	−12.55	14496	1.43
Angiotensin deprotonated	−17.97	20729	−17.61	14477	1.43
Angiotensin zwitterion	−16.78	20915	−16.61	14593	1.43
Beta-carotene	−2.42	5747	−2.11	4026	1.42
CNT$_{20}$	4.81	3032	4.49	2908	1.04
CNT$_{40}$	4.73	23963	4.46	21173	1.13
CNT$_{80}$	18.01	116538	19.57	89610	1.30
CNT$_{160}$	−5.66	634820	−0.50	394721	1.60
CNT (6,3)$_8$	−145.37	3318623	−149.03	1563661	2.12
DNA$_1$	−8.78	4714	−8.65	3706	1.27
DNA$_2$	−17.15	26586	−16.73	18638	1.42
DNA$_4$	−35.74	96807	−35.35	59166	1.63
DNA$_8$	−52.72	243378	−51.62	138320	1.75
DNA$_{16}$	−109.55	550829	−107.78	304185	1.81
Diamond$_{102}$	−15.17	33457	−14.82	29360	1.13
Diamond$_{470}$	−146.87	1872628	−159.96	1187355	1.57
Graphite$_{24}$ ($C_{24}H_{12}$)	−2.95	3444	−2.38	3132	1.09
Graphite$_{54}$ ($C_{54}H_{18}$)	−9.54	21503	−5.73	17165	1.25
Graphite$_{96}$ ($C_{94}H_{24}$)	−15.07	72514	−18.00	53609	1.35
$(H_2O)_{68}$	−21.42	3036	−21.50	1818	1.66
$(H_2O)_{142}$	−46.32	9230	−46.71	5012	1.84
$(H_2O)_{285}$	−109.31	24753	−110.04	12568	1.96
$(H_2O)_{569}$	−234.04	59980	−235.55	28891	2.07
$(LiF)_{32}$	5.36	9591	5.46	8524	1.12
$(LiF)_{72}$	50.31	168574	39.48	150494	1.12
$(LiF)_{288}$	17.46[a]	15874061[a]	−96.16[a]	13231982[a]	1.19[a]
Phthalocyanine complex ($CuPcF_{16}$)	0.32[b]	59986[b]	0.00[b]	64987[b]	0.92[b]
Polyethyne$_{64}$ ($C_{64}H_{66}$)	−12.98	6883	−12.74	4206	1.63
Polyethyne$_{128}$ ($C_{128}H_{130}$)	−20.47	18318	−19.88	9659	1.89
Polyethyne$_{512}$ ($C_{512}H_{514}$)	−54.38	80962	−52.23	39064	2.07
Polyyne$_{64}$ ($C_{64}H_2$)	34.59	4956	3.99[c]	4770[c]	1.03[c]
Polyyne$_{1024}$ ($C_{1024}H_2$)	505.38	210740	112.26[c]	266948[c]	0.78[c]
$(S_8)_5$	−1.83	6611	−1.97	4784	1.38
$(S_8)_{20}$	−40.18	116281	−40.23	63562	1.82
Triphenylmethyl	−0.01[b]	5613[b]	0.00[b]	6452[b]	0.86[b]
Zeolite LTA	−5.39	590275	−0.26	330466	1.78
Zeolite SOD	5.84	126784	7.67	84718	1.49

[a] QQ ($\vartheta_K = 10^{-9}$) and QQR ($\vartheta_K = 10^{-9}$).

[b] QQ ($\vartheta_K = 10^{-9}$) and QQR ($\vartheta_K = 10^{-10}$).

[c] QQ ($\vartheta_K = 10^{-8}$) and QQR ($\vartheta_K = 10^{-9}$).

the QQR value with the same threshold (17.6 μhartree). On the other hand a few lines show negative slopes, which means that the QQR error with $\vartheta_K = 10^{-8}$ was fortuitously good and thereby more accurate than the result with $\vartheta_K = 10^{-9}$. As mentioned above this is a common behavior that arises also for pure Schwarz-type screening. The individual points in the lower left part of the diagram should be considered in connection with the slopes of the remaining lines that indicate that the integral to error ratio is superior to the pure Schwarz calculations in these cases as well. The leftmost point in Figure 6(a) corresponds to the polyyne $C_{1024}H_2$. While the comparison of the QQ ($\vartheta_K = 10^{-8}$) and QQR ($\vartheta_K = 10^{-9}$) values might be inconclusive for the performance in this particular case, tighter thresholds again confirm the good

This article is copyrighted as indicated in the article. Reuse of AIP content is subject to the terms at: http://scitation.aip.org/termsconditions. Downloaded to IP: 92.230.182.222 On: Sat, 14 Dec 2013 21:59:43

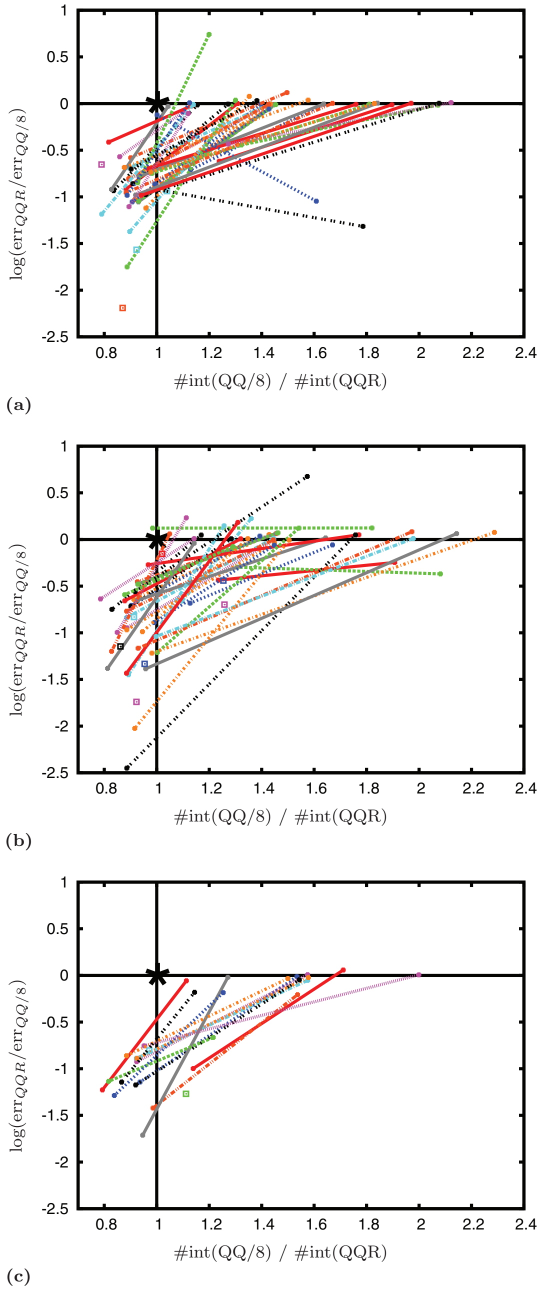

FIG. 6. Error and speedup (via ratio of integrals) with the (a) 6-31G*, (b) SV(P), and (c) cc-pVTZ basis set for QQR calculations (right endpoint: $\vartheta_K = 10^{-8}$ and left endpoint: $\vartheta_K = 10^{-9}$) of the whole test set relative to the values of a pure Schwarz calculation with $\vartheta_K = 10^{-8}$. The Schwarz reference is indicated as a black asterisk. Values to the right of this reference point indicate increased speed, while values below the reference indicate improved accuracy. Data tables can be found in the supplementary information.[50]

QQR performance since the QQ ($\vartheta_K = 10^{-9}$) error is 20.0 μhartree, while QQR ($\vartheta_K = 10^{-10}$) reduces the error to only 7.7 μhartree at essentially the same cost (203.6 and 203.5 billion exchange integrals, respectively).

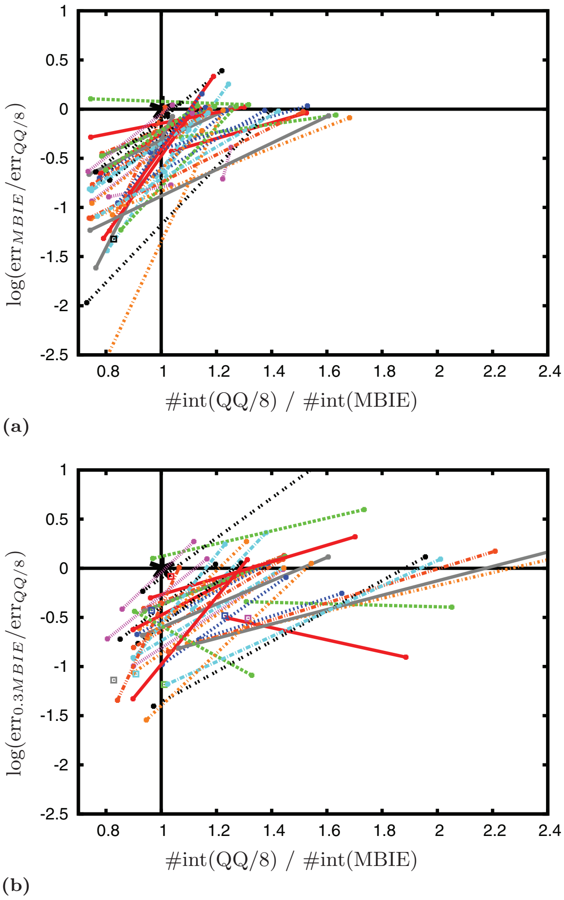

FIG. 7. Error and speedup (via ratio of integrals) for (a) MBIE and (b) scaled MBIE (scaling factor 0.3) calculations (right endpoint: $\vartheta_K = 10^{-8}$ and left endpoint: $\vartheta_K = 10^{-9}$) of the whole test set in the SV(P) basis relative to the values of a pure Schwarz calculation with $\vartheta_K = 10^{-8}$. The Schwarz reference is indicated as a black asterisk. Values to the right of this reference point indicate increased speed, while values below the reference indicate improved accuracy. Data tables can be found in the supplementary information.[50]

Results for the rigorous MBIE bound are exemplarily shown for the SV(P) basis in Figure 7(a). In comparison to the QQR results in Figure 6(b) the performance gain with the MBIE screening is obviously significantly smaller. The line corresponding to the DNA$_{16}$ system passes above the reference point in the rigorous case for the same reasons stated above.

As argued in Sec. III A it can be expected that scaling the MBIE bounds should lead to a screening nearly as effective as the QQR screening because of similar standard deviations on the logarithmic scale. Figure 7(b) shows the results where the MBIE estimates were scaled down by a factor of 0.3. This value is assumed to be quite optimal based on preliminary calculations on smaller molecules with different scaling factors and indeed offers a performance that is close to the QQR method, however, less uniform across the test set. The performance of MBIE and scaled MBIE in 6-31G* and

This article is copyrighted as indicated in the article. Reuse of AIP content is subject to the terms at: http://scitation.aip.org/termsconditions. Downloaded to IP: 92.230.182.222 On: Sat, 14 Dec 2013 21:59:43

cc-pVTZ basis is similar and the corresponding data and diagrams can be found in the supplementary information.[50]

Therefore, the QQR screening is clearly our most favored screening. In addition, the QQR screening is cheaper and much easier to implement than MBIE. Also it can be much more easily extended to other two-electron integrals like those in AO-based correlation methods. Finally, it seems that the QQR screening offers a quite optimum performance: for some randomly chosen smaller test systems, there is a very good agreement of the number of numerically significant integrals selected by our QQR screening with those numbers based on counting the explicit integrals themselves (as in a perfect screening over shells) and interpolation to the same error in the energy. This suggests that there might be little room for further improvements upon QQR.

IV. CONCLUSION

The QQR integral estimates for preselecting four-center two-electron integrals introduced in the present work allow to account for the $1/R$ distance decay between the two charge distributions. Although the QQR estimates are not rigorous upper bounds to the two-electron integrals, they offer tight estimates for well-separated bra- and ket-charge distributions. The performance of the QQR estimates is demonstrated to be useful for screening, e.g., exchange integrals within SCF theory. Most importantly, the QQR estimates can be readily extended to any screening of two-electron integrals such as, e.g., in AO-based correlation methods which we plan to report on soon.[38]

For testing screening methods in general, we presented a benchmark set of large molecules covering a wide range of chemical compounds such as insulating, delocalized, radical, and ionic systems. The test set is well suited for assessing screening methods especially in combination with the described statistical diagrammatic analysis but might as well be useful for benchmarking other approximations for large systems. Furthermore, since most of the systems are included in various sizes, it is also well suited to investigate the scaling behavior.

The results of our extensive tests indicate the good performance of the new QQR screening and its superiority to our previous, rigorous MBIE screening. This shows that reliable tightness of estimates is more important than rigorous upper bounds in the present context. In addition, the new bounds are much simpler and easier to implement, so that they are the recommended choice.

ACKNOWLEDGMENTS

We dedicate this work in honour of Professor Dr. Christoph Bräuchle (LMU Munich) on the occasion of his 65th birthday. C.O. thanks Professor Dr. Peter Pulay (University of Arkansas) for his question during a conference in Bad Herrenalb in 2006 whether the rigorous bound property of integral estimates is essential. While C.O. answered at that time, also by citing the work of Jan Almlöf that a rigorous bound is expected to be crucial, we believe that *reliable tightness* is more important in the present context as exemplified by our present work. The authors also thank Dr. Jörg Kussmann (University of Munich, LMU) for valuable discussions and an anonymous referee for useful comments on our manuscript. Furthermore, C.O. acknowledges financial support by the Volkswagen Stiftung within the funding initiative "New Conceptual Approaches to Modeling and Simulation of Complex Systems."

APPENDIX A: DERIVATION OF RIGOROUS MBIE BOUNDS

This derivation assumes two charge distributions A and B, that are well separated such that the multipole expansion of the two-electron integrals is valid:

$$\begin{aligned}(A \mid B) &= \int \Omega_A(\boldsymbol{r}_1)\frac{1}{r_{12}}\Omega_B(\boldsymbol{r}_2)\mathrm{d}\boldsymbol{r}_1\mathrm{d}\boldsymbol{r}_2\\ &= \int \Omega_A(\boldsymbol{r}_1)\sum_{n=0}^{\infty}\frac{\Delta r_{12}^n}{R^{n+1}}P_n(cos\phi)\Omega_B(\boldsymbol{r}_2)\mathrm{d}\boldsymbol{r}_1\mathrm{d}\boldsymbol{r}_2.\end{aligned} \tag{A1}$$

Based on the experience with CFMM we furthermore assume that restricting the multipole expansion to orders up to a chosen order n_{max} (∼15–25) allows to reproduce the value of the two-electron integral to within numerical accuracy.

The centers of the multipole expansion of the charge distributions A and B coincide with the origins of $\boldsymbol{r}_1$ and $\boldsymbol{r}_2$, respectively. Obviously Δr_{12} is bound as

$$\Delta r_{12} = |\boldsymbol{r}_1 - \boldsymbol{r}_2| \leq r_1 + r_2 \tag{A2}$$

with the notation $r_n = |\boldsymbol{r}_n|$. Using $P_n(\cos\phi) \leq 1$ we can formulate an upper bound to the integral (A1):

$$\begin{aligned}(A \mid B) &\leq \int \left| \Omega_A(\boldsymbol{r}_1)\sum_{n=0}^{\infty}\frac{(r_1+r_2)^n}{R^{n+1}}\Omega_B(\boldsymbol{r}_2)\right| \mathrm{d}\boldsymbol{r}_1\mathrm{d}\boldsymbol{r}_2\\ &= \sum_{n=0}^{\infty}\frac{1}{R^{n+1}}\sum_{i=0}^{n}\binom{n}{i}\int \left|\Omega_A(\boldsymbol{r}_1)r_1^{n-i}\right|\mathrm{d}\boldsymbol{r}_1\\ &\quad \times \int \left|\Omega_B(\boldsymbol{r}_2)r_2^{i}\right|\mathrm{d}\boldsymbol{r}_2\\ &= \sum_{n=0}^{\infty}\frac{1}{R^{n+1}}\sum_{i=0}^{n}\binom{n}{i}\mathcal{M}_A^{(n-i)}\mathcal{M}_B^{(i)}\end{aligned} \tag{A3}$$

with the absolute multipole integrals

$$\mathcal{M}_A^{(i)} = \int \left|\Omega_A(\boldsymbol{r})r^{i}\right|\mathrm{d}\boldsymbol{r}. \tag{A4}$$

This article is copyrighted as indicated in the article. Reuse of AIP content is subject to the terms at: http://scitation.aip.org/termsconditions. Downloaded to IP: 92.230.182.222 On: Sat, 14 Dec 2013 21:59:43

We choose our estimates to be of the form $\frac{\mathcal{M}_A^{\prime(0)}\mathcal{M}_B^{\prime(0)}}{R-\mathrm{ext}_A-\mathrm{ext}_B}$ and rewrite using the limit of the geometric series

$$\begin{aligned}
&\frac{\mathcal{M}_A^{\prime(0)}\mathcal{M}_B^{\prime(0)}}{R-\mathrm{ext}_A-\mathrm{ext}_B}\\
&\quad=\frac{\mathcal{M}_A^{\prime(0)}\mathcal{M}_B^{\prime(0)}}{R}\frac{1}{1-\frac{\mathrm{ext}_A+\mathrm{ext}_B}{R}}\\
&\quad=\frac{\mathcal{M}_A^{\prime(0)}\mathcal{M}_B^{\prime(0)}}{R}\sum_{n=0}^{\infty}\left(\frac{\mathrm{ext}_A+\mathrm{ext}_B}{R}\right)^n\\
&\quad=\mathcal{M}_A^{\prime(0)}\mathcal{M}_B^{\prime(0)}\sum_{n=0}^{\infty}\frac{(\mathrm{ext}_A+\mathrm{ext}_B)^n}{R^{n+1}}\\
&\quad=\sum_{n=0}^{\infty}\frac{1}{R^{n+1}}\sum_{i=0}^{n}\binom{n}{i}\mathrm{ext}_A^{n-i}\mathcal{M}_A^{\prime(0)}\mathrm{ext}_B^{i}\mathcal{M}_B^{\prime(0)}. \qquad \text{(A5)}
\end{aligned}$$

Comparing to Eq. (A3) we see that the estimate is an upper bound to the two-electron integral if ext_A and $\mathcal{M}_A^{\prime(0)}$ are chosen such that

$$\mathrm{ext}_A^i\mathcal{M}_A^{\prime(0)} \geq \mathcal{M}_A^{(i)} \quad \forall \quad i: 0 \leq i \leq n_{max} \qquad \text{(A6)}$$

with identical requirements for ext_B and $\mathcal{M}_B^{\prime(0)}$.

In the following we will first examine the case of charge distributions described by a single Gaussian-type function:

$$\begin{aligned}
g(\boldsymbol{r}) &= n_g x^{l_x} y^{l_y} z^{l_z} e^{-\zeta r^2}\\
&= n_g r^{l_x+l_y+l_z} e^{-\zeta r^2}\cos^{l_z}(\theta)\sin^{l_x+l_y}(\theta)\cos^{l_x}(\phi)\sin^{l_y}(\phi),
\end{aligned} \qquad \text{(A7)}$$

where $n_g = e \cdot a_0^{-(l_x+l_y+l_z+3)}$ (e being the elementary charge and a_0 being the Bohr radius) is a trivial prefactor that adjusts the units to be consistent with a charge distribution. We deliberately did not choose a properly normalized function here, since these distributions will be used as non-normalized contributions in the Gaussian product theorem (GPT) later on. It should be noted that the factor n_g (which is 1 in atomic units) is usually considered to be included in parts in the contraction coefficients of the basis functions, the expansion coefficients of the GPT, and the $1/r$ operator as appropriate. The derivation could of course be done either way yielding the same result, but it is conceptually clearer if $g(\boldsymbol{r})$ is a proper charge distribution.

For the case of two simple Gaussian-type distributions (A7) and multipole centers that coincide with the centers of the corresponding charge distribution, a natural choice to fulfill inequality (A6) for $i = 0$ is

$$\mathcal{M}_g^{\prime(0)} = \mathcal{M}_g^{(0)} = \int |g(\boldsymbol{r})|\,\mathrm{d}\boldsymbol{r}. \qquad \text{(A8)}$$

Applying this definition to inequality (A6) for $i > 0$ yields

$$\mathrm{ext}_g^i \geq \frac{\int |g(\boldsymbol{r})r^i|\,\mathrm{d}\boldsymbol{r}}{\int |g(\boldsymbol{r})|\,\mathrm{d}\boldsymbol{r}} = \frac{\int g(r)r^i r^2\mathrm{d}r}{\int g(r)r^2\mathrm{d}r} = \frac{\int r^i r^l e^{-\zeta r^2}r^2\mathrm{d}r}{\int r^l e^{-\zeta r^2}r^2\mathrm{d}r}. \qquad \text{(A9)}$$

where the angle-dependent integrals cancel since they are the same in the numerator and denominator. By substituting $r \rightarrow \frac{r}{\sqrt{\zeta}}$ we obtain

$$\mathrm{ext}_g^i \geq \frac{1}{\zeta^{\frac{i}{2}}}\frac{\int r^i r^l e^{-r^2}r^2\mathrm{d}r}{\int r^l e^{-r^2}r^2\mathrm{d}r} = \frac{1}{\zeta^{\frac{i}{2}}}\frac{\Gamma\{(i+l+3)/2\}}{\Gamma\{(l+3)/2\}} \qquad \text{(A10)}$$

and end up with the requirement for the extents ext_g:

$$\mathrm{ext}_g \geq \frac{1}{\sqrt{\zeta}}\left(\frac{\Gamma\{(i+l+3)/2\}}{\Gamma\{(l+3)/2\}}\right)^{1/i} \quad \forall \quad i: 1 \leq i \leq n_{max}. \qquad \text{(A11)}$$

Numerical tests for $0 \leq l \leq 10$ and $1 \leq i \leq 100$ showed that for constant ζ the maximum of the RHS of inequality (A11) corresponds to $i = n_{max}$ so that

$$\mathrm{ext}_g(l,\zeta) = \frac{1}{\sqrt{\zeta}}\left(\frac{\Gamma\{(n_{max}+l+3)/2\}}{\Gamma\{(l+3)/2\}}\right)^{1/n_{max}} \qquad \text{(A12)}$$

ensures that inequality (A6) is fulfilled.

In practice, one usually uses contracted basis functions which lead to charge distributions that are described by sums over products of primitive basis functions. Each product of primitives can be expanded in a sum of Gaussian-type functions with a common origin but different angular momenta by virtue of the GPT:

$$\begin{aligned}
\Omega_{\mu\nu}(\boldsymbol{r}) &= \sum_{p\in\mu} c_{p\mu}\sum_{q\in\nu} c_{q\nu}\Omega_{pq}(\boldsymbol{r}-\boldsymbol{r}_{\mu\nu,pq}),\\
\Omega_{pq}(\boldsymbol{r}-\boldsymbol{r}_{\mu\nu,pq}) &= \sum_{g}^{\mathrm{GPT}} c_g g(\boldsymbol{r}-\boldsymbol{r}_{\mu\nu,pq})
\end{aligned} \qquad \text{(A13)}$$

with $c_{p\mu}$ and $c_{q\nu}$ being the contraction coefficients (including normalization constants), c_g being the prefactors in the Gaussian product theorem, and $\boldsymbol{r}_{\mu\nu,pq}$ being the distance vector between contracted and primitive centers.

Starting with the RHS of inequality (A6) for contracted basis functions, a bound can be formulated as follows:

$$\begin{aligned}
&\int |\Omega_{\mu\nu}(\boldsymbol{r})|\boldsymbol{r}|^i|\mathrm{d}\boldsymbol{r}\\
&\quad= \int \left|\sum_{p\in\mu} c_{p\mu}\sum_{q\in\nu} c_{q\nu}\Omega_{pq}(\boldsymbol{r}-\boldsymbol{r}_{\mu\nu,pq})|\boldsymbol{r}|^i\right|\mathrm{d}\boldsymbol{r}\\
&\quad\leq \sum_{p\in\mu}\sum_{q\in\nu}|c_{p\mu}c_{q\nu}|\int |\Omega_{pq}(\boldsymbol{r}-\boldsymbol{r}_{\mu\nu,pq})|\boldsymbol{r}|^i|\mathrm{d}\boldsymbol{r}\\
&\quad= \sum_{p\in\mu}\sum_{q\in\nu}|c_{p\mu}c_{q\nu}|\int |\Omega_{pq}(\boldsymbol{r})|\boldsymbol{r}+\boldsymbol{r}_{\mu\nu,pq}|^i|\mathrm{d}\boldsymbol{r}\\
&\quad\leq \sum_{p\in\mu}\sum_{q\in\nu}\sum_{g}^{\mathrm{GPT}}|c_{p\mu}c_{q\nu}c_g|\int |g(\boldsymbol{r})|\boldsymbol{r}+\boldsymbol{r}_{\mu\nu,pq}|^i|\mathrm{d}\boldsymbol{r}
\end{aligned}$$

This article is copyrighted as indicated in the article. Reuse of AIP content is subject to the terms at: http://scitation.aip.org/termsconditions. Downloaded to IP: 92.230.182.222 On: Sat, 14 Dec 2013 21:59:43

$$
\begin{aligned}
&\leq \sum_{p\in\mu}\sum_{q\in\nu}\sum_{g}^{\mathrm{GPT}} |c_{p\mu}c_{q\nu}c_g| \int |g(\boldsymbol{r})(r + r_{\mu\nu,pq})^i|\mathrm{d}\boldsymbol{r} \\
&= \sum_{p\in\mu}\sum_{q\in\nu}\sum_{g}^{\mathrm{GPT}} |c_{p\mu}c_{q\nu}c_g| \sum_{t=0}^{i}\binom{i}{t} r_{\mu\nu,pq}^{i-t} \int |g(\boldsymbol{r})r^t|\mathrm{d}\boldsymbol{r} \\
&\leq \sum_{p\in\mu}\sum_{q\in\nu}\sum_{g}^{\mathrm{GPT}} |c_{p\mu}c_{q\nu}c_g| \sum_{t=0}^{i}\binom{i}{t} r_{\mu\nu,pq}^{i-t}\mathrm{ext}_g^t \int |g(\boldsymbol{r})|\mathrm{d}\boldsymbol{r} \\
&= \sum_{p\in\mu}\sum_{q\in\nu}\sum_{g}^{\mathrm{GPT}} |c_{p\mu}c_{q\nu}c_g| (r_{\mu\nu,pq} + \mathrm{ext}_g)^i \int |g(\boldsymbol{r})|\mathrm{d}\boldsymbol{r},
\end{aligned}
\tag{A14}
$$

where ext_g has to fulfill Eq. (A12). Recalling inequality (A6) and substituting the RHS with the derived upper bound yields

$$
\mathrm{ext}_{\mu\nu}^i \mathcal{M}_{\mu\nu}^{\prime(0)} \geq \sum_{p\in\mu}\sum_{q\in\nu}\sum_{g}^{\mathrm{GPT}} |c_{p\mu}c_{q\nu}c_g|(r_{\mu\nu,pq} + \mathrm{ext}_g)^i \times \int |g(\boldsymbol{r})|\,\mathrm{d}\boldsymbol{r}. \tag{A15}
$$

Defining

$$
\mathcal{M}_{\mu\nu}^{\prime(0)} = \sum_{p\in\mu}\sum_{q\in\nu}\sum_{g}^{\mathrm{GPT}} |c_{p\mu}c_{q\nu}c_g| \int |g(\boldsymbol{r})|\,\mathrm{d}\boldsymbol{r} \tag{A16}
$$

to satisfy inequality (A15) for the case $i = 0$ leads to

$$
\begin{aligned}
&\mathrm{ext}_{\mu\nu}^i \mathcal{M}_{\mu\nu}^{\prime(0)} \geq \sum_{p\in\mu}\sum_{q\in\nu}\sum_{g}^{\mathrm{GPT}} |c_{p\mu}c_{q\nu}c_g|(r_{\mu\nu,pq} + \mathrm{ext}_g)^i \mathcal{M}_{pq}^{(0)}, \\
&\mathrm{ext}_{\mu\nu} \geq \left(\frac{\sum_{p\in\mu}\sum_{q\in\nu}\sum_{g}^{\mathrm{GPT}} |c_{p\mu}c_{q\nu}c_g|(r_{\mu\nu,pq} + \mathrm{ext}_g)^i \mathcal{M}_{pq}^{(0)}}{\mathcal{M}_{\mu\nu}^{\prime(0)}}\right)^{1/i}
\end{aligned}
\tag{A17}
$$

for all i with $1 \leq i \leq n_{max}$.

With the absolute multipoles Eq. (A16) and extents that satisfy inequality (A17), the MBIE estimates (Eq. (1)) are bounds to the multipole terms up to order n_{max} but furthermore all multipole terms up to infinite order are taken into account in the estimates owing to the infinite geometric series (see Eq. (A5)). The higher multipole terms are still estimated very conservatively and therefore n_{max} can be chosen much smaller than the maximum order in CFMM theory. In this work we used $n_{max} = 5$ throughout and no underestimations were observed (see Sec. III A).

1. Implementational details

At the beginning of all calculations one sets up a list of the factors

$$
f(l) = \left(\frac{\Gamma\{(n_{max} + l + 3)/2\}}{\Gamma\{(l + 3)/2\}}\right)^{1/n_{max}} \tag{A18}
$$

for given n_{max} and all occurring total angular momenta $l = l_x + l_y + l_z$ so that the individual primitive extents (A12) are easily accessible by scaling with $\frac{1}{\sqrt{\zeta}}$, where ζ is the primitive pair exponent $\zeta = \zeta_p + \zeta_q$.

The absolute monopole integrals over primitive Gaussians $g(\boldsymbol{r})$ can be conveniently calculated in spherical coordinates (skipping the trivial prefactor $n_g = 1$ in atomic units):

$$
\begin{aligned}
\int |g(\boldsymbol{r})|\,\mathrm{d}\boldsymbol{r} &= R\cdot\Theta\cdot\Phi, \\
R &= \int r^{l_x+l_y+l_z+2}e^{-\zeta r^2}\mathrm{d}r \\
&= \zeta^{-\frac{l_x+l_y+l_z+3}{2}} \int r^{l_x+l_y+l_z+2}e^{-r^2}\mathrm{d}r, \\
\Theta &= \int |\cos^{l_z}(\theta)\sin^{l_x+l_y+1}(\theta)|\mathrm{d}\theta, \\
\Phi &= \int |\cos^{l_x}(\phi)\sin^{l_y}(\phi)|\mathrm{d}\phi.
\end{aligned}
\tag{A19}
$$

In the evaluation of R the substitution $r \rightarrow \frac{r}{\sqrt{\zeta}}$ was used. Putting everything together we obtain

$$
\int |g(\boldsymbol{r})|\,\mathrm{d}\boldsymbol{r} = \zeta^{-\frac{l_x+l_y+l_z+3}{2}} f(l_x, l_y, l_z). \tag{A20}
$$

The factors $f(l_x, l_y, l_z)$ are also tabulated at the beginning of the calculation, so that the evaluation of primitive absolute multipoles is cheap later on. The contracted absolute multipoles are then determined according to Eq. (A16). Calculation of contracted extents finally requires evaluation of the RHS of Eq. (A17) for all n_{max} possible values of i.

APPENDIX B: DEFINITIONS OF CENTERS AND WELL-SEPARATEDNESS EXTENTS

Since the choice of the multipole centers is not unique, we provide the explicit definitions we used in our implementation. The center of primitive charge distributions is calculated as

$$
\vec{r}_{pq} = \frac{\zeta_p\vec{r}_p + \zeta_q\vec{r}_q}{\zeta_p + \zeta_q}, \tag{B1}
$$

while the contracted centers are defined as

$$
\vec{r}_{\mu\nu} = \frac{\sum\limits_{p\in\mu,q\in\nu} |c_p c_q|\vec{r}_{pq}}{\sum\limits_{p\in\mu,q\in\nu} |c_p c_q|} \tag{B2}
$$

with the contraction coefficients c_p and c_q

The well-separatedness extents of primitive charge distributions are calculated as in CFMM theory[10]

$$
\mathrm{ext}'_{pq} = \sqrt{\frac{2}{\zeta_p + \zeta_q}}\mathrm{erfc}^{-1}(\vartheta_{thr}). \tag{B3}
$$

with ζ_p and ζ_q being the exponents of the primitive basis functions. To ensure well separatedness for contracted charge distributions, we add the distance of the primitive and contracted center $r_{\mu\nu,pq}$ to the corresponding primitive extent and

This article is copyrighted as indicated in the article. Reuse of AIP content is subject to the terms at: http://scitation.aip.org/termsconditions. Downloaded to IP: 92.230.182.222 On: Sat, 14 Dec 2013 21:59:43

take the maximum of these values:

$$\mathrm{ext}'_{\mu\nu} = \max_{p\in\mu,q\in\nu} \left\{\mathrm{ext}'_{pq} + r_{\mu\nu,pq}\right\}. \tag{B4}$$

APPENDIX C: CONNECTION BETWEEN QQR AND MBIE

For the trivial case of primitive s-functions there is a simple relation between the QQR and MBIE estimate through

$$Q_{s_1s_2} = \left(\frac{2}{\pi}\right)^{(1/4)} (\zeta_{s_1} + \zeta_{s_2})^{(1/4)} \mathcal{M}_{s_1s_2}. \tag{C1}$$

Similar relations might be derived for higher angular momenta in the special case of charge distributions described by single Gaussian-type distributions. However, this is not possible for the general case where there is a sum of contributions either due to contracted basis functions or owing to the Gaussian product theorem in the case where the centers of primitive functions do not coincide. For these general cases, the MBIE derivation requires the use of absolute values of the contraction/expansion coefficients to reduce the absolute multipole integrals to primitive contributions (see Eq. (A14)). This contrasts to the Schwarz integrals, where all coefficients can be applied with the appropriate sign and therefore primitive contributions might partially cancel out, whereas a positive value of the final integral is ensured. Therefore, a direct connection between the Schwarz and MBIE integrals cannot be established for the general case. Furthermore, it should be noted that the overestimations, that occur by applying the absolute values of the contraction/expansion coefficients in the MBIE integrals, show one of the main disadvantages of MBIE compared to the QQR estimate, for which all integrals can be evaluated exactly.

APPENDIX D: ORIGIN OF THE DIMENSIONAL FACTOR

In the QQR integral estimate Eq. (2) the right hand side includes a factor of 1 a.u. of length that was skipped in the expression assuming all quantities in atomic units. Concerning the origin of this dimensional factor, one can argue that it appears since the $1/R$ factor needs to be dimensionless, if one considers QQR as a distance scaled Schwarz estimate. Nevertheless, we briefly discuss in the following, how the factor evolves if one starts the route to the QQR estimates from the two-electron integral that should be estimated.

We consider a two-electron integral with charge distributions denoted as Ω_A and Ω_B that have centers $\mathbf{R}_A$ and $\mathbf{R}_B$. For simplicity we choose the coordinate system such that both centers are located on one of the coordinate axis, which is possible without loss of generality, since we discuss a single integral. In this case, the interelectronic distance r_{12}, that occurs in the Coulomb operator, can be considered as a function of the bra-ket distance $R_{AB} = |\mathbf{R}_A - \mathbf{R}_B|$ as well as the electron coordinates relative to the bra and ket centers, $\boldsymbol{r}_{1A} = \boldsymbol{r}_1 - \mathbf{R}_A$ and $\boldsymbol{r}_{2B} = \boldsymbol{r}_2 - \mathbf{R}_B$. The two-electron integral therefore depends implicitly on the bra-ket distance through the function r_{12}. To get an explicit dependence on the bra-ket separation (for large values) we use the functional dependence on R_{AB}, derived from the multipole expansion, for an empirical separation:

$$\begin{aligned}(\Omega_A|\Omega_B) &= \int \frac{\Omega_A(\boldsymbol{r}_{1A})\Omega_B(\boldsymbol{r}_{2B})}{r_{12}(\boldsymbol{r}_{1A}, \boldsymbol{r}_{2B}, R_{AB})} \mathrm{d}r_1\mathrm{d}r_2 \\ &\approx \int \frac{\Omega_A(\boldsymbol{r}_{1A})\Omega_B(\boldsymbol{r}_{2B})}{r_{12}(\boldsymbol{r}_{1A}, \boldsymbol{r}_{2B}, 0)} \mathrm{d}r_1\mathrm{d}r_2 \cdot g(R_{AB}),\end{aligned} \tag{D1}$$

where the function $g(R_{AB})$ describes the asymptotic 1/R decay known from MBIE theory. The dependence on R_{AB} is completely removed from the remaining integral with the last argument of the function r_{12}, i.e., R_{AB}, set to zero. As the unit of length connected to R_{AB} remains in the integral (the zero value is dimensionful), the values of the function $g(R_{AB})$ need to be dimensionless, so that the final form is

$$g(R_{AB}) = \frac{a_0}{R_{AB} - \mathrm{ext}'_{\mu\nu} - \mathrm{ext}'_{\lambda\sigma}} \tag{D2}$$

with a_0 being the Bohr radius, which is 1 in atomic units and therefore not listed in Eq. (2). It should be further noted that the final integral in Eq. (D1) is identical to the two-electron integral for the case that one of the charge distributions was translated such that the centers of A and B coincide. We can therefore efficiently estimate this new integral using the common Schwarz bound, so that the product of this estimated intermediate and the function $g(R_{AB})$ directly yields the final expression of the QQR estimate Eq. (2).

[1] A. Szabo and N. S. Ostlund, *Modern Quantum Chemistry: Introduction to Advanced Electronic Structure Theory* (Macmillan, New York, 1982).
[2] R. G. Parr and W. Yang, *Density-Functional Theory of Atoms and Molecules* (Oxford University Press, New York, 1994).
[3] T. Helgaker, P. Jørgensen, and J. Olsen, *Molecular Electronic-Structure Theory* (Wiley-VCH, Weinheim, 2000).
[4] R. Ahlrichs, Theor. Chim. Acta **33**, 157 (1974).
[5] J. Almlöf, K. Faegri, and K. Korsell, J. Comput. Chem. **3**, 385 (1982).
[6] D. Cremer and J. Gauss, J. Comput. Chem. **7**, 274 (1986).
[7] J. L. Whitten, J. Chem. Phys. **58**, 4496 (1973).
[8] M. Häser and R. Ahlrichs, J. Comput. Chem. **10**, 104 (1989).
[9] P. M. W. Gill, B. G. Johnson, and J. A. Pople, Chem. Phys. Lett. **217**, 65 (1994).
[10] C. A. White, B. G. Johnson, P. M. W. Gill, and M. Head-Gordon, Chem. Phys. Lett. **230**, 8 (1994).
[11] M. Challacombe, E. Schwegler, and J. Almlöf, J. Chem. Phys. **104**, 4685 (1996).
[12] M. C. Strain, G. E. Scuseria, and M. J. Frisch, Science **271**, 51 (1996).
[13] E. Schwegler, M. Challacombe, and M. Head-Gordon, J. Chem. Phys. **106**, 9708 (1997).
[14] C. Ochsenfeld, C. A. White, and M. Head-Gordon, J. Chem. Phys. **109**, 1663 (1998).
[15] E. Schwegler and M. Challacombe, J. Chem. Phys. **111**, 6223 (1999).
[16] C. Ochsenfeld, J. Kussmann, and D. S. Lambrecht, in *Reviews in Computational Chemistry*, edited by K. B. Lipkowitz and T. R. Cundari (Wiley-VCH, 2007), Vol. 23, pp. 1–81.
[17] C. A. White, B. G. Johnson, P. M. W. Gill, and M. Head-Gordon, Chem. Phys. Lett. **253**, 268 (1996).
[18] C. Ochsenfeld, Chem. Phys. Lett. **327**, 216 (2000).
[19] B. G. Johnson, C. A. White, Q. Zhang, B. Chen, R. L. Graham, P. M. W. Gill, and M. Head-Gordon, in *Recent Developments and Applications of Modern Density Functional Theory*, edited by J. Seminario (Elsevier, Amsterdam, 1996), pp. 441–464.
[20] P. Sałek, S. Høst, L. Thøgersen, P. Jørgensen, P. Manninen, J. Olsen, B. Jansík, S. Reine, F. Pawłowski, E. Tellgren, T. Helgaker, and S. Coriani, J. Chem. Phys. **126**, 114110 (2007).
[21] E. Rudberg, E. H. Rubensson, and P. Sałek, J. Chem. Theory Comput. **7**, 340 (2011).

This article is copyrighted as indicated in the article. Reuse of AIP content is subject to the terms at: http://scitation.aip.org/termsconditions. Downloaded to IP: 92.230.182.222 On: Sat, 14 Dec 2013 21:59:43

[22] C. Ochsenfeld, J. Kussmann, and F. Koziol, Angew. Chem., Int. Ed. **43**, 4485 (2004).

[23] J. Zienau, J. Kussmann, and C. Ochsenfeld, Mol. Phys. **108**, 333 (2010).

[24] C. Ochsenfeld and M. Head-Gordon, Chem. Phys. Lett. **270**, 399 (1997).

[25] J. Kussmann and C. Ochsenfeld, J. Chem. Phys. **127**, 054103 (2007).

[26] M. Beer, J. Kussmann, and C. Ochsenfeld, J. Chem. Phys. **134**, 74102 (2011).

[27] D. S. Lambrecht and C. Ochsenfeld, J. Chem. Phys. **123**, 184101 (2005).

[28] J. Almlöf, Chem. Phys. Lett. **181**, 319 (1991).

[29] M. Häser and J. Almlöf, J. Chem. Phys. **96**, 489 (1992).

[30] M. Häser, Theor. Chim. Acta **87**, 147 (1993).

[31] A. K. Wilson and J. Almlöf, Theor. Chim. Acta **95**, 49 (1997).

[32] P. Y. Ayala and G. E. Scuseria, J. Chem. Phys. **110**, 3660 (1999).

[33] D. S. Lambrecht, B. Doser, and C. Ochsenfeld, J. Chem. Phys. **123**, 184102 (2005).

[34] B. Doser, D. S. Lambrecht, J. Kussmann, and C. Ochsenfeld, J. Chem. Phys. **130**, 64107 (2009).

[35] B. Doser, J. Zienau, L. Clin, D. S. Lambrecht, and C. Ochsenfeld, Z. Phys. Chem. **224**, 397 (2010).

[36] P. Jurecka, J. Sponer, J. Cerný, and P. Hobza, Phys. Chem. Chem. Phys. **8**, 1985 (2006).

[37] See http://www.cup.uni-muenchen.de/pc/ochsenfeld/download.html for structure files.

[38] S. A. Maurer, D. S. Lambrecht, and C. Ochsenfeld, "Efficient integral screening in linear-scaling Møller-Plesset perturbation theory" (unpublished).

[39] J. Almlöf, in *Lecture Notes in Quantum Chemistry II*, Lecture Notes in Chemistry, Vol. 64, edited by B. Roos (Springer, Berlin, 1994).

[40] Y. Shao, L. F. Molnar, Y. Jung, J. Kussmann, C. Ochsenfeld, S. T. Brown, A. T. Gilbert, L. V. Slipchenko, S. V. Levchenko, D. P. O'Neill, R. A. DiStasio, Jr., R. C. Lochan, T. Wang, G. J. Beran, N. A. Besley, J. M. Herbert, C. Yeh Lin, T. Van Voorhis, S. H. Chien, A. Sodt, R. P. Steele, V. A. Rassolov, P. E. Maslen, P. P. Korambath, R. D. Adamson, B. Austin, J. Baker, E. F. C. Byrd, H. Dachsel, R. J. Doerksen, A. Dreuw, B. D. Dunietz, A. D. Dutoi, T. R. Furlani, S. R. Gwaltney, A. Heyden, S. Hirata, C.-P. Hsu, G. Kedziora, R. Z. Khalliulin, P. Klunzinger, A. M. Lee, M. S. Lee, W. Liang, I. Lotan, N. Nair, B. Peters, E. I. Proynov, P. A. Pieniazek, Y. M. Rhee, J. Ritchie, E. Rosta, C. D. Sherrill, A. C. Simmonett, J. E. Subotnik, H. L. Woodcock III, W. Zhang, A. T. Bell, A. K. Chakraborty, D. M. Chipman, F. J. Keil, A. Warshel, W. J. Hehre, H. F. Schaefer III, J. Kong, A. I. Krylov, P. M. W. Gill, and M. Head-Gordon, Phys. Chem. Chem. Phys. **8**, 3172 (2006).

[41] M. Head-Gordon and J. A. Pople, J. Chem. Phys. **89**, 5777 (1988).

[42] P. Pulay, Chem. Phys. Lett. **73**, 393 (1980).

[43] T. Van Voorhis and M. Head-Gordon, Mol. Phys. **100**, 1713 (2002).

[44] W. J. Hehre, R. Ditchfield, and J. A. Pople, J. Chem. Phys. **56**, 2257 (1972).

[45] P. C. Hariharan and J. A. Pople, Theor. Chim. Acta **28**, 213 (1973).

[46] A. Schäfer, H. Horn, and R. Ahlrichs, J. Chem. Phys. **97**, 2571 (1992).

[47] T. H. Dunning, J. Chem. Phys. **90**, 1007 (1989).

[48] R. A. Kendall, T. H. Dunning, and R. J. Harrison, J. Chem. Phys. **96**, 6796 (1992).

[49] P. M. W. Gill, B. G. Johnson, and J. A. Pople, Chem. Phys. Lett. **209**, 506 (1993).

[50] See supplementary material at http://dx.doi.org/10.1063/1.3693908 for remaining figures and data tables.

This article is copyrighted as indicated in the article. Reuse of AIP content is subject to the terms at: http://scitation.aip.org/termsconditions. Downloaded to IP: 92.230.182.222 On: Sat, 14 Dec 2013 21:59:43

Supplementary Information to ”Distance-Dependent Schwarz-Based Integral Estimates for Two-Electron Integrals — Reliable Tightness vs. Rigorous Upper Bounds”

Simon A. Maurer, Daniel S. Lambrecht[a)], Denis Flaig, and Christian Ochsenfeld[b)]

Chair of Theoretical Chemistry, Department of Chemistry,
University of Munich (LMU), Butenandtstr. 7, D-81377 München, Germany

[a)] Present address: Dept. of Chemistry, University of California, Berkeley, CA 94720, USA

[b)] Electronic mail: christian.ochsenfeld@uni-muenchen.de

I. ERROR STATISTICS

	MBIE					QQR				
Basis	$\overline{F}$	F_{min}	F_{max}	$\sigma(F)_{avg}$	$\sigma(log(F))_{avg}$	$\overline{F}$	F_{min}	F_{max}	$\sigma(F)_{avg}$	$\sigma(log(F))_{avg}$
6-31G*	3.23	1.00	46.4	1.37	0.18	1.63	0.45	16.6	0.79	0.17
SV(P)	7.71	1.00	$1{\cdot}10^5$	85.26	0.38	3.18	0.37	$7{\cdot}10^4$	42.76	0.34
cc-pVTZ	9.86	1.00	$6{\cdot}10^5$	119.27	0.39	3.20	0.33	$1{\cdot}10^5$	34.40	0.34

TABLE I. Comparison of error statistics for MBIE and QQR far-field integrals. The statistic is restricted to cases where the MBIE/QQR estimate was actually smaller than the corresponding Schwarz estimate. Shown are the statistics of the ratio $F = I_{estimate}/I_{exact}$ as the average $\overline{F}$, its smallest and largest values (F_{min},F_{max}) and the standard deviations of F and $log(F)$ averaged over all iterations.

II. CALCULATIONS ON S22 TEST SET

A. Results for the remaining basis sets

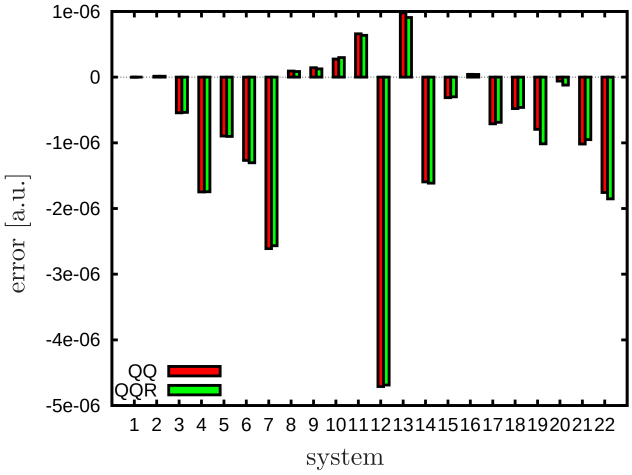

FIG. 1. Errors in S22 test set calculations with Schwarz and QQR screening with 6-31G* basis set ($\vartheta_K = 10^{-8}$). Reference for the errors are QQ ($\vartheta_K = 10^{-10}$) calculations.

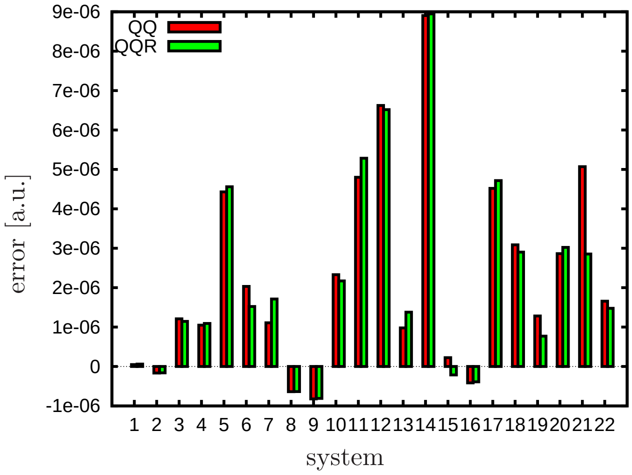

FIG. 2. Errors in S22 test set calculations with Schwarz and QQR screening with cc-pVTZ basis set ($\vartheta_K = 10^{-8}$). Reference for the errors are QQ ($\vartheta_K = 10^{-10}$) calculations.

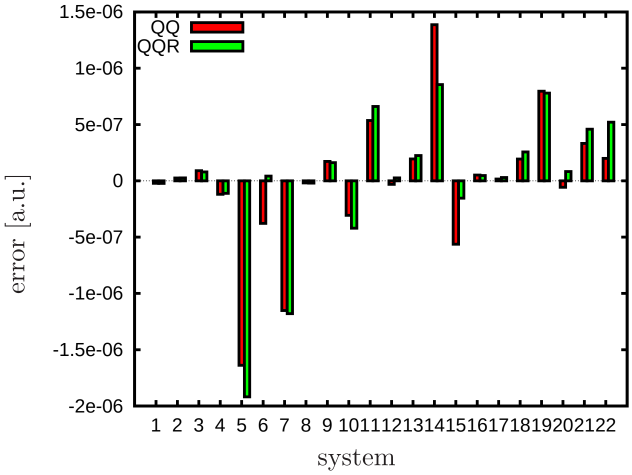

FIG. 3. Errors in S22 test set calculations with Schwarz and QQR screening with aug-cc-pVTZ basis. A tighter threshold ($\vartheta_K = 10^{-9}$) is applied. Reference for the errors are QQ ($\vartheta_K = 10^{-10}$) calculations.

B. Distance dependent error fluctuation

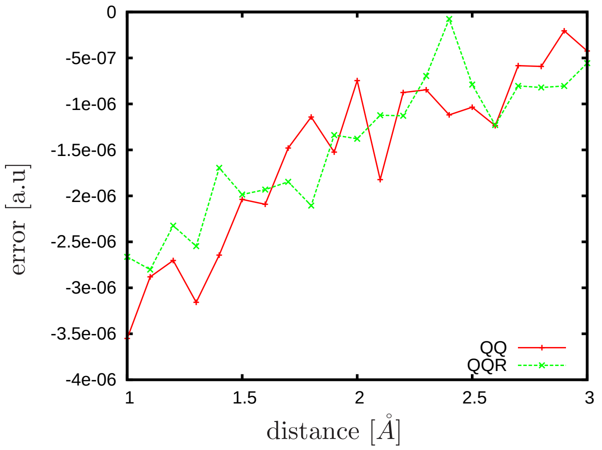

FIG. 4. Errors of Schwarz and QQR screening with respect to the distance along the h-bonds in the h-bonded uracil dimer (#5) of the S22 test set with aug-cc-pVTZ basis ($\vartheta_K = 10^{-9}$).

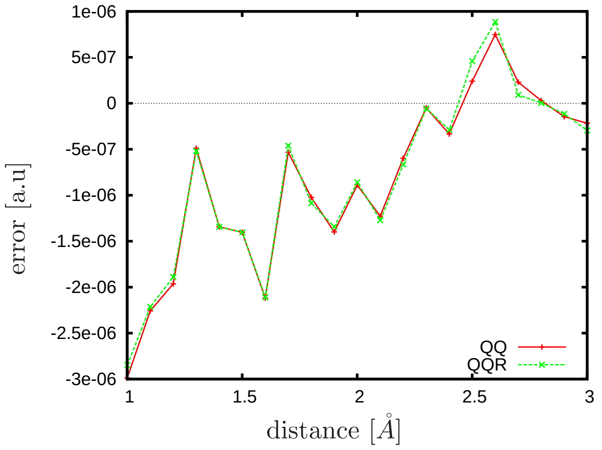

FIG. 5. Errors of Schwarz and QQR screening with respect to the distance of the frontmost hydrogen to the second benzene plane in the t-shaped benzene dimer (#20) of the S22 test set with 6-31G* basis ($\vartheta_K = 10^{-8}$).

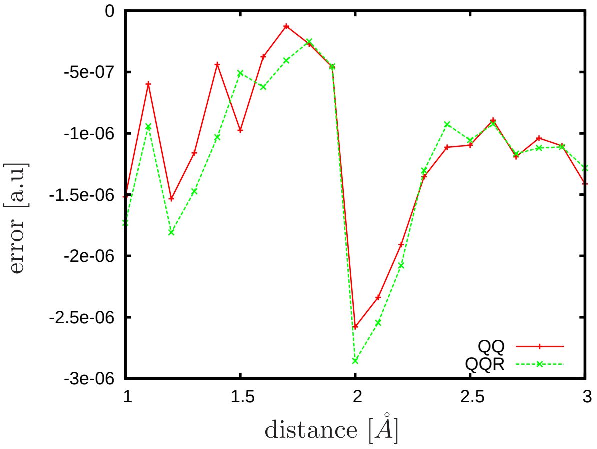

FIG. 6. Errors of Schwarz and QQR screening with respect to the distance along the h-bond in the 2-pyridoxine · 2-aminopyridine complex (#6) of the S22 test set with SV(P) basis ($\vartheta_K = 10^{-8}$).

C. Plots of error to integral number

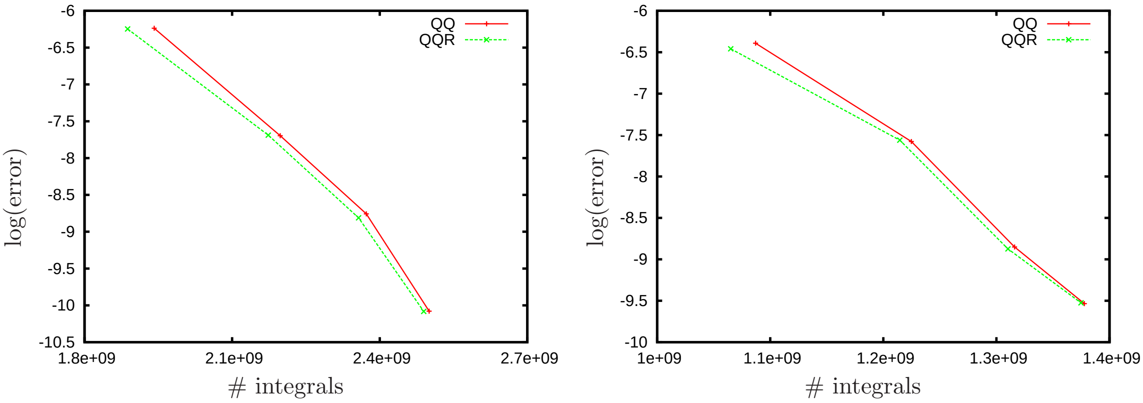

(a) #1

(b) #2

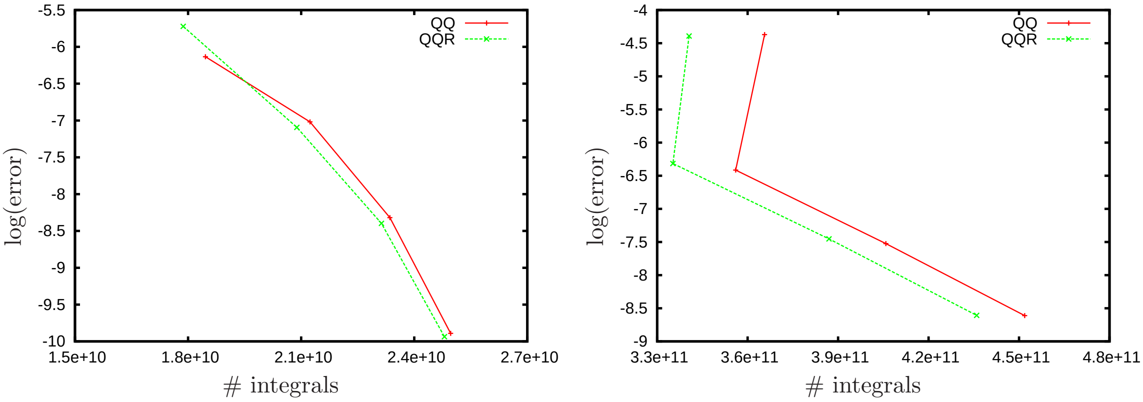

(c) #3

(d) #6 (additional iteration for $\vartheta_K = 10^{-8}$)

FIG. 7. Error vs. number of integrals for Schwarz and QQR screening with different thresholds ϑ_K for systems of the S22 test set with aug-cc-pVTZ basis set. The points correspond to calculations with ϑ_K values of 10^{-8}, 10^{-9}, 10^{-10}, and 10^{-11}.

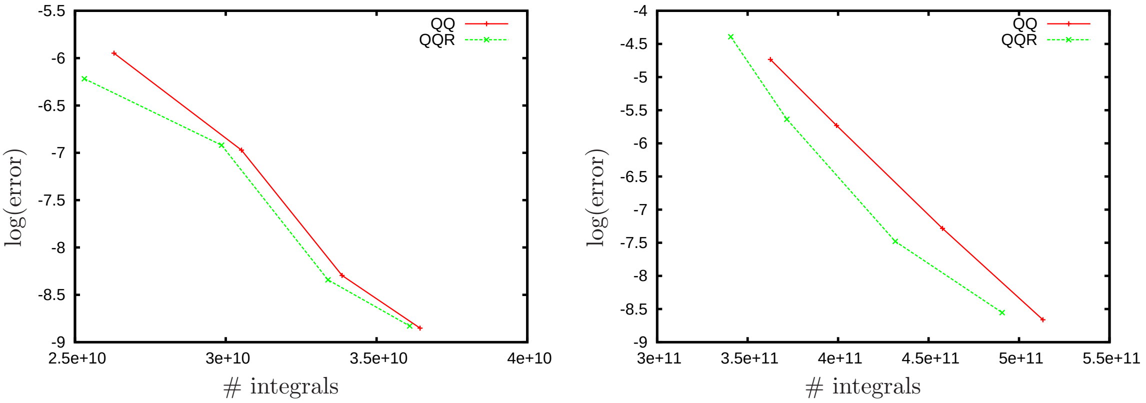

(a) #4 (b) #5

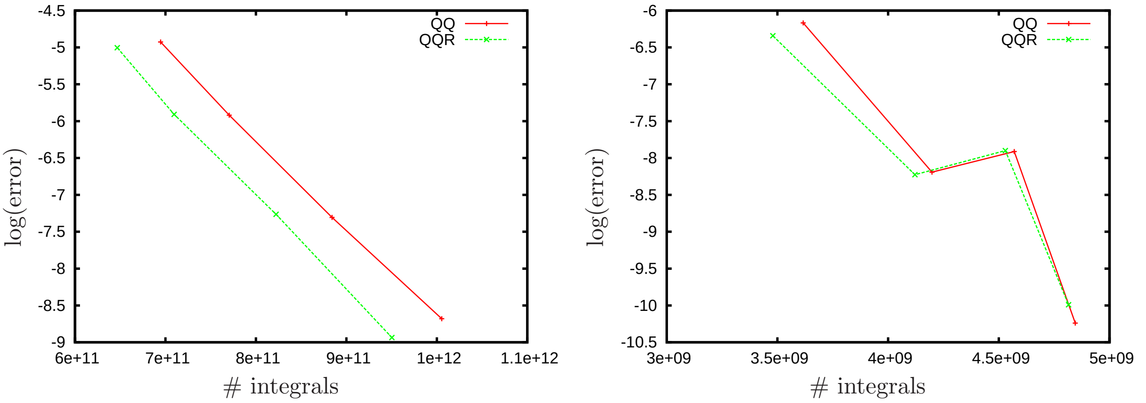

(c) #7 (d) #8

FIG. 8. Error vs. number of integrals for Schwarz and QQR screening with different thresholds ϑ_K for systems of the S22 test set with aug-cc-pVTZ basis set. The points correspond to calculations with ϑ_K values of 10^{-8}, 10^{-9}, 10^{-10}, and 10^{-11}.

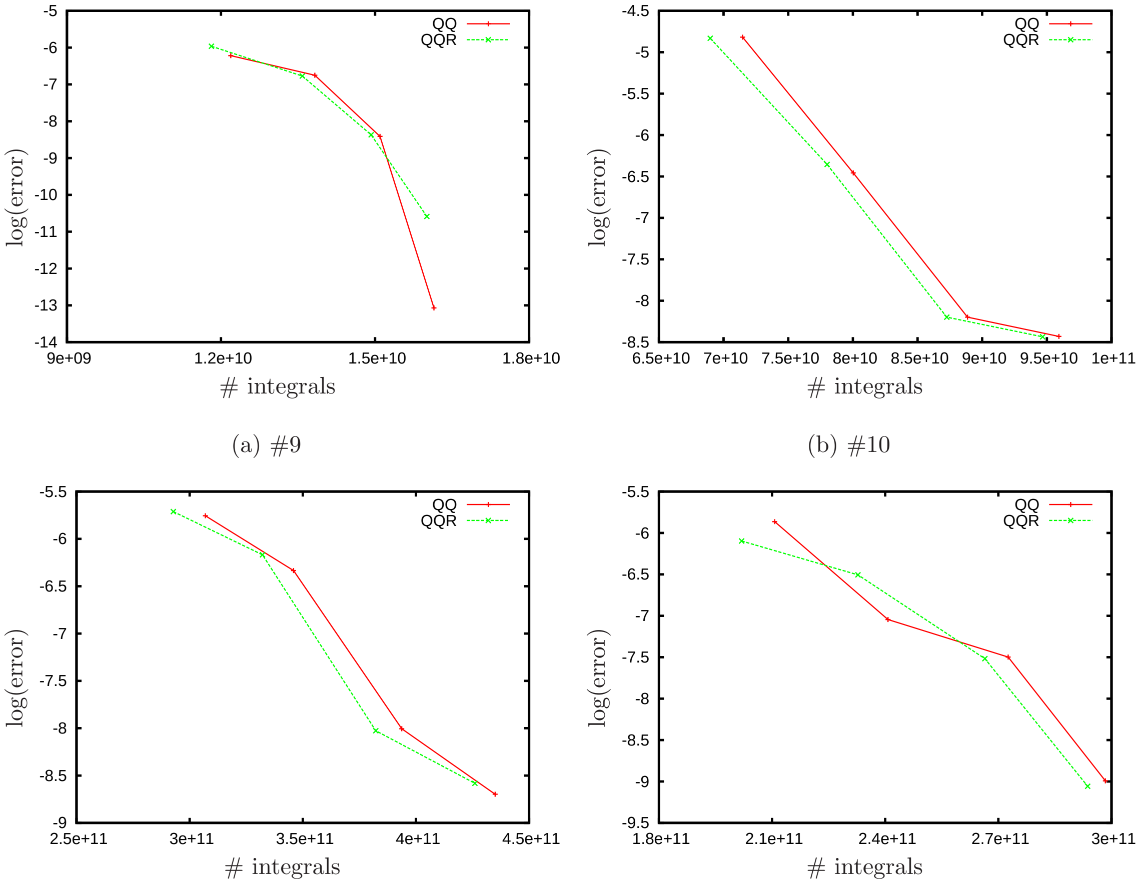

(a) #9

(b) #10

(c) #11

(d) #12

FIG. 9. Error vs. number of integrals for Schwarz and QQR screening with different thresholds ϑ_K for systems of the S22 test set with aug-cc-pVTZ basis set. The points correspond to calculations with ϑ_K values of 10^{-8}, 10^{-9}, 10^{-10}, and 10^{-11}.

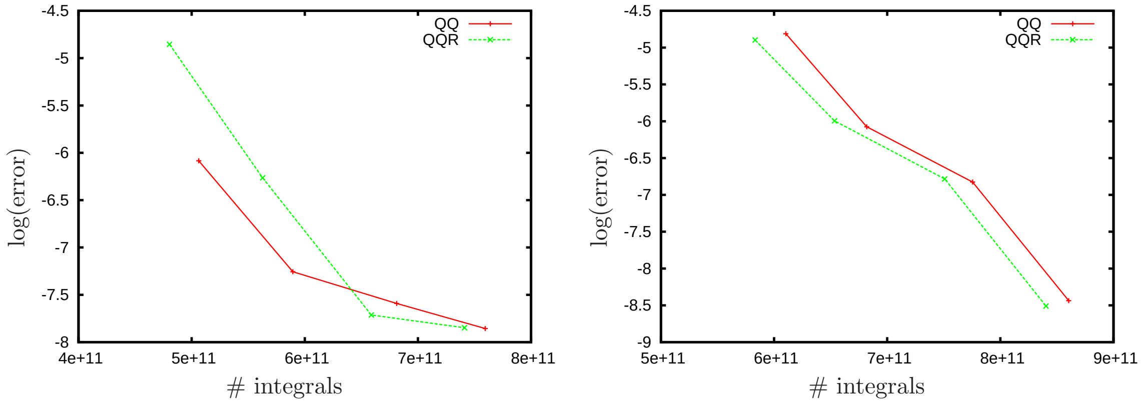

(a) #13

(b) #14

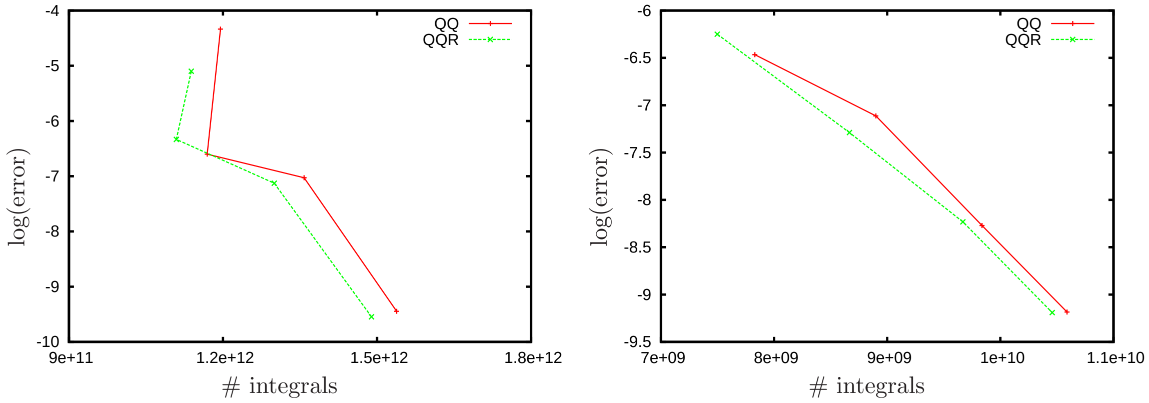

(c) #15 (additional iteration for $\vartheta_K = 10^{-8}$)

(d) #16

FIG. 10. Error vs. number of integrals for Schwarz and QQR screening with different thresholds ϑ_K for systems of the S22 test set with aug-cc-pVTZ basis set. The points correspond to calculations with ϑ_K values of 10^{-8}, 10^{-9}, 10^{-10}, and 10^{-11}.

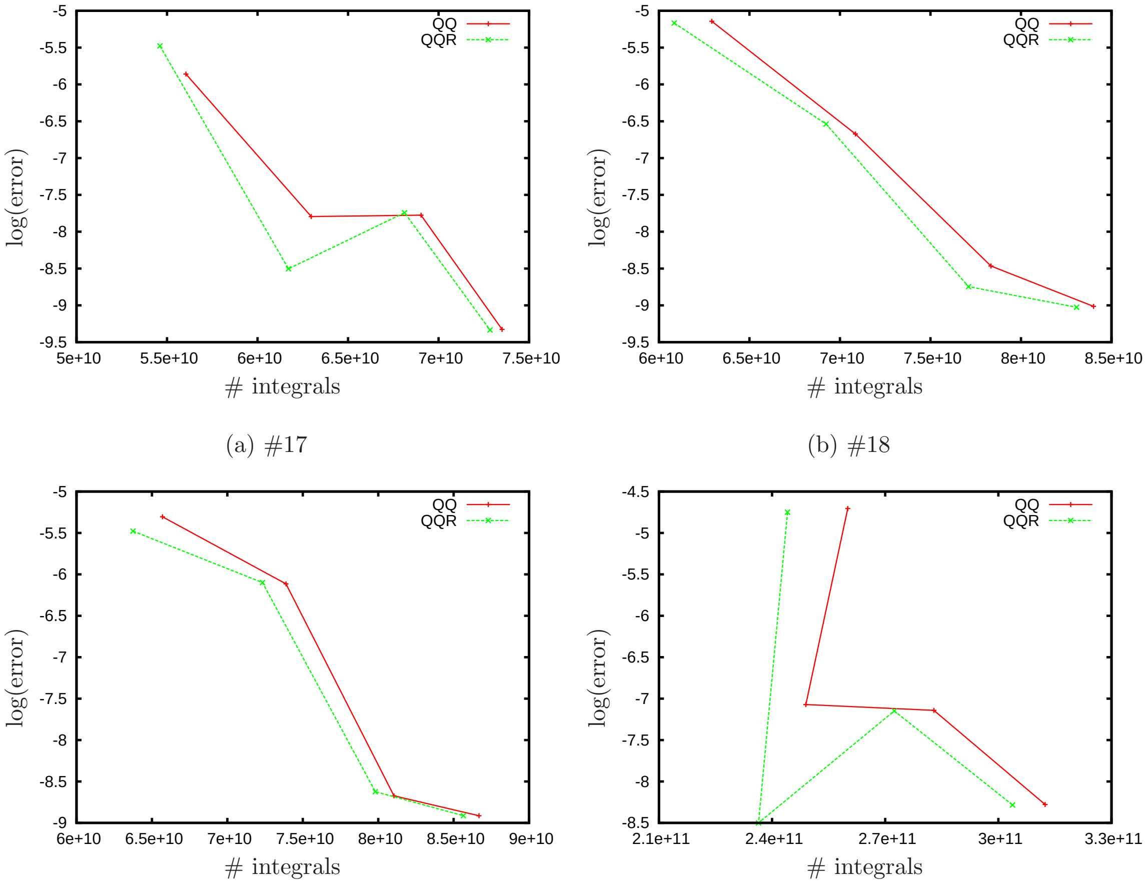

(a) #17

(b) #18

(c) #19

(d) #20 (additional iteration for $\vartheta_K = 10^{-8}$)

FIG. 11. Error vs. number of integrals for Schwarz and QQR screening with different thresholds ϑ_K for systems of the S22 test set with aug-cc-pVTZ basis set. The points correspond to calculations with ϑ_K values of 10^{-8}, 10^{-9}, 10^{-10}, and 10^{-11}.

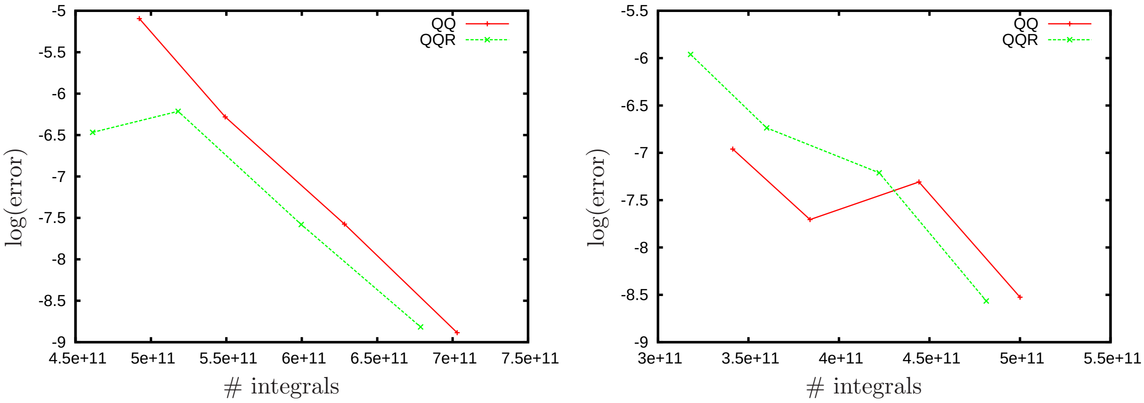

(a) #21 (b) #22

FIG. 12. Error vs. number of integrals for Schwarz and QQR screening with different thresholds ϑ_K for systems of the S22 test set with aug-cc-pVTZ basis set. The points correspond to calculations with ϑ_K values of 10^{-8}, 10^{-9}, 10^{-10}, and 10^{-11}.

III. CALCULATIONS ON THE NEW LARGE SCALE BENCHMARK SET

The zeolithe LTA system is excluded for the SV(P) basis, since even the Schwarz calculation (QQ, $\vartheta_K = 10^{-9}$) did not converge with the same number of iterations as the reference (QQ, $\vartheta_K = 10^{-10}$). For the cc-pVTZ basis the reference calculation of the zeolithe SOD system did not converge, so that we discarded this case, since the origin of this behavior is in no relation with our present work.

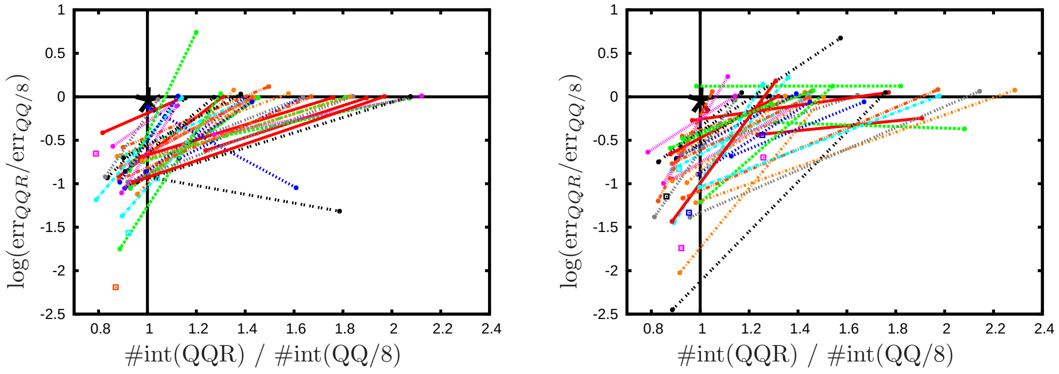

(a)6-31G*

(b)SV(P)

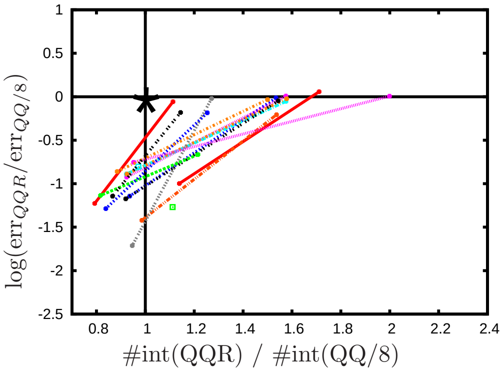

(c)cc-pVTZ

FIG. 13. Error and speedup (via ratio of integrals) for QQR calculations (right endpoint: $\vartheta_K = 10^{-8}$, left endpoint: $\vartheta_K = 10^{-9}$) of the whole test set relative to the values of a pure Schwarz calculation with $\vartheta_K = 10^{-8}$. The Schwarz reference is indicated as a black asterisk. Values to the right of this reference point indicate increased speed, while values below the reference indicate improved accuracy.

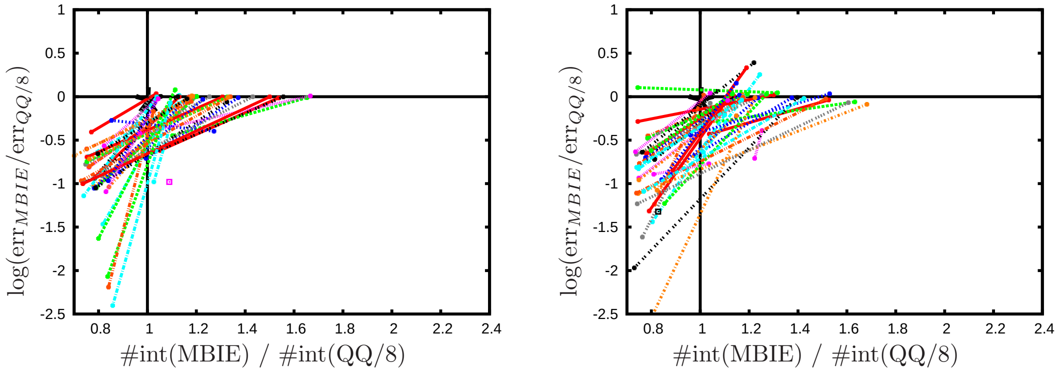

(a)6-31G* (b)SV(P)

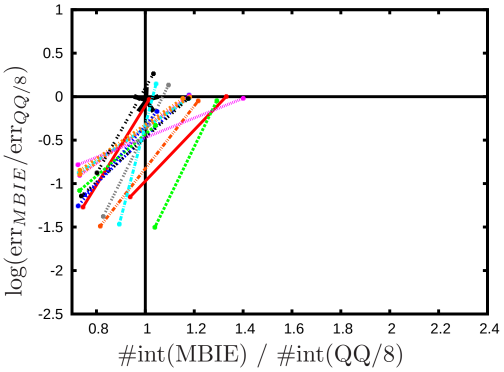

(c)cc-pVTZ

FIG. 14. Error and speedup (via ratio of integrals) for MBIE calculations (right endpoint: $\vartheta_K = 10^{-8}$, left endpoint: $\vartheta_K = 10^{-9}$) of the whole test set relative to the values of a pure Schwarz calculation with $\vartheta_K = 10^{-8}$. The Schwarz reference is indicated as a black asterisk. Values to the right of this reference point indicate increased speed, while values below the reference indicate improved accuracy.

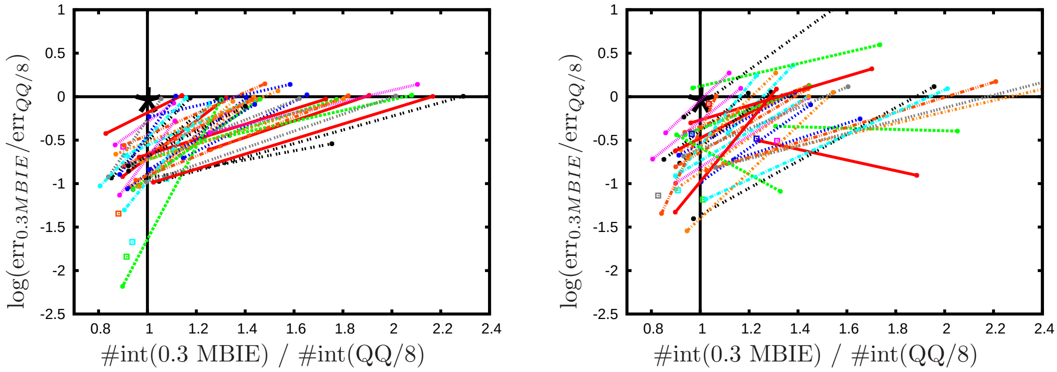

(a)6-31G*

(b)SV(P)

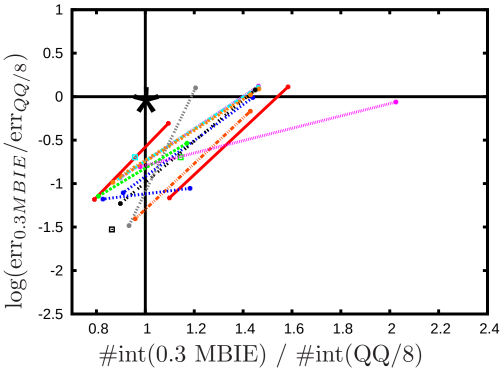

(c)cc-pVTZ

FIG. 15. Error and speedup (via ratio of integrals) for scaled MBIE (scaling factor 0.3) calculations (right endpoint: $\vartheta_K = 10^{-8}$, left endpoint: $\vartheta_K = 10^{-9}$) of the whole test set relative to the values of a pure Schwarz calculation with $\vartheta_K = 10^{-8}$. The Schwarz reference is indicated as a black asterisk. Values to the right of this reference point indicate increased speed, while values below the reference indicate improved accuracy.

	QQ ($\vartheta_K = 10^{-10}$)	QQ ($\vartheta_K = 10^{-8}$)		QQR ($\vartheta_K = 10^{-8}$)			QQR ($\vartheta_K = 10^{-9}$)		
System	E(SCF)	err [μhartree]	#int [10^6]	err [μhartree]	#int [10^6]	speedup	err [μhartree]	#int [10^6]	speedup
Amylose$_2$	-1290.37187964	-7.18	2574	-6.94	2229	1.15	-0.83	3080	0.83
Amylose$_4$	-2504.77075216	-11.85	7808	-11.86	5967	1.30	-1.43	8842	0.88
Amylose$_8$	-4933.56833606	-26.54	19482	-25.99	13950	1.39	-2.34	21492	0.90
Amylose$_{16}$	-9791.16338707	-51.17	42899	-50.11	29968	1.43	-4.77	46832	0.91
Amylose$_{32}$	-19506.35401792	-64.08	83312	-62.68	57623	1.44	-5.86	89677	0.92
Amylose$_{48}$	-29221.54544476	-96.49	126797	-94.44	87372	1.45	-8.52	136301	0.93
Amylose$_{64}$	-38936.73733674	-128.44	170311	-125.18	117159	1.45	-11.56	182959	0.93
Angiotensin	-3541.05432236	-12.62	20779	-12.55	14496	1.43	-2.58	23246	0.89
Angiotensin deprotonated	-3539.84839477	-17.97	20729	-17.61	14477	1.43	-2.77	23177	0.89
Angiotensin zwitterion	-3540.78865674	-16.78	20915	-16.61	14593	1.43	-2.66	23374	0.89
Beta-Carotene	-1547.18049647	-2.42	5747	-2.11	4026	1.42	-0.33	5791	0.99
CNT$_{20}$	-762.65937554	4.81	3032	4.49	2908	1.04	-0.57	3664	0.82
CNT$_{40}$	-1519.66990375	4.73	23963	4.46	21173	1.13	-1.82	29336	0.81
CNT$_{80}$	-3033.88767039	18.01	116538	19.57	89610	1.30	-0.32	131364	0.88
CNT$_{160}$	-6062.09254743	-5.66	634820	-0.50	394721	1.60	4.26	633851	1.00
CNT (6,3)$_8$	-25459.11269501	-145.37	3318623	-149.03	1563661	2.12	-53.31	2607727	1.27
DNA$_1$	-1753.05874673	-8.78	4714	-8.65	3706	1.27	-1.21	5186	0.90
DNA$_2$	-4486.05364783	-17.15	26586	-16.73	18638	1.42	-2.67	29772	0.89
DNA$_4$	-9952.02667330	-35.74	96807	-35.35	59166	1.63	-5.88	103836	0.93
DNA$_8$	-20883.98970789	-52.72	243378	-51.62	138320	1.75	-10.60	251119	0.96
DNA$_{16}$	-42747.91684662	-109.55	550829	-107.78	304185	1.81	-19.57	560954	0.98
Diamond$_{102}$	-1623.01308017	-15.17	33457	-14.82	29360	1.13	-0.99	42348	0.79
Diamond$_{470}$	-9657.94199985	-146.87	1872628	-159.96	1187355	1.57	-30.35	2137272	0.87
Graphite$_{24}$ ($C_{24}H_{12}$)	-915.91889839	-2.95	3444	-2.38	3132	1.09	-0.79	4011	0.85
Graphite$_{54}$ ($C_{54}H_{18}$)	-2054.81438451	-9.54	21503	-5.73	17165	1.25	-0.40	23977	0.89
Graphite$_{96}$ ($C_{94}H_{24}$)	-3648.83474243	-15.07	72514	-18.00	53609	1.35	-1.14	75644	0.95
$(H_2O)_{68}$	-5169.25891018	-21.42	3036	-21.50	1818	1.66	-2.37	3438	0.88
$(H_2O)_{142}$	-10794.90830507	-46.32	9230	-46.71	5012	1.84	-4.84	10041	0.91
$(H_2O)_{285}$	-21666.21529719	-109.31	24753	-110.04	12568	1.96	-11.33	26315	0.94
$(H_2O)_{569}$	-43256.80918149	-234.04	59980	-235.55	28891	2.07	-24.83	62581	0.95
(LiF)$_{32}$	-1712.41286542	5.36	9591	5.46	8524	1.12	0.55	10813	0.88
(LiF)$_{72}$	-3853.29566346	50.31	168574	39.48	150494	1.12	3.94	188528	0.89
(LiF)$_{288}$	-15414.53483159	17.46	15874061	-96.16	13231982	1.19	-2.47	17116531	0.92
Phthalocyanine complex (CuPcF$_{16}$)	-4876.89913554	0.32	59986	nc	nc	nc	0.00	64987	0.92
Polyethyne$_{64}$ ($C_{64}H_{66}$)	-2461.52238938	-12.98	6883	-12.74	4206	1.63	-2.53	6097	1.12
Polyethyne$_{128}$ ($C_{128}H_{130}$)	-4921.90399086	-20.47	18318	-19.88	9659	1.89	-4.93	14793	1.23
Polyethyne$_{512}$ ($C_{512}H_{514}$)	-19684.19284824	-54.38	80962	-52.23	39064	2.07	-19.56	61215	1.32
Polyyne$_{64}$ ($C_{64}H_2$)	-2422.52577559	34.59	4956	nc	nc	nc	3.99	4770	1.03
Polyyne$_{1024}$ ($C_{1024}H_2$)	-38743.17183228	505.38	210740	nc	nc	nc	112.26	266948	0.78
$(S_8)_5$	-15900.34492647	-1.83	6611	-1.97	4784	1.38	-0.36	7327	0.90
$(S_8)_{20}$	-63601.24366822	-40.18	116281	-40.23	63562	1.82	-7.41	118978	0.97
Triphenylmethyl	-728.21066709	-0.01	5613	nc	nc	nc	0.00	6452	0.86
Zeolite LTA	-22852.73100170	-5.39	590275	-0.26	330466	1.78	0.64	589060	1.00
Zeolite SOD	-11426.37970013	5.84	126784	7.67	84718	1.49	1.53	140800	0.90

$\vartheta_K = 10^{-9}$

$\vartheta_K = 10^{-10}$

QQ ($\vartheta_K = 10^{-9}$) vs QQR ($\vartheta_K = 10^{-9}$)

QQ ($\vartheta_K = 10^{-9}$) vs QQR ($\vartheta_K = 10^{-10}$)

TABLE II. QQR benchmark calculations in a 6-31G* basis. Errors are given with respect to the QQ ($\vartheta_K = 10^{-10}$) reference calculations. Speedups are given as the ratio of the number of integrals. Entries ”nc” indicate that the SCF procedure did not converge with the same number of iterations as the reference calculation.

	QQ ($\vartheta_K = 10^{-10}$)	QQ ($\vartheta_K = 10^{-8}$)		QQR ($\vartheta_K = 10^{-8}$)			QQR ($\vartheta_K = 10^{-9}$)		
System	E(SCF)	err [μhartree]	#int [10^6]	err [μhartree]	#int [10^6]	speedup	err [μhartree]	#int [10^6]	speedup
Amylose$_2$	-1289.30958143	-6.35	2422	-7.08	2071	1.16	-1.13	2922	0.82
Amylose$_4$	-2502.71579749	-8.44	7458	-8.58	5649	1.32	-1.85	8494	0.87
Amylose$_8$	-4929.52810178	-18.74	19125	-20.37	13726	1.39	-3.69	21180	0.90
Amylose$_{16}$	-9783.15265090	-34.63	42997	-39.08	30097	1.42	-7.87	47098	0.91
Amylose$_{32}$	-19490.40206365	-31.91	83006	-36.90	57050	1.45	-11.25	89617	0.92
Amylose$_{48}$	-29197.65208374	-50.64	126526	-59.47	86684	1.45	-16.87	136399	0.92
Amylose$_{64}$	-38904.90287130	-67.50	170095	-79.54	116315	1.46	-22.36	183218	0.92
Angiotensin	-3538.20114216	-14.98	20496	-15.44	14174	1.44	-2.17	23164	0.88
Angiotensin deprotonated	-3537.00928396	-19.17	20462	-19.01	14148	1.44	-2.16	23103	0.88
Angiotensin zwitterion	-3537.93473984	-19.48	20668	-17.97	14267	1.44	-2.09	23328	0.88
Beta-Carotene	-1545.91399372	-6.48	5952	-5.63	4110	1.44	-0.83	6010	0.99
CNT$_{20}$	-762.06679416	20.09	3068	23.05	2924	1.04	1.27	3707	0.82
CNT$_{40}$	-1518.49484348	23.73	27114	21.63	23731	1.14	0.98	33374	0.81
CNT$_{80}$	-3031.55496379	89.03	131035	135.81	100080	1.30	3.28	148100	0.88
CNT$_{160}$	-6057.68082564	322.57	601196	426.77	389851	1.54	19.84	600037	1.00
CNT (6,3)$_8$	-25439.62697511	206.36	3388781	nc	nc	nc	-74.79	2702319	1.25
DNA$_1$	-1751.64058502	-7.51	4344	-7.65	3382	1.28	-1.44	4819	0.90
DNA$_2$	-4482.78611747	-16.51	24247	-16.34	16786	1.44	-2.81	27400	0.88
DNA$_4$	-9945.06024869	-26.19	88343	-27.20	53742	1.64	-5.84	95365	0.92
DNA$_8$	-20869.62777355	-17.03	226352	-19.10	127841	1.77	-9.12	233960	0.96
DNA$_{16}$	-42718.76127383	-13.33	519786	-17.70	285522	1.82	-17.63	528246	0.98
Diamond$_{102}$	-1621.67114256	-33.55	36738	-34.31	32151	1.14	-7.74	46765	0.78
Diamond$_{470}$	-9650.31570380	-345.70	2318696	nc	nc	nc	-51.04	2539409	0.91
Graphite$_{24}$ ($C_{24}H_{12}$)	-915.20812240	1.36	3435	2.33	3087	1.11	-0.13	4045	0.84
Graphite$_{54}$ ($C_{54}H_{18}$)	-2053.25903530	19.15	21217	26.84	16884	1.25	-0.68	23772	0.89
Graphite$_{96}$ ($C_{94}H_{24}$)	-3646.06798350	34.37	72139	35.08	53540	1.34	-3.53	76297	0.94
$(H_2O)_{68}$	-5164.46587098	-5.80	2897	-6.49	1648	1.75	0.02	3270	0.88
$(H_2O)_{142}$	-10784.92701965	-6.06	9187	-7.34	4657	1.97	0.41	9889	0.92
$(H_2O)_{285}$	-21646.23236033	-9.25	25332	-10.68	11819	2.14	0.38	26452	0.95
$(H_2O)_{569}$	-43216.96018556	-21.44	62878	-25.54	27487	2.28	1.29	64057	0.98
(LiF)$_{32}$	-1711.00561734	-4.15	777	-3.48	602	1.29	1.06	885	0.87
(LiF)$_{72}$	-3850.17688483	-135.62	11207	nc	nc	nc	-6.29	11749	0.95
(LiF)$_{288}$	-15402.26182395	-64.88[a]	976056[a]	nc	nc	nc	-45.55[b]	956575[b]	1.02[c]
Phthalocyanine complex (CuPcF$_{16}$)	-4874.37702111	0.16[a]	41925[a]	nc	nc	nc	0.00[b]	45434[b]	0.92[c]
Polyethyne$_{64}$ ($C_{64}H_{66}$)	-2459.56030662	-15.99	6433	-13.97	3852	1.67	-3.32	5708	1.12
Polyethyne$_{128}$ ($C_{128}H_{130}$)	-4917.98300322	-15.96	15193	-9.05	7965	1.90	-5.84	12307	1.23
Polyethyne$_{512}$ ($C_{512}H_{514}$)	-19668.52013958	-46.92	72417	-20.05	34788	2.08	-23.68	55430	1.30
Polyyne$_{64}$ ($C_{64}H_2$)	-2420.70590851	11.20	4620	18.78	3397	1.36	2.45	4214	1.09
Polyyne$_{1024}$ ($C_{1024}H_2$)	-38714.13056060	213.69	230505	nc	nc	nc	42.87	183223	1.25
$(S_8)_5$	-15896.03282019	-18.96	3461	-18.67	2299	1.50	-0.17	3778	0.91
$(S_8)_{20}$	-63584.04120698	-93.16	46923	-95.53	23722	1.97	-8.50	47021	0.99
Triphenylmethyl	-727.63533135	0.11[a]	6095[a]	nc	nc	nc	0.00[b]	7073[b]	0.86[c]
Zeolite SOD	-11420.46415460	-9.24	81055	-43.75	51495	1.57	-2.55	88327	0.91

[a] $\vartheta_K = 10^{-9}$

[b] $\vartheta_K = 10^{-10}$

[c] QQ ($\vartheta_K = 10^{-9}$) vs QQR ($\vartheta_K = 10^{-9}$)

[d] QQ ($\vartheta_K = 10^{-9}$) vs QQR ($\vartheta_K = 10^{-10}$)

TABLE III. QQR benchmark calculations in a SV(P) basis. Errors are given with respect to the QQ ($\vartheta_K = 10^{-10}$) reference calculations. Speedups are given as the ratio of the number of integrals. Entries "nc" indicate that the SCF procedure did not converge with the same number of iterations as the reference calculation.

	QQ ($\vartheta_K = 10^{-10}$)	QQ ($\vartheta_K = 10^{-8}$)		QQR ($\vartheta_K = 10^{-8}$)			QQR ($\vartheta_K = 10^{-9}$)		
System	E(SCF)	err [μhartree]	#int [10^6]	err [μhartree]	#int [10^6]	speedup	err [μhartree]	#int [10^6]	speedup
Amylose$_8$	-4935.50037018	38.47	594819	37.32	387616	1.53	2.77	635395	0.93
Angiotensin	-3542.29774594	19.89	624237	17.59	396236	1.57	2.56	676690	0.92
Angiotensin deprotonated	-3541.09955031	16.87	625414	17.20	397072	1.57	2.00	677241	0.92
Angiotensin zwitterion	-3542.04128890	22.52	636455	21.37	403302	1.57	2.90	688281	0.92
Beta-Carotene	-1547.69227412	13.76	237345	8.55	154426	1.53	-0.52	240739	0.98
CNT$_{20}$	-762.89139947	-11.73	87453	-10.28	78564	1.11	0.69	110313	0.79
CNT$_{40}$	-1520.10192384	13.93	519652	3.01	427594	1.21	1.02	636611	0.81
DNA$_2$	-4487.55380469	18.87	651975	16.95	422354	1.54	1.26	708988	0.91
Diamond$_{102}$	-1623.54040194	-37.50	1288697	-24.50	1028128	1.25	-1.93	1537478	0.83
Graphite$_{54}$ ($C_{54}H_{18}$)	-2055.39466151	-10.39	504678	-9.92	397069	1.27	0.20	533315	0.94
$(H_2O)_{68}$	-5172.25099200	-12.25	155406	-12.43	77733	1.99	-2.15	163299	0.95
(LiF)$_{72}$	-3854.48445742	-17.14[a]	4328105[a]	nc	nc	nc	-2.69[b]	4455747[b]	0.97[d]
Polyethyne$_{64}$ ($C_{64}H_{66}$)	-2462.36305423	-13.58	244446	-15.52	142857	1.71	-1.36	214585	1.13
Polyyne$_{64}$ ($C_{64}H_2$)	-2423.26066309	-19.29	106011	nc	nc	nc	-1.03	95365	1.11
$(S_8)_5$	-15901.99827795	-7.60	75104	-7.05	50069	1.49	-1.04	84886	0.88
Triphenylmethyl	-728.43312233	0.10[a]	186660[a]	0.06[a]	163137[a]	1.14[c]	0.00[b]	215572[b]	0.86[d]

[a] $\vartheta_K = 10^{-9}$

[b] $\vartheta_K = 10^{-10}$

[c] QQ ($\vartheta_K = 10^{-9}$) vs QQR ($\vartheta_K = 10^{-9}$)

[d] QQ ($\vartheta_K = 10^{-9}$) vs QQR ($\vartheta_K = 10^{-10}$)

TABLE IV. QQR benchmark calculations in a cc-pVTZ basis. Errors are given with respect to the QQ ($\vartheta_K = 10^{-10}$) reference calculations. Speedups are given as the ratio of the number of integrals. Entries ”nc” indicate that the SCF procedure did not converge with the same number of iterations as the reference calculation.

	QQ ($\vartheta_K = 10^{-10}$)	QQ ($\vartheta_K = 10^{-8}$)		MBIE ($\vartheta_K = 10^{-8}$)			MBIE ($\vartheta_K = 10^{-9}$)		
System	E(SCF)	err [μhartree]	#int [10^6]	err [μhartree]	#int [10^6]	speedup	err [μhartree]	#int [10^6]	speedup
Amylose$_2$	-1290.37187964	-7.18	2574	-7.23	2440	1.05	-0.82	3285	0.78
Amylose$_4$	-2504.77075216	-11.85	7808	-11.82	6912	1.12	-1.42	9933	0.78
Amylose$_8$	-4933.56833606	-26.54	19482	-26.47	16628	1.17	-2.34	24916	0.78
Amylose$_{16}$	-9791.16338707	-51.17	42899	-51.17	36113	1.18	-4.77	54989	0.78
Amylose$_{32}$	-19506.35401792	-64.08	83312	-64.41	69523	1.19	-5.88	105341	0.79
Amylose$_{48}$	-29221.54544476	-96.49	126797	-96.96	105615	1.20	-8.54	160402	0.79
Amylose$_{64}$	-38936.73733674	-128.44	170311	-128.99	141713	1.20	-11.58	215480	0.79
Angiotensin	-3541.05432236	-12.62	20779	-12.51	17705	1.17	-2.59	27340	0.75
Angiotensin deprotonated	-3539.84839477	-17.97	20729	-17.95	17680	1.17	-2.77	27260	0.76
Angiotensin zwitterion	-3540.78865674	-16.78	20915	-16.63	17830	1.17	-2.65	27509	0.76
Beta-Carotene	-1547.18049647	-2.42	5747	-2.26	4687	1.22	-0.33	6480	0.88
CNT$_{20}$	-762.65937554	4.81	3032	4.78	2997	1.01	-0.59	3724	0.81
CNT$_{40}$	-1519.66990375	4.73	23963	5.11	23133	1.03	-1.85	31090	0.77
CNT$_{80}$	-3033.88767039	18.01	116538	21.64	104643	1.11	-0.42	145746	0.79
CNT$_{160}$	-6062.09254743	-5.66	634820	-2.26	499014	1.27	3.02	744009	0.85
CNT (6,3)$_8$	-25459.11269501	-145.37	3318623	-148.14	1991185	1.66	-54.53	3424861	0.96
DNA$_1$	-1753.05874673	-8.78	4714	-8.79	4194	1.12	-1.22	5713	0.82
DNA$_2$	-4486.05364783	-17.15	26586	-16.85	22749	1.16	-2.68	34895	0.76
DNA$_4$	-9952.02667330	-35.74	96807	-35.61	77220	1.25	-5.94	129570	0.74
DNA$_8$	-20883.98970789	-52.72	243378	-52.35	186230	1.30	-10.66	323311	0.75
DNA$_{16}$	-42747.91684662	-109.55	550829	-108.83	414927	1.32	-19.63	732099	0.75
Diamond$_{102}$	-1623.01308017	-15.17	33457	-15.07	32235	1.03	-1.09	45259	0.73
Diamond$_{470}$	-9657.94199985	-146.87	1872628	-148.27	1580006	1.18	-30.71	2674035	0.70
Graphite$_{24}$ ($C_{24}H_{12}$)	-915.91889839	-2.95	3444	-2.67	3340	1.03	-0.80	4187	0.82
Graphite$_{54}$ ($C_{54}H_{18}$)	-2054.81438451	-9.54	21503	-7.20	19647	1.09	-0.32	26301	0.81
Graphite$_{96}$ ($C_{94}H_{24}$)	-3648.83474243	-15.07	72514	-15.43	61374	1.18	-1.38	86060	0.84
$(H_2O)_{68}$	-5169.25891018	-21.42	3036	-21.35	2267	1.33	-2.31	4161	0.72
$(H_2O)_{142}$	-10794.90830507	-46.32	9230	-46.23	6451	1.43	-4.65	12559	0.73
$(H_2O)_{285}$	-21666.21529719	-109.31	24753	-108.84	16497	1.50	-10.91	33644	0.73
$(H_2O)_{569}$	-43256.80918149	-234.04	59980	-233.12	38540	1.55	-23.86	81406	0.73
(LiF)$_{32}$	-1712.41286542	5.36	9591	5.08	9190	1.04	0.58	11412	0.84
(LiF)$_{72}$	-3853.29566346	50.31	168574	47.60	161431	1.04	4.06	203057	0.83
(LiF)$_{288}$	-15414.53483159	17.46[a]	15874061[a]	10.86[a]	14793247[a]	1.07[c]	0.14[b]	18963045[b]	0.83[d]
Phthalocyanine complex (CuPcF$_{16}$)	-4876.89913554	0.32[a]	59986[a]	0.27[a]	54855[a]	1.09[c]	0.00[b]	69926[b]	0.85[d]
Polyethyne$_{64}$ ($C_{64}H_{66}$)	-2461.52238938	-12.98	6883	-12.66	5020	1.37	-2.53	6923	0.99
Polyethyne$_{128}$ ($C_{128}H_{130}$)	-4921.90399086	-20.47	18318	-19.78	11925	1.53	-4.91	17420	1.05
Polyethyne$_{512}$ ($C_{512}H_{514}$)	-19684.19284824	-54.38	80962	-52.96	48983	1.65	-19.37	73429	1.10
Polyyne$_{64}$ ($C_{64}H_2$)	-2422.52577559	34.59	4956	35.81	4387	1.12	3.62	4830	1.02
Polyyne$_{1024}$ ($C_{1024}H_2$)	-38743.17183228	505.38	210740	nc	nc	nc	52.90	193468	1.08
$(S_8)_5$	-15900.34492647	-1.83	6611	-1.73	5690	1.16	-0.40	8294	0.79
$(S_8)_{20}$	-63601.24366822	-40.18	116281	-39.63	87432	1.32	-7.72	152528	0.76
Triphenylmethyl	-728.21066709	-0.01[a]	5613[a]	-0.01[a]	5478[a]	1.02[c]	0.00[b]	6676[b]	0.84[d]
Zeolite LTA	-22852.73100170	-5.39	590275	-4.69	445519	1.32	0.48	749037	0.78
Zeolite SOD	-11426.37970013	5.84	126784	5.14	107483	1.17	1.46	168683	0.75

[a] $\vartheta_K = 10^{-9}$

[b] $\vartheta_K = 10^{-10}$

[c] QQ ($\vartheta_K = 10^{-9}$) vs MBIE ($\vartheta_K = 10^{-9}$)

[d] QQ ($\vartheta_K = 10^{-9}$) vs MBIE ($\vartheta_K = 10^{-10}$)

TABLE V. MBIE benchmark calculations in a 6-31G* basis. Errors are given with respect to the QQ ($\vartheta_K = 10^{-10}$) reference calculations. Speedups are given as the ratio of the number of integrals. Entries "nc" indicate that the SCF procedure did not converge with the same number of iterations as the reference calculation.

	QQ ($\vartheta_K = 10^{-10}$)	QQ ($\vartheta_K = 10^{-8}$)		MBIE ($\vartheta_K = 10^{-8}$)			MBIE ($\vartheta_K = 10^{-9}$)		
System	E(SCF)	err [μhartree]	#int [10^6]	err [μhartree]	#int [10^6]	speedup	err [μhartree]	#int [10^6]	speedup
Amylose$_2$	-1289.30958143	-6.35	2422	-7.32	2275	1.06	-1.17	3123	0.77
Amylose$_4$	-2502.71579749	-8.44	7458	-8.62	6559	1.13	-1.86	9559	0.78
Amylose$_8$	-4929.52810178	-18.74	19125	-19.52	16482	1.16	-3.72	24646	0.77
Amylose$_{16}$	-9783.15265090	-34.63	42997	-36.91	36747	1.17	-7.92	55519	0.77
Amylose$_{32}$	-19490.40206365	-31.91	83006	-33.59	69723	1.19	-11.29	105659	0.78
Amylose$_{48}$	-29197.65208374	-50.64	126526	-53.29	106204	1.19	-16.91	161219	0.78
Amylose$_{64}$	-38904.90287130	-67.50	170095	-72.11	142565	1.19	-22.47	216766	0.78
Angiotensin	-3538.20114216	-14.98	20496	-14.99	17416	1.17	-2.22	27412	0.74
Angiotensin deprotonated	-3537.00928396	-19.17	20462	-18.47	17388	1.17	-2.22	27326	0.74
Angiotensin zwitterion	-3537.93473984	-19.48	20668	-18.54	17562	1.17	-2.15	27590	0.74
Beta-Carotene	-1545.91399372	-6.48	5952	-6.26	4816	1.23	-0.82	6778	0.87
CNT$_{20}$	-762.06679416	20.09	3068	20.90	3027	1.01	1.16	3775	0.81
CNT$_{40}$	-1518.49484348	23.73	27114	19.93	26056	1.04	0.57	35523	0.76
CNT$_{80}$	-3031.55496379	89.03	131035	91.73	116811	1.12	4.31	165656	0.79
CNT$_{160}$	-6057.68082564	322.57	601196	345.77	472834	1.27	19.03	704040	0.85
CNT (6,3)$_8$	-25439.62697511	206.36	3388781	222.76	2215658	1.52	-74.81	3529908	0.96
DNA$_1$	-1751.64058502	-7.51	4344	-7.49	3853	1.12	-1.42	5341	0.81
DNA$_2$	-4482.78611747	-16.51	24247	-16.31	20634	1.17	-2.81	32297	0.75
DNA$_4$	-9945.06024869	-26.19	88343	-27.05	70597	1.25	-5.69	119615	0.73
DNA$_8$	-20869.62777355	-17.03	226352	-17.90	174083	1.30	-8.82	303971	0.74
DNA$_{16}$	-42718.76127383	-13.33	519786	-14.81	394882	1.31	-16.97	698295	0.74
Diamond$_{102}$	-1621.67114256	-33.55	36738	-36.97	35302	1.04	-7.79	49980	0.73
Diamond$_{470}$	-9650.31570380	-345.70	2318696	-315.94	1981994	1.16	-53.11	3134818	0.73
Graphite$_{24}$ ($C_{24}H_{12}$)	-915.20812240	1.36	3435	-0.23	3318	1.03	-0.17	4243	0.80
Graphite$_{54}$ ($C_{54}H_{18}$)	-2053.25903530	19.15	21217	11.79	19283	1.10	-0.69	26384	0.80
Graphite$_{96}$ ($C_{94}H_{24}$)	-3646.06798350	34.37	72139	20.74	62854	1.14	-2.88	87611	0.82
$(H_2O)_{68}$	-5164.46587098	-5.80	2897	-5.68	2075	1.39	0.06	3968	0.73
$(H_2O)_{142}$	-10784.92701965	-6.06	9187	-5.72	6069	1.51	0.47	12430	0.73
$(H_2O)_{285}$	-21646.23236033	-9.25	25332	-7.91	15773	1.60	0.54	34131	0.74
$(H_2O)_{569}$	-43216.96018556	-21.44	62878	-17.51	37386	1.68	1.65	84325	0.74
(LiF)$_{32}$	-1711.00561734	-4.15	777	-4.48	686	1.13	0.99	972	0.79
(LiF)$_{72}$	-3850.17688483	-135.62	11207	-193.76	9766	1.14	-15.08	13302	0.84
(LiF)$_{288}$	-15402.26182395	-64.88[a]	976056[a]	-139.52[a]	820657[a]	1.18[c]	-9.27[b]	1098568[b]	0.88[d]
Phthalocyanine complex (CuPcF$_{16}$)	-4874.37702111	0.16[a]	41925[a]	0.14[a]	37693[a]	1.11[c]	0.00[b]	49413[b]	0.84[d]
Polyethyne$_{64}$ ($C_{64}H_{66}$)	-2459.56030662	-15.99	6433	-15.53	4680	1.37	-3.35	6588	0.97
Polyethyne$_{128}$ ($C_{128}H_{130}$)	-4917.98300322	-15.96	15193	-14.61	9957	1.52	-5.94	14651	1.03
Polyethyne$_{512}$ ($C_{512}H_{514}$)	-19668.52013958	-46.92	72417	-40.82	44355	1.63	-24.29	67539	1.07
Polyyne$_{64}$ ($C_{64}H_2$)	-2420.70590851	11.20	4620	20.14	3716	1.24	2.56	4560	1.01
Polyyne$_{1024}$ ($C_{1024}H_2$)	-38714.13056060	213.69	230505	87.17	183958	1.25	41.72	188561	1.22
$(S_8)_5$	-15896.03282019	-18.96	3461	-18.48	2827	1.22	0.04	4418	0.78
$(S_8)_{20}$	-63584.04120698	-93.16	46923	-89.09	32944	1.42	-7.57	61062	0.76
Triphenylmethyl	-727.63533135	0.11[a]	6095[a]	nc	nc	nc	0.00[b]	7362[b]	0.82[d]
Zeolite SOD	-11420.46415460	-9.24	81055	-22.71	66462	1.21	-2.12	106345	0.76

[a] $\vartheta_K = 10^{-9}$

[b] $\vartheta_K = 10^{-10}$

[c] QQ ($\vartheta_K = 10^{-9}$) vs MBIE ($\vartheta_K = 10^{-9}$)

[d] QQ ($\vartheta_K = 10^{-9}$) vs MBIE ($\vartheta_K = 10^{-10}$)

TABLE VI. MBIE benchmark calculations in a SV(P) basis. Errors are given with respect to the QQ ($\vartheta_K = 10^{-10}$) reference calculations. Speedups are given as the ratio of the number of integrals. Entries "nc" indicate that the SCF procedure did not converge with the same number of iterations as the reference calculation.

	QQ ($\vartheta_K = 10^{-10}$)	QQ ($\vartheta_K = 10^{-8}$)		MBIE ($\vartheta_K = 10^{-8}$)			MBIE ($\vartheta_K = 10^{-9}$)		
System	E(SCF)	err [μhartree]	#int [10^6]	err [μhartree]	#int [10^6]	speedup	err [μhartree]	#int [10^6]	speedup
Amylose$_8$	-4935.50037018	38.47	594819	40.14	504517	1.17	2.86	791174	0.75
Angiotensin	-3542.29774594	19.89	624237	18.96	529739	1.17	2.64	856139	0.72
Angiotensin deprotonated	-3541.09955031	16.87	625414	17.30	530175	1.17	2.09	855007	0.73
Angiotensin zwitterion	-3542.04128890	22.52	636455	22.25	538689	1.18	2.86	869863	0.73
Beta-Carotene	-1547.69227412	13.76	237345	12.28	195142	1.21	-0.44	291002	0.81
CNT$_{20}$	-762.89139947	-11.73	87453	-10.86	86152	1.01	0.63	117412	0.74
CNT$_{40}$	-1520.10192384	13.93	519652	6.51	498786	1.04	1.15	711175	0.73
DNA$_2$	-4487.55380469	18.87	651975	17.91	554603	1.17	1.35	883547	0.73
Diamond$_{102}$	-1623.54040194	-37.50	1288697	-25.35	1230002	1.04	-2.07	1777832	0.72
Graphite$_{54}$ ($C_{54}H_{18}$)	-2055.39466151	-10.39	504678	-14.12	460980	1.09	-0.43	609635	0.82
$(H_2O)_{68}$	-5172.25099200	-12.25	155406	-11.74	110959	1.40	-2.01	214637	0.72
(LiF)$_{72}$	-3854.48445742	-17.14[a]	4328105[a]	-24.03[a]	4145896[a]	1.04[c]	-0.58[b]	4845183[b]	0.89[d]
Polyethyne$_{64}$ ($C_{64}H_{66}$)	-2462.36305423	-13.58	244446	-13.63	183620	1.33	-0.95	260623	0.93
Polyyne$_{64}$ ($C_{64}H_2$)	-2423.26066309	-19.29	106011	17.33	82019	1.29	-0.60	102064	1.03
$(S_8)_5$	-15901.99827795	-7.60	75104	-7.25	65117	1.15	-1.08	102550	0.73
Triphenylmethyl	-728.43312233	0.10[a]	186660[a]	0.19[a]	180680[a]	1.03[c]	0.01[b]	232712[b]	0.80[d]

[a] $\vartheta_K = 10^{-9}$

[b] $\vartheta_K = 10^{-10}$

[c] QQ ($\vartheta_K = 10^{-9}$) vs MBIE ($\vartheta_K = 10^{-9}$)

[d] QQ ($\vartheta_K = 10^{-9}$) vs MBIE ($\vartheta_K = 10^{-10}$)

TABLE VII. MBIE benchmark calculations in a cc-pVTZ basis. Errors are given with respect to the QQ ($\vartheta_K = 10^{-10}$) reference calculations. Speedups are given as the ratio of the number of integrals. Entries "nc" indicate that the SCF procedure did not converge with the same number of iterations as the reference calculation.

	QQ ($\vartheta_K = 10^{-10}$)	QQ ($\vartheta_K = 10^{-8}$)		MBIE ($\vartheta_K = 10^{-8}$)			MBIE ($\vartheta_K = 10^{-9}$)		
System	E(SCF)	err [μhartree]	#int [10^6]	err [μhartree]	#int [10^6]	speedup	err [μhartree]	#int [10^6]	speedup
Amylose$_2$	-1290.37187964	-7.18	2574	-6.92	2191	1.17	-0.83	3019	0.85
Amylose$_4$	-2504.77075216	-11.85	7808	-11.50	5901	1.32	-1.42	8693	0.89
Amylose$_8$	-4933.56833606	-26.54	19482	-25.51	13874	1.40	-2.30	21228	0.91
Amylose$_{16}$	-9791.16338707	-51.17	42899	-49.45	29871	1.43	-4.69	46349	0.92
Amylose$_{32}$	-19506.35401792	-64.08	83312	-60.01	57311	1.45	-5.66	88626	0.94
Amylose$_{48}$	-29221.54544476	-96.49	126797	-90.81	86931	1.45	-8.23	134748	0.94
Amylose$_{64}$	-38936.73733674	-128.44	170311	-120.54	116568	1.46	-11.13	180893	0.94
Angiotensin	-3541.05432236	-12.62	20779	-11.91	14478	1.43	-2.65	22980	0.90
Angiotensin deprotonated	-3539.84839477	-17.97	20729	-17.03	14454	1.43	-2.84	22912	0.90
Angiotensin zwitterion	-3540.78865674	-16.78	20915	-16.56	14578	1.43	-2.70	23117	0.90
Beta-Carotene	-1547.18049647	-2.42	5747	-1.97	3994	1.43	-0.35	5712	1.00
CNT$_{20}$	-762.65937554	4.81	3032	4.55	2871	1.05	-0.57	3610	0.84
CNT$_{40}$	-1519.66990375	4.73	23963	4.88	21005	1.14	-1.78	28881	0.82
CNT$_{80}$	-3033.88767039	18.01	116538	16.68	89489	1.30	-0.11	129765	0.89
CNT$_{160}$	-6062.09254743	-5.66	634820	7.83	400818	1.58	3.32	630837	1.00
CNT (6,3)$_8$	-25459.11269501	-145.37	3318623	-201.53	1576486	2.10	-56.04	2644229	1.25
DNA$_1$	-1753.05874673	-8.78	4714	-8.40	3667	1.28	-1.22	5108	0.92
DNA$_2$	-4486.05364783	-17.15	26586	-15.87	18614	1.42	-2.68	29429	0.90
DNA$_4$	-9952.02667330	-35.74	96807	-33.96	59696	1.62	-5.92	103400	0.93
DNA$_8$	-20883.98970789	-52.72	243378	-49.37	140686	1.72	-10.63	251906	0.96
DNA$_{16}$	-42747.91684662	-109.55	550829	-102.05	310536	1.77	-19.66	564715	0.97
Diamond$_{102}$	-1623.01308017	-15.17	33457	-14.71	28891	1.15	-1.42	41490	0.80
Diamond$_{470}$	-9657.94199985	-146.87	1872628	-170.85	1220571	1.53	-31.97	2150888	0.87
Graphite$_{24}$ ($C_{24}H_{12}$)	-915.91889839	-2.95	3444	-2.48	3109	1.10	-0.82	3970	0.86
Graphite$_{54}$ ($C_{54}H_{18}$)	-2054.81438451	-9.54	21503	-8.02	17135	1.25	-0.47	23741	0.90
Graphite$_{96}$ ($C_{94}H_{24}$)	-3648.83474243	-15.07	72514	-13.30	53735	1.34	-1.39	75026	0.96
$(H_2O)_{68}$	-5169.25891018	-21.42	3036	-21.94	1667	1.82	-2.34	3187	0.95
$(H_2O)_{142}$	-10794.90830507	-46.32	9230	-47.07	4579	2.01	-4.82	9271	0.99
$(H_2O)_{285}$	-21666.21529719	-109.31	24753	-110.12	11420	2.16	-11.34	24164	1.02
$(H_2O)_{569}$	-43256.80918149	-234.04	59980	-236.79	26166	2.29	-24.82	57283	1.04
(LiF)$_{32}$	-1712.41286542	5.36	9591	5.44	8593	1.11	0.68	10822	0.88
(LiF)$_{72}$	-3853.29566346	50.31	168574	26.54	151596	1.11	3.70	190307	0.88
(LiF)$_{288}$	-15414.53483159	17.46[a]	15874061[a]	nc	nc	nc	-0.25[b]	17354896[b]	0.91[c]
Phthalocyanine complex (CuPcF$_{16}$)	-4876.89913554	0.32[a]	59986[a]	nc	nc	nc	0.00[b]	63934[b]	0.93[c]
Polyethyne$_{64}$ ($C_{64}H_{66}$)	-2461.52238938	-12.98	6883	-13.64	4165	1.65	-2.55	6004	1.14
Polyethyne$_{128}$ ($C_{128}H_{130}$)	-4921.90399086	-20.47	18318	-21.16	9604	1.90	-5.03	14619	1.25
Polyethyne$_{512}$ ($C_{512}H_{514}$)	-19684.19284824	-54.38	80962	-56.49	38893	2.08	-19.39	60601	1.33
Polyyne$_{64}$ ($C_{64}H_2$)	-2422.52577559	34.59	4956	nc	nc	nc	3.93	4602	1.07
Polyyne$_{1024}$ ($C_{1024}H_2$)	-38743.17183228	505.38	210740	nc	nc	nc	134.77	233901	0.90
$(S_8)_5$	-15900.34492647	-1.83	6611	-1.42	4719	1.40	-0.29	7166	0.92
$(S_8)_{20}$	-63601.24366822	-40.18	116281	-37.84	64542	1.80	-7.17	119063	0.97
Triphenylmethyl	-728.21066709	-0.01[a]	5613[a]	nc	nc	nc	0.00[b]	6367[b]	0.88[c]
Zeolite LTA	-22852.73100170	-5.39	590275	-1.55	336420	1.75	0.61	593198	0.99
Zeolite SOD	-11426.37970013	5.84	126784	8.21	85636	1.48	1.61	140264	0.90

[a] $\vartheta_K = 10^{-9}$

[b] $\vartheta_K = 10^{-10}$

[c] QQ ($\vartheta_K = 10^{-9}$) vs MBIE ($\vartheta_K = 10^{-9}$)

[d] QQ ($\vartheta_K = 10^{-9}$) vs MBIE ($\vartheta_K = 10^{-10}$)

TABLE VIII. Scaled MBIE (scaling factor 0.3) benchmark calculations in a 6-31G* basis. Errors are given with respect to the QQ ($\vartheta_K = 10^{-10}$) reference calculations. Speedups are given as the ratio of the number of integrals. Entries ”nc” indicate that the SCF procedure did not converge with the same number of iterations as the reference calculation.

	QQ ($\vartheta_K = 10^{-10}$)	QQ ($\vartheta_K = 10^{-8}$)		MBIE ($\vartheta_K = 10^{-8}$)			MBIE ($\vartheta_K = 10^{-9}$)		
System	E(SCF)	err [μhartree]	#int [10^6]	err [μhartree]	#int [10^6]	speedup	err [μhartree]	#int [10^6]	speedup
Amylose$_2$	-1289.30958143	-6.35	2422	-6.98	2024	1.19	-1.20	2846	0.85
Amylose$_4$	-2502.71579749	-8.44	7458	-8.63	5583	1.33	-2.00	8306	0.89
Amylose$_8$	-4929.52810178	-18.74	19125	-20.97	13787	1.38	-3.97	20967	0.91
Amylose$_{16}$	-9783.15265090	-34.63	42997	-41.24	30569	1.40	-8.46	46709	0.92
Amylose$_{32}$	-19490.40206365	-31.91	83006	-42.99	57441	1.44	-12.41	88612	0.93
Amylose$_{48}$	-29197.65208374	-50.64	126526	-66.80	87361	1.44	-18.61	134911	0.93
Amylose$_{64}$	-38904.90287130	-67.50	170095	-88.53	117353	1.44	-24.58	181311	0.93
Angiotensin	-3538.20114216	-14.98	20496	-15.13	14212	1.44	-1.84	22822	0.89
Angiotensin deprotonated	-3537.00928396	-19.17	20462	-18.67	14195	1.44	-1.94	22756	0.89
Angiotensin zwitterion	-3537.93473984	-19.48	20668	-19.56	14311	1.44	-1.68	22971	0.89
Beta-Carotene	-1545.91399372	-6.48	5952	-5.23	4099	1.45	-0.68	5931	1.00
CNT$_{20}$	-762.06679416	20.09	3068	20.42	2882	1.06	0.91	3646	0.84
CNT$_{40}$	-1518.49484348	23.73	27114	nc	nc	nc	1.72	32758	0.82
CNT$_{80}$	-3031.55496379	89.03	131035	108.73	99903	1.31	4.18	145954	0.89
CNT$_{160}$	-6057.68082564	322.57	601196	nc	nc	nc	21.13	594765	1.01
CNT (6,3)$_8$	-25439.62697511	206.36	3388781	nc	nc	nc	-68.01	2754581	1.23
DNA$_1$	-1751.64058502	-7.51	4344	-8.49	3368	1.28	-1.29	4743	0.91
DNA$_2$	-4482.78611747	-16.51	24247	-20.35	16829	1.44	-2.58	26952	0.89
DNA$_4$	-9945.06024869	-26.19	88343	-34.12	55048	1.60	-5.42	94773	0.93
DNA$_8$	-20869.62777355	-17.03	226352	-35.63	132988	1.70	-8.51	235556	0.96
DNA$_{16}$	-42718.76127383	-13.33	519786	-52.76	299619	1.73	-16.76	536391	0.96
Diamond$_{102}$	-1621.67114256	-33.55	36738	-41.82	31518	1.16	-6.42	45639	0.80
Diamond$_{470}$	-9650.31570380	-345.70	2318696	nc	nc	nc	-28.97	2553085	0.90
Graphite$_{24}$ ($C_{24}H_{12}$)	-915.20812240	1.36	3435	2.56	3072	1.11	-0.52	4002	0.85
Graphite$_{54}$ ($C_{54}H_{18}$)	-2053.25903530	19.15	21217	33.68	17235	1.23	-2.31	23550	0.90
Graphite$_{96}$ ($C_{94}H_{24}$)	-3646.06798350	34.37	72139	64.28	55125	1.30	-6.72	75946	0.94
$(H_2O)_{68}$	-5164.46587098	-5.80	2897	-7.59	1480	1.95	0.22	2980	0.97
$(H_2O)_{142}$	-10784.92701965	-6.06	9187	-9.05	4158	2.20	0.85	8954	1.02
$(H_2O)_{285}$	-21646.23236033	-9.25	25332	-13.82	10496	2.41	1.42	23810	1.06
$(H_2O)_{569}$	-43216.96018556	-21.44	62878	-34.62	24315	2.58	3.66	57430	1.09
(LiF)$_{32}$	-1711.00561734	-4.15	777	-0.33	585	1.32	1.51	860	0.90
(LiF)$_{72}$	-3850.17688483	-135.62	11207	nc	nc	nc	-50.56	11611	0.96
(LiF)$_{288}$	-15402.26182395	-64.88[a]	976056[a]	nc	nc	nc	-53.56[b]	943147[b]	1.03[c]
Phthalocyanine complex (CuPcF$_{16}$)	-4874.37702111	0.16[a]	41925[a]	nc	nc	nc	0.00[b]	44525[b]	0.94[c]
Polyethyne$_{64}$ ($C_{64}H_{66}$)	-2459.56030662	-15.99	6433	-8.89	3890	1.65	-3.00	5658	1.13
Polyethyne$_{128}$ ($C_{128}H_{130}$)	-4917.98300322	-15.96	15193	1.98	8055	1.88	-4.96	12248	1.24
Polyethyne$_{512}$ ($C_{512}H_{514}$)	-19668.52013958	-46.92	72417	18.85	35284	2.05	-21.43	55364	1.30
Polyyne$_{64}$ ($C_{64}H_2$)	-2420.70590851	11.20	4620	25.77	3348	1.37	4.25	4149	1.11
Polyyne$_{1024}$ ($C_{1024}H_2$)	-38714.13056060	213.69	230505	nc	nc	nc	66.23	175386	1.31
$(S_8)_5$	-15896.03282019	-18.96	3461	-21.24	2242	1.54	0.54	3658	0.94
$(S_8)_{20}$	-63584.04120698	-93.16	46923	-115.32	23326	2.01	-6.17	45866	1.02
Triphenylmethyl	-727.63533135	0.11[a]	6095[a]	nc	nc	nc	0.00[b]	6974[b]	0.87[c]
Zeolite SOD	-11420.46415460	-9.24	81055	-108.60	51452	1.57	-5.38	86855	0.93

[a] $\vartheta_K = 10^{-9}$

[b] $\vartheta_K = 10^{-10}$

[c] QQ ($\vartheta_K = 10^{-9}$) vs MBIE ($\vartheta_K = 10^{-9}$)

[d] QQ ($\vartheta_K = 10^{-9}$) vs MBIE ($\vartheta_K = 10^{-10}$)

TABLE IX. Scaled MBIE (scaling factor 0.3) benchmark calculations in a SV(P) basis. Errors are given with respect to the QQ ($\vartheta_K = 10^{-10}$) reference calculations. Speedups are given as the ratio of the number of integrals. Entries ”nc” indicate that the SCF procedure did not converge with the same number of iterations as the reference calculation.[23]

	QQ ($\vartheta_K = 10^{-10}$)	QQ ($\vartheta_K = 10^{-8}$)		MBIE ($\vartheta_K = 10^{-8}$)			MBIE ($\vartheta_K = 10^{-9}$)		
System	E(SCF)	err [μhartree]	#int [10^6]	err [μhartree]	#int [10^6]	speedup	err [μhartree]	#int [10^6]	speedup
Amylose$_8$	-4935.50037018	38.47	594819	37.58	413211	1.43	3.01	654115	0.90
Angiotensin	-3542.29774594	19.89	624237	25.61	427001	1.46	2.31	698153	0.89
Angiotensin deprotonated	-3541.09955031	16.87	625414	22.32	427490	1.46	1.95	697765	0.89
Angiotensin zwitterion	-3542.04128890	22.52	636455	27.64	434516	1.46	2.76	709770	0.89
Beta-Carotene	-1547.69227412	13.76	237345	9.35	166000	1.42	-0.54	247629	0.95
CNT$_{20}$	-762.89139947	-11.73	87453	-5.78	79924	1.09	0.77	110469	0.79
CNT$_{40}$	-1520.10192384	13.93	519652	4.06	443962	1.17	0.99	643168	0.80
DNA$_2$	-4487.55380469	18.87	651975	22.51	449791	1.44	1.11	726245	0.89
Diamond$_{102}$	-1623.54040194	-37.50	1288697	3.30	1089556	1.18	-2.48	1559866	0.82
Graphite$_{54}$ ($C_{54}H_{18}$)	-2055.39466151	-10.39	504678	-13.11	418694	1.20	-0.34	540827	0.93
$(H_2O)_{68}$	-5172.25099200	-12.25	155406	-10.63	76730	2.02	-1.91	158886	0.97
(LiF)$_{72}$	-3854.48445742	-17.14[a]	4328105[a]	nc	nc	nc	-3.44[b]	4521238[b]	0.95[c]
Polyethyne$_{64}$ ($C_{64}H_{66}$)	-2462.36305423	-13.58	244446	-17.60	154348	1.58	-0.93	222492	1.09
Polyyne$_{64}$ ($C_{64}H_2$)	-2423.26066309	-19.29	106011	nc	nc	nc	-3.88	92620	1.14
$(S_8)_5$	-15901.99827795	-7.60	75104	-7.99	52500	1.43	-0.78	86612	0.86
Triphenylmethyl	-728.43312233	0.10[a]	186660[a]	nc	nc	nc	0.00[b]	216285[b]	0.86[c]

[a] $\vartheta_K = 10^{-9}$

[b] $\vartheta_K = 10^{-10}$

[c] QQ ($\vartheta_K = 10^{-9}$) vs MBIE ($\vartheta_K = 10^{-9}$)

[d] QQ ($\vartheta_K = 10^{-9}$) vs MBIE ($\vartheta_K = 10^{-10}$)

TABLE X. Scaled MBIE (scaling factor 0.3) benchmark calculations in a cc-pVTZ basis. Errors are given with respect to the QQ ($\vartheta_K = 10^{-10}$) reference calculations. Speedups are given as the ratio of the number of integrals. Entries ”nc” indicate that the SCF procedure did not converge with the same number of iterations as the reference calculation.

5.2 Paper II: "Efficient distance-including integral screening in linear-scaling Møller-Plesset perturbation theory",

S. A. Maurer, D. S. Lambrecht, J. Kussmann, C. Ochsenfeld,

***J. Chem. Phys.*, 138, 014101 (2013)**

THE JOURNAL OF CHEMICAL PHYSICS **138**, 014101 (2013)

Efficient distance-including integral screening in linear-scaling Møller-Plesset perturbation theory

Simon A. Maurer, Daniel S. Lambrecht,[a] Jörg Kussmann, and Christian Ochsenfeld[b]
Chair of Theoretical Chemistry, Department of Chemistry, University of Munich (LMU), Butenandtstr. 7, D-81377 München, Germany

(Received 7 September 2012; accepted 26 November 2012; published online 2 January 2013)

Efficient estimates for the preselection of two-electron integrals in atomic-orbital based Møller-Plesset perturbation theory (AO-MP2) theory are presented, which allow for evaluating the AO-MP2 energy with computational effort that scales linear with molecular size for systems with a significant HOMO-LUMO gap. The estimates are based on our recently introduced QQR approach [S. A. Maurer, D. S. Lambrecht, D. Flaig, and C. Ochsenfeld, J. Chem. Phys. **136**, 144107 (2012)], which exploits the asympotic decay of the integral values with increasing bra-ket separation as deduced from the multipole expansion and combines this decay behavior with the common Schwarz bound to a tight and simple estimate. We demonstrate on a diverse selection of benchmark systems that our AO-MP2 method in combination with the QQR-type estimates produces reliable results for systems with both localized and delocalized electronic structure, while in the latter case the screening essentially reverts to the common Schwarz screening. For systems with localized electronic structure, our AO-MP2 method shows an early onset of linear scaling as demonstrated on DNA systems. The favorable scaling behavior allows to compute systems with more than 1000 atoms and 10 000 basis functions on a single core that are clearly not accessible with conventional MP2 methods. Furthermore, our AO-MP2 method is particularly suited for parallelization and we present benchmark calculations on a protein-DNA repair complex comprising 2025 atoms and 20 371 basis functions. *© 2013 American Institute of Physics*. [http://dx.doi.org/10.1063/1.4770502]

I. INTRODUCTION

The accurate description of electron-correlation effects in quantum-chemical calculations is often essential for reliable studies on chemical and biochemical systems. Especially, the effect of London dispersion interactions is not accounted for properly if the correlation treatment is insufficient. Unfortunately, correlation methods are usually expensive and often exhibit a strong increase of the computational cost with system size.

One option to account for correlation effects is density-functional theory (DFT),[1] which nowadays is widely used in chemistry. In the Kohn-Sham formulation of DFT,[2] the computational cost is typically comparable to the uncorrelated Hartree-Fock (HF) calculations and can be realized to scale linearly with system size.[3–12] However, most of the commonly used density functionals, such as the popular B3LYP,[13,14] are known to fail in describing dispersion interactions despite their inclusion of correlation effects. There have been several attempts to include dispersion description in DFT by introducing a large number of fitting parameters or including empirical approximations to the dispersion energy (see Ref. 15 for a recent review), but on top of the undesired empiricism none of the approaches so far proved to be generally applicable to both energetics and molecular response properties. Furthermore, it has been recently reported that DFT calculations on large molecules using some pure GGA functionals can suffer from severe convergence problems due to a vanishing HOMO-LUMO gap.[16] It seems that a significant portion of Hartree-Fock exchange is necessary for large scale DFT calculations at this stage of development of functionals. In contrast, the common Hartree-Fock method, while unable to give a description of correlation effects, in general shows stable convergence of the self-consistent field (SCF) procedure even for large systems and is, therefore, ideally suited as a starting point for subsequent correlation calculations.

Wave-function based methods, such as Møller-Plesset (MP) perturbation theory or the coupled-cluster approach, provide general and systematic routes to account for correlation effects based on a Hartree-Fock solution. Among these correlation methods, the MP2 approach, which truncates the Møller-Plesset expansion at second-order, is one of the most economical ones, which usually allows to recover a substantial part of the correlation energy at moderate cost (see, e.g., Ref. 17 for a recent review). Nevertheless, the scaling behavior is unfavorable in the general canonical MP2 approach since the computation time grows asymptotically with the fifth power of the system size N (abbreviated as $\mathcal{O}(N^5)$ in the following).

There have been several attempts to reduce the computational cost and/or the scaling behavior of MP2 using local correlation domains,[18–25] the Laplace transformation of the energy denominator,[26–32] the resolution-of-the-identity (RI) (also known as density fitting),[25,33–36] the Cholesky decomposition,[37] or pseudospectral approaches.[38,39]

---

[a] Present address: Department of Chemistry, University of Pittsburgh, Pittsburgh, Pennsylvania 15260, USA.

[b] Electronic mail: christian.ochsenfeld@uni-muenchen.de.

This article is copyrighted as indicated in the article. Reuse of AIP content is subject to the terms at: http://scitation.aip.org/termsconditions. Downloaded to IP: 92.230.182.222 On: Sat, 14 Dec 2013 21:52:55

Furthermore, the use of explicitly correlated wave-functions has been successfully applied to MP2[40,41] and allows to reduce the errors of incomplete basis sets and local correlation domains.

Among these approaches, low-scaling algorithms are achieved either by *a priori* restriction of the correlation domains, which is the basis of "local" methods, or by preselecting individual integrals based on their estimated values. The errors due to restricted correlation domains are hard to predict and recent developments, such as the DEC-MP2 approach,[42] try to overcome this problem by dynamically expanding the domain sizes to convergence. In contrast to local methods the advantage of the integral screening approach employed in our present work is a more direct control of the accuracy: In combination with the Laplace expansion of the energy denominator, integral products can be directly screened according to their estimated contribution to the final energy.

Nevertheless, the ultimate goal of a linear-scaling algorithm based on integral screening has been hampered for a long time due to unsuitable estimates that did not account for the decay of the integral value with increasing separation of the bra and ket charge distribution. A two-electron integral in the atomic orbital (AO) basis usually shows an asymptotic 1/R decay with the bra-ket separation as exemplarily shown in Fig. 1. Since common estimates such as the widely used Schwarz bound[28,43] do not account for the decay, they can severely overestimate the true integral value. A first account of the decay with the bra-ket separation has been realized by the multipole-based integral estimates introduced by Lambrecht and Ochsenfeld in 2005.[44] Recently, we reported improved estimates, named QQR,[45] which describe the integral decay well and have been shown to yield significant savings in the evaluation of the exchange contribution in Hartree-Fock calculations. The idea behind the QQR approach is to combine the Schwarz estimate with the decay behavior that can be derived from the multipole expansion. This approach yields estimates which are both simple and tight.

In the following, we will introduce QQR-type estimates in AO-MP2 theory, where their application in screening allows for a linear-scaling evaluation of the MP2 energy, while the error remains fully controlled by the screening threshold. In Sec. II A, we will review the basic equations of the Laplace AO-MP2 formulation, while the QQR estimates for AO-MP2 are discussed in Sec. II B. After giving computational details, we provide extensive tests and benchmark calculations on a selection from our previously introduced benchmark set[45] in Sec. IV. The data show that our AO-MP2 method using screening based on QQR estimates provides reliable results for large molecular systems and exhibits linear-scaling with system size allowing calculations on systems with more than 1000 atoms and 10 000 basis functions on a single core. Furthermore, we show benchmark results of a parallelized version of our method, calculating cutouts of a protein-DNA complex relevant in the DNA repair process of oxidative damages, where each calculated system comprises 2025 atoms and 20 371 basis functions.

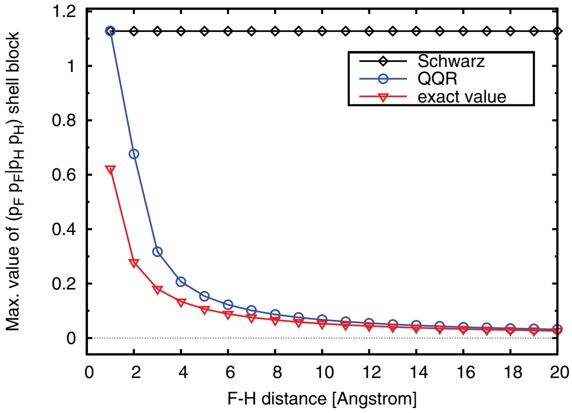

FIG. 1. Decay behavior of a $(p_F p_F|p_H p_H)$ integral shell block in a HF$\cdots$HF dimer (6-31G** basis).

II. THEORY

A. Laplace AO-MP2

Our linear-scaling MP2 implementation is based on the Laplace AO-MP2 approach introduced by Almlöf and Häser in 1991–1993.[26–28] The denominator in the MP2 expression is replaced by virtue of a Laplace transform and evaluated as a finite quadrature sum

$$\frac{1}{\epsilon_a + \epsilon_b - \epsilon_i - \epsilon_j} \approx \sum_\alpha \omega^{(\alpha)} e^{-(\epsilon_a+\epsilon_b-\epsilon_i-\epsilon_j)t^{(\alpha)}}. \qquad (1)$$

The resulting AO-MP2 energy expression

$$E_{\mathrm{AO-MP2}} = -\sum_\alpha \left(2e_J^{(\alpha)} - e_K^{(\alpha)}\right) \qquad (2)$$

typically requires 5–8 quadrature points to allow for μHartree accuracy.

The Coulomb-type term $e_J^{(\alpha)}$ and the exchange-type term $e_K^{(\alpha)}$ can be expressed in terms of half-transformed integrals (HTIs),

$$e_J^{(\alpha)} = \sum_{\mu\nu\lambda\sigma} (\underline{\mu}\overline{\nu}|\lambda\sigma)(\mu\nu|\underline{\lambda}\overline{\sigma}), \qquad (3)$$

$$e_K^{(\alpha)} = \sum_{\mu\nu\lambda\sigma} (\underline{\mu}\nu|\underline{\lambda}\sigma)(\mu\overline{\sigma}|\lambda\overline{\nu}), \qquad (4)$$

where the underline and overline denote transformations with the occupied and virtual pseudo-density matrix, respectively. The transformation of a HTI reads

$$(\underline{\mu}\overline{\nu}|\lambda\sigma) = \sum_{\mu'\nu'} \underline{P}_{\mu\mu'}\overline{P}_{\nu\nu'}(\mu'\nu'|\lambda\sigma) \qquad (5)$$

with analogous expressions for transformations of other indices. The corresponding pseudo-densities are defined as

$$\begin{aligned} \underline{P}_{\mu\nu} &= (\omega_\alpha)^{\frac{1}{4}} \sum_i c_{\mu i} e^{\epsilon_i t_\alpha} c_{\nu i} = (\omega_\alpha)^{\frac{1}{4}} (e^{t_\alpha \mathbf{PF}}\mathbf{P})_{\mu\nu}, \\ \overline{P}_{\mu\nu} &= (\omega_\alpha)^{\frac{1}{4}} \sum_a c_{\mu a} e^{-\epsilon_a t_\alpha} c_{\nu a} = (\omega_\alpha)^{\frac{1}{4}} (e^{-t_\alpha \mathbf{QF}}\mathbf{Q})_{\mu\nu} \end{aligned} \qquad (6)$$

with the quadrature weights ω_α, the quadrature exponents t_α, the Fock matrix $\mathbf{F}$, and the occupied and virtual

This article is copyrighted as indicated in the article. Reuse of AIP content is subject to the terms at: http://scitation.aip.org/termsconditions. Downloaded to IP: 92.230.182.222 On: Sat, 14 Dec 2013 21:52:55

one-particle density matrices **P** and **Q**, respectively. The second expression in Eq. (6) using matrix exponentials allows for a fully linear-scaling evaluation, since the involved matrices are sparse and only AO-quantities are involved,[30,46,47] so that it can be combined with true linear-scaling diagonalization-free SCF algorithms (see, e.g., Ref. 48 for a recent review).

In the exchange-type term (Eq. (4)) all of the four AO-indices are coupled with each other via the coupling occurring within function products (bra or ket). In contrast to the Coulomb term (Eq. (3)), the coupling between bra and ket of one integral is hence mediated by the couplings within bra and ket of the second integral, which results in a much stronger decay. Since the transformed basis functions inherit the decay behavior from the density matrix, which decays exponentially for systems with non-vanishing HOMO-LUMO gap, the AO-indices are all exponentially coupled in the exchange term. Setting up a linear-scaling screening algorithm for this term is therefore straightforward using existing estimates and screening schemes.[28,49]

In the present work, we focus on the Coulomb-type term (Eq. (3)), where a linear-scaling scheme needs to account for the decay of the integral products that comes with increasing distance between the bra and ket charge distribution. The Coulomb-type term is identical to the opposite-spin (OS) term, which is used in the scaled-opposite spin (SOS-)MP2 method.[35] In this approach, the opposite-spin contribution is empirically scaled, so that the scaling approximately compensates for the exchange-term and often allows to statistically improve results upon conventional MP2. The SOS-AO-MP2 energy can be written as

$$E_{\mathrm{SOS-AO-MP2}} = -c_{\mathrm{OS}} \sum_{\alpha} e_J^{(\alpha)}, \tag{7}$$

where the scaling factor c_{OS} is 1.3.[35]

It should be noted that the MP2 energy expression is formally analogous to the Kohn-Sham second-order perturbation theory (PT2) energy term used in double-hybrid density functionals such as, e.g., B2-PLYP,[50] where the Kohn-Sham orbitals substitute the Hartree-Fock orbitals. Some of the functionals, such as PTPSS or PWPB95,[51] rely on the opposite-spin PT2 contribution only, which corresponds to the Coulomb-type MP2 term. The approach described here could be applied to the OS-PT2 term without further modifications (using Kohn-Sham orbitals as input) and in combination with the well-established techniques for the remaining hybrid-GGA part[3,7,52] allows for linear-scaling evaluation of this class of functionals.

B. Integral estimates

The classical Schwarz estimate[43] can be applied to a four-center two-electron integral with two arbitrary charge distributions Ω_A and Ω_B,

$$|(\Omega_A|\Omega_B)| \leq (\Omega_A|\Omega_A)^{\frac{1}{2}} (\Omega_B|\Omega_B)^{\frac{1}{2}}. \tag{8}$$

Based on the general Schwarz estimates, Häser[28] introduced estimates for half- and fully transformed integrals that read

$$\begin{aligned} (\underline{\mu}\overline{\nu}|\lambda\sigma) &\leq Z_{\underline{\mu}\overline{\nu}} Q_{\lambda\sigma}, \\ (\underline{\mu}\overline{\nu}|\underline{\lambda}\overline{\sigma}) &\leq Z_{\underline{\mu}\overline{\nu}} Z_{\underline{\lambda}\overline{\sigma}} \end{aligned} \tag{9}$$

with the common Schwarz integrals

$$Q_{\mu\nu} = (\mu\nu|\mu\nu)^{\frac{1}{2}} \tag{10}$$

and the pseudo-Schwarz matrix

$$\begin{aligned} Z_{\underline{\mu}\overline{\nu}} &= \min\left(\sum_{\lambda} (\underline{\mu}\lambda|\underline{\mu}\lambda)^{\frac{1}{2}} |\overline{P}_{\lambda\nu}|, \sum_{\lambda} |\underline{P}_{\mu\lambda}| (\lambda\overline{\nu}|\lambda\overline{\nu})^{\frac{1}{2}} \right) \\ &\geq (\underline{\mu}\overline{\nu}|\underline{\mu}\overline{\nu})^{\frac{1}{2}} \end{aligned} \tag{11}$$

that was introduced to circumvent the costly exact transformation involved in the calculation of $(\underline{\mu}\overline{\nu}|\underline{\mu}\overline{\nu})^{1/2}$ while retaining the upper bound property.

The Schwarz estimates obviously ignore the dependence of the integral value on the bra-ket separation, which results in severe overestimation. The actual decay behavior of the integral values can be deduced from the multipole expansion, which can be applied if the charge distributions in bra and ket are well-separated,

$$(\Omega_A|\Omega_B) = \sum_{m=0}^{\infty} \sum_{n=0}^{\infty} \sum_{i=-m}^{m} \sum_{j=-n}^{n} \frac{q_{mi}^A T'_{mi,nj} q_{nj}^B}{R_{AB}^{m+n+1}}, \tag{12}$$

where q_{mi}^A are the multipoles of the charge distribution Ω_A with multipole order m with the index i running over the $(2m + 1)$ individual spherical multipoles of the given order. The denominator includes the bra-ket separation R_{AB}, i.e., the distance between the expansion centers, and only depends on the orders of the interacting multipoles. Finally, T' accounts for the relative orientation of the two multipole moments. Please note, that we split the interaction tensor $T_{mi,nj} = T'_{mi,nj}/R_{AB}^{m+n+1}$ into its two components in our notation to highlight the dependence on the bra-ket separation.

Analyzing the first few terms of the multipole expansion

$$\begin{aligned} (\Omega_A|\Omega_B) = {} & \frac{q_{00}^A q_{00}^B}{R_{AB}} + \frac{q_{00}^A \left(\sum_{j=-1}^{1} T'_{00,1j} q_{1j}^B \right)}{R_{AB}^2} \\ & + \frac{\left(\sum_{i=-1}^{1} q_{1i}^A T'_{1i,00} \right) q_{00}^B}{R_{AB}^2} + \mathcal{O}\left(\mathrm{R}_{\mathrm{AB}}^{-3}\right) \end{aligned} \tag{13}$$

clearly shows the asymptotic 1/R decay for the general case, since the first term, describing the monopole-monopole interaction will dominate for large distances.

For the case of a half-transformed integral $(\underline{\mu}\overline{\nu}|\lambda\sigma)$, the monopole of the bra distribution is zero

$$q_{00}^{\underline{\mu}\overline{\nu}} = S_{\underline{\mu}\overline{\nu}} = \sum_{\mu'\nu'} \underline{P}_{\mu'\mu} S_{\mu\nu} \overline{P}_{\nu\nu'} = 0 \tag{14}$$

due to the orthogonality of the occupied and virtual subspace. As a result, the first and second terms in the expansion Eq. (13) vanish for the half-transformed integrals and the

This article is copyrighted as indicated in the article. Reuse of AIP content is subject to the terms at: http://scitation.aip.org/termsconditions. Downloaded to IP: 92.230.182.222 On: Sat, 14 Dec 2013 21:52:55

asymptotic decay is $1/R^2$, as determined by the third term. This leads to a total $1/R^4$-decay for the HTI products in Eq. (3), which is the well-known distance decay for the Coulomb-type AO-MP2 contribution.[30,53]

For fully transformed integrals $(\underline{\mu}\overline{\nu}|\underline{\lambda}\overline{\sigma})$ the decay is stronger, since the monopoles of both, the bra and ket distribution, vanish and so the third term in the expansion is zero as well. For large separations, the expansion is then dominated by the dipole-dipole terms that decay with $1/R^3$. Using fully-transformed integrals in the Coulomb term, the contributions read $(\underline{\mu}\overline{\nu}|\underline{\lambda}\overline{\sigma})(\mu\nu|\lambda\sigma)$ and the contraction with the untransformed integrals again leads to a total $1/R^4$-decay for this term. It is worthwhile to note that the asymptotic $1/R^3$ decay as deduced for fully transformed AO-integrals also applies to integrals over local molecular orbitals (MOs) or local pseudo-MOs as in the Cholesky-decomposed density MP2 (CDD-MP2) approach,[54] so that the following ideas can be readily applied in these methods as well.

Recently, we introduced the QQR integral estimates,[45] which efficiently combine the decent description of the coupling within a basis function pair provided by the Schwarz estimates with the asymptotic $1/R^n$ distance decay with bra-ket separation derived from the multipole expansion. In contrast to previous attempts by us, the QQR estimate does not constitute an upper bound on the integral but rather provides a tighter estimate close to the true value, which was shown to be clearly advantageous. Furthermore, the QQR estimate is simple and easy to implement and has been shown to allow for efficient screening in the context of Hartree-Fock theory.[45] The QQR-type estimates in AO-MP2 read (in atomic units),

$$\begin{aligned}(\underline{\mu}\overline{\nu}|\lambda\sigma) &\approx \frac{Z_{\underline{\mu}\overline{\nu}} Q_{\lambda\sigma}}{(R - \mathrm{ext}_{\underline{\mu}\overline{\nu}} - \mathrm{ext}_{\lambda\sigma})^2}, \\ (\underline{\mu}\overline{\nu}|\underline{\lambda}\overline{\sigma}) &\approx \frac{Z_{\underline{\mu}\overline{\nu}} Z_{\underline{\lambda}\overline{\sigma}}}{(R - \mathrm{ext}_{\underline{\mu}\overline{\nu}} - \mathrm{ext}_{\underline{\lambda}\overline{\sigma}})^3}\end{aligned} \tag{15}$$

and may be applied if the bra and ket charge distributions are well separated, i.e., the bra-ket distance R is larger than the sum of the extents $\mathrm{ext}_{\underline{\mu}\overline{\nu}/\mu\nu}$ of the two distributions. Integrals with such well-separated charge distributions will collectively be referred to as far-field. For all integrals with smaller bra-ket separation (near-field), the common Schwarz-type estimates will be used. As usual, the estimates Eq. (15) implicitly include a dimension factor of a_0^n (with a_0 being the Bohr radius and $n = 2, 3$), that makes the $1/R^n$ factors dimensionless (cf. Appendix D of Ref. 45). This factor is 1 in atomic units and is therefore skipped in the expression. The explicit formulas for the untransformed extents $\mathrm{ext}_{\mu\nu}$ and the definition of the centers of the multipole expansion as used in our implementation can be found in Appendix B of Ref. 45 (note that we dropped the prime in the notation of the extents here). Since the multipole expansion is valid independent of the choice of the expansion centers (provided that the charge distributions remain well separated with respect to the chosen centers), the same centers are used for both untransformed and transformed basis function products. The extents are defined with respect to the expansion centers so that well separatedness is always ensured.

The crucial point is the definition of the transformed extents $\mathrm{ext}_{\underline{\mu}\overline{\nu}}$, since robust estimates have to account properly for the localization as well as possible delocalization of the transformed functions to ensure that the far-field QQR-type estimates are only applied in cases where the multipole expansion is valid. In general, the extents define a sphere around each expansion center, and two charge distributions are considered well-separated if these spheres do not intersect. In this sense, the sphere defined by the transformed extents has to include all untransformed distributions that significantly contribute to the transformed charge distribution.

To measure the significance of the untransformed contribution, we first assign for each transformed pair $\underline{\mu}\overline{\nu}$ a relative weight to each untransformed AO contribution $\mu'\nu'$,

$$c_{\underline{\mu}\overline{\nu}}^{\mu'\nu'} = \frac{|\underline{P}_{\mu\mu'} S_{\mu'\nu'} \overline{P}_{\nu'\nu}|}{\sum_{\lambda\sigma} |\underline{P}_{\mu\lambda} S_{\lambda\sigma} \overline{P}_{\sigma\nu}|}. \tag{16}$$

For systems with significant HOMO-LUMO gap, there is asymptotically a constant number of untransformed pairs $\mu'\nu'$ that have a significant weight within a given transformed pair $\underline{\mu}\overline{\nu}$ due to the sparsity of the pseudo-densities.

The transformed extent of a pair $\underline{\mu}\overline{\nu}$ is chosen such that it covers all untransformed charge distributions whose weight $c_{\underline{\mu}\overline{\nu}}^{\mu'\nu'}$ is larger than some chosen transformation threshold ϑ_t. Therefore, we take the distance between the expansion center and each significantly contributing untransformed pair and each time add the individual untransformed extent scaled by the relative weight. The maximum of all these values defines the transformed extent

$$\mathrm{ext}_{\underline{\mu}\overline{\nu}} = \max_{\left\{\mu',\nu' | c_{\underline{\mu}\overline{\nu}}^{\mu'\nu'} > \vartheta_t\right\}} \left\{ r_{\underline{\mu}\overline{\nu},\mu'\nu'} + c_{\underline{\mu}\overline{\nu}}^{\mu'\nu'} \mathrm{ext}_{\mu'\nu'} \right\}, \tag{17}$$

where $r_{\underline{\mu}\overline{\nu},\mu'\nu'}$ is the distance between the centers of $\underline{\mu}\overline{\nu}$ and $\mu'\nu'$.

For efficiency reasons, we perform all screening steps over shells in the actual implementation, which is advantageous both in terms of screening time as well as memory requirements. All screening matrices contain the maximum element for the corresponding shell pair and we also evaluate Eqs. (16) and (17) in the way that we perform all loops and sums over shells and substitute the matrix elements over basis functions by their individual shell pair maxima.

With these definitions we perform a screening on the HTI products of Eq. (3) based on the QQR estimates

$$(\underline{\mu}\overline{\nu}|\lambda\sigma)(\mu\nu|\underline{\lambda}\overline{\sigma}) \approx \frac{Z_{\underline{\mu}\overline{\nu}} Q_{\lambda\sigma} Q_{\mu\nu} Z_{\underline{\lambda}\overline{\sigma}}}{{R'_{\underline{\mu}\overline{\nu},\lambda\sigma}}^2 {R'_{\mu\nu,\underline{\lambda}\overline{\sigma}}}^2}, \tag{18}$$

where we introduced the reduced distance $R'_{\underline{\mu}\overline{\nu},\lambda\sigma} = R_{\underline{\mu}\overline{\nu},\lambda\sigma} - \mathrm{ext}_{\underline{\mu}\overline{\nu}} - \mathrm{ext}_{\lambda\sigma}$ for a more compact notation. We abbreviate this screening procedure as QQZZR4 in the following. In the context of AO-MP2, this screening of significant HTIs is also termed the "external" screening, since there is another screening step involved in the transformation steps in Eq. (5) (the "internal" screening) to select significant contributions. Our implementation of the "internal" screening is described in detail in Ref. 32 and currently employs the Schwarz estimate only.

This article is copyrighted as indicated in the article. Reuse of AIP content is subject to the terms at: http://scitation.aip.org/termsconditions. Downloaded to IP: 92.230.182.222 On: Sat, 14 Dec 2013 21:52:55

Finally, the QQR estimates are no longer upper bounds to the integral value, but rather provide tight estimates which might as well slightly underestimate the true value. However, this does not have any practical consequences, since tightness of integral estimates can be considered more important than a rigorous upper bound in the present context of preselecting integrals in quantum chemical schemes: Due to the vast amount of neglected contributions, even a screening based on upper bounds will not provide a useful upper bound on the total energy for any reasonable threshold. In Ref. 45, we provide a numerical example in the context of Hartree-Fock theory and a more thorough discussion of the issue, from which we conclude that, in general, tightness of integral estimates is much more important in practice than an upper bound property.

III. COMPUTATIONAL DETAILS

All calculations were performed with a development version of Q-CHEM.[55] The density convergence criterion of the SCF procedure was set to a maximum DIIS error of 10^{-7}, which results in energy steps below 0.5 μHartree in the final iteration. In all the MP2 calculations, the frozen core approximation was applied. In the AO-MP2 calculations, we used 5 quadrature points, which has been found to be sufficient for Laplace errors as small as a few μHartree.[32] The Laplace points were determined for each system using the Levenberg-Marquardt algorithm as described in Ref. 32. If nothing else is indicated, the threshold for the internal screening, i.e., the screening of the transformation steps towards HTIs, was chosen identical to the external screening threshold of the HTI products. The threshold for the determination of the untransformed QQR extents was set to 0.1, which has been shown to provide reliable results in the Hartree-Fock case.[45] The threshold for transformed extents in Eq. (17) was chosen as 10^{-3}, which is considered a reasonable compromise between accuracy and performance based on preliminary calculations. The sparsity threshold for the neglect of small matrix elements was conservatively chosen as 10^{-10}. The basis sets 6-31G*/6-31G**,[56,57] SV(P),[58] and cc-pVTZ[59] were used as noted.

IV. RESULTS

A. Robustness and efficiency of QQZZR4 screening

The definition of the transformed extents is crucial for the reliability as well as efficiency of the QQZZR4 screening. While the MP2 method is mainly applied to systems with localized electron distribution, robust approximations should reliably reproduce the canonical result even for delocalized systems since there is a smooth transition. In Table I, we compare the pure Schwarz results with our proposed QQZZR4 screening (right column) as well as a modified version dubbed "QQZZR4$_{\text{untrf}}$," where the transformed extents were simply substituted by the untransformed ones. The latter approach may of course lead to inappropriate application of the estimates for integrals where the bra and ket charge distributions are not actually well separated but it was included to demonstrate a potential pitfall when developing quantum-chemical methods for large systems: While an approach might provide good results for localized systems, it may still fail for larger molecules with delocalized electronic structure. In the case of the simplistic "untrf" approach the results for hydrogen-chains clearly reveal its defects.

TABLE I. Errors in the opposite-spin MP2 term for DNA_2 (128 atoms) and $Amylose_8$ (171 atoms) in 6-31G* basis and hydrogen chains with 6-31G** basis. Pure Schwarz screening (QQZZ), a modified—not recommended—QQZZR4 screening using only untransformed extents (QQZZR4 untrf), and the usual QQZZR4 screening are compared for a screening threshold of $\vartheta = 10^{-7}$.

	QQZZ		QQZZR4 untrf[a]		QQZZR4[b]	
System	#int[10^6]	err[μH]	#int[10^6]	err[μH]	#int[10^6]	err[μH]
$Amylose_8$	153 111	23.57	38 463	18.33	46 150	13.13
DNA_2	118 498	42.77	44 007	45.31	54 913	58.43
H_{16}	7	− 5.04	3	200.66	5	− 1.38
H_{32}	29	− 8.95	6	526.00	14	− 4.22
H_{64}	118	− 20.09	14	1186.17	32	− 6.42
H_{128}	479	− 41.61	28	2519.34	67	− 15.82

[a] All extents in the estimates are untransformed, the threshold for untransformed extents was raised to 10^{-3}.

[b] Common QQZZR4 screening with thresholds 10^{-1} for untransformed and 10^{-3} for transformed extents.

Our newly proposed QQZZR4 screening with properly transformed extents works reliably for both localized as well as delocalized systems. We conclude, that it is not sufficient to test a new approach only for localized systems, if one aims for an approximation that reliably reproduces the results of the underlying method. Hydrogen chains seem to provide an excellent test case due to the strong delocalization combined with short calculation times.

To get an impression of the efficiency of the QQZZR4 screening, we compare the number of HTIs and the resulting error with a hypothetical screening based on "exact" estimates, that was simulated using the calculated integral values. The data for QQZZR4, pure Schwarz (QQZZ) and this exact screening are plotted in Fig. 2 for different screening thresholds and for the example of $C_{40}H_{82}$. The plot clearly shows that QQZZR4 improves significantly upon pure Schwarz in terms of the number of HTIs that have to be calculated, while the error is of similar size in both cases. Compared to the exact screening, QQZZR4 (naturally) requires more integrals to reach the same accuracy. Taking the connecting lines in Fig. 2 as rough interpolation for intermediate thresholds, one can estimate that reaching the same accuracy with QQZZR4 requires approximately 2 times the amount of HTIs compared to an exact screening. In contrast, pure Schwarz screening requires 6 to 8 times the number of integrals compared to exact screening with the same accuracy and this ratio will increase with system size (because pure Schwarz deteriorates with increasing bra-ket separation).

Similar reference calculations as for the example described above are too expensive for the extensive test set employed in Fig. 3. However, a cheap estimate of the QQZZR4 performance is also possible, if the *a posteriori* screening based on the exact integral values is restricted to those integrals selected by a QQZZR4 screening with a reasonable

This article is copyrighted as indicated in the article. Reuse of AIP content is subject to the terms at: http://scitation.aip.org/termsconditions. Downloaded to IP: 92.230.182.222 On: Sat, 14 Dec 2013 21:52:55

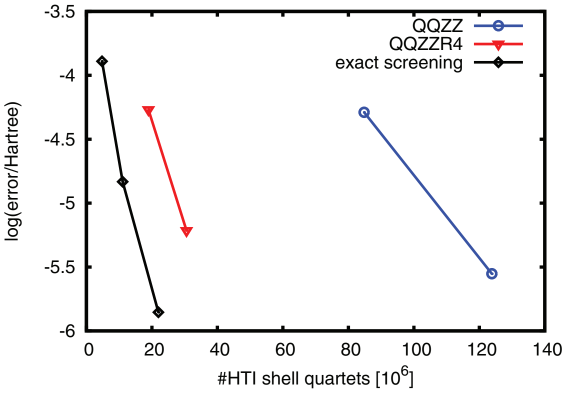

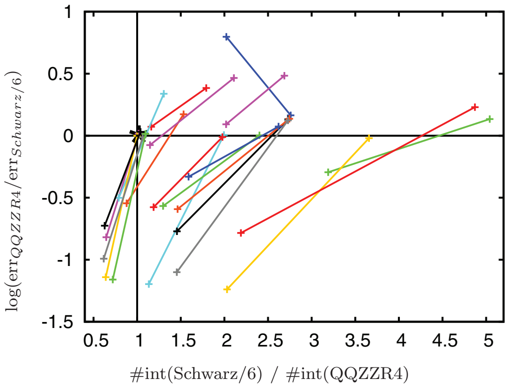

FIG. 2. Dependence of the error of the Coulomb-type term for the first Laplace point on the number of calculated HTI shell quartets in QQZZR4 and pure Schwarz (QQZZ) screening calculations for a linear alkane $C_{40}H_{82}$ (6-31G* basis) with external thresholds of $\vartheta = 10^{-6}$ (left point) and 10^{-7} (right point) as well as results based on a hypothetical exact screening with thresholds of $\vartheta = 10^{-8}$, 10^{-9}, 10^{-10} (from left to right). The reference energy corresponds to a pure Schwarz calculation with $\vartheta = 10^{-10}$. The exact screening is simulated by neglecting all integral shell blocks whose largest actual value is smaller than the chosen threshold. The internal screening threshold was fixed to 10^{-10} in all calculations.

FIG. 3. Error in the opposite-spin MP2 term and speedup (via ratio of integrals) for QQZZR4 AO-MP2 calculations of the whole test set with the 6-31G* basis set (right endpoint: $\vartheta = 10^{-6}$, left endpoint: $\vartheta = 10^{-7}$) relative to the values of a pure Schwarz (QQZZ) calculation with $\vartheta = 10^{-6}$. The Schwarz reference is indicated as a black asterisk at the intersection of the horizontal and vertical line. Values to the right of this reference point indicate increased speed, while values below the reference indicate improved accuracy. The lines that end close to the reference point correspond to very compact or delocalized systems, where QQZZR4 essentially reverts to pure Schwarz screening. The underlying data to the plot can be found in Table II. System sizes in the test set range from 30 to 204 atoms and 250 to 1499 basis functions.

threshold: We chose a screening threshold of $\vartheta = 10^{-7}$ and checked which of the selected integrals were actually negligibly small and had, therefore, been overestimated in the screening process. In these calculations, integrals with values below 10^{-10} can be considered negligible, since their neglect introduces a mean error of only 2.7 μHartree compared to the full summation whereby the number of HTI products is reduced by a factor of 2.3 on average (the average includes the first quadrature point of all the QQZZR4 ($\vartheta = 10^{-7}$) calculations listed in Table II). In contrast, neglecting also integrals with values below 10^{-9} results in an average error of 53.7 μHartree which is significant compared to the accuracy

TABLE II. Total number of half-transformed integrals (HTIs) and error of the opposite-spin AO-MP2 energy with respect to MO-MP2 for calculations in the 6-31G* basis. The absolute energies as well as the canonical reference values are provided in the supplementary material.[76]

	$\vartheta = 10^{-7}$				$\vartheta = 10^{-6}$			
	QQZZ		QQZZR4		QQZZ		QQZZR4	
System	#int[10^6]	err[μH]	#int[10^6]	err[μH]	#int[10^6]	err[μH]	#int[10^6]	err[μH]
Amylose_4	37 432	12.66	20 400	9.00	23 126	141.28	11 596	143.20
Amylose_8	153 111	23.57	46 150	13.13	93 716	227.68	25 628	217.21
Angiotensin	99 646	60.78	41 378	70.65	60 555	276.11	22 063	378.11
Angiotensin deprotonated	97 954	23.43	40 883	38.18	59 533	225.37	21 811	305.03
Angiotensin zwitterion	96 516	6.95	40 284	20.83	58 591	262.58	21 470	348.75
Beta-Carotene	26 292	39.97	10 685	39.50	16 986	84.61	6482	100.29
CNT_{20}	12 216	13.25	12 215	13.25	7818	183.08	7818	182.99
CNT_{40}	75 114	62.95	73 165	70.87	45 905	376.86	44 189	404.97
CNT_{80}	366 158	84.96	251 056	264.94	220 766	928.77	144 090	1383.71
Diamond_{102}	127 361	59.64	122 059	61.49	75 349	603.47	70 825	586.01
DNA_1	19 596	24.18	10 715	33.98	12 731	128.01	6438	124.84
DNA_2	118 498	42.77	54 913	58.43	71 239	215.39	29 663	216.89
Graphite_{24} ($C_{24}H_{12}$)	12 412	25.19	12 295	25.47	7934	167.77	7811	174.42
Graphite_{54} ($C_{54}H_{18}$)	86 884	81.20	69 890	149.95	55 074	475.07	42 178	1034.98
$(H_2O)_{68}$	15 905	6.18	3984	11.04	8723	67.14	1791	113.96
$(\text{LiF})_{32}$	39 371	− 2.73	36 934	− 2.56	26 602	37.03	24 273	38.32
Polyethyne_{64}	39 032	13.47	8417	28.94	26 844	− 57.03	5325	77.64
Polyyne_{64}	29 864	1.05	11 847	2.33	23 924	1.89	8902	5.75
Polyyne_{64} (rotated)	26 792	− 260.25	10 242	− 257.82	20 711	41.09	7505	60.00
$(S_8)_5$	27 531	− 10.17	14 777	7.15	16 952	− 8.52	8039	− 24.87

This article is copyrighted as indicated in the article. Reuse of AIP content is subject to the terms at: http://scitation.aip.org/termsconditions. Downloaded to IP: 92.230.182.222 On: Sat, 14 Dec 2013 21:52:55

of the full summation based on a QQZZR4 ($\vartheta = 10^{-7}$) screening (cf. Table II).

We therefore estimate the amount of integrals that are non-essential in these calculations to be roughly equal to those integrals with a value smaller than 10^{-10} and conclude that our QQZZR4 method overestimates the number of HTI products for the examples listed in Fig. 3 by a factor of roughly 2–2.5 on average.

TABLE III. Total number of half-transformed integrals (HTIs) and error of the opposite-spin AO-MP2/QQZZR4 energy with respect to MO-MP2 for calculations in the SV(P) basis. The absolute energies as well as the canonical reference values are provided in the supplementary material.[76]

	$\vartheta = 10^{-7}$		$\vartheta = 10^{-6}$	
System	#int[10^6]	err[μH]	#int[10^6]	err[μH]
Amylose$_4$	14 522	25.00	7875	253.10
Amylose$_8$	32 927	51.48	17 476	441.67
Angiotensin	30 476	62.82	15 390	864.75
Angiotensin deprotonated	30 079	45.88	15 215	840.05
Angiotensin zwitterion	29 528	58.15	14 945	915.72
Beta-Carotene	8157	30.30	4726	566.61
CNT$_{20}$	9702	−13.28	6047	287.70
CNT$_{40}$	60 482	28.15	36 000	527.23
Diamond$_{102}$	65 063	142.04	39 990	1049.86
DNA$_1$	7090	29.85	4023	292.77
DNA$_2$	36 007	71.07	18 338	669.16
Graphite$_{24}$ ($C_{24}H_{12}$)	9200	9.49	5604	423.59
Graphite$_{54}$ ($C_{54}H_{18}$)	30 728	321.49	18 968	1790.77
H_{64}	5	−27.92	3	109.27
H_{128}	10	−74.12	7	180.75
$(H_2O)_{68}$	2525	73.55	1062	708.46
$(LiF)_{32}$	1057	22.79	484	51.54
Polyethyne$_{64}$	5736	−0.35	3450	258.14
Polyyne$_{64}$	6466	3.75	4442	1025.49
Polyyne$_{64}$ (rotated)	5446	92.67	3645	1851.77
$(S_8)_5$	4679	−44.70	2323	447.73

B. Benchmark calculations

We performed extensive calculations on a subset of our previously presented benchmark set,[45] where we selected systems that allow for MO-MP2 reference calculations within a reasonable time frame. The structure files of the full benchmark set are available for download.[60] In Table II, we compare the results of AO-MP2 using pure Schwarz screening (QQZZ) with our new QQZZR4 approach in a 6-31G* basis. We find that, in general, the QQZZR4 errors are comparable to the errors of the common Schwarz approach with the same threshold. At the same time, the number of HTIs needed for the calculations is drastically reduced compared to QQZZ for most of the systems. As expected, the only exceptions are the very compact $(LiF)_{32}$ and the delocalized carbon nanotubes (CNT) and graphite systems. For all but the delocalized CNT and graphite systems a threshold of 10^{-6} can be recommended, since it allows for errors below 400 μHartree or less than 1 kJ/mol, i.e., so called chemical accuracy.

A graphical representation of the data is given in Fig. 3 where all the QQZZR4 results are plotted with respect to the pure Schwarz calculation with threshold $\vartheta = 10^{-6}$. The connecting lines in the plot can be interpreted as a rough interpolation for intermediate thresholds. The intersection points with the horizontal reference line allow to estimate the savings assuming the same accuracy as the Schwarz calculation. It can be seen that QQZZR4 allows for speedups between 2 and 4.5 compared to Schwarz even for the smaller system sizes studied here. However, it should be noted that the number of selected HTIs scales asymptotically linear for QQZZR4, while it scales quadratic with conventional Schwarz screening, so that the speedups increase roughly linearly with system size for larger systems. The lines that end close to the reference point in Fig. 3 correspond to the delocalized or very compact systems, where the screening essentially reverts—as expected—to pure Schwarz screening.

The notable exception in Fig. 3 is the line on the top with negative slope. This is the very special case of Polyyne$_{64}$, which is essentially a linear carbon chain with alternating bond lengths. This system was calculated not only in standard orientation, like all the other systems, but another time oriented along the (1,1,1)-direction (labeled "rotated"). For the latter case, the unusual behavior is observed (cf. the data in Table II). The reason is the occurence of exceptionally large elements in the virtual pseudo-densities (in the order of 10^4 a.u.), that are due to the extraordinary electronic structure of the system and that increase the internal screening error for individual contributions. Since the system is also very homogenous, i.e., there are many nearly identical contributions, error compensation is variable, which is the reason for the strong dependence on the orientation as well as the error fluctuation with the screening threshold. We want to emphasize that these observations are not connected to the new QQZZR4 screening, but also occur for pure Schwarz screening, and that the QQZZR4 approach reproduces the Schwarz results very well. The problem could be fixed by adjusting the internal screening threshold according to the maximum pseudo-density elements, but we did not make use of this approach. Neither the electronic structure nor the exceptional homogeneity of this tough test case is representative for systems usually studied with MP2 and for common cases, i.e., all the remaining benchmark systems, the new QQR-type screening is shown to be highly reliable.

In Table III, the QQZZR4 results in a SV(P) basis are given. The very expensive CNT$_{80}$ calculations were skipped, but two hydrogen chains were added to represent larger delocalized systems. In comparison with the results in the 6-31G* basis using the same threshold (Table II), it is observed that the error is larger but the number of HTIs is reduced with the SV(P) basis set. This is due to the screening procedure that runs over shells instead of basis functions for efficiency reasons. Since the 6-31G* basis uses shared-sp shells, more functions are selected than in the case of a SV(P) basis, where the s and p shells are estimated separately and the screening is, therefore, more stringent. Due to this, a tighter threshold needs to be applied to reach the same accuracy (cf. Fig. 2 where the "exact" screening needs thresholds 2–3 orders of magnitude tighter than QQZZR4 or Schwarz) and it turns out that a threshold of $\vartheta = 10^{-7}$ in a SV(P) basis gives results

This article is copyrighted as indicated in the article. Reuse of AIP content is subject to the terms at: http://scitation.aip.org/termsconditions. Downloaded to IP: 92.230.182.222 On: Sat, 14 Dec 2013 21:52:55

TABLE IV. The number of basis functions, the total number of half-transformed integrals (HTIs), the scaling with system size, and the error of the opposite-spin AO-MP2/QQZZR4 energy with respect to MO-MP2 for calculations on linear alkanes.

	6-31G*, $\vartheta = 10^{-6}$				cc-pVTZ, $\vartheta = 10^{-9}$			
System	N_{bas}	#int[10^6]	scaling[a]	err[μH]	N_{bas}	#int[10^6]	scaling[a]	err[μH]
C_5H_{12}	99	143		9.71	318	12 613		2.92
$C_{10}H_{22}$	194	550	2.00	8.78	608	45 766	1.99	5.39
$C_{20}H_{42}$	384	1414	1.38	– 28.23	1188	11 7291	1.40	…[b]

[a] Scaling exponent for the number of half-transformed integrals (HTIs) with respect to the next smaller alkane.

[b] Only the external screening part of the calculation has been performed.

comparable to $\vartheta = 10^{-6}$ in a 6-31G* basis both in terms of accuracy as well as the number of HTIs.

For the larger cc-pVTZ basis set, we performed test calculations on linear alkanes, where the results are shown in Table IV. For the scaling of the number of HTIs with increasing basis set size N at fixed molecule size one expects an N^4 behavior. Comparing the 6-31G* and cc-pVTZ bases this corresponds to an expected factor for the integral numbers of roughly $3.1^4 \approx 90$ for larger linear alkanes which is well represented by the QQZZR4 screening results presented in Table IV, where the screening thresholds were chosen to provide comparable accuracies in both bases (i.e., $\vartheta = 10^{-6}$ and $\vartheta = 10^{-9}$, respectively). This observation indicates a consistently good performance of our QQR-type screening even for larger basis sets in line with the observation for the SCF case.[45] In this context, it should be noted that also analogous scaling *with system size* for both the 6-31G* and cc-pVTZ basis is observed as expected.

As confirmed by the data in Tables II and III, a systematic improvement of the errors is generally possible by tightening the threshold. We therefore conclude that, for a wide range of molecular systems, our AO-MP2 in combination with the QQZZR4 screening provides reliable results, and the accuracy is fully controlled.

Our benchmark calculations allow to choose the threshold such that the error in the absolute energies is satisfactory for the system sizes studied. For very large systems, the error in the absolute energy of course grows (approximately linearly) with the number of atoms. Usually, this does not pose any problems in practice, since the errors can be expected to largely cancel for relative energies, which are the quantity of interest in most cases. We performed calculations on the well-known S22 test set[61] for interaction energies to study this effect as shown below.

The root-mean-square deviation (RMSD) of the interaction energies for the whole S22 set is given in Table V and confirms that a threshold of 10^{-6} is enough to reach an error well below 1 kcal/mol for relative energies. The second row in Table V shows the RMSD of a worst case estimate that simulates missing error compensation and is simply determined by adding up the (unsigned) errors in the absolute energies of the monomer and dimer calculations for each system. Comparing this worst case estimate with the actual RMSD shows that a significant error compensation occurs for a threshold of $\vartheta = 10^{-6}$, while the error compensation is smaller in the case of $\vartheta = 10^{-7}$. The reason for this observation lies in the different dominating error contributions: In the case of the tighter threshold $\vartheta = 10^{-7}$ the remaining (small) error is mainly determined by the Laplace quadrature, which amounts to approximately 0.001–0.1 kcal/mol with 5 quadrature points. For the small test systems of S22, we conclude that the Laplace error does not exhibit any significant error cancellation for interaction energies. It should be noted that the Laplace error in these counterpoise-corrected calculations is enhanced by high-lying virtual ghost functions that essentially correspond to core orbitals of the ghost atoms and thus the error could be further reduced by applying the "frozen virtual" approximation as described in Ref. 32. In addition to that, it might be useful to choose identical quadrature points for the monomer and dimer calculations to facilitate error compensation, while in all our calculations the Laplace points were determined in each calculation individually.

For the case of the generally recommended threshold $\vartheta = 10^{-6}$ the error in the interaction energies is mainly determined by the neglect of integral contributions. Since these contributions describe local correlation effects, the error is mostly canceled for interaction energies. For large interacting systems, where the contact area is small compared to the size of an individual monomer, we also expect favorable error compensation. The reason is that the intramonomer errors, which are large on an absolute scale, will largely cancel when forming energy differences. We therefore expect that the thresholds, which provide satisfactory accuracy in absolute energies for our benchmark set (see above), will provide accurate interaction energies even for very large interacting systems. Of course, the accuracy can always be verified and systematically improved in our AO-MP2 method by incrementally tightening the threshold and increasing the number of quadrature points.

TABLE V. Counterpoise-corrected SOS-AO-MP2/QQZZR4 results for the S22 test set with a SVP basis. The root-mean-square deviation (RMSD) of the errors in the interaction energy with respect to full SOS-MO-MP2 are given.

	RMSD [kcal/mol]	
S22 interaction energies	$\vartheta = 10^{-6}$	$\vartheta = 10^{-7}$
Error in the interaction energy	0.139	0.051
Worst case estimate[a]	0.431	0.072

[a] For the worst case estimate we summed up the errors in the absolute energies of the monomer and dimer calculations for each test system.

This article is copyrighted as indicated in the article. Reuse of AIP content is subject to the terms at: http://scitation.aip.org/termsconditions. Downloaded to IP: 92.230.182.222 On: Sat, 14 Dec 2013 21:52:55

TABLE VI. Number of basis functions and HTI products as well as the scaling behavior of the number of HTIs with respect to the next smaller system for DNA double-strands with a 6-31G* basis set ($\vartheta = 10^{-6}$).

	N	#HTI [10^6]	scaling
DNA_1	579	6438	
DNA_2	1252	29 663	1.98
DNA_4	2598	81 901	1.39
DNA_8	5290	186 869	1.16
DNA_{16}	10 674	396 853	1.07

C. Scaling behavior and timings

Using our new QQZZR4 screening, our AO-MP2 method shows an early onset of linear scaling for systems with significant HOMO-LUMO gap. The scaling of the number of HTI products for DNA systems is given in Table VI. From two to four DNA base pairs, the scaling is already down to 1.39, while for the larger systems it is almost perfectly linear (1.07). For the larger cc-pVTZ basis set we found in test calculations on linear alkanes that the scaling of the number of half-transformed integrals is essentially the same as in the 6-31G* basis (see Table IV). If the basis set contains diffuse functions the onset of linear scaling is naturally shifted to larger systems: While in a 6-31G* or cc-pVTZ basis the scaling of HTIs is very close to $N^{2.0}$ from C_5H_{12} to $C_{10}H_{22}$, the scaling for calculations in a 6-31++G** basis is still $N^{2.1}$ from $C_{20}H_{42}$ to $C_{40}H_{82}$.

In Fig. 4, we plotted timings with the 6-31G* basis set for SOS variants of MO-MP2, RI-MP2, and our AO-MP2 method as well as conventional RI-MP2. The calculations were run on a single core of an Intel Xeon E5620 using 48 GB RAM. It should be noted, that the RI errors in absolute MP2 energies are usually much larger than the errors of our AO-MP2 method, if one of the generally recommended basis/auxiliary basis combinations is applied in the RI calculation (so that the comparison is not entirely fair for AO-MP2). While the deviations in absolute energies introduced by the RI approach are usually not a problem in practice, since the errors cancel to a large extent when relative energies are considered, AO-MP2 in contrast exhibits small errors even for absolute energies and fast convergence to the canonical result with the screening threshold and the number of Laplace quadrature points.

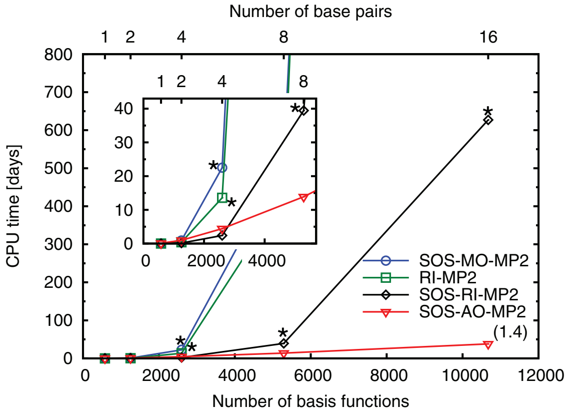

FIG. 4. CPU times for SOS-MO-MP2, RI-MP2, and SOS-RI-MP2 (both with aux-SVP auxiliary basis) as well as SOS-AO-MP2 ($\vartheta = 10^{-6}$) calculations on DNA systems with the 6-31G* basis. The number in brackets indicates the scaling behavior with respect to the previous point. Neither the common MO-MP2 nor any of the RI-MP2 versions are feasible for the largest systems due to their steep scaling with system size, so the data points (*) were extrapolated conservatively with the scaling behavior of the previous points (MO-MP2 4.41, RI-MP2 4.85, SOS-RI-MP2 3.94).

The canonical SOS-MO-MP2 formally scales as $\mathcal{O}(N^5)$ and is therefore only competitive for smaller systems with less than 1500 basis functions. The conventional RI-MP2 method shows the same $\mathcal{O}(N^5)$ scaling with a reduced prefactor but due to the steep scaling the prefactor reduction does not extend the accessible system sizes substantially compared to MO-MP2. The SOS-RI-MP2 implementation of Jung *et al.*[35] is clearly more efficient than conventional $\mathcal{O}(N^5)$ schemes by reducing the asymptotic scaling to $\mathcal{O}(N^4)$ using a Laplace approach, while being constrained to the Coulomb-type MP2 contraction (opposite-spin component). For the larger systems, the $\mathcal{O}(N^4)$ scaling of SOS-RI-MP2 clearly shows the limitation of this efficient scheme to medium sized molecules. Due to the steep scaling of MO-MP2 and the RI variants, calculations on the larger systems were not feasible. The timings were extrapolated with the scaling behavior of the previous points, which can be considered a conservative estimate, since for larger systems the regime of the (higher) asymptotic scaling behavior of the methods would presumably be reached.

In contrast our SOS-AO-MP2 method using QQZZR4 screening shows an early onset of linear scaling with a scaling exponent from 8 to 16 DNA base pairs of 1.4. The crossover of our linear-scaling method occurs as compared to SOS-MO-MP2 roughly around two DNA base pairs (1200/1300 basisfunctions), to RI-MP2 for roughly three DNA basepairs (1700/1800 basis functions), and to the fourth-order scaling SOS-RI-MP2 method for about five DNA basepairs (roughly 3400 basis functions).

With our linear-scaling AO-MP2 method the largest system computed, so far, on a single core comprises 1052 atoms corresponding to 16 DNA base pairs with 10674 basis functions in a 6-31G* basis. The full calculation took approximately two months, whereas the estimated calculation time for the SOS-RI-MP2 approach would be close to two years and for the conventional MO-MP2 calculation more than three decades even with our conservative extrapolation. It should be noted that the RI methodology can also be applied within our AO-MP2 approach to speed up the calculation,[62] but the linear scaling behavior would be lost if no *a priori* restriction of the fitting domains[25] or a local fitting metric[63,64] is employed, which we have not exploited so far and which shows that the comparison to the RI schemes is not entirely fair for our AO-MP2 method.

D. Parallelization and application to the MutM-DNA complex

Our AO-MP2 method is also particularly suited for parallelization since both the Coulomb and exchange-type contribution (Eqs. (3) and (4)) can be conveniently split into smaller batches of HTI products that can be evaluated independently.

This article is copyrighted as indicated in the article. Reuse of AIP content is subject to the terms at: http://scitation.aip.org/termsconditions. Downloaded to IP: 92.230.182.222 On: Sat, 14 Dec 2013 21:52:55

Since only the screening matrices (calculated once in the beginning) and the final energy contribution have to be communicated between the computing nodes there is only minimal overhead.

We performed SOS-AO-MP2 calculations on a system of a DNA strand containing an 8-oxoguanine lesion interacting with the enzyme MutM that is responsible for DNA repair. The setup was based on a crystal structure of the syn-conformer (PDB 1R2Y), which was edited by saturating with hydrogen atoms and adding water and counter ions and then minimized using the AMBER force-field.[65,66] The anti-conformer was obtained by manual rotation and subsequent molecular dynamics for the inner region (5 Å around the lesion) in order to remove sterical clashes. After a final minimization, all residues within 11 Å of the lesion in both conformers were selected for the quantum-chemical calculation. Further details of the system setup will be given in an upcoming publication.[66]

The SOS-AO-MP2 calculations were performed for the cutouts of both conformers which each comprises 2025 atoms and 20 371 basis functions with a 6-31G* basis set and correspond to the system plotted in Fig. 5 (the anti-conformer is shown exemplarily). A screening threshold of 10^{-6} was applied (see Tables II and V for benchmark data). The main part of the calculation, i.e., the evaluation of the HTI products, was performed on 20 nodes each equipped with two Intel Xeon E5620 (total of 160 cores) and 48 GB RAM. The wall time for this dominating step was approximately 7.5 days. In addition, the screening matrices have been calculated in advance on 5 nodes with two Intel Xeon E5620 CPUs and 96 GB RAM in less than 1 day, so that the calculation of one conformer required approximately 8.5 days in total.

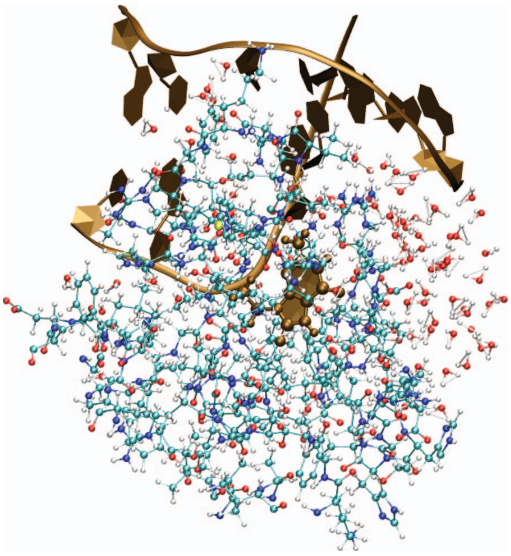

FIG. 5. Cutout of the X-ray structure of a DNA double strand with an 8-oxoguanine lesion in complex with the MutM repair protein. Calculations of two conformers were performed at the SOS-AO-MP2 level of theory. The cutout comprises 2025 atoms and 20 371 basis functions in a 6-31G** basis. The SOS-AO-MP2 calculation took 8.5 days on a cluster with 160 cores in parallel.

While these results for the repair complex are more of a benchmark calculation at this stage, our preliminary findings are qualitatively in line with the results of the force-field molecular dynamics studies of Ref. 67 that indicate the syn-conformer to form a more stable complex by about 2.7 kcal/mol for the 8-oxoguanine lesion. At the SOS-AO-MP2/6-31G** level of theory, we find an energy difference between the complex with syn- and anti-conformer (with two different but fixed geometries) of 24.1 kcal/mol in favor of the syn-conformer.

The calculation shows that our linear-scaling AO-MP2 method allows to handle very large systems which is expected to be useful for biochemical studies by providing a wave-function based description of electron correlation. At the Hartree-Fock level of theory it has been found that accurate descriptions of isomerization energies or nuclear magnetic resonance (NMR) shifts require to include large parts of the environment of about 6–10 Å around the region of interest in the quantum-chemical description.[68–70] While it is still a question under study how large the environment needs to be chosen to converge the influence of correlation effects, our AO-MP2 method is well suited for these kinds of studies since systems including residues within more than 10 Å around the region of interest are accessible.

V. CONCLUSION AND OUTLOOK

We have introduced QQR-type integral estimates into AO-MP2 theory, that account efficiently for the integral decay with the bra-ket separation in both untransformed and transformed integrals and allow for evaluating the correlation energy with linear-scaling computational cost. The QQR estimates exploit the asymptotic decay behavior of the two-electron integrals, deduced from the multipole expansion, and combine this decay with the common Schwarz bound to a simple and tight estimate. Using the QQR estimates in the screening of the Coulomb-type MP2 term allows to exploit the $1/R^4$ coupling between bra and ket charge distributions, so that a linear-scaling number of significant integral products can be preselected for systems with significant HOMO-LUMO gaps. Furthermore, our QQR estimates are quite generally applicable to two-electron quantities in quantum chemistry, so that they can also be straightforwardly applied to preselect two-electron integrals in other local methods or, e.g., the Cholesky decomposed density MP2.[54]

We have provided benchmark calculations of our AO-MP2 method on a diverse selection of test systems, which show that AO-MP2 produces reliable results for localized as well as delocalized systems, where in the latter case, the screening essentially reverts to pure Schwarz screening. It was further shown for the example of DNA systems, that our implementation shows an early onset of linear-scaling for systems with significant HOMO-LUMO gap which allows to outperform conventional MP2 methods for systems larger than a few base pairs. The favorable scaling of our method allows to perform calculations on systems with more than 1000 atoms and more than 10 000 basis functions on a single core. Our AO-MP2 method is also particularly suited for parallelization, where we presented benchmark calculations on a

This article is copyrighted as indicated in the article. Reuse of AIP content is subject to the terms at: http://scitation.aip.org/termsconditions. Downloaded to IP: 92.230.182.222 On: Sat, 14 Dec 2013 21:52:55

cutout of a protein-DNA repair complex, where the calculated system comprised 2025 atoms and 20 371 basis functions.

Furthermore, our AO-MP2 method is an ideal starting point for calculating molecular properties of large systems. In contrast to, e.g., empirical dispersion corrections to DFT, which do not depend directly on the electronic structure, the AO-MP2 approach takes full account of correlation even in the case of response properties. Besides the linear-scaling formulation of MP2 gradients that was recently developed in our group,[47] we aim for second derivatives of the MP2 energy: Using our new QQR-type screening we have an ideal starting point for such developments, where a major goal is to extend our linear- and sublinear-scaling methods for calculating NMR shieldings at HF or DFT level[71–74] to the MP2 level.[75] Such MP2 NMR shieldings are expected to provide another important and reliable link to experimental studies.

ACKNOWLEDGMENTS

C.O. acknowledges financial support by the Volkswagen Stiftung within the funding initiative "New Conceptual Approaches to Modeling and Simulation of Complex Systems" and by the SFB 749 "Dynamik und Intermediate molekularer Transformationen" (DFG).

[1] R. G. Parr and W. Yang, *Density-Functional Theory of Atoms and Molecules* (Oxford University Press, New York, 1994).
[2] W. Kohn and L. J. Sham, Phys. Rev. **140**, A1133 (1965).
[3] C. A. White, B. G. Johnson, P. M. W. Gill, and M. Head-Gordon, Chem. Phys. Lett. **230**, 8 (1994).
[4] M. Challacombe, E. Schwegler, and J. Almlöf, J. Chem. Phys. **104**, 4685 (1996).
[5] M. C. Strain, G. E. Scuseria, and M. J. Frisch, Science **271**, 51 (1996).
[6] E. Schwegler, M. Challacombe, and M. Head-Gordon, J. Chem. Phys. **106**, 9708 (1997).
[7] C. Ochsenfeld, C. A. White, and M. Head-Gordon, J. Chem. Phys. **109**, 1663 (1998).
[8] E. Schwegler and M. Challacombe, J. Chem. Phys. **111**, 6223 (1999).
[9] C. Ochsenfeld, J. Kussmann, and D. S. Lambrecht, in *Reviews in Computational Chemistry*, edited by K. B. Lipkowitz and T. R. Cundari (Wiley-VCH, 2007), Vol. 23, pp. 1–81.
[10] A. Palser and D. Manolopoulos, Phys. Rev. B **58**, 12704 (1998).
[11] Y. Shao, C. Saravanan, M. Head-Gordon, and C. A. White, J. Chem. Phys. **118**, 6144 (2003).
[12] A. M. N. Niklasson, C. J. Tymczak, and M. Challacombe, J. Chem. Phys. **118**, 8611 (2003).
[13] A. D. Becke, J. Chem. Phys. **98**, 5648 (1993).
[14] P. J. Stephens, F. J. Devlin, C. F. Chabalowski, and M. J. Frisch, J. Phys. Chem. **98**, 11623 (1994).
[15] S. Grimme, WIREs Comput. Mol. Sci. **1**, 211 (2011).
[16] E. Rudberg, E. H. Rubensson, and P. Sałek, J. Chem. Theory Comput. **7**, 340 (2011).
[17] D. Cremer, WIREs Comput. Mol. Sci. **1**, 509 (2011).
[18] P. Pulay and S. Saebø, Theor. Chim. Acta **69**, 357 (1986).
[19] C. Hampel and H.-J. Werner, J. Chem. Phys. **104**, 6286 (1996).
[20] P. Maslen and M. Head-Gordon, Chem. Phys. Lett. **283**, 102 (1998).
[21] M. Schütz, G. Hetzer, and H.-J. Werner, J. Chem. Phys. **111**, 5691 (1999).
[22] M. S. Lee, P. E. Maslen, and M. Head-Gordon, J. Chem. Phys. **112**, 3592 (2000).
[23] G. Hetzer, M. Schütz, H. Stoll, and H.-J. Werner, J. Chem. Phys. **113**, 9443 (2000).
[24] S. Saebø and P. Pulay, J. Chem. Phys. **115**, 3975 (2001).
[25] H.-J. Werner, F. R. Manby, and P. J. Knowles, J. Chem. Phys. **118**, 8149 (2003).
[26] J. Almlöf, Chem. Phys. Lett. **181**, 319 (1991).
[27] M. Häser and J. Almlöf, J. Chem. Phys. **96**, 489 (1992).
[28] M. Häser, Theor. Chim. Acta **87**, 147 (1993).
[29] A. K. Wilson and J. Almlöf, Theor. Chim. Acta **95**, 49 (1997).
[30] P. Y. Ayala and G. E. Scuseria, J. Chem. Phys. **110**, 3660 (1999).
[31] G. E. Scuseria and P. Y. Ayala, J. Chem. Phys. **111**, 8330 (1999).
[32] B. Doser, D. S. Lambrecht, J. Kussmann, and C. Ochsenfeld, J. Chem. Phys. **130**, 064107 (2009).
[33] M. Feyereisen, G. Fitzgerald, and A. Komornicki, Chem. Phys. Lett. **208**, 359 (1993).
[34] F. Weigend, M. Häser, H. Patzelt, and R. Ahlrichs, Chem. Phys. Lett. **294**, 143 (1998).
[35] Y. Jung, R. C. Lochan, A. D. Dutoi, and M. Head-Gordon, J. Chem. Phys. **121**, 9793 (2004).
[36] Y. Jung, Y. Shao, and M. Head-Gordon, J. Comput. Chem. **28**, 1953 (2007).
[37] H. Koch, A. Sánchez de Merás, and T. B. Pedersen, J. Chem. Phys. **118**, 9481 (2003).
[38] T. J. Martinez and E. A. Carter, J. Chem. Phys. **100**, 3631 (1994).
[39] R. B. Murphy, M. D. Beachy, R. A. Friesner, and M. N. Ringnalda, J. Chem. Phys. **103**, 1481 (1995).
[40] H.-J. Werner and F. R. Manby, J. Chem. Phys. **124**, 054114 (2006).
[41] T. B. Adler, H.-J. Werner, and F. R. Manby, J. Chem. Phys. **130**, 054106 (2009).
[42] K. Kristensen, I.-M. Høyvik, B. Jansik, P. Jørgensen, T. Kjærgaard, S. Reine, and J. Jakowski, Phys. Chem. Chem. Phys. **14**, 15706 (2012).
[43] M. Häser and R. Ahlrichs, J. Comput. Chem. **10**, 104 (1989).
[44] D. S. Lambrecht and C. Ochsenfeld, J. Chem. Phys. **123**, 184101 (2005); **136**, 149901 (2012).
[45] S. A. Maurer, D. S. Lambrecht, D. Flaig, and C. Ochsenfeld, J. Chem. Phys. **136**, 144107 (2012).
[46] P. Surjan, Chem. Phys. Lett. **406**, 318 (2005).
[47] S. Schweizer, B. Doser, and C. Ochsenfeld, J. Chem. Phys. **128**, 154101 (2008).
[48] J. Kussmann, M. Beer, and C. Ochsenfeld, "Linear-scaling self-consistent field methods for large molecules," WIREs Comput. Mol. Sci. (to be published).
[49] C. Ochsenfeld, Chem. Phys. Lett. **327**, 216 (2000).
[50] S. Grimme, J. Chem. Phys. **124**, 034108 (2006).
[51] L. Goerigk and S. Grimme, J. Chem. Theory Comput. **7**, 291 (2011).
[52] B. G. Johnson, C. A. White, Q. Zhang, B. Chen, R. L. Graham, P. M. W. Gill, and M. Head-Gordon, in *Recent Developments and Applications of Modern Density Functional Theory*, edited by J. Seminario (Elsevier, Amsterdam, 1996), pp. 441–464.
[53] D. S. Lambrecht, B. Doser, and C. Ochsenfeld, J. Chem. Phys. **123**, 184102 (2005).
[54] J. Zienau, L. Clin, B. Doser, and C. Ochsenfeld, J. Chem. Phys. **130**, 204112 (2009).
[55] Y. Shao, L. F. Molnar, Y. Jung, J. Kussmann, C. Ochsenfeld, S. T. Brown, A. T. Gilbert, L. V. Slipchenko, S. V. Levchenko, D. P. O'Neill, R. A. DiStasio, Jr., R. C. Lochan, T. Wang, G. J. Beran, N. A. Besley, J. M. Herbert, C. Yeh Lin, T. Van Voorhis, S. Hung Chien, A. Sodt, R. P. Steele, V. A. Rassolov, P. E. Maslen, P. P. Korambath, R. D. Adamson, B. Austin, J. Baker, E. F. C. Byrd, H. Dachsel, R. J. Doerksen, A. Dreuw, B. D. Dunietz, A. D. Dutoi, T. R. Furlani, S. R. Gwaltney, A. Heyden, S. Hirata, C.-P. Hsu, G. Kedziora, R. Z. Khalliulin, P. Klunzinger, A. M. Lee, M. S. Lee, W. Liang, I. Lotan, N. Nair, B. Peters, E. I. Proynov, P. A. Pieniazek, Y. Min Rhee, J. Ritchie, E. Rosta, C. David Sherrill, A. C. Simmonett, J. E. Subotnik, H. Lee Woodcock III, W. Zhang, A. T. Bell, A. K. Chakraborty, D. M. Chipman, F. J. Keil, A. Warshel, W. J. Hehre, H. F. Schaefer III, J. Kong, A. I. Krylov, P. M. W. Gill, and M. Head-Gordon, Phys. Chem. Chem. Phys. **8**, 3172 (2006).
[56] W. J. Hehre, R. Ditchfield, and J. A. Pople, J. Chem. Phys. **56**, 2257 (1972).
[57] P. C. Hariharan and J. A. Pople, Theor. Chim. Acta **28**, 213 (1973).
[58] A. Schäfer, H. Horn, and R. Ahlrichs, J. Chem. Phys. **97**, 2571 (1992).
[59] T. H. Dunning, J. Chem. Phys. **90**, 1007 (1989).
[60] See http://www.cup.uni-muenchen.de/pc/ochsenfeld/download.html for structure files.
[61] P. Jurecka, J. Sponer, J. Cerný, and P. Hobza, Phys. Chem. Chem. Phys. **8**, 1985 (2006).
[62] J. Zienau, "Low-order scaling second-order Møller-Plesset perturbation theory using auxiliary basis sets and quantum-chemical calculation of NMR chemical shifts for supramolecular systems," Ph.D. dissertation (Ochsenfeld group, University of Tuebingen, 2009).
[63] Y. Jung, A. Sodt, P. M. W. Gill, and M. Head-Gordon, Proc. Natl. Acad. Sci. U.S.A. **102**, 6692 (2005).

This article is copyrighted as indicated in the article. Reuse of AIP content is subject to the terms at: http://scitation.aip.org/termsconditions. Downloaded to IP: 92.230.182.222 On: Sat, 14 Dec 2013 21:52:55

[64] D. S. Lambrecht, K. Brandhorst, W. H. Miller, C. W. McCurdy, and M. Head-Gordon, J. Phys. Chem. A **115**, 2794 (2011).

[65] D. Case, T. Darden, T. C. Cheatham III, C. Simmerling, J. Wang, R. Duke, R. Luo, M. Crowley, R. C. Walker, W. Zhang, K. Merz, B. Wang, S. Hayik, A. Roitberg, G. Seabra, I. Kolossváry, K. F. Wong, F. Paesani, J. Vanicek, X. Wu, S. Brozell, T. Steinbrecher, H. Gohlke, L. Yang, C. Tan, J. Mongan, V. Hornak, G. Cui, D. Mathews, M. Seetin, C. Sagui, V. Babin, and P. Kollman, AMBER 10, Technical Report (University of California, San Francisco, 2008).

[66] D. Flaig, K. Sadeghian, S. A. Maurer, and C. Ochsenfeld, "A quantum-chemical study of DNA repair processes" (unpublished).

[67] K. Song, V. Hornak, C. de Los Santos, A. P. Grollman, and C. Simmerling, Biochemistry **45**, 10886 (2006).

[68] C. V. Sumowski and C. Ochsenfeld, J. Phys. Chem. A **113**, 11734 (2009).

[69] C. V. Sumowski, B. B. T. Schmitt, S. Schweizer, and C. Ochsenfeld, Angew. Chem. Int. Ed. **49**, 9951 (2010).

[70] D. Flaig, M. Beer, and C. Ochsenfeld, J. Chem. Theory Comput. **8**, 2260 (2012).

[71] C. Ochsenfeld, J. Kussmann, and F. Koziol, Angew. Chem. Int. Ed. **43**, 4485 (2004).

[72] J. Kussmann and C. Ochsenfeld, J. Chem. Phys. **127**, 054103 (2007).

[73] M. Beer and C. Ochsenfeld, J. Chem. Phys. **128**, 221102 (2008).

[74] M. Beer, J. Kussmann, and C. Ochsenfeld, J. Chem. Phys. **134**, 074102 (2011).

[75] M. Maurer and C. Ochsenfeld, "A linear-scaling MP2 method for the calculation of NMR shieldings" (unpublished).

[76] See supplementary material at http://dx.doi.org/10.1063/1.4770502 for data tables of absolute AO-MP2 energies and reference values.

This article is copyrighted as indicated in the article. Reuse of AIP content is subject to the terms at: http://scitation.aip.org/termsconditions. Downloaded to IP: 92.230.182.222 On: Sat, 14 Dec 2013 21:52:55

Supplementary Information to ”Efficient distance-including integral screening in linear-scaling Møller-Plesset perturbation theory”

Simon A. Maurer, Daniel S. Lambrecht[a)], Jörg Kussmann, and Christian Ochsenfeld[b)]

Chair of Theoretical Chemistry, Department of Chemistry,

University of Munich (LMU), Butenandtstr. 7, D-81377 München, Germany

[a)] Present address: Dept. of Chemistry, University of Pittsburgh, Pittsburgh, PA 15260, USA

[b)] Electronic mail: christian.ochsenfeld@uni-muenchen.de

System	E_{SCF}	E_{OS}^{MP2}	E_{SS}^{MP2}	E_{corr}^{MP2}
Amylose$_4$	-2504.77076388	-5.07941431	-1.85890756	-6.93832187
Amylose$_8$	-4933.56835921	-10.01542195	-3.67149775	-13.68691971
Angiotensin	-3541.05434831	-7.87539979	-2.89191349	-10.76731328
Angiotensin deprotonated	-3539.84841707	-7.87886769	-2.90075622	-10.77962391
Angiotensin zwitterion	-3540.78868347	-7.89114594	-2.90140661	-10.79255255
Beta-Carotene	-1547.18051370	-3.87302407	-1.32400691	-5.19703098
CNT$_{20}$	-762.65937688	-1.91738425	-0.75912234	-2.67650659
CNT$_{40}$	-1519.66993613	-3.85642067	-1.63657694	-5.49299760
CNT$_{80}$	-3033.88778035	-7.59539153	-3.29840179	-10.89379332
Diamond$_{102}$	-1623.01308246	-4.30485565	-1.62253785	-5.92739350
DNA$_1$	-1753.05875675	-3.71269490	-1.39079153	-5.10348642
DNA$_2$	-4486.05367572	-8.11171862	-3.08070025	-11.19241887
Graphite$_{24}$ ($C_{24}H_{12}$)	-915.91890811	-2.19309157	-0.86212825	-3.05521981
Graphite$_{54}$ ($C_{54}H_{18}$)	-2054.81443025	-5.02016432	-2.02144373	-7.04160805
$(\mathrm{H_2O})_{68}$	-5169.25891993	-9.55780460	-3.37558409	-12.93338870
$(\mathrm{LiF})_{32}$	-1712.41286653	-2.27451608	-0.89863502	-3.17315110
Polyethyne$_{64}$	-2461.52240281	-6.00452511	-2.07366626	-8.07819137
Polyyne$_{64}$	-2422.52579175	-5.74981142	-2.14945437	-7.89926580
Polyyne$_{64}$ (rotated)	-2422.52579057	-5.74981006	-2.14945423	-7.89926429
$(\mathrm{S_8})_5$	-15900.34495487	-3.61805261	-1.33812056	-4.95617317

TABLE A. Hartree-Fock energies (E_{SCF}), opposite-spin (E_{OS}^{MP2}) and same-spin (E_{SS}^{MP2}) MP2 contributions as well as the total MP2 energy ($\mathrm{E}_{corr}^{MP2} = \mathrm{E}_{OS}^{MP2} + \mathrm{E}_{SS}^{MP2}$) in a 6-31G* basis for the systems listed in table II of the paper. The comparison to AO-MP2 in the paper is restricted to E_{OS}^{MP2}, the other values are given for future benchmarks.

	$\vartheta = 10^{-7}$		$\vartheta = 10^{-6}$	
System	QQZZ	QQZZR4	QQZZ	QQZZR4
Amylose$_4$	-5.07940165	-5.07940531	-5.07927303	-5.07927111
Amylose$_8$	-10.01539839	-10.01540882	-10.01519427	-10.01520475
Angiotensin	-7.87533901	-7.87532914	-7.87512368	-7.87502168
Angiotensin deprotonated	-7.87884425	-7.87882951	-7.87864232	-7.87856266
Angiotensin zwitterion	-7.89113899	-7.89112511	-7.89088336	-7.89079718
Beta-Carotene	-3.87298410	-3.87298457	-3.87293947	-3.87292379
CNT$_{20}$	-1.91737101	-1.91737100	-1.91720118	-1.91720126
CNT$_{40}$	-3.85635771	-3.85634980	-3.85604381	-3.85601569
CNT$_{80}$	-7.59530657	-7.59512659	-7.59446276	-7.59400782
Diamond$_{102}$	-4.30479600	-4.30479415	-4.30425217	-4.30426964
DNA$_1$	-3.71267072	-3.71266092	-3.71256688	-3.71257006
DNA$_2$	-8.11167585	-8.11166019	-8.11150323	-8.11150173
Graphite$_{24}$ ($C_{24}H_{12}$)	-2.19306637	-2.19306609	-2.19292380	-2.19291715
Graphite$_{54}$ ($C_{54}H_{18}$)	-5.02008312	-5.02001437	-5.01968925	-5.01912934
$(H_2O)_{68}$	-9.55779842	-9.55779357	-9.55773747	-9.55769065
$(LiF)_{32}$	-2.27451881	-2.27451864	-2.27447905	-2.27447776
Polyethyne$_{64}$	-6.00451165	-6.00449617	-6.00458214	-6.00444747
Polyyne$_{64}$	-5.74981037	-5.74980909	-5.74980954	-5.74980568
Polyyne$_{64}$ (rotated)	-5.75007032	-5.75006788	-5.74976897	-5.74975007
$(S_8)_5$	-3.61806277	-3.61804545	-3.61806112	-3.61807748

TABLE B. Opposite-spin AO-MP2 energies with Schwarz (QQZZ) or QQR-type screening (QQZZR4) in a 6-31G* basis. The values in table II of the paper are the difference between the values in this table and the canonical reference E_{OS}^{MP2} values provided in table A.

System	E_{SCF}	E_{OS}^{MP2}	E_{SS}^{MP2}	E_{corr}^{MP2}
Amylose$_4$	-2502.71580805	-5.08036056	-1.83341489	-6.91377545
Amylose$_8$	-4929.52812295	-10.01567411	-3.62104055	-13.63671466
Angiotensin	-3538.20116588	-7.80047080	-2.85746119	-10.65793199
Angiotensin deprotonated	-3537.00930470	-7.80243290	-2.86604429	-10.66847719
Angiotensin zwitterion	-3537.93476480	-7.81589138	-2.86701488	-10.68290626
Beta-Carotene	-1545.91401152	-3.78680325	-1.30609081	-5.09289407
CNT$_{20}$	-762.06679523	-1.89013234	-0.75456001	-2.64469235
CNT$_{40}$	-1518.49486494	-3.81414607	-1.63157657	-5.44572264
Diamond$_{102}$	-1621.67114578	-4.22712703	-1.60654552	-5.83367256
DNA$_1$	-1751.64059417	-3.68518126	-1.37081311	-5.05599437
DNA$_2$	-4482.78614256	-8.07040192	-3.04093262	-11.11133454
Graphite$_{24}$ ($C_{24}H_{12}$)	-915.20813101	-2.15585491	-0.85301206	-3.00886697
Graphite$_{54}$ ($C_{54}H_{18}$)	-2053.25907528	-4.94997989	-2.00449839	-6.95447828
H$_{64}$	-33.41799921	-0.77126130	-0.12100887	-0.89227017
H$_{128}$	-66.83866647	-1.54405345	-0.25092614	-1.79497960
$(H_2O)_{68}$	-5164.46588204	-9.71832034	-3.34446025	-13.06278059
(LiF)$_{32}$	-1711.00561791	-2.34866025	-0.90545452	-3.25411477
Polyethyne$_{64}$	-2459.56032011	-5.86991588	-2.04390673	-7.91382260
Polyyne$_{64}$	-2420.70591842	-5.65260748	-2.12357071	-7.77617819
Polyyne$_{64}$ (rotated)	-2420.70591752	-5.65260627	-2.12357035	-7.77617662
$(S_8)_5$	-15896.03282630	-3.74241683	-1.40884823	-5.15126505

TABLE C. Hartree-Fock energies (E_{SCF}), opposite-spin (E_{OS}^{MP2}) and same-spin (E_{SS}^{MP2}) MP2 contributions as well as the total MP2 energy ($E_{corr}^{MP2} = E_{OS}^{MP2} + E_{SS}^{MP2}$) in a SV(P) basis for the systems listed in table III of the paper. The comparison to AO-MP2 in the paper is restricted to E_{OS}^{MP2}, the other values are given for future benchmarks.

System	$\vartheta = 10^{-7}$	$\vartheta = 10^{-6}$
Amylose$_4$	-5.08033555	-5.08010746
Amylose$_8$	-10.01562263	-10.01523244
Angiotensin	-7.80040797	-7.79960605
Angiotensin deprotonated	-7.80238703	-7.80159285
Angiotensin zwitterion	-7.81583324	-7.81497566
Beta-Carotene	-3.78677296	-3.78623664
CNT$_{20}$	-1.89014562	-1.88984464
CNT$_{40}$	-3.81411793	-3.81361885
Diamond$_{102}$	-4.22698499	-4.22607718
DNA$_1$	-3.68515141	-3.68488849
DNA$_2$	-8.07033085	-8.06973275
Graphite$_{24}$ ($C_{24}H_{12}$)	-2.15584542	-2.15543132
Graphite$_{54}$ ($C_{54}H_{18}$)	-4.94965841	-4.94818912
H$_{64}$	-0.77128923	-0.77115203
H$_{128}$	-1.54412757	-1.54387270
(H$_2$O)$_{68}$	-9.71824679	-9.71761188
(LiF)$_{32}$	-2.34863746	-2.34860871
Polyethyne$_{64}$	-5.86991623	-5.86965774
Polyyne$_{64}$	-5.65260372	-5.65158199
Polyyne$_{64}$ (rotated)	-5.65251360	-5.65075450
(S$_8$)$_5$	-3.74246153	-3.74196909

TABLE D. Opposite-spin AO-MP2 energies with Schwarz (QQZZ) or QQR-type screening (QQZZR4) in a SV(P) basis. The values in table III of the paper are the difference between the values in this table and the canonical reference E_{OS}^{MP2} values provided in table C.

5.3 Paper III: ”Cholesky-decomposed density MP2 with density fitting: accurate MP2 and double-hybrid DFT energies for large systems”,

S. A. Maurer, L. Clin, C. Ochsenfeld,

(submitted)

Cholesky-decomposed density MP2 with density fitting: accurate MP2 and double-hybrid DFT energies for large systems

Simon A. Maurer, Lucien Clin, and Christian Ochsenfeld[a)]

Chair of Theoretical Chemistry, Department of Chemistry,
University of Munich (LMU), Butenandtstr. 7, D-81377 Munich, Germany
and
Center for Integrated Protein Science (CIPSM) at the Department of Chemistry,
University of Munich (LMU), Butenandtstr. 5-13, D-81377 Munich, Germany

Our recently developed QQR-type integral screening is introduced in our Cholesky-decomposed pseudo-densities Møller-Plesset perturbation theory of second order (CDD-MP2) method. We use the resolution-of-the-identity (RI) approximation in combination with efficient integral transformations employing sparse matrix multiplications. The RI-CDD-MP2 method shows an asymptotic cubic scaling behavior with system size and a small prefactor that results in an early crossover to conventional methods for both small and large basis sets. We also explore the use of local fitting approximations which allow to further reduce the scaling behavior for very large systems. The reliability of our method is demonstrated on test sets for interaction and reaction energies of medium sized systems and on a diverse selection from our own benchmark set for total energies of larger systems. Timings on DNA systems show that fast calculations for systems with more than 500 atoms are feasible using a single processor core. Parallelization extends the range of accessible system sizes on one computing node with multiple cores to more than 1000 atoms in a double-zeta basis and more than 500 atoms in a triple-zeta basis.

a)Electronic mail: christian.ochsenfeld@uni-muenchen.de

I. INTRODUCTION

The efficient account of electron correlation is a central challenge in the development of quantum-chemical methods. The importance of a reliable correlation description is a requirement to describe the London dispersion effects which are important in many chemical and biochemical systems. The least expensive wave-function based method that allows for a non-empirical account of dispersion effects is the second-order energy correction in Møller-Plesset perturbation theory (MP2) [1] which has therefore been extensively studied [2]. While MP2 scales with the fifth power of the molecular size in its MO-based formulation, the development of efficient low-order scaling methods for computing the MP2 energy has seen tremendous advancements in the last decade (see, e.g., Ref. [2] for a recent review). In contrast to MP2, conventional functionals in the density functional theory (DFT) approach [3] require either a large number of fitting parameters or empirical correction terms to describe dispersive contributions (see Ref. [4] for a recent review). The modern double-hybrid DFT functionals – a class of functionals which was pioneered by Grimme in 2006 [5] with the B2-PLYP functional – show better results than conventional functionals in many respects including the dispersion description [5]. However, the double-hybrid functionals contain a perturbative term which is equivalent to the MP2 expression except that Kohn-Sham orbitals from a conventional functional are used as input instead of the Hartree-Fock orbitals in MP2 theory. Therefore, the efficient evaluation of the MP2 expression is an equally important goal for MP2 theory as well as for modern double-hybrid DFT functionals.

An important step in the development of efficient MP2 methods was the use of the resolution-of-the-identity (RI) approximation [6] (also known as density fitting). The RI approximation significantly reduces the prefactor of the calculation while the fifth-power scaling of the computational cost with system size remains for a full RI-MP2 calculation. Only in combination with a neglect of the exchange-type term, as in the scaled opposite-spin (SOS-)MP2 method [7] the scaling behavior can be reduced to a fourth-order scaling. Closely connected to the RI approach are methods that use a Cholesky decomposition of the two-electron integral matrix [8, 9] which is similar to an on-the-fly creation of an auxiliary RI basis. Other developments in MP2 theory include pseudospectral methods [10] and the recent introduction of a tensor decomposition of the ERI integrals [11] where the latter also provides a promising fourth-order scaling evaluation of the MP2 expression.

Low-order scaling MP2 methods were initiated by the seminal work of Pulay and Saebø [12, 13] who introduced a reformulation of MP2 theory that allows to employ localized orbitals and to impose local restrictions on the correlation space. This non-canonical MP2 method requires an iterative procedure to determine the MP2 amplitudes but the whole calculation can be realized with linear-scaling cost [14]. Further improvements include local density fitting approximations to reduce the prefactor of the calculations [15]. In recent work, a dynamic expansion of the correlation space in local methods has been explored in the divide-expand-consolidate MP2 method [16].

A second pathway to low-order scaling MP2 theory was developed by Häser and Almlöf [17–19] using a Laplace transform to eliminate the energy denominator which allows for a purely atomic orbital-based (AO) expression of the MP2 energy. Different linear-scaling methods have been developed based on the non-iterative AO-MP2 approach [20–24]. In contrast to local MP2 methods based on the Pulay/Saebø approach which usually apply spatial restrictions of the correlation space, practical AO-MP2 methods rely on integral estimates to preselect significant contributions [23, 24]. In previous work, we succesfully employed our recently developed QQR-type estimates [24, 25] within AO-MP2, which allow to perform SOS-AO-MP2 calculations on molecules with more than 2000 atoms and 20000 basis functions [24]. Based on the AO-MP2 approach, the linear-scaling formulation of gradients [26], shielding tensors for nuclear-magnetic resonance measurements [27] and the dispersion interaction contribution in symmetry-adapted perturbation theory [28] have been developed where even sublinear-scaling is possible for local perturbations [27, 28].

While our linear-scaling AO-MP2 method is particularly suited for large systems and moderate basis sets, the prefactor is significantly increased for large basis sets due to the redundancies in the set of atomic orbital basis functions which is particularly pronounced for the occupied space. One way to circumvent the problem is the use of small basis sets in combination with an explicitly correlated approach as recently proposed by Hollman et al. [29]. Explicitly correlated MP2 is known to significantly reduce the basis set incompleteness error and therefore lower the requirements for the basis set quality but additional costs arise from the computation of the explicitly correlated terms involving three-electron integrals [30].

In this work, we follow another approach, where the dependency on the basis set size of AO-MP2 is reduced by restoring the restrictions to non-redundant sets of occupied and virtual functions using a Cholesky decomposition of the pseudo-densities (CDD). The theory and a pilot implementation of the SOS-CDD-MP2 method was presented in 2009 [31]. In the present work, we report on a full CDD-MP2 implementation that employs our new QQR-type integral estimates in the screening procedure and efficient sparse matrix algebra in the integral transformation steps. We show that, with these improvements, RI-based CDD-MP2 is a very efficient cubic scaling MP2 method which shows an early crossover to the conventional RI-MP2 method with both small and large basis sets. Furthermore, for an interesting range of molecules the RI-CDD-MP2 method shows smaller prefactors than our linear-scaling AO-MP2 scheme that allowed for the calculation of a DNA-repair complex with 2025 atoms and 20 371 basis functions [24]. Therefore, for a certain molecular-size window RI-CDD-MP2 seems currently the method of choice for calculating reliable and fully numerically controlled MP2 and double-hybrid DFT energies despite the non-linear scaling behavior at this stage.

In section II we discuss the theory of QQR-based CDD-MP2 while some important properties of the Cholesky decomposition of the pseudo-densities are discussed in more detail in the appendix. Benchmark results for the S66 test set [32], the set of reaction energies of Riplinger et al. [33], and our benchmark set of large systems [25] are presented in section IV A and show that small and well-controlled errors are obtained with our RI-CDD-MP2 method. In section IV B, we discuss timings of our method for model systems of linear alkanes where we also explore local RI fitting. As realistic examples, calculations on DNA systems with more than 500 atoms and more than 5000 basis functions on a single CPU core are presented. Results for calculations with more than 10000 basis functions using parallelization are presented in section V where the largest systems contained 1052 atoms with a double-zeta basis and 524 atoms with a triple-zeta basis and were calculated on one computing node with multiple cores.

II. THEORY

Our method is based on the Laplace AO-MP2 approach, which was pioneered by Almlöf and Häser [17, 34, 35]. In this approach, the Laplace transform allows to express the MP2 energy using only AO quantities [35]

$$E_{AO-MP2} = -\sum_{\alpha} \sum_{\substack{\mu\nu\lambda\sigma \\ \mu'\nu'\lambda'\sigma'}} \underline{P}_{\mu\mu'} \overline{P}_{\nu\nu'} \underline{P}_{\sigma\sigma'} \overline{P}_{\lambda\lambda'} \left[2(\mu\nu|\lambda\sigma) - (\mu\sigma|\lambda\nu)\right] (\mu'\nu'|\lambda'\sigma') \tag{1}$$

where the first sum runs over the quadrature points of the Laplace expansion. The MO coefficients and orbital energies are contracted into the so-called pseudo-densities

$$\begin{aligned} \underline{P}_{\mu\nu} &= (\omega_\alpha)^{\frac{1}{4}} \sum_{i}^{\text{occ}} c_{\mu i} e^{\epsilon_i t_\alpha} c_{\nu i} \\ \overline{P}_{\mu\nu} &= (\omega_\alpha)^{\frac{1}{4}} \sum_{a}^{\text{virt}} c_{\mu a} e^{-\epsilon_a t_\alpha} c_{\nu a} \end{aligned} \tag{2}$$

where the alpha-dependent parameters are the coefficients of the Laplace expansion.

The derivation of our Cholesky-decomposed pseudo-density (CDD-)MP2 method [31] starts from Eq. 1 where a Cholesky decomposition with complete pivoting [36, 37] is performed on $\underline{\mathbf{P}}$ and $\overline{\mathbf{P}}$

$$\underline{\mathbf{P}} = \underline{\mathbf{L}}\,\underline{\mathbf{L}}^T \qquad \overline{\mathbf{P}} = \overline{\mathbf{L}}\,\overline{\mathbf{L}}^T. \tag{3}$$

The pivoting procedure is required to extend the applicability of the Cholesky decomposition to positive semi-definite matrices like the pseudo-densities. The columns of $\underline{\mathbf{L}}$ ($\overline{\mathbf{L}}$) can be considered as the coefficients of localized occupied (virtual) pseudo-MOs, which in contrast to regular MOs include the effect of the orbital energies. The number of pseudo-MOs is equal or smaller than the number of occupied (virtual) MOs as discussed in Appendix

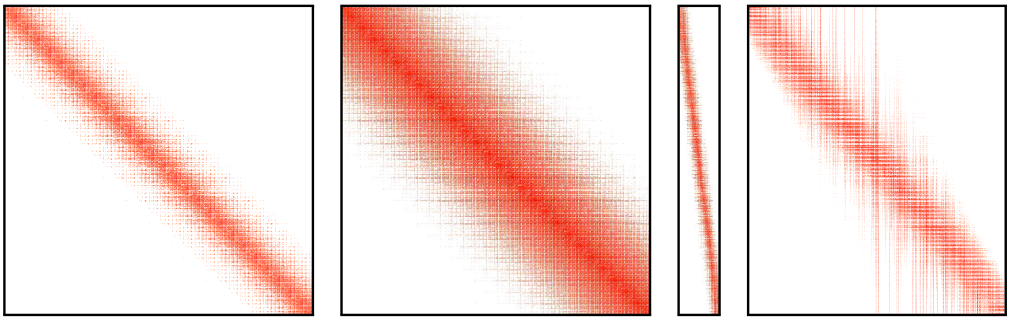

(a) $\underline{\mathbf{P}}$ (b) $\overline{\mathbf{P}}$ (c) $\underline{\mathbf{L}}$ (d) $\overline{\mathbf{L}}$

Figure 1. Sparsity pattern of the pseudo-density matrices and the coefficient matrices of the Cholesky pseudo-MOs for the example of $C_{80}H_{162}$

A. Furthermore, the pseudo-MOs mostly inherit the locality from the pseudo-densities as already noted by Aquilante et al. [38] for the decomposition of the standard density matrix and depicted in Fig. 1. In our method, we reorder the columns of $\underline{\mathbf{L}}$ /$\overline{\mathbf{L}}$ as described in detail in Sec. III which does not affect the validity of the decomposition but makes the sparsity pattern better visible and more suitable for the sparse formats that use a block structure. Due to the local features of the pseudo-MOs we will abbreviate them as LPMOs (local pseudo-MOs) in the following.

The expression for the CDD-MP2 energy then reads

$$E_{CDD-MP2} = -\sum_{\alpha}\sum_{ij}^{\text{occ}}\sum_{ab}^{\text{virt}} \left[2(\underline{i}\overline{a}|\underline{j}\overline{b}) - (\underline{i}\overline{b}|\underline{j}\overline{a})\right] (\underline{i}\overline{a}|\underline{j}\overline{b}) \tag{4}$$

with the two-electron integrals in the basis of the LPMOs

$$(\underline{i}\overline{a}|\underline{j}\overline{b}) = \sum_{\mu\nu\lambda\sigma} \underline{L}_{\mu i}\overline{L}_{\nu a}\underline{L}_{\lambda j}\overline{L}_{\sigma b}(\mu\nu|\lambda\sigma). \tag{5}$$

The LPMO basis is non-redundant and the *formal* number of contributions in CDD-MP2 is therefore only $N_{occ}^2 N_{virt}^2$ per Laplace point (N_{occ} and N_{virt} are the number of occupied and virtual MOs) instead of N_{basis}^4 in the AO-MP2 expression (see Ref. [24]) with N_{basis} denoting the number of basis functions. As both MP2 methods are based on local functions, the number of *significant* contributions scales linear in both cases

Similar to our AO-MP2 method [24], we use our efficient QQR-type estimates for the screening of significant integral products. In the basis of the LPMOs, every $(\underline{i}\overline{a}|\underline{j}\overline{b})$ integral shows an asymptotic $1/R^3$ decay with increasing bra-ket separation which can be deduced from the multipole expansion. The monopole of both bra- and ket-charge distributions are zero, i.e.,

$$\underline{\mathbf{L}}^T\mathbf{S}\overline{\mathbf{L}} = \mathbf{0} \tag{6}$$

which is proven in appendix B. The first (slowest decaying) non-zero term in the multipole expansion is therefore the dipole-dipole term which determines the asymptotic $1/R^3$ decay [24]. The appropriate QQR-type integral estimates take the form [24]

$$(\underline{i}\overline{a}|\underline{j}\overline{b}) \approx \frac{Z_{\underline{i}\overline{a}}Z_{\underline{j}\overline{b}}}{(R_{\underline{i}\overline{a},\underline{j}\overline{b}} - \mathrm{ext}_{\underline{i}\overline{a}} - \mathrm{ext}_{\underline{j}\overline{b}})^3} \tag{7}$$

with the pseudo-Schwarz integrals $Z_{\underline{i}\overline{a}} = (\underline{i}\overline{a}|\underline{i}\overline{a})^{\frac{1}{2}}$ and the distance $R_{\underline{i}\overline{a},\underline{j}\overline{b}}$ between the two charge distributions. The centers of the LPMO products as well as the extents $\mathrm{ext}_{\underline{i}\overline{a}}$ are defined in Appendix C. It should be noted that we do not use the estimate for $Z_{\underline{i}\overline{a}}$ which is conventionally employed in AO-MP2 (based on the Schwarz-integrals for singly transformed distributions, see, e.g., Eq. (31-33) in Ref. [35]) but instead calculate the $(\underline{i}\overline{a}|\underline{i}\overline{a})$ integrals using the RI-approach (see below) without further approximations.

Based on the decay behavior of the individual integrals, the behavior of the Coulomb-type integral products $(\underline{i}\overline{a}|\underline{j}\overline{b})(\underline{i}\overline{a}|\underline{j}\overline{b})$ follows as $1/R^6$, while the decay of the exchange-type contributions $(\underline{i}\overline{a}|\underline{j}\overline{b})(\underline{i}\overline{b}|\underline{j}\overline{a})$ is stronger due to the additional direct coupling of all indices within the function products of either bra or ket. Using the estimates of Eq. 7, the asymptotic decay behavior of all terms is efficiently taken into account in the screening procedure which allows to preselect a linear-scaling number of significant (i,j,a,b) combinations.

To reduce the cost of the screening procedure, we furthermore include a pre-screening of electron pairs (i,j). We take the maximum Schwarz estimate for a given (i,j) combination and any possible index a and b to build the corresponding QQR-type estimate

$$(\underline{i}\overline{a}|\underline{j}\overline{b}) \lessapprox \frac{Z_{\underline{i},\max}Z_{\underline{j},\max}}{(R_{\underline{i},\underline{j}} - \mathrm{ext}_{\underline{i}} - \mathrm{ext}_{\underline{j}})^3} \tag{8}$$

with $Z_{\underline{i},\max} = \max_{\overline{a}} Z_{\underline{i},\overline{a}}$ and the centers and extents assigned to occupied LPMOs as defined in appendix C. Exploiting the sparsity of the pseudo-Schwarz matrix $\mathbf{Z}$, this pre-screening procedure scales quadratically with system size with negligible cost and allows to reduce the scaling of the remaining screening steps according to Eq. 7 to linear.

For an efficient evaluation of the ERIs in the LPMO basis, we use the density-fitting/RI approximation [6]

$$(\underline{i}\overline{a}|\underline{j}\overline{b}) = \sum_{PQ} (\underline{i}\overline{a}|P) \left[\mathbf{J}^{-1}\right]_{PQ} (Q|\underline{j}\overline{b}) \tag{9}$$

where the matrix $\mathbf{J}$ contains the two-center Coulomb integrals $(P|Q)$ in the auxiliary basis. For efficient evaluation this expression can be recast into the following form

$$\begin{aligned}
(\underline{i}\overline{a}|\underline{j}\overline{b}) &= \sum_{P} B_{\underline{i}\overline{a},P} B_{\underline{j}\overline{b},P} \\
B_{\underline{i}\overline{a},P} &= \sum_{\mu\nu} \underline{L}_{\mu\underline{i}} \overline{L}_{\nu\overline{a}} B_{\mu\nu,P} \\
B_{\mu\nu,P} &= \sum_{Q} (\mu\nu|Q) \left[\mathbf{J}^{-\frac{1}{2}}\right]_{QP} .
\end{aligned} \tag{10}$$

The formation of the AO elements $B_{\mu\nu,P}$ shows an asymptotically cubic scaling with system size but has to be performed only once and will become only significant for very large systems, so that we have not put any effort into elaborating on this step. The following transformations to the LPMO basis (required for every Laplace point) are realized in an asymptotic quadratic scaling way by exploiting the sparsity of the LPMO coefficient matrices. We perform this step using sparse matrix multiplications with the very efficient block-compressed sparse row (BCSR) format [39, 40] that uses highly optimized basic linear algebra subroutines (BLAS) for the multiplication of significant blocks. The final contraction step to the integrals $(\underline{i}\overline{a}|\underline{j}\overline{b})$ again scales quadratically with system size and can be performed using dense matrix multiplications after collecting the appropriate (i,j,a,b) combinations.

It is also possible to reduce the scaling in the transformation and contraction steps in the RI procedure to asymptotically linear with system size, if the auxiliary functions are restricted to atoms where the charge distributions of either bra or ket have significant contributions (local fitting) [15]. In this case the sums in Eq. 9 are restricted to a constant number of elements per integral at the expense of a recalculation of the inverse of the matrix $\mathbf{J}$ for each restricted set of auxiliary functions. As a simple criterion to determine the fitting functions assigned to an occupied orbital, we compare the maximum LPMO coefficient on each atom with a chosen threshold (default: 10^{-3}) and assign all RI functions on these selected atoms to this LPMO. We then follow the approach of Werner et al. [15] and merge all the fit domains of all the occupied orbitals that build pairs with a given LPMO i into a larger set of fitting functions (called *orbital fit domains* in Ref. [15]) that is used as auxiliary space for all (i,j) pairs. Despite the larger auxiliary space, we found this approach beneficial. It reduces the number of times the inverse of the matrix $\mathbf{J}$ in Eq. 9 has to be calculated from once per (i,j) pair to once per occupied orbital, which overcompensates the increased cost due to the larger number of fit functions. We furthermore merge the orbital fit domains of several (default: 30) occupied LPMOs into an even larger set of fitting functions to further reduce this cost and make the local fit competitive for reasonably sized systems.

To determine double-hybrid DFT energies, Eq. 4 is evaluated with Kohn-Sham orbitals. No modification of the MP2 code is required and only the SCF part of the calculation is substituted by a Kohn-Sham calculation. The energy obtained with Eq. 4 is finally scaled with a functional-dependent parameter and added to the DFT SCF result to obtain the double-hybrid DFT energy.

III. COMPUTATIONAL DETAILS

All calculations were performed with the newly developed QM package FermiONs++ [41]. If nothing else is indicated, we use 6 quadrature points for the Laplace expansion and a screening threshold of 10^{-9} in our QQR-type screening. The underlying Hartree-Fock calculations have been converged to a maximum element of the DIIS error matrix below 10^{-7}. The extents for the QQR-type estimates are determined with the same thresholds as in our AO-MP2 approach [24], i.e., the untransformed (AO) extents are based on a threshold of 0.1 and the threshold for transformed extents in Eq. C4 is 10^{-3}. The basis sets cc-pVTZ [42, 43] and def2-SVP [44] were used as noted, together with the corresponding auxiliary basis sets for the RI expansion in MP2 [45, 46]. The frozen core approximation was used in all MP2 calculations.

The sparsity criterion for the BCSR matrix blocks is chosen as 10^{-6}. Details of our BCSR implementation are given in Ref. [40]. The reverse Cuthill-McKee algorithm [47, 48] is applied to reorder the atoms in the molecule by reducing the bandwith of the connectivity matrix. It should be noted that this approach provides banded pseudo-density matrices for elongated systems while their Cholesky decomposition as obtained by the algorithm for semi-definite matrices does not immediately reflect this property due to the pivoting procedure. The banded structure has to be reestablished by reordering the columns in a suitable way. In this work, we reorder the columns in a two step procedure. In the first step, we determine the indices of the first and last significant entry in each column, take the average and pre-order the columns according to this value. In the next step, we optimize for the BCSR format and determine the first and last significant block of each single column. The comparison in the final sorting procedure is then based on the index of the last significant block if this value differs by more than 1, otherwise the index of the first significant block is compared.

IV. RESULTS

A. Benchmark calculations

We performed benchmark calculations on the S66 test set for interaction energies [32] as well as the test set for reaction energies of Riplinger et al. (see table II of Ref. [33]). The error statistics for these test sets are compared to a canonical RI-MP2 reference in table I: The errors obtained with our method are virtually negligible for these test sets (smaller than 0.05 kcal/mol in all cases). As we are aiming for large systems and the error increases with system size, we consider the high accuracy appropriate for these small test systems.

For benchmark calculations on larger systems we compared absolute energies for molecules from our own benchmark set [25] similar to the set used in our AO-MP2 studies (table II of Ref. [24]), where we did not consider the larger carbon nanotubes due to convergence problems in the cc-pVTZ basis and replaced the $Li_{16}F_{16}$ system by the larger $Li_{36}F_{36}$ cutout. The

	S66 test set for interactions	Reaction test set of Ref. [33]
RMSD	0.018	0.008
MAE	0.014	0.005
MAX	0.039	0.022

Table I. Root mean square deviation (RMSD), mean absolute error (MAE) and maximum error (MAX) for the RI-CDD-MP2 method in a cc-pVTZ basis compared to RI-MP2 reference results for the S66 set of interaction energies [32] and the test set for reaction energies of Riplinger et al. [33]. All values are given in kcal/mol.

results are given in table II. Besides our default choice for the screening threshold ($\vartheta = 10^{-9}$) we also compare to the results for thresholds 10^{-8} and 10^{-10}. Our default threshold results in errors smaller than 1.5 mHartree for systems with significant HOMO-LUMO gap and the error shows a smooth convergence behavior with the threshold for all but the small gap (5,0)CNT and graphene systems. For these systems with very small HOMO-LUMO gap the default number of Laplace points needs to be increased and smooth convergence of the accuracy with increasing number of Laplace points is observed. To reach sub-mHartree accuracy the (5,0)CNT requires 9 Laplace points while the graphene $C_{54}H_{18}$ only needs 7 expansion points. As we focus on systems with localized electronic structure and significant HOMO-LUMO gap, we consider the default of 6 Laplace points and a threshold of $\vartheta = 10^{-9}$ a reliable choice. It should be noted that the RI-CDD-MP2 energies can always be converged with these parameters to check the validity of the results also in the case that no benchmark values are available.

B. Scaling behavior and timings

We analyzed the performance of our RI-CDD-MP2 method with full auxiliary basis and the variant with local RI fitting on linear alkanes as model systems. The timings are plotted

			Error [μHartree]		
System	# atoms	# bf	$\vartheta = 10^{-10}$	$\vartheta = 10^{-9}$	$\vartheta = 10^{-8}$
Amylose$_4$	87	1938	57	386	3306
Amylose$_8$	171	3818	210	1025	7567
Angiotensin	146	3244	135	994	7724
Angiotensin deprotonated	144	3216	137	1008	7922
Angiotensin zwitterion	146	3244	136	982	7787
Diamond $C_{42}H_{60}$	102	2100	18	419	6930
DNA$_1$	62	1428	29	174	1608
DNA$_2$	128	3016	139	995	7958
Li$_{36}$F$_{36}$	72	2160	89	992	15500
Polyyne $C_{64}H_2$	66	1948	159	559	4762
Polyyne $C_{64}H_2$ (rotated)	66	1948	224	1318	14768
(S$_8$)$_5$	40	1360	26	587	5573
(5.0)CNT $C_{20}H_{10}$	30	740	3316 [a]	3326 [a]	3613
Beta-Carotene	96	1984	134	362	2759
Graphene $C_{24}H_{12}$	36	888	252 [a]	275	740
Graphene $C_{54}H_{18}$	72	1872	1164 [a]	1348 [a]	4595
Polyethyne $C_{64}H_{66}$	130	2844	325	609	3605

[a] The error with the tighter thresholds can be attributed mainly to the Laplace expansion in these small gap systems and decreases consistently with increasing number of Laplace points. For the default threshold 10^{-9}, errors below 1 mHartree are obtained with 9 (7) points for the CNT $C_{20}H_{10}$ (Graphene $C_{54}H_{18}$) system.

Table II. Error of RI-CDD-MP2 with respect to canonical RI-MP2 results for different screening thresholds ϑ. The number of atoms and basis functions are given for each system. The selected systems are part of our previously published benchmark set [25] and the structure files are available for download from our website [49]. The systems in the lower part of the table have a delocalized structure in combination with a small HOMO-LUMO gap ($\lesssim 0.3\,a.u.$ in the cc-pVTZ basis).

in Fig. 2 and details including the scaling behavior are summarized in Tab. III. The timings of our RI-CDD-MP2 method show an early crossover with canonical RI-MP2 calculations at system sizes between 20 and 40 carbon atoms. For systems with 80 carbon atoms the speedup with our new method is almost a factor of 10 compared to the canonical approach. The scaling exponent of RI-CDD-MP2 with full RI basis is around 2.5 for larger systems and approaches 3 in the asymptotic limit. For very large systems the local fitting approximation shows significant savings compared to the RI-CDD-MP2 method with full auxiliary basis. The local fitting implementation scales close to linear in many steps but there are still some quadratic remnants in the code (most importantly the calculation of all $(\mu\nu|P)$ integrals) which have an adverse effect on the scaling for the largest alkane systems (more than 160 carbon atoms). The scaling behavior of our RI-CDD-MP2 method with full auxiliary basis and the speedups compared to the canonical approach are similar in both the def2-SVP and cc-pVTZ basis. For the local fitting variant the scaling is slightly higher in the cc-pVTZ basis as compared to the def2-SVP basis. As the local fitting approach becomes faster than the calculations with full auxiliary space only for systems with more than 80 carbon atoms and still shows close to quadratic scaling for these system sizes, we restricted the following studies to the full RI approach.

We also compared our RI-CDD-MP2 method with our linear-scaling SOS-AO-MP2 method for the case of the linear alkane with 80 carbon atoms. The number of significant contributions in a def2-SVP basis is $8.6 \cdot 10^9$ for SOS-AO-MP2 and $1.9 \cdot 10^9$ which amounts to a reduction by a factor of 4.5. This is the result of the reduced number of formal contributions and the stronger decay behavior of the contributions in RI-CDD-MP2 as discussed in Sec. II. The calculation time for this example system is 17.1 h for SOS-AO-MP2 compared to 2.7 h for RI-CDD-MP2 which is due to the efficient RI treatment in the latter method in combination with the reduced number of significant contributions.

Besides the alkane model systems we also performed timings on DNA strands where the results are plotted in Fig. 3 and details including the scaling behavior are given in Tab. IV. Again, the RI-CDD-MP2 method shows an early crossover with RI-MP2 for system sizes

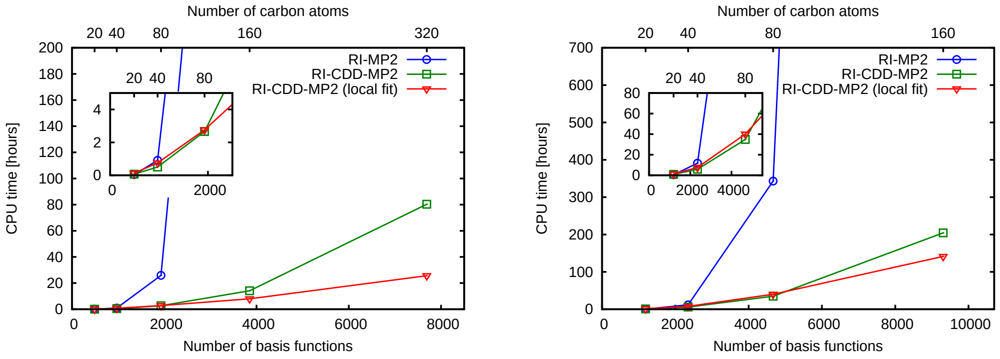

(a) def2-SVP (b) cc-pVTZ

Figure 2. CPU times for canonical RI-MP2 and RI-CDD-MP2 calculations with full auxiliary basis as well as local fitting on linear alkanes. The RI-MP2 values for systems with more than 80 carbon atoms have been conservatively extrapolated with the scaling behavior of the two previous points.

between one and two DNA base pairs. Already for four DNA base pairs the speedup is more than a factor of 4 compared to the canonical approach in both the def2-SVP and cc-pVTZ basis (using conservatively extrapolated values for RI-MP2/cc-pVTZ). For the largest system with eight base pairs in def2-SVP the estimated RI-MP2 calculation time would be more than one order of magnitude larger than the time required with our RI-CDD-MP2 method.

V. LARGE-SCALE CALCULATIONS

We performed calculations on very large DNA systems using multi-core computing nodes and an OpenMP parallelized code. On the triple-zeta level we performed a calculation on a system with 8 DNA base pairs with 524 atoms and 12544 basis functions on a node with four Xeon E7-4820 processor (32 cores in total) using roughly 60 GB of RAM. The MP2 calculation finished in ∼40.5 days, where more than half of the time (∼25 days) is due to (serial) hard-disk input-output (I/O) access reading batches of RI integrals from disk. The calculation might therefore be significantly sped up by simultaneous execution of the expensive RI multiplications and I/O operations, but we did not yet exploit this approach

def2-SVP basis		RI-MP2		RI-CDD-MP2		RI-CDD-MP2 (local fit)	
System	#bf	time [h]	scaling	time [h]	scaling	time [h]	scaling
$C_{20}H_{42}$	490	0.04	-	0.07	-	0.13	-
$C_{40}H_{82}$	970	0.91	4.68	0.50	2.79	0.75	2.60
$C_{80}H_{162}$	1930	25.92	4.87	2.66	2.44	2.76	1.89
$C_{160}H_{322}$	3850	789.31	4.95	14.10	2.42	7.99	1.54
$C_{320}H_{642}$	7690	-	-	80.29	2.51	25.63	1.68
cc-pVTZ basis		RI-MP2		RI-CDD-MP2		RI-CDD-MP2 (local fit)	
System	#bf	time [h]	scaling	time [h]	scaling	time [h]	scaling
$C_{20}H_{42}$	1188	0.46	-	0.88	-	1.30	-
$C_{40}H_{82}$	2348	11.75	4.77	5.87	2.78	7.59	2.59
$C_{80}H_{162}$	4668	343.01	4.91	34.81	2.59	40.06	2.42
$C_{160}H_{322}$	9308	-	-	204.54	2.57	141.37	1.83

Table III. CPU times and scaling behavior with respect to the number of basis functions for canonical RI-MP2 and RI-CDD-MP2 calculations both with full auxiliary basis and local fitting approximations on linear alkane systems in a def2-SVP and cc-pVTZ basis (all calculations on one CPU core).

in our present implementation.

The largest system containing 16 base pairs and 1052 atoms was calculated in a def2-SVP basis comprising 11230 basis functions. This calculation was performed on a node with two Xeon E5645 processors (12 cores in total) where roughly 50 GB of RAM were used and the total RI-CDD-MP2 calculation time was ∼49.5 days. In contrast, for a conventional RI-MP2 calculation even an unrealisticly optimistic extrapolation assuming perfect parallelization on the 12 CPU cores and no hard disk limitations would amount to two years of CPU time and one additional year of serial I/O operations.

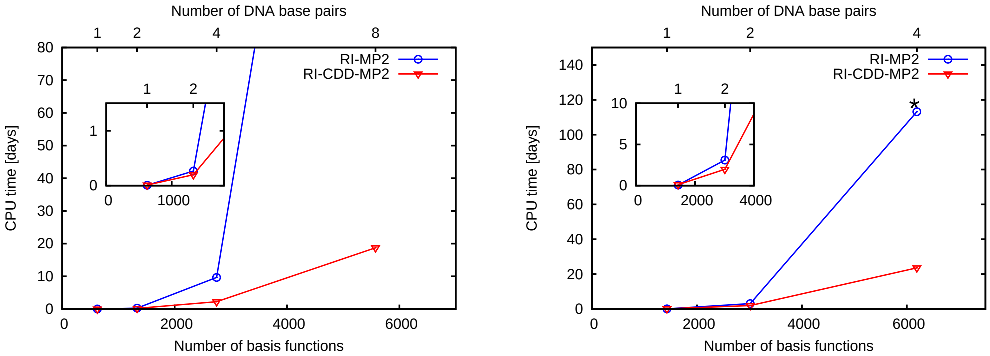

(a) def2-SVP (b) cc-pVTZ

Figure 3. Timings of our RI-CDD-MP2 method in comparison to canonical RI-MP2 on DNA systems. The RI-MP2 values for the largest DNA systems (8 base pairs in def2-SVP, 4 base pairs in cc-pVTZ) have been conservatively extrapolated with the scaling behavior of the two previous points.

def2-SVP basis		RI-MP2		RI-CDD-MP2	
System	#bf	time [h]	scaling	time [h]	scaling
DNA_1	625	0.16	-	0.23	-
DNA_2	1332	6.36	4.87	4.75	4.02
DNA_4	2746	231.63	4.97	53.22	3.34
DNA_8	5574	-	-	449.53	3.01
cc-pVTZ basis		**RI-MP2**		**RI-CDD-MP2**	
System	#bf	time [h]	scaling	time [h]	scaling
DNA_1	1428	1.73	-	2.73	-
DNA_2	3016	74.45	5.03	47.64	3.82
DNA_4	6192	-	-	566.37	3.44

Table IV. CPU times and scaling behavior with respect to the number of basis functions for canonical RI-MP2 as well as RI-CDD-MP2 calculations with full auxiliary basis on DNA systems in a def2-SVP and cc-pVTZ basis (all calculations on one CPU core).

VI. CONCLUSION

We demonstrated the efficiency of our RI-CDD-MP2 method with QQR-type integral estimates to preselect significant contributions. In addition, the Cholesky decomposition of the pseudo-densities provides local occupied and virtual pseudo-MOs that allow for an efficient preselection of the linear-scaling number of significant energy contributions. The use of efficient BCSR sparse matrix multiplications in the integral transformation steps in combination with an RI-based formulation leads to a small prefactor and an early crossover to conventional RI-MP2. Our method scales asymptotically cubically with system size while for extended systems local restrictions on the auxiliary space can be used to further reduce the scaling behavior.

Our method provides small and well-controlled errors as shown for calculations on the S66 test set of interaction energies [32], a set of reaction energies also selected by Riplinger et al. [33], and a diverse selection of systems from our own benchmark set [25]. The efficiency of our method was demonstrated for DNA systems, where calculations on systems with eight base pairs and more than 500 atoms and 5000 basis functions in a double-zeta basis could be performed on a single CPU core. Using parallelization, the range of accessible system sizes can be further increased and calculations with more than 1000 atoms in a double-zeta basis and more than 500 atoms in a triple-zeta basis can be performed on a single computing node.

Further speedups might be possible by improving the locality of the LPMOs using an additional localization step on top of the Cholesky decomposition. As the LPMOs do not form an orthonormal set, this approach requires new localization techniques. Recent developments [50, 51] provide robust optimization techniques for both occupied and virtual functions and extensions applicable to the Cholesky LPMOs are under development in our group.

VII. ACKNOWLEDGEMENTS

C. O. acknowledges financial support by the 'Deutsche Forschungsgemeinschaft' (DFG) for the project Oc35/4-1. Further funding was provided by the DFG via the initiatives SFB 749 'Dynamik und Intermediate molekularer Transformationen' (project C7) and the DFG cluster of excellence EXC 114 'Center for Integrative Protein Science Munich' (CIPSM).

Appendix A: Cholesky decomposition with complete pivoting

In the following, the implications of the Cholesky decomposition with complete pivoting with special focus on the number of pseudo-orbitals that are obtained with decomposition of the pseudo-densities are discussed.

A description of an algorithm for the Cholesky decomposition using complete pivoting can be found, e.g., in Ref. [36]. For any symmetric, positive semi-definite $m \times m$ matrix $\mathbf{A}$ the decomposition can be written as

$$\mathbf{A} = \mathbf{P}\mathbf{L}'\mathbf{L}'^{\mathbf{T}}\mathbf{P}^{\mathbf{T}} \tag{A1}$$

The matrix $\mathbf{L}'$ is an $m \times r$ rectangular matrix ($r < m$) with a special form where the first r rows form an $r \times r$ lower triangular matrix with all positive (non-zero) diagonal elements. The (unitary) $m \times m$ permutation matrix $\mathbf{P}$ follows from the pivoting procedure and interchanges rows of $\mathbf{L}'$. Due to the special form of $\mathbf{L}'$, which is a direct consequence of the decomposition algorithm, it is easy to show that the number of rows of $\mathbf{L}'$ is equal to the rank of the matrix $\mathbf{A}$: The first r rows of the matrix $\mathbf{L}'$ are linearly independent since the determinant of the corresponding lower triangular $r \times r$ matrix is non-zero (it is the product of the non-zero diagonal elements). As the (row) rank of the matrix is therefore at least r and at the same time the rank cannot be larger than the number of columns, it follows that the rank of $\mathbf{L}'$ is equal to the number of columns r. As the number of linearly independent rows is not changed by the permutation matrix $\mathbf{P}$, the rank of the matrix $\mathbf{L} = \mathbf{P}\mathbf{L}'$ is also r which implies that $\mathbf{L}$ has r non-zero singular values. Due to $\mathbf{A} = \mathbf{L}\mathbf{L}^{\mathbf{T}}$ the singular values of $\mathbf{A}$ are the squares of the singular values of $\mathbf{L}$ and therefore both $\mathbf{A}$ and $\mathbf{L}$ have the same rank, which is equal to the number of columns of $\mathbf{L}$.

The rank of the matrices $\underline{\mathbf{P}}$ ($\overline{\mathbf{P}}$) is lower or equal the number of occupied (virtual) orbitals as can be seen from a reformulation of Eq. 2

$$\underline{\mathbf{P}} = \underline{\mathbf{C}}\,\underline{\mathbf{C}}^T \qquad \overline{\mathbf{P}} = \overline{\mathbf{C}}\,\overline{\mathbf{C}}^T \tag{A2}$$

with the weighted MO coefficients $\underline{\mathbf{C}}$ and $\overline{\mathbf{C}}$ defined as

$$\begin{aligned}\underline{C}_{\mu i} &= (\omega_\alpha)^{\frac{1}{8}} C_{\mu i} e^{\frac{1}{2}\epsilon_i t_\alpha} \\ \overline{C}_{\mu a} &= (\omega_\alpha)^{\frac{1}{8}} C_{\mu a} e^{-\frac{1}{2}\epsilon_a t_\alpha}\end{aligned} \tag{A3}$$

The rank of $\underline{\mathbf{C}}$ and $\overline{\mathbf{C}}$ is connected to the rank of the matrices of regular occupied and virtual MO coefficients: The vectors of occupied (virtual) MOs are linearly independent therefore the rank of the corresponding matrix $\mathbf{C_{occ}}$ ($\mathbf{C_{virt}}$) is equal to the number of occupied (virtual) orbitals. The matrix $\underline{\mathbf{C}}$ ($\overline{\mathbf{C}}$) only differs from $\mathbf{C_{occ}}$ ($\mathbf{C_{virt}}$) due to the scaling of each column/MO by a Laplace factor dependent on the quadrature point. This scaling does not change the linear independence of the columns except for the case, where the scaling factor is (numerically) zero. In most cases, the rank of $\underline{\mathbf{C}}$ ($\overline{\mathbf{C}}$) is therefore equal to the number of occupied (virtual) MOs, while for some quadrature points with large exponents the columns of low-lying occupied or high-lying virtual orbitals are essentially zero and the (numerical) rank of the matrices is slightly reduced.

As discussed above for the case of $\mathbf{A} = \mathbf{L}\mathbf{L}^\mathbf{T}$ it follows from Eq. A2 that the rank of $\underline{\mathbf{C}}$ ($\overline{\mathbf{C}}$) is equal to the rank of $\underline{\mathbf{P}}$ ($\overline{\mathbf{P}}$), which is at the same time equal to the number of columns (and the rank) of $\underline{\mathbf{L}}$ ($\overline{\mathbf{L}}$) resulting from the Cholesky decomposition. The number of occupied (virtual) Cholesky pseudo-MOs is therefore often equal and in a few cases – for quadrature points with large exponents – slightly smaller than the number of regular occupied (virtual) MOs.

Appendix B: Proof of $\underline{\mathbf{L}}^\mathbf{T}\mathbf{S}\overline{\mathbf{L}} = \mathbf{0}$

Starting with the scaled MO coefficient matrices defined in Eq. A3, it follows that

$$\underline{\mathbf{C}}^\mathbf{T}\mathbf{S}\overline{\mathbf{C}} = \mathbf{0} \tag{B1}$$

as it is equivalent to

$$(\omega_\alpha)^{\frac{1}{4}} e^{\frac{1}{2}(\epsilon_i-\epsilon_a)t_\alpha} \sum_{\mu\nu} C_{\mu i} S_{\mu\nu} C_{\mu a} = 0 \tag{B2}$$

where the sum is zero due to the orthogonality of the occupied and virtual MO space. In the following, we will prove that $\underline{\mathbf{L}}$ and $\overline{\mathbf{L}}$ are connected to $\underline{\mathbf{C}}$ and $\overline{\mathbf{C}}$ by a unitary transformation, which is a direct consequence of $\underline{\mathbf{L}}\underline{\mathbf{L}}^T = \underline{\mathbf{C}}\underline{\mathbf{C}}^T = \underline{\mathbf{P}}$ and the corresponding expression for the virtual matrices.

We use the singular value decomposition of a real $m \times n$ matrix $\mathbf{A}$ that can be expressed as [52]

$$\mathbf{A} = \mathbf{V_A \Sigma_A U_A^T} \tag{B3}$$

where $\mathbf{V}_A$ is the unitary $m \times m$ matrix of the left singular vectors, $\mathbf{U}_A$ is the unitary $n \times n$ matrix of the right singular vectors and $\mathbf{\Sigma}_A$ is an $m \times n$ matrix which is zero except for the singular values on its diagonal. The singular values are the square roots of the (positive, non-zero) eigenvalues of $\mathbf{AA^T}$ (and also of $\mathbf{A^T A}$). The left singular vectors are the eigenvectors of $\mathbf{AA^T}$.

Any two real $m \times n$ matrices $\mathbf{A}$ and $\mathbf{B}$ for which

$$\mathbf{AA^T} = \mathbf{BB^T} \tag{B4}$$

therefore share the same singular values and left singular vectors and can be expressed as

$$\begin{aligned} \mathbf{A} &= \mathbf{V \Sigma U_A^T} \\ \mathbf{B} &= \mathbf{V \Sigma U_B^T} \end{aligned} \tag{B5}$$

Therefore

$$\mathbf{A} = \mathbf{B U_B U_A^T} = \mathbf{BU} \tag{B6}$$

with a unitary $m \times m$ matrix $\mathbf{U} = \mathbf{U}_B \mathbf{U}_A^T$.

If $\underline{\mathbf{L}}$ ($\overline{\mathbf{L}}$) and $\underline{\mathbf{C}}$ ($\overline{\mathbf{C}}$) have the same dimensions, it follows that

$$\underline{\mathbf{L}} = \underline{\mathbf{C}}\mathbf{U_{occ}} \tag{B7}$$

where $\mathbf{U_{occ}}$ is a unitary matrix of the appropriate dimension and corresponding expression for the virtual matrices apply. Therefore

$$\underline{\mathbf{L}}^T \mathbf{S} \overline{\mathbf{L}} = \mathbf{U_{occ}^T} \underline{\mathbf{C}}^\mathbf{T} \mathbf{S} \overline{\mathbf{C}} \mathbf{U_{virt}} = \mathbf{0} \tag{B8}$$

as a consequence of Eq. B1. If the dimension of $\underline{\mathbf{L}}$ ($\overline{\mathbf{L}}$) is smaller than the dimension of $\underline{\mathbf{C}}$ ($\overline{\mathbf{C}}$) as discussed in Appendix A the proof still holds if matrices $\tilde{\underline{\mathbf{L}}}$ ($\tilde{\overline{\mathbf{L}}}$) are considered, where additional zero columns have been added, to match the dimensions of $\underline{\mathbf{C}}$ ($\overline{\mathbf{C}}$). The proof above gives $\tilde{\underline{\mathbf{L}}}^T\mathbf{S}\tilde{\overline{\mathbf{L}}} = \mathbf{0}$ and it follows trivially that $\underline{\mathbf{L}}^T\mathbf{S}\overline{\mathbf{L}} = \mathbf{0}$ for the submatrices with smaller dimensions.

Appendix C: Definition of centers and extents

In the following we use M, N, K, and L to denote shells. The centers of the LPMO products are defined as

$$\vec{r}_{\underline{i}\overline{a}} = \frac{\sum_{MN} |\underline{L}_{M\underline{i}} S_{MN} \overline{L}_{N\overline{a}}| \vec{r}_{MN}}{\sum_{MN} |\underline{L}_{M\underline{i}} S_{MN} \overline{L}_{N\overline{a}}|} \tag{C1}$$

where the sum runs over all shell pairs and a matrix element indexed with M or N is the maximum of all corresponding AO matrix elements within the shell:

$$S_{MN} = \max_{\mu\in M,\nu\in N} |S_{\mu\nu}| \qquad \underline{L}_{M\underline{i}} = \max_{\mu\in M} |\underline{L}_{\mu\underline{i}}| \tag{C2}$$

The centers of the AO products $\vec{r}_{MN}$ are defined in Eq. (B2) of Ref. [25] and are the same for all the basis function products of a shell pair. For the pre-screening of (i,j) pairs the center assigned to a single occupied LPMO $\underline{i}$ is calculated as in Eq. C1 where $\overline{L}_{N\overline{a}}$ is replaced by $\underline{L}_{N\underline{i}}$.

The extents are defined similarly to the approach in AO-MP2 [24]. For every LPMO pair, relative weights of the AO contributions are calculated

$$c_{\underline{i}\overline{a}}^{MN} = \frac{|\underline{L}_{M\underline{i}} S_{MN} \overline{L}_{N\overline{a}}|}{\sum_{KL} |\underline{L}_{K\underline{i}} S_{KL} \overline{L}_{L\overline{a}}|}. \tag{C3}$$

All AO contributions with relative weight larger than the chosen extent threshold ϑ_{trf} (10^{-3} in our work) are taken into account to determine the extent of the LPMO pair according to

$$\mathrm{ext}_{\underline{i}\overline{a}} = \max_{\{M,N|c_{\underline{i}\overline{a}}^{MN} > \vartheta_{trf}\}} \left\{ R_{\underline{i}\overline{a},MN} + c_{\underline{i}\overline{a}}^{MN} \mathrm{ext}_{MN} \right\}. \tag{C4}$$

The AO extents ext_{MN} are defined in Eq. (B4) of Ref. [25] and, like the AO centers, they have a distinct value for each shell pair.

For the pre-screening of (i,j) pairs, the extent assigned to a single occupied LPMO is determined with respect to the center of this orbital

$$\mathrm{ext}_{\underline{i}} = \max_{\{M,N,\overline{a}|c^{MN}_{\underline{i}\overline{a}} > \vartheta_{trf}\}} \left\{ R_{\underline{i},MN} + c^{MN}_{\underline{i}\overline{a}} \mathrm{ext}_{MN} \right\} . \tag{C5}$$

where the maximum is now taken over any virtual LPMO and every shell pair.

To reduce the computational cost for determining the centers and extents, we restrict all calculations to significant $(\underline{i},\overline{a})$ pairs and take only significant shell pairs into account. Furthermore, the sparsity of the LPMO coefficient matrices is exploited, which leads to an asymptotically linear-scaling cost for these steps.

[1] C. Møller and M. S. Plesset, Phys. Rev. **46**, 618 (1934).

[2] D. Cremer, WIREs Comput. Mol. Sci. **1**, 509 (2011).

[3] R. G. Parr and W. Yang, *Density-Functional Theory of Atoms and Molecules* (Oxford University Press, New York, 1994).

[4] S. Grimme, WIREs Comput. Mol. Sci. **1**, 211 (2011).

[5] S. Grimme, J. Chem. Phys. **124**, 034108 (2006).

[6] M. Feyereisen, G. Fitzgerald, and A. Komornicki, Chem. Phys. Lett. **208**, 359 (1993).

[7] Y. Jung, R. C. Lochan, A. D. Dutoi, and M. Head-Gordon, J. Chem. Phys. **121**, 9793 (2004).

[8] H. Koch, A. Sánchez de Merás, and T. B. Pedersen, J. Chem. Phys. **118**, 9481 (2003).

[9] J. Boström, M. Pitoák, F. Aquilante, P. Neogrády, T. B. Pedersen, and R. Lindh, J. Chem. Theory Comput. **8**, 1921 (2012).

[10] T. J. Martinez and E. A. Carter, J. Chem. Phys. **100**, 3631 (1994).

[11] E. G. Hohenstein, R. M. Parrish, and T. J. Martínez, J. Chem. Phys. **137**, 044103 (2012).

[12] P. Pulay, Chem. Phys. Lett. **100**, 151 (1983).

[13] P. Pulay and S. Saebø, Theor. Chim. Acta **69**, 357 (1986).

[14] M. Schütz, G. Hetzer, and H.-J. Werner, J. Chem. Phys. **111**, 5691 (1999).

[15] H.-J. Werner, F. R. Manby, and P. J. Knowles, J. Chem. Phys. **118**, 8149 (2003).

[16] K. Kristensen, I.-M. Høyvik, B. Jansík, P. Jørgensen, T. Kjærgaard, S. Reine, and J. Jakowski, Phys. Chem. Chem. Phys. **14**, 15706 (2012).

[17] J. Almlöf, Chem. Phys. Lett. **181**, 319 (1991).

[18] M. Häser and J. Almlöf, J. Chem. Phys. **96**, 489 (1992).

[19] M. Häser, Theor. Chim. Acta **87**, 147 (1993).

[20] P. Y. Ayala and G. E. Scuseria, J. Chem. Phys. **110**, 3660 (1999).

[21] D. S. Lambrecht, B. Doser, and C. Ochsenfeld, J. Chem. Phys. **123**, 184102 (2005).

[22] D. S. Lambrecht, B. Doser, and C. Ochsenfeld, J. Chem. Phys. **136**, 149902 (2012).

[23] B. Doser, D. S. Lambrecht, J. Kussmann, and C. Ochsenfeld, J. Chem. Phys. **130**, 64107 (2009).

[24] S. A. Maurer, D. S. Lambrecht, J. Kussmann, and C. Ochsenfeld, J. Chem. Phys. **138**, 014101 (2013).

[25] S. A. Maurer, D. S. Lambrecht, D. Flaig, and C. Ochsenfeld, J. Chem. Phys. **136**, 144107 (2012).

[26] S. Schweizer, B. Doser, and C. Ochsenfeld, J. Chem. Phys. **128**, 154101 (2008).

[27] M. Maurer and C. Ochsenfeld, J. Chem. Phys. **138**, 174104 (2013).

[28] S. A. Maurer, M. Beer, D. S. Lambrecht, and C. Ochsenfeld, J. Chem. Phys. **139**, 184104 (2013).

[29] D. S. Hollman, J. J. Wilke, and H. F. Schaefer, J. Chem. Phys. **138**, 064107 (2013).

[30] W. Klopper, F. R. Manby, S. Ten-No, and E. F. Valeev, Int. Rev. Phys. Chem. **25**, 427 (2006).

[31] J. Zienau, L. Clin, B. Doser, and C. Ochsenfeld, J. Chem. Phys. **130**, 204112 (2009).

[32] J. Rezáč, K. E. Riley, and P. Hobza, J. Chem. Theory Comput. **7**, 2427 (2011).

[33] C. Riplinger and F. Neese, J. Chem. Phys. **138**, 034106 (2013).

[34] M. Häser and J. Almlöf, J. Chem. Phys. **96**, 489 (1992).

[35] M. Häser, Theoret. Chim. Acta **87**, 147 (1993).

[36] N. J. Higham, WIREs Comput. Stat. **1**, 251 (2009).

[37] H. Harbrecht, M. Peters, and R. Schneider, Appl. Num. Math. **62**, 428 (2012).

[38] F. Aquilante, T. B. Pedersen, A. Sánchez de Merás, and H. Koch, J. Chem. Phys. **125**, 174101 (2006).

[39] F. G. Gustavson, ACM Trans. Math. Softw. **4**, 250 (1978).

[40] J. Kussmann and C. Ochsenfeld, J. Chem. Phys. **127**, 54103 (2007).

[41] J. Kussmann and C. Ochsenfeld, J. Chem. Phys. **138**, 134114 (2013).

[42] T. H. Dunning, J. Chem. Phys. **90**, 1007 (1989).

[43] D. E. Woon and T. H. Dunning, J. Chem. Phys. **98**, 1358 (1993).

[44] F. Weigend and R. Ahlrichs, Phys. Chem. Chem. Phys. **7**, 3297 (2005).

[45] F. Weigend, A. Köhn, and C. Hättig, J. Chem. Phys. **116**, 3175 (2002).

[46] F. Weigend, M. Häser, H. Patzelt, and R. Ahlrichs, Chem. Phys. Lett. **294**, 143 (1998).

[47] E. Cuthill and J. McKee, in *Proceedings of the 1969 24th National Conference* (ACM, New York, NY, USA, 1969) pp. 157–172.

[48] J. George, *Computer implementation of the finite element method*, Tech. Rep. STAN-CS-71-208 (Stanford University (Stanford,CA US), 1971).

[49] Structure files are available for download from our homepage `http://www.cup.uni-muenchen.de/pc/ochsenfeld/download.html`.

[50] B. Jansík, S. Høst, K. Kristensen, and P. Jørgensen, J. Chem. Phys. **134**, 194104 (2011).

[51] I.-M. Høyvik, B. Jansík, and P. Jørgensen, J. Chem. Theory Comput. **8**, 3137 (2012).

[52] I. N. Bronstein, K. A. Semendjajew, G. Musiol, and H. Mühlig, *Taschenbuch der Mathematik*, 7th ed. (Verlag Harri Deutsch GmbH, Frankfurt am Main, 2008).

5.4 Paper IV: ”Linear-scaling symmetry-adapted perturbation theory with scaled dispersion”, S. A. Maurer, M. Beer, D. S. Lambrecht, C. Ochsenfeld, *J. Chem. Phys.*, 139, 184104 (2013)

THE JOURNAL OF CHEMICAL PHYSICS **139**, 184104 (2013)

Linear-scaling symmetry-adapted perturbation theory with scaled dispersion

Simon A. Maurer, Matthias Beer, Daniel S. Lambrecht,[a)] and Christian Ochsenfeld[b)]
Chair of Theoretical Chemistry, Department of Chemistry, University of Munich (LMU), Butenandtstr. 7, D-81377 Munich, Germany

(Received 20 July 2013; accepted 15 October 2013; published online 11 November 2013)

We present a linear-scaling symmetry-adapted perturbation theory (SAPT) method that is based on an atomic orbital (AO) formulation of zeroth-order SAPT (SAPT0). The non-dispersive terms are realized with linear-scaling cost using both the continuous fast multipole method (CFMM) and the linear exchange (LinK) approach for integral contractions as well as our efficient Laplace-based coupled-perturbed self-consistent field method (DL-CPSCF) for evaluating response densities. The reformulation of the dispersion term is based on our linear-scaling AO Møller-Plesset second-order perturbation theory (AO-MP2) method, that uses our recently introduced QQR-type screening [S. A. Maurer, D. S. Lambrecht, J. Kussmann, and C. Ochsenfeld, J. Chem. Phys. **138**, 014101 (2013)] for preselecting numerically significant energy contributions. Similar to scaled opposite-spin MP2, we neglect the exchange-dispersion term in SAPT and introduce a scaling factor for the dispersion term, which compensates for the error and at the same time accounts for basis set incompleteness effects and intramonomer correlation. We show in extensive benchmark calculations that the new scaled-dispersion (sd-)SAPT0 approach provides reliable results for small and large interacting systems where the results with a small 6-31G** basis are roughly comparable to supermolecular MP2 calculations in a triple-zeta basis. The performance of our method is demonstrated with timings on cellulose fragments, DNA systems, and cutouts of a protein-ligand complex with up to 1100 atoms on a single computer core. © *2013 AIP Publishing LLC*. [http://dx.doi.org/10.1063/1.4827297]

I. INTRODUCTION

Non-covalent interactions play a key role in molecular processes of chemical and biological systems. Pattern recognition, such as antigen binding, cell communication via signal transduction cascades, enzymatic catalysis, or conservation of information in the genetic code altogether depend on weak intermolecular interactions. Reversible, non-covalent interactions are the fundamental link to process dynamic information within complex systems such as cells and living organisms. Here, the reliable calculation of intermolecular interaction potentials can provide important insights.

There are in general two approaches for the calculation of interaction energies with quantum-chemical methods. In the conceptionally simpler supermolecular approach, one computes the difference in the total energy of the interacting complex and the separated systems, which is the interaction energy. This approach has the advantage that it can be used with any method which allows to calculate total energies and is therefore quite universal. On the other hand the total energy of a system is several orders of magnitude larger than (non-covalent) interaction energies which sets high requirements on the accuracy of the individual energy calculations for obtaining the small energy difference correctly. Among the available quantum-chemical methods, the Hartree-Fock (HF) approach and Kohn-Sham density-functional theory (KS-DFT) with conventional functionals fail to provide a reasonable description of dispersion interactions and one usually has to resort to the more expensive coupled-cluster methods[1] or perturbation theory[2] for a wave-function based description of dispersive effects. Alternatively, also very useful empirical corrections to HF or DFT are available[3] that, however, sacrifice the *ab initio* character and with it the systematic improvability.

In the second approach, the interaction energy is directly calculated, usually as a sum of physically interpretable components. One of the most successful ansätze in this category is symmetry-adapted perturbation theory (SAPT),[4,5] which derives interaction contributions by perturbative expansion of the total energy in the intermolecular potential and applies permutation operators to (approximately) re-establish the anti-symmetry of the solutions. Intramolecular correlation can be included in the theory using a double-perturbation expansion that takes the fluctuation potential of the monomers into account,[4] while in some more recent developments the SAPT energy terms have been rederived based on a coupled-cluster description of the monomers.[6–8] In an alternative approach, KS-DFT has been applied for the calculation of the monomers to account for intramonomer correlation effects which yields the SAPT(DFT)[9] or DFT-SAPT[10,11] methods.

Restricting the SAPT perturbation expansion to second-order terms is the simplest SAPT approach that yields reasonably accurate results. This approximation covers the dominant contributions of the classical picture, i.e.,

---

[a)] Present address: Department of Chemistry, University of Pittsburgh, Pittsburgh, Pennsylvania 15260, USA.
[b)] Electronic mail: christian.ochsenfeld@uni-muenchen.de

This article is copyrighted as indicated in the article. Reuse of AIP content is subject to the terms at: http://scitation.aip.org/termsconditions. Downloaded to IP: 92.230.182.222 On: Sat, 14 Dec 2013 22:00:25

electrostatic interactions, induction, dispersion, and, in addition, the corresponding exchange effects. If the intramolecular correlation is neglected, this leads to so-called zeroth-order SAPT, which we denote SAPT0 following Hohenstein and Sherrill.[12] This approach (also known as SAPT(0) in the earlier literature, see, e.g., Ref. 13) is zeroth-order in the fluctuation potential and second-order in the intermolecular potential. In contrast to the supermolecular approach, intramonomer correlation is no requirement to capture the dominant dispersive interaction components in SAPT, and the low-order SAPT0 method describes dispersion terms with a quality roughly comparable to supermolecular Møller-Plesset perturbation theory of second-order (MP2).

Several groups have developed efficient code for the low-order terms of SAPT using density-fitting (DF)/resolution-of-the-identity (RI) methods,[12,14,15] or Cholesky decomposition of the two-electron integrals.[12] Using DF in combination with Laplace expansion techniques, Hohenstein *et al.* showed[16] that it is possible to reduce the scaling of all SAPT0 contributions except for the exchange-dispersion term to at most $\mathcal{O}(\mathrm{M}^4)$, while the latter retains an unfavorable $\mathcal{O}(\mathrm{M}^5)$ behavior. In contrast to the existing SAPT approaches, there are several low-order or even linear-scaling variants of Coupled-Cluster theory or MP2 available (see, e.g., Refs. 17–21 for recent developments) that can be applied in the supermolecular approach.

In this work, we apply techniques developed for linear-scaling energy and property calculations[20,22] to present for the first time a linear-scaling SAPT method. Starting with a formulation entirely in the atomic-orbital (AO) basis, we use the continuous fast multipole method (CFMM)[23,24] and the linear exchange (LinK)[25,26] method to calculate Coulomb- and exchange-type matrices in the non-dispersive terms and make use of our efficient density matrix-based Laplace-transformed coupled-perturbed self-consistent field method (DL-CPSCF).[27] Linear-scaling cost for the dispersion term is achieved using our QQR-type integral screening, which has recently been introduced in the context of Hartree-Fock theory[28] and our linear-scaling atomic orbital-based MP2 method[20] which is closely connected to the SAPT dispersion term. It is worthwhile to stress that we refer to linear scaling with respect to molecular size (while the size of the atom-centered basis is unchanged). For increasing basis set size – while the molecular size is kept constant – our method scales as the fifth power of the number of basis functions per atom. Our present approach focuses on linear-scaling cost for large systems with modest basis sets using a fully AO-based formulation, while further developments for larger basis sets might preferably use our Cholesky-decomposed density approach.[29,30]

While our approaches in principle allow for linear-scaling calculations of all the SAPT0 terms, we introduce an economical simplification that is motivated by the success of the scaled-opposite spin (SOS) MP2[31] method. We neglect the exchange-dispersion term and scale the dispersion component to correct for the error which at the same time partially corrects for intramonomer correlation and for basis set incompleteness effects. The latter effect, which is dominant for small basis sets as discussed below, has also been observed by Řezáč and Hobza[32] who proposed scaling of both the dispersion and exchange-dispersion contribution in DFT-SAPT calculations to estimate the complete basis set (CBS) limit.

We present extensive benchmark calculations of our scaled-dispersion (sd-)SAPT0 method that show a consistently good performance, especially for small basis sets like 6-31G**, roughly comparable to MP2 calculations in a triple-zeta basis. In Sec. V, we present timings that show the linear and in some situations even sublinear scaling-behavior of our method with system size, which allows to perform SAPT calculations on compact protein systems with more than 1000 atoms on a single CPU core.

II. LINEAR-SCALING SCALED-DISPERSION SAPT0

Our approach is based on zeroth-order SAPT (which we denote SAPT0 following Hohenstein and Sherrill[12]) where the interaction energy is expanded to second order in the intermolecular potential with the intramonomer correlation neglected. This leads to the following expression for the interaction energy:

$$E^{SAPT0} = E^{(10)}_{pol} + E^{(10)}_{exch} + E^{(20)}_{ind,resp} + E^{(20)}_{exch-ind,resp} + E^{(20)}_{disp} + E^{(20)}_{exch-disp}, \tag{1}$$

where $E^{(10)}_{pol}$ is the electrostatic, $E^{(10)}_{exch}$ is the exchange, $E^{(20)}_{ind,resp}$ is the coupled induction, $E^{(20)}_{exch-ind,resp}$ is the coupled exchange induction, $E^{(20)}_{disp}$ is the dispersion, and $E^{(20)}_{exch-disp}$ is the exchange-dispersion energy component.

The non-dispersive energy terms

$$E_{non-disp} = E^{(10)}_{pol} + E^{(10)}_{exch} + E^{(20)}_{ind,resp} + E^{(20)}_{exch-ind,resp} \tag{2}$$

have been recently formulated in the AO basis by Hesselmann *et al.*[14] In our present work, we combine this AO-based formulation with our linear-scaling density matrix-based schemes. Thus, we employ sparse matrix multiplications,[33] construct the Coulomb- and exchange-type matrices via CFMM[23,24] and the LinK[25,26] method, and employ our DL-CPSCF[27] method in order to compute the induction-response density matrix. This leads to an asymptotic linear-scaling cost for the non-dispersive terms with respect to the system size. In cases where the monomers interact only via a constant number of atoms, while the rest of the molecule extends into regions far away from the area of interaction, the calculation of the non-dispersive terms even scales sublinearly with the size of the extended monomer provided that the density of both monomers and the multipoles of the CFMM box hierarchy are known from preceding SCF calculation of the monomers. Of course, the SCF calculation for the monomers scales linearly with its size so that this linear-scaling component remains in all cases.

We furthermore extended the linear-scaling formulation to the dispersion term, which reads in the uncoupled approximation[16,34]

$$E^{(20)}_{disp} = -4 \sum_{ia}^{A} \sum_{jb}^{B} \frac{|(i^A a^A|j^B b^B)|^2}{\varepsilon_a^A - \varepsilon_i^A + \varepsilon_b^B - \varepsilon_j^B}, \tag{3}$$

This article is copyrighted as indicated in the article. Reuse of AIP content is subject to the terms at: http://scitation.aip.org/termsconditions. Downloaded to IP: 92.230.182.222 On: Sat, 14 Dec 2013 22:00:25

where the superscripts refer to the MOs and orbital energies of monomer A or B. The expression is very similar to the formula for the opposite-spin term of the MP2 correlation energy except that the results of two separate SCF calculations of the monomers are used. We follow the AO-MP2 approach[35–37] and replace the denominator using the Laplace transform with a finite quadrature sum

$$\frac{1}{\varepsilon_a^A - \varepsilon_i^A + \varepsilon_b^B - \varepsilon_j^B} \approx \sum_\alpha \omega^{(\alpha)} e^{-(\varepsilon_a^A - \varepsilon_i^A + \varepsilon_b^B - \varepsilon_j^B)t^{(\alpha)}}. \quad (4)$$

By expanding the MOs of Eq. (3) in the dimer-centered basis set[38] and substitution of the energy denominator, the summation over the MO indices can be carried out which yields the AO based expression

$$E_{disp}^{(20)} = -4 \sum_\alpha \sum_{\substack{\mu\nu\lambda\sigma \\ \mu'\nu'\lambda'\sigma'}} \underline{P}_{\mu\mu'}^A \overline{P}_{\nu\nu'}^A (\mu'\nu'|\lambda\sigma) \underline{P}_{\lambda\lambda'}^B \overline{P}_{\sigma\sigma'}^B (\mu\nu|\lambda'\sigma'), \quad (5)$$

where the pseudo-densities of monomer A are defined as

$$\begin{aligned} \underline{P}_{\mu\nu}^A &= (\omega_\alpha)^{\frac{1}{4}} \sum_i^A c_{\mu i}^A e^{\epsilon_i^A t_\alpha} c_{\nu i}^A, \\ \overline{P}_{\mu\nu}^A &= (\omega_\alpha)^{\frac{1}{4}} \sum_a^A c_{\mu a}^A e^{-\epsilon_a^A t_\alpha} c_{\nu a}^A \end{aligned} \quad (6)$$

with corresponding expressions for monomer B.

To reduce the computational cost for the dispersion term, we employ our recently introduced QQR-type screening[20] to estimate individual energy contributions. Following our AO-MP2 approach,[20,39] we use half-transformed integrals (HTIs)

$$(\underline{\mu}^A \overline{\nu}^A|\lambda\sigma) = \sum_{\mu'\nu'} \underline{P}_{\mu\mu'}^A \overline{P}_{\nu\nu'}^A (\mu'\nu'|\lambda\sigma), \quad (7)$$

as intermediates, which show an asymptotic $1/R^2$ decay with increasing separation of the bra and ket charge distribution. With this definition the individual contributions to the dispersion energy can be expressed as products of two HTIs. The number of significant contributions scales linear with system size, since each HTI product shows an asymptotic $1/R^4$ decay with the bra-ket separation.

The HTIs are estimated using QQR-type estimates

$$(\underline{\mu}^A \overline{\nu}^A|\lambda\sigma) \approx \frac{Z_{\underline{\mu}\overline{\nu}}^A Q_{\lambda\sigma}}{(R - \mathrm{ext}_{\underline{\mu}\overline{\nu}} - \mathrm{ext}_{\lambda\sigma})^2} \quad (8)$$

with the (pseudo) Schwarz-matrices Z^A and Q, the bra-ket separation R, and the extents $\mathrm{ext}_{\underline{\mu}\overline{\nu}}$ and $\mathrm{ext}_{\lambda\sigma}$. Detailed definitions of all quantities are given in Refs. 20 and 28. Since the integral estimates reflect the correct asymptotic $1/R^4$ decay of the HTI products, the number of significant contributions preselected by our screening procedure scales linear with system size. In combination with additional screening in the transformation steps in Eq. (7) as described in Ref. 39, this leads to an overall linear-scaling cost of the dispersion term. As in the case of the non-dispersive contributions, even sublinear scaling can be achieved in cases where the interacting systems are expanded in regions far away from the contact surface.

TABLE I. Optimized values of the scaling factor for the dispersion term and the corresponding root-mean-square deviation (RMSD) from the reference values in kcal/mol for the S22 training set.

Basis	c_{disp}	RMSD
6-31G**	1.19	0.40
SVP	1.14	0.59
cc-pVTZ	0.89	0.73

While a linear-scaling formulation of the remaining exchange-dispersion term is also possible, it is computationally more demanding. We therefore follow here the idea of the scaled-opposite spin (SOS-)MP2 method by Head-Gordon and co-workers[31] and adapt it to the SAPT0 expression. In SOS-MP2, the exchange-type MP2 contribution is neglected and the error corrected by scaling the Coulomb-type term. Similar to this approach for MP2, we neglect here the exchange-dispersion contribution and scale the dispersion energy in what we call the scaled-dispersion (sd-)SAPT0 method

$$E^{sd-SAPT0} = E_{non-disp} + c_{disp} E_{disp}^{(20)}. \quad (9)$$

This approach is also closely connected to the method of Řezáč and Hobza[32] who scaled the sum of both the dispersion and exchange-dispersion contribution to improve DFT-SAPT results in small basis sets as compared to the CBS limit.

We determine the scaling parameter for the dispersion term c_{disp} by linear least-squares fit of the sd-SAPT0 interaction energies to the reference values of the S22 test set.[40] The optimal scaling factors are given in Table I together with the corresponding RMSD with respect to the reference values. In the larger cc-pVTZ basis the optimal scaling parameter is smaller than one, in line with the neglect of the repulsive exchange-dispersion contribution. At the same time, the scaling factor accounts for some of the missing intramonomer correlation and remaining basis set incompleteness. For the smaller double-zeta basis sets the scaling factors are larger than one indicating that the basis set incompleteness effect dominates over the neglect of the repulsive exchange-dispersion in these cases.

Nevertheless, the RMSD shows that the fit for double-zeta basis sets is actually significantly better than for the cc-pVTZ basis, since the smaller basis sets lead to rather balanced errors for hydrogen-bonded and dispersion bound systems, which can be cured to a large extent by a single scaling factor. We will show in the following that this balanced description with sd-SAPT0 in double-zeta basis sets seems transferable to other systems, which makes sd-SAPT0 a low-cost alternative to existing methods, rendering it particularly useful for large systems due to the favorable scaling with system size.

III. COMPUTATIONAL DETAILS

All SAPT calculations were performed with a development version of Q-CHEM.[41] The 6-31G** (Refs. 42 and 43) def2-SVP Ref. 44) and cc-pVTZ (Ref. 45) basis sets have been used. The density convergence criterion of the SCF

This article is copyrighted as indicated in the article. Reuse of AIP content is subject to the terms at: http://scitation.aip.org/termsconditions. Downloaded to IP: 92.230.182.222 On: Sat, 14 Dec 2013 22:00:25

TABLE II. Root-mean-square deviation (RMSD), mean absolute deviation (MAD), and maximum deviation (MAX) from the reference results for the S66 test set in kcal/mol.

	sd-SAPT0		SOS(MI)-MP2			MP2			SCS(MI)-MP2
	6-31G**	SVP	6-31G**[a]	SVP[a]	CBS[b]	6-31G**	SVP	CBS[c]	CBS[c]
RMSD	0.48	0.57	2.42	2.72	0.80	1.91	1.99	0.69	0.38
MAD	0.36	0.48	1.75	2.11	0.58	1.69	1.77	0.45	0.28
MAX	1.09	1.31	7.73	7.63	2.44	4.11	4.24	2.11	1.04

[a] The basis set dependent scaling factors have been obtained using the protocol of Ref. 48 (c_{OS}(6-31G**) = 2.6, c_{OS}(SVP) = 2.3).

[b] Derived from the MP2 results published on www.begdb.com[49] using the SOS(MI)-MP2 scaling factor for cc-pV(TQ)Z extrapolation of Ref. 48 (c_{OS} = 1.70).

[c] Statistics of the results published on www.begdb.com.[49]

procedure was set to a maximum DIIS error of 10^{-7} and the threshold for the neglect of small contributions in the calculation of Coulomb and exchange-type matrices was set to 10^{-10}. The convergence criterion for the CPSCF equations was set to 10^{-4}. In the Laplace quadrature we use the tabulated values of Hackbusch and co-workers[46] and a default of 5 Laplace points was chosen, which covered the required range of orbital differences for all but the MutM repair enzyme complexes. In the case of the largest MutM system the range of orbital differences in the denominator of DL-CPSCF was extraordinarily large and only tabulated value sets with at least 7 Laplace points were available for this range[46] so that this number was used as the default for the MutM calculations.

In the dispersion term, 5 Laplace points were used in all cases (the deviation to 6 Laplace points is <0.001 kcal/mol for S22 in the 6-31G** basis). The threshold for integral screening in the dispersion term as well as the threshold for matrix sparsity were set to 10^{-6}. Tightening both of these thresholds by one order of magnitude resulted in only small deviations (<0.1 kcal/mol or <3% of the dispersion energy for the S22 set), so that these values are considered a reliable choice. All timings were performed on a single core of a Xeon E5620 CPU with a total of 48 GB of available RAM.

IV. RESULTS

A. S66/S66x8 benchmarks

We performed extensive benchmark calculations on the S66 test set of interaction energies and the corresponding dissociation curves, the S66x8 set.[47] In Table II, the sd-SAPT0 results for the S66 set of equilibrium geometries are compared to results for MP2 as well as the SCS(MI)-MP2 and SOS(MI)-MP2 methods[48] all including the counterpoise correction. The SOS(MI)-MP2 method is the one most closely connected to our sd-SAPT0 method since the SAPT dispersion term is formally and computationally very similar to the opposite-spin term of MP2 and both methods use a single parameter (optimized for the S22 test set in both cases). However, sd-SAPT0 achieves much better results than SOS(MI)-MP2, with the latter being even inferior to conventional MP2. In comparison with the other methods, sd-SAPT0 with the small basis 6-31G** provides results much better than MP2 in the same basis, significantly better than the CBS extrapolated MP2 values, and of comparable accuracy to the CBS extrapolated SCS(MI)-MP2 results. The same holds for the dissociation curves of S66x8 in Table III where again MP2 is only competitive in a large basis and even then requires additional component-scaling to improve upon the sd-SAPT0 results in a simple double-zeta basis.

B. Protein-ligand interactions

High accuracy reference calculations are very expensive for larger systems, so benchmark sets for interaction energies mainly focus on small molecules. One of the few exceptions is the benchmark set of Neese, Grimme, and co-workers[50] which used LPNO-CEPA/TZVP results in combination with MP2/CBS values to get estimates of the interaction energies suitable for benchmarking. It should be noted that these results are, of course, not of comparable accuracy as the reference results for the smaller test sets (S22, S66, S66x8). The estimated uncertainty in the reference results according to Antony *et al.*[50] is 2–3 kcal/mol for the weaker interactions (interaction energy <10 kcal/mol) and 5%–10% for the stronger interacting systems.

Table IV shows the sd-SAPT0 interaction energies in a 6-31G** basis and corresponding errors with respect to the reference as well as counterpoise-corrected RI-MP2 and SCS(MI)-MP2 results in a cc-pVTZ basis for comparison. Only those systems are listed for which reference values are available (see the supplementary material[51] for the remaining results). The threshold for the sd-SAPT0 calculations was our default value of $\vartheta = 10^{-6}$. Tightening the threshold to $\vartheta = 10^{-7}$ resulted in only minor changes (max. deviation 0.21 kcal/mol, RMSD 0.10 kcal/mol), which again confirms that $\vartheta = 10^{-6}$ is a suitable choice also for larger systems.

The maximum deviation of our sd-SAPT0 results from the reference is 2.80 kcal/mol and the errors are comparable to the much more expensive RI-MP2 and scaled RI-MP2 results in a triple-zeta basis. Most of these results are within

TABLE III. Root-mean-square deviation (RMSD), mean absolute deviation (MAD), and maximum deviation (MAX) from the reference results for the S66x8 test set in kcal/mol. The RMSD values of the MP2 and SCS(MI)-MP2 CBS results are taken from Ref. 47.

	sd-SAPT0		MP2			SCS(MI)-MP2
	6-31G**	SVP	6-31G**	SVP	CBS[47]	CBS[47]
RMSD	0.46	0.52	1.63	1.68	0.67	0.32
MAD	0.33	0.37	1.21	1.26	…	…
MAX	2.02	2.45	5.79	6.28	…	…

This article is copyrighted as indicated in the article. Reuse of AIP content is subject to the terms at: http://scitation.aip.org/termsconditions. Downloaded to IP: 92.230.182.222 On: Sat, 14 Dec 2013 22:00:25

TABLE IV. Interaction energies ΔE_{PL} and errors compared to the protein-ligand interaction test set of Antony *et al.*[50] Only those systems are listed for which reference values are available (see the supplementary material[51] for the full table). The basis set used for sd-SAPT0 is 6-31G**, while the RI-MP2 and SCS(MI)-MP2 results both use the much larger cc-pVTZ basis in the RI-approximation and include counterpoise correction.

	sd-SAPT0/6-31G**		RI-MP2/cc-pVTZ		SCS-(MI)-MP2/cc-pVTZ	
System	ΔE_{PL}	Error	ΔE_{PL}	Error	ΔE_{PL}	Error
1	1.78	−1.58	2.12	−1.92	2.43	−2.23
2	−2.74	−1.86	−3.67	−0.93	−2.94	−1.66
3	−4.81	−2.79	−6.15	−1.45	−5.69	−1.91
4	−14.28	1.68	−11.45	−1.15	−12.14	−0.46
5	−14.18	0.58	−11.35	−2.25	−11.76	−1.84
6	−16.61	0.71	−14.51	−1.39	−15.88	−0.02
7	−17.14	1.04	−14.73	−1.37	−16.16	0.06
8	−17.79	1.29	−15.09	−1.41	−16.64	0.14
9	−20.20	2.80	−15.31	−2.09	−16.29	−1.11
10	−20.93	1.63	−14.79	−4.51	−16.11	−3.19
11	−21.58	−1.22	−20.15	−2.65	−21.36	−1.44
12	−22.77	−2.23	−21.73	−3.27	−22.10	−2.90
14	−32.38	−0.92	−29.70	−3.60	−31.89	−1.41
15	−36.41	−0.09	−33.39	−3.11	−35.05	−1.45
23	−64.19	0.89	−61.03	−2.27	−63.90	0.60

the error estimates of the reference values, where only a few deviations for the stronger interacting systems (>10 kcal/mol) are slightly higher than the estimated 10% uncertainty of Ref. 50 (maximum deviation is 16% for sd-SAPT0/6-31G**, 23% for MP2/cc-pVTZ, and 17% for SCS(MI)-MP2/cc-pVTZ). We conclude that our sd-SAPT0 method with the chosen small 6-31G** basis provides reasonable interaction energies also for larger systems with errors of similar magnitude as the standard MP2 approach with a triple-zeta basis.

V. TIMINGS

In Table V, we present timings of our linear-scaling sd-SAPT0 method for a cellulose strand interacting with a small cellulose fragment located abreast one end of the strand. Due to the finite range of the interactions, which is reflected by our SAPT method, the calculation time for the SAPT contributions is sublinear with increasing size of the cellulose strand in the rate determining steps. The scaling of the SCF calculation for the strand remains linear, which is reflected by the timings in Table V. The observed increase in calculation time for the small fragment (of constant size) is due to the increasing number of basis functions on ghost atoms in the dimer centered basis and the corresponding increased cost of the diagonalization step.

In general, the cost of our method increases asymptotically linearly with the number of atoms in the contact surface between the two monomers. The scaling behavior with system size is therefore either sublinear in case of constant contact surface (see cellulose example above) or linear when the contact surface grows proportional to the system size. An example of the latter is given in Fig. 1 for the case of

TABLE V. CPU times in hours for sd-SAPT0 calculations on two cellulose systems with the 6-31G** basis. The interaction between a small 2-unit fragment of one strain and either a 12 or 20 unit fragment of an adjacent strain is calculated and compared. The number of electrons and atoms is given for the large fragment. Timings for the SCF calculations on the monomers, the non-dispersive SAPT terms (Eq. (2)), and the dispersion contribution (Eq. (5)) as well as the scaling with respect to the number of electrons are given. The 2-unit cellulose block is located abreast of one end of the adjacent fragment, so that the computational cost for the sd-SAPT0 calculation scales sublinear with the size of the larger fragment. The SCF calculation of the larger fragment scales linear with its size, while the SCF time for the 2-unit fragment increases due to the increasing size of the dimer-centered basis.

# Glucose units	12	20	
# Electrons	1042	1730	Scaling
# Atoms	255	423	$\mathcal{O}(N^x)$
SCF 2-unit frag.	1.2	1.9	0.95
SCF 12/20-unit frag.	3.6	6.5	1.16
$E_{non-disp}$	2.6	3.9	0.79
E_{disp}	13.0	15.3	0.32

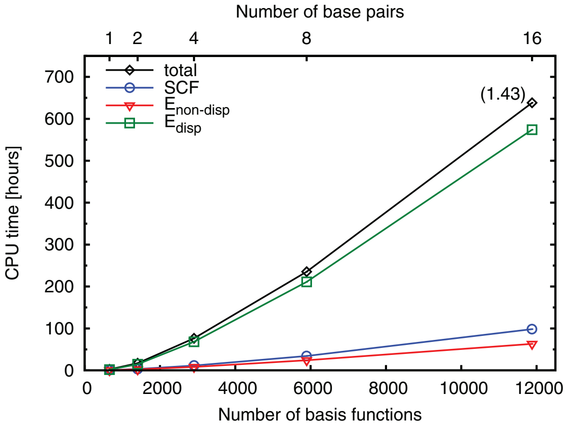

FIG. 1. CPU times for sd-SAPT0 calculations on DNA systems with the 6-31G** basis. The calculation times for the SCF calculations on the monomers, the non-dispersive terms (Eq. (2)) as well as for the dispersion term (Eq. (5)) are given.

This article is copyrighted as indicated in the article. Reuse of AIP content is subject to the terms at: http://scitation.aip.org/termsconditions. Downloaded to IP: 92.230.182.222 On: Sat, 14 Dec 2013 22:00:25

TABLE VI. CPU times in hours for sd-SAPT0 calculations on the repair enzyme MutM in complex with an 8oxoG lesion. The basis set is 6-31G**. The number of electrons and atoms is given for the enzyme cutout. Timings for the SCF calculations on the monomers, the non-dispersive SAPT terms (Eq. (2)), and the dispersion contribution (Eq. (5)) as well as the scaling with respect to the number of electrons are given. The increasing cost for the SCF calculation of the 8-oxoG lesion is due to the increasing size of the dimer-centered basis.

Cutout radius	7.0 Å	12.0 Å	
# Electrons	1136	4066	Scaling
# Atoms	307	1100	$\mathcal{O}(N^x)$
SCF 8-oxoG	5.5	25.3	1.19
SCF enzyme	10.0	133.4	2.03[a]
$E_{non-disp}$	12.0	64.7	1.32
E_{disp}	103.2	433.9	1.13

[a] The number of SCF iterations increases by 50% due to a smaller HOMO-LUMO gap in the larger system. The scaling of the average cost per iteration is $\mathcal{O}(N^{1.7})$.

interacting DNA strands. The CPU times of the SCF calculations on the two monomers as well as the calculation of the non-dispersive SAPT terms and the dispersion term all scale linearly with system size. The scaling exponent of the total CPU time is 1.43 from DNA$_8$ to DNA$_{16}$. A table of the CPU timings can be found in the supplementary material.[51]

Finally, we studied the case of a small fragment interacting with a larger three-dimensional environment for the example of an oxidized DNA base (8oxoG) interacting with cutouts of the MutM repair enzyme, where the 8oxoG lesion is located in the active pocket of the enzyme. The timings are given in Table VI. Besides the SCF calculations for the enzyme, all the dominating steps of the calculation scale close to linearly with the size of the protein cutout.

VI. CONCLUSION

In this work, we have presented the first linear-scaling SAPT method. Our approach is based on the SAPT0 method and formulated entirely in the AO-basis, which allows to employ our linear-scaling techniques for Hartree-Fock energy and response property calculations as well as screening techniques from our AO-MP2 method. In the non-dispersive terms we use CFMM and LinK for Coulomb- and exchange-type contractions, while for the expensive solution of the CPSCF equations we use our efficient DL-CPSCF approach. For the dispersion term we employ our QQR-type screening to take the $1/R^4$ decay of the AO-based contributions into account, so that a linear-scaling number of integrals is pre-selected.

In an approach similar to the SOS-MP2 method, we neglect the exchange-dispersion term and introduce one scaling parameter for the dispersion term that corrects for this error and at the same time accounts for basis set incompleteness effects and intramonomer correlation. Extensive benchmark calculations on the S66 and S66x8 sets as well as for a set of larger protein-ligand interactions show that this scaled-dispersion zeroth-order SAPT (sd-SAPT0) approach yields reliable results for small and large systems. Our sd-SAPT0 method is especially useful with small basis sets where the rather balanced errors can be efficiently cured by a single parameter. The benchmarks show that sd-SAPT0 in a 6-31G** basis provides errors roughly comparable to supermolecular MP2 calculations in a triple-zeta basis for a whole range of test systems.

The timings for DNA systems illustrate the linear-scaling behavior of our method, with a scaling behavior similar to our efficient AO-MP2 method. In cases where the molecules are expanded in areas far away from the interaction region, the method even shows effective sublinear scaling with the size of the large monomer as shown for interacting cellulose fragments. Further timing calculations for the case of an 8-oxoG lesion interacting with different cutouts of the MutM repair protein illustrate the possibility to perform with our sd-SAPT0 method calculations comprising more than 1000 atoms on a single CPU core.

The combination of linear or even sublinear scaling cost with system size and good results for very modest basis sets makes our sd-SAPT0 method an efficient approach for calculating interaction energies for medium sized up to very large molecular systems. In large biochemical systems, where quantum-chemical treatment is necessarily restricted to cutouts around the active site, our method is ideally suited to study the convergence of the different interaction components, which also might provide further insight on how to define the size of QM regions[52–54] used in layered models like combined quantum-chemical/molecular-mechanical (QM/MM) calculations.

ACKNOWLEDGMENTS

C.O. acknowledges financial support by the Volkswagen Stiftung within the funding initiative "New Conceptual Approaches to Modeling and Simulation of Complex Systems," by the SFB 749 "Dynamik und Intermediate molekularer Transformationen" (DFG, Project C7), and the DFG cluster of excellence EXC 114 "Center for Integrative Protein Science Munich" (CIPSM).

[1] R. J. Bartlett, WIREs Comput. Mol. Sci. **2**, 126 (2012).
[2] D. Cremer, WIREs Comput. Mol. Sci. **1**, 509 (2011).
[3] S. Grimme, WIREs Comput. Mol. Sci. **1**, 211 (2011).
[4] B. Jeziorski, R. Moszynski, and K. Szalewicz, Chem. Rev. **94**, 1887 (1994).
[5] K. Szalewicz, WIREs Comput. Mol. Sci. **2**, 254 (2012).
[6] T. Korona and B. Jeziorski, J. Chem. Phys. **128**, 144107 (2008).
[7] T. Korona, J. Chem. Phys. **128**, 224104 (2008).
[8] T. Korona, J. Chem. Theory Comput. **5**, 2663 (2009).
[9] H. L. Williams and C. F. Chabalowski, J. Phys. Chem. A **105**, 646 (2001).
[10] G. Jansen and A. Hesselmann, J. Phys. Chem. A **105**, 11156 (2001).
[11] A. Hesselmann and G. Jansen, Chem. Phys. Lett. **357**, 464 (2002).
[12] E. G. Hohenstein and C. D. Sherrill, J. Chem. Phys. **132**, 184111 (2010).
[13] K. Szalewicz, K. Patkowski, and B. Jeziorski, Struct. Bonding **116**, 43 (2005).
[14] A. Hesselmann, G. Jansen, and M. Schütz, J. Chem. Phys. **122**, 014103 (2005).
[15] R. Podeszwa, R. Bukowski, and K. Szalewicz, J. Chem. Theory Comput. **2**, 400 (2006).
[16] E. G. Hohenstein, R. M. Parrish, C. D. Sherrill, J. M. Turney, and H. F. Schaefer, J. Chem. Phys. **135**, 174107 (2011).
[17] H.-J. Werner and M. Schütz, J. Chem. Phys. **135**, 144116 (2011).
[18] I.-M. Høyvik, K. Kristensen, B. Jansik, and P. Jørgensen, J. Chem. Phys. **136**, 014105 (2012).
[19] J. Yang, G. K.-L. Chan, F. R. Manby, M. Schütz, and H.-J. Werner, J. Chem. Phys. **136**, 144105 (2012).

This article is copyrighted as indicated in the article. Reuse of AIP content is subject to the terms at: http://scitation.aip.org/termsconditions. Downloaded to IP: 92.230.182.222 On: Sat, 14 Dec 2013 22:00:25

[20] S. A. Maurer, D. S. Lambrecht, J. Kussmann, and C. Ochsenfeld, J. Chem. Phys. **138**, 014101 (2013).

[21] C. Riplinger and F. Neese, J. Chem. Phys. **138**, 034106 (2013).

[22] J. Kussmann, M. Beer, and C. Ochsenfeld, WIREs Comput. Mol. Sci. **3**, 614 (2013).

[23] C. A. White, B. G. Johnson, P. M. W. Gill, and M. Head-Gordon, Chem. Phys. Lett. **230**, 8 (1994).

[24] C. A. White, B. G. Johnson, P. M. W. Gill, and M. Head-Gordon, Chem. Phys. Lett. **253**, 268 (1996).

[25] C. Ochsenfeld, C. A. White, and M. Head-Gordon, J. Chem. Phys. **109**, 1663 (1998).

[26] C. Ochsenfeld, Chem. Phys. Lett. **327**, 216 (2000).

[27] M. Beer and C. Ochsenfeld, J. Chem. Phys. **128**, 221102 (2008).

[28] S. A. Maurer, D. S. Lambrecht, D. Flaig, and C. Ochsenfeld, J. Chem. Phys. **136**, 144107 (2012).

[29] J. Zienau, L. Clin, B. Doser, and C. Ochsenfeld, J. Chem. Phys. **130**, 204112 (2009).

[30] S. A. Maurer, L. Clin, and C. Ochsenfeld, “Cholesky-decomposed density MP2 with density fitting: accurate MP2 and double-hybrid DFT energies for large systems” (unpublished).

[31] Y. Jung, R. C. Lochan, A. D. Dutoi, and M. Head-Gordon, J. Chem. Phys. **121**, 9793 (2004).

[32] J. Řezáč and P. Hobza, J. Chem. Theory Comput. **7**, 685 (2011).

[33] J. Kussmann and C. Ochsenfeld, J. Chem. Phys. **127**, 054103 (2007).

[34] A. Hesselmann and G. Jansen, Chem. Phys. Lett. **367**, 778 (2003).

[35] J. Almlöf, Chem. Phys. Lett. **181**, 319 (1991).

[36] M. Häser and J. Almlöf, J. Chem. Phys. **96**, 489 (1992).

[37] M. Häser, Theor. Chim. Acta **87**, 147 (1993).

[38] H. L. Williams, E. M. Mas, K. Szalewicz, and B. Jeziorski, J. Chem. Phys. **103**, 7374 (1995).

[39] B. Doser, D. S. Lambrecht, J. Kussmann, and C. Ochsenfeld, J. Chem. Phys. **130**, 064107 (2009).

[40] P. Jurecka, J. Sponer, J. Černý, and P. Hobza, Phys. Chem. Chem. Phys. **8**, 1985 (2006).

[41] Y. Shao, L. F. Molnar, Y. Jung, J. Kussmann, C. Ochsenfeld, S. T. Brown, A. T. Gilbert, L. V. Slipchenko, S. V. Levchenko, D. P. O’Neill, R. A. DiStasio, Jr., R. C. Lochan, T. Wang, G. J. Beran, N. A. Besley, J. M. Herbert, C. Yeh Lin, T. Van Voorhis, S. Hung Chien, A. Sodt, R. P. Steele, V. A. Rassolov, P. E. Maslen, P. P. Korambath, R. D. Adamson, B. Austin, J. Baker, E. F. C. Byrd, H. Dachsel, R. J. Doerksen, A. Dreuw, B. D. Dunietz, A. D. Dutoi, T. R. Furlani, S. R. Gwaltney, A. Heyden, S. Hirata, C.-P. Hsu, G. Kedziora, R. Z. Khalliulin, P. Klunzinger, A. M. Lee, M. S. Lee, W. Liang, I. Lotan, N. Nair, B. Peters, E. I. Proynov, P. A. Pieniazek, Y. Min Rhee, J. Ritchie, E. Rosta, C. David Sherrill, A. C. Simmonett, J. E. Subotnik, H. Lee Woodcock III, W. Zhang, A. T. Bell, A. K. Chakraborty, D. M. Chipman, F. J. Keil, A. Warshel, W. J. Hehre, H. F. Schaefer III, J. Kong, A. I. Krylov, P. M. W. Gill, and M. Head-Gordon, Phys. Chem. Chem. Phys. **8**, 3172 (2006).

[42] W. J. Hehre, R. Ditchfield, and J. A. Pople, J. Chem. Phys. **56**, 2257 (1972).

[43] P. C. Hariharan and J. A. Pople, Theor. Chim. Acta **28**, 213 (1973).

[44] F. Weigend and R. Ahlrichs, Phys. Chem. Chem. Phys. **7**, 3297 (2005).

[45] T. H. Dunning, J. Chem. Phys. **90**, 1007 (1989).

[46] A. Takatsuka, S. Ten-No, and W. Hackbusch, J. Chem. Phys. **129**, 044112 (2008).

[47] J. Řezáč, K. E. Riley, and P. Hobza, J. Chem. Theory Comput. **7**, 2427 (2011).

[48] R. A. Distasio and M. Head-Gordon, Mol. Phys. **105**, 1073 (2007).

[49] J. Řezáč, P. Jurečka, K. E. Riley, J. Černý, H. Valdes, K. Pluháčková, K. Berka, T. Rezáč, M. Pitoák, J. Vondrášek, and P. Hobza, Collect. Czech. Chem. Commun. **73**, 1261 (2008).

[50] J. Antony, S. Grimme, D. G. Liakos, and F. Neese, J. Phys. Chem. A **115**, 11210 (2011).

[51] See supplementary material at http://dx.doi.org/10.1063/1.4827297 for remaining data tables.

[52] C. V. Sumowski and C. Ochsenfeld, J. Phys. Chem. A **113**, 11734 (2009).

[53] C. V. Sumowski, B. B. T. Schmitt, S. Schweizer, and C. Ochsenfeld, Angew. Chem. Int. Ed. **49**, 9951 (2010).

[54] D. Flaig, M. Beer, and C. Ochsenfeld, J. Chem. Theory Comput. **8**, 2260 (2012).

This article is copyrighted as indicated in the article. Reuse of AIP content is subject to the terms at: http://scitation.aip.org/termsconditions. Downloaded to IP: 92.230.182.222 On: Sat, 14 Dec 2013 22:00:25

Supplementary Information to "Linear-Scaling Symmetry-Adapted Perturbation Theory with Scaled Dispersion"

Simon A. Maurer, Matthias Beer, Daniel S. Lambrecht[a], and Christian Ochsenfeld[b]

Chair of Theoretical Chemistry, Department of Chemistry,
University of Munich (LMU), Butenandtstr. 7, D-81377 Munich, Germany

[a] Present address: Dept. of Chemistry, University of Pittsburgh, Pittsburgh, PA 15260, USA

[b] Electronic mail: christian.ochsenfeld@uni-muenchen.de

system	sd-SAPT0/6-31G**
1	1.78
2	-2.74
3	-4.81
4	-14.28
5	-14.18
6	-16.61
7	-17.14
8	-17.79
9	-20.20
10	-20.93
11	-21.58
12	-22.77
13	-30.25
14	-32.38
15	-36.41
16	-31.17
17	-41.65
18	-46.42
19	-48.00
20	-53.68
21	-50.01
22	-65.32
23	-64.19
24	-77.19

TABLE A. Interaction energies in kcal/mol for the full protein-ligand interaction test set of Antony et al. [J. Phys. Chem. A **115**, 11210 (2011)].

		SCF		$E_{non-disp}$		E_{disp}	
system	N_{bas}	time [h]	scal.	time [h]	scal.	time [h]	scal.
DNA_1	660	0.58	-	0.47	-	1.89	-
DNA_2	1408	3.23	2.27	2.36	2.13	14.64	2.70
DNA_4	2904	11.51	1.76	8.16	1.71	68.16	2.12
DNA_8	5896	34.40	1.55	24.00	1.52	211.16	1.60
DNA_{16}	11880	98.32	1.50	63.19	1.38	574.11	1.43

TABLE B. CPU times for sd-SAPT0 calculations on DNA systems with the 6-31G** basis. Timings for the SCF calculations on the monomers, the non-dispersive SAPT terms, and the dispersion contribution as well as the scaling with respect to the number of basis functions are given.

Curriculum vitae

Personal Details

Date of birth	April 20, 1984
Place of birth	Waiblingen
Nationality	German

Education

since 03/2010	PhD student at the University of Munich (LMU) in the group of Prof. Dr. C. Ochsenfeld
11/2009–02/2010	PhD student at the University of Tübingen in the group of Prof. Dr. C. Ochsenfeld
10/2009	Diploma in chemistry, University of Tübingen, 1.16 (very good) Thesis: ”Atomorbital-basierte CIS(D)-Theorie für elektronisch angeregte Zustände” Supervisor: Prof. Dr. C. Ochsenfeld
01/2008–10/2009	Studies in chemistry at the University of Tübingen
08/2007–12/2007	Studies in chemistry at the Royal Institute of Technology (KTH) in Stockholm
10/2006–07/2007	Studies in chemistry at the University of Tübingen
09/2006	Prediploma in chemistry, University of Stuttgart, very good
10/2004–09/2006	Studies in chemistry at the University of Stuttgart

Awards/Fellowships

05/2005–06/2009	Fellowship of the ”Studienstiftung des deutschen Volkes”
08/2007–12/2007	Fellowship of the ”Landesstiftung Baden-Württemberg” for studies at KTH
01/2007	BASF advancement award for excellent achievements in prediploma studies